

Some outstanding problems concerning heterogeneous polymerizations in aqueous media : thermodynamics, kinetics and modeling

Citation for published version (APA):

Kurja, J. (1997). *Some outstanding problems concerning heterogeneous polymerizations in aqueous media : thermodynamics, kinetics and modeling*. [Phd Thesis 1 (Research TU/e / Graduation TU/e), Chemical Engineering and Chemistry]. Technische Universiteit Eindhoven. <https://doi.org/10.6100/IR492641>

DOI:

[10.6100/IR492641](https://doi.org/10.6100/IR492641)

Document status and date:

Published: 01/01/1997

Document Version:

Publisher's PDF, also known as Version of Record (includes final page, issue and volume numbers)

Please check the document version of this publication:

- A submitted manuscript is the version of the article upon submission and before peer-review. There can be important differences between the submitted version and the official published version of record. People interested in the research are advised to contact the author for the final version of the publication, or visit the DOI to the publisher's website.
- The final author version and the galley proof are versions of the publication after peer review.
- The final published version features the final layout of the paper including the volume, issue and page numbers.

[Link to publication](#)

General rights

Copyright and moral rights for the publications made accessible in the public portal are retained by the authors and/or other copyright owners and it is a condition of accessing publications that users recognise and abide by the legal requirements associated with these rights.

- Users may download and print one copy of any publication from the public portal for the purpose of private study or research.
- You may not further distribute the material or use it for any profit-making activity or commercial gain
- You may freely distribute the URL identifying the publication in the public portal.

If the publication is distributed under the terms of Article 25fa of the Dutch Copyright Act, indicated by the "Taverne" license above, please follow below link for the End User Agreement:

www.tue.nl/taverne

Take down policy

If you believe that this document breaches copyright please contact us at:

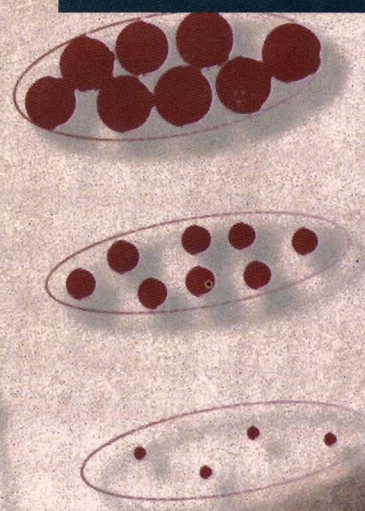
openaccess@tue.nl

providing details and we will investigate your claim.

Some Outstanding Problems concerning Heterogeneous Polymerizations in Aqueous Media

Thermodynamics,
Kinetics
and Modeling

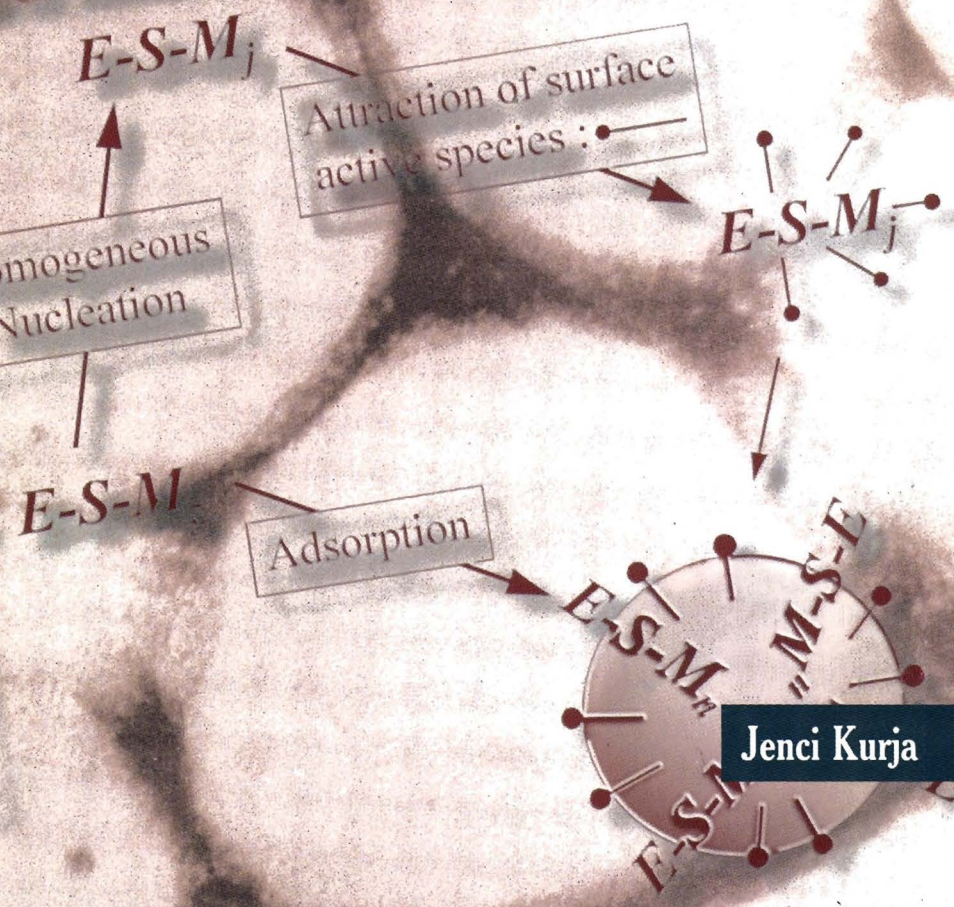
Particle growth
Nucleation



anucleation

Degree of Accumulation

Initiation and Propagation in the cytoplasm



Jenci Kurja

**Some Outstanding Problems concerning
Heterogeneous Polymerizations
in Aqueous Media**

Thermodynamics, Kinetics and Modeling

CIP-DATA LIBRARY TECHNISCHE UNIVERSITEIT EINDHOVEN

Kurja, Jenö

Some outstanding problems concerning heterogeneous polymerizations in aqueous media:
thermodynamics, kinetics and modeling/ by Jenci Kurja.-Eindhoven

Technische Universiteit Eindhoven, 1997

Proefschrift.-

ISBN 90-386-0387-8

NUGI 813

Trefw.: emulsiepolymerisatie

Subject Headings: emulsion polymerization

© Copyright 1997, J.Kurja

Omslagontwerp: Ben Mobach, TUE

Druk: Universiteitsdrukkerij, TUE

**Some Outstanding Problems concerning
Heterogeneous Polymerizations
in Aqueous Media**

Thermodynamics, Kinetics and Modeling

Proefschrift

ter verkrijging van de graad van doctor aan de Technische Universiteit Eindhoven,
op gezag van de Rector Magnificus, prof.dr. M. Rem, voor een commissie
aangewezen door het College van Dekanen in het openbaar te verdedigen
op woensdag 18 juni 1997 om 16.00 uur

door

Jenö Kurja

geboren te Maastricht

Dit proefschrift is goedgekeurd door de promotoren:

prof.dr. P.J. Lemstra

prof.dr.ir. A.L. German

Copromotor:

dr. I.A. Maxwell

Voor allen die in hun hart
ruimte maken voor mij

Contents

CHAPTER 1

Introduction

1.1	Introduction	1
1.2	Classification of Polymerization Reaction	3
1.3	Heterogeneous Polymerization Processes	3
1.4	Emulsion Polymerization	5
	1.4.1 Emulsion Polymerization Kinetics	5
	1.4.2 Monomer Partitioning during Emulsion Polymerization	10
1.5	Some Outstanding Problems in Emulsion Polymerization-like Systems	11
1.6	Objective of the Thesis	12
1.7	Survey of the Thesis	13
1.8	References	15

CHAPTER 2

Thermodynamics of Polymer Solutions

2.1	Introduction	19
2.2	Flory-Huggins Theory	19
2.3	Thermodynamics of Polymer Solutions	22
	2.3.1 Phase Separation Behavior of Polymer Solutions	22
	2.3.2 Phase Behavior of Amorphous Polymers in Solution	24
	2.3.3 Phase Behavior of Semi-Crystalline Polymers in Solution	27
2.4	Thermally vs. Chemically induced Phase Separation	29
2.5	References	31

CHAPTER 3

Partial Swelling of Latex Particles

3.1	Introduction	34
3.2	Theory	34
3.3	Experimental	37
3.4	Results and Discussion	40
	3.4.1 Influence of Temperature	40
	3.4.2 Influence of the Radius of the Latex Particles	41
	3.4.3 Influence of the Molar Mass of the Polymer	44
	3.4.4 Influence of the Cross-link Density	45
	3.4.5 Influence of Copolymer Composition	45
	3.4.6 Influence of Water Solubility of Monomer/Solvent	47
	3.4.7 Influence of Specific Interaction between Monomer/Solvent and Polymer	50
3.5	Estimation of Monomer Partitioning	52
3.6	Conclusions	54
3.7	References	56

CHAPTER 4**Saturation Swelling of Latex Particles****1. Ideal Systems**

4.1	Introduction	57
4.2	Theory	58
4.3	Experimental	63
4.4	Results and Discussion	66
	4.4.1 Experimental Results	66
	4.4.2 Modeling of Saturation Swelling of Latex Particles	71
4.5	Concluding Remarks	77
4.6	References	78

CHAPTER 5**Saturation Swelling of Latex Particles****2. Non-Ideal Systems: The Styrene-Acrylonitrile-Butadiene Case**

5.1	Introduction	81
5.2	Theory	83
5.3	Experimental Partitioning Results and Discussion	87
	5.3.1 Partial Swelling of PB Particles by One Monomer	87
	5.3.2 Saturation Swelling of PB and SAN Latex Particles by One Monomer	88
	5.3.3 Saturation Swelling of SAN latex Particles by Two Monomers	89
5.4	Modeling and Prediction of Monomer Partitioning in Non-ideal Latex Systems	93
	5.4.1 Partial Swelling of PB Latices by One Monomer	93
	5.4.2 Saturation Swelling by One Monomer	95
	5.4.3 Saturation Swelling by Two Monomers	97
5.5	Concluding Remarks	110
5.6	References	110

CHAPTER 6**Phase Diagrams of Emulsion Polymerization Systems**

6.1	Introduction	113
6.2	Ternary Phase Diagrams	114
6.3	Ternary Phase Diagrams of Emulsion polymerization Systems: The Swelling of Latex Particles by One Monomer	115
	6.3.1 Definition of Edges and Axis in Ternary Phase Diagrams of Latices Swollen by One Monomer	116
	6.3.2 The Different factors influencing the Ternary Phase Diagram of Latices Swollen by One Monomer	120
6.4	Quaternary Phase Diagrams of Emulsion Polymerization Systems: The Swelling of Latex Particles by Two Monomers	123

6.5	The Use of Phase Diagrams in Emulsion Polymerization Processes	125
6.5.1	Seeded Emulsion Polymerization	125
6.5.2	<i>Ab initio</i> Emulsion Homopolymerization	126
6.6	Concluding Remarks	127
6.7	Appendix A: The Gibbs Phase Rule	128
6.8	References	130

CHAPTER 7

Polymerization in Vesicles

7.1	Introduction	131
7.2	Guidelines for the <i>Polymerization in Vesicles</i>	132
7.3	Kinetic processes during the <i>Polymerization in Vesicles</i>	134
7.4	Concluding Remarks	138
7.5	References	138

CHAPTER 8

Swelling of Vesicles

8.1	Introduction	141
8.2	Theory	143
8.3	Results and Discussion	151
8.4	Conclusions	159
8.5	Appendix A: Surface Phenomena in Vesicle Bilayers and the Gibbs Phase Rule	161
8.6	References	163

CHAPTER 9

Unconventional Emulsion Polymerizations

9.1	Introduction	165
9.2	Unconventional Free-radical Emulsion Polymerizations	168
9.2.1	Chemically-Initiated Vinyl Polymerizations	168
9.2.2	Ultrasound Polymerizations	168
9.2.3	Polymerization in Vesicles	169
9.2.4	Conducting Polymer Latices	169
9.3	Ionic Emulsion polymerizations	170
9.4	Transition Metal Catalyzed Emulsion Polymerizations	171
9.4.1	Transition Metal Catalyzed Vinyl Polymerizations	172
9.4.2	Ring-Opening Metathesis Polymerization (ROMP)	172
9.5	Enzyme Catalyzed Emulsion Polymerizations	174
9.5.1	Bacterial Polyhydroxyalkanoates	174
9.5.2	Natural Rubber	175
9.5.3	Cellulose	176
9.6	Concluding Remarks	177
9.7	References	178

CHAPTER 10**The Accumulation of Poly-(R)-3-hydroxybutyrate in *Alcaligenes eutrophus*****1. Kinetics and Metabolic Regulation**

10.1	Introduction	181
10.2	Theory	183
10.2.1	Synthetic Polycondensations versus the Biosynthesis of <i>b</i> -PHAs	183
10.2.1.1	Synthetic Polycondensations	183
10.2.1.2	Biosynthesis of <i>b</i> -PHAs	185
10.2.2	Enzyme Kinetics: Analyzing Enzyme Rate Data	188
10.2.2.1	Initial Rate Method	188
10.2.2.2	Kinetic Analysis of Progress Curves	191
10.3	Experimental	194
10.4	Results and Discussion	195
10.4.1	Straightforward Analysis of Kinetic Data	196
10.4.2	The Use of the Integrated Rate Equation for the Analysis of Kinetic Data	198
10.5	Concluding Remarks	200
10.6	References	201

CHAPTER 11**The Accumulation of Poly-(R)-3-hydroxybutyrate in *Alcaligenes eutrophus*****2. Granule Growth**

11.1	Introduction	203
11.2	Theory	204
11.2.1	Emulsion Polymerization	205
11.2.2	Accumulation of Poly-(R)-3-hydroxybutyrate	207
11.2.3	Physical Model for the PHB Accumulation in <i>Alcaligenes eutrophus</i>	207
11.2.3.1	Formation of Granules	208
11.2.3.2	Growth of Granules	208
11.2.4	Kinetic Model for the Accumulation of PHB in <i>Alcaligenes eutrophus</i>	209
11.2.4.1	Initiation	209
11.2.4.2	Propagation in the Cytoplasm	210
11.2.4.3	Adsorption of Polymer-Polymerase Conjugates onto Granules	210
11.2.4.4	Propagation at the Granule Surface	211
11.2.4.5	Chain Transfer at the Granule Surface	212
11.2.4.6	Molar Mass of Polymer	213
11.3	Granule Growth: Comparison with Experiment	215
11.3.1	Rate of Polymerization	215
11.3.2	Molar Mass	222
11.4	Conclusions	223
11.5	References	224

CHAPTER 12**The Accumulation of Poly-(R)-3-hydroxybutyrate in *Alcaligenes eutrophus*****3. Granule Formation**

12.1	Introduction	227
12.2	Latex Particle Formation in Emulsion Polymerization Processes	228
12.2.1	Synthetic Emulsion Polymerizations	228
12.2.2	Latex Particle Formation in Biological Emulsion Polymerizations	230
12.2.2.1	The Biosynthesis of Poly- <i>cis</i> -isoprene (Natural Rubber)	230
12.2.2.2	The Biosynthesis of Cellulose	232
12.2.2.3	The Biosynthesis of Poly-3-hydroxyalkanoates	232
12.3	Granule Formation during the Biosynthesis of PHB in <i>Alcaligenes eutrophus</i>	235
12.3.1	Initiation	235
12.3.2	Propagation in the Cytoplasm	236
12.3.3	Chain Transfer in the Cytoplasm	237
12.3.4	Quantitative Description of Granule Formation during PHB Accumulation	238
12.3.5	Influence of Granule Formation on the Molar Mass of the Polymer	239
12.4	Experimental Molar Mass versus Accumulation Time and Conversion	241
12.4.1	Molar Mass of PHB formed during a Two-step Batch Fermentation	241
12.4.2	Influence of Multiple Carbon Source Addition on Accumulation Process	243
12.5	Concluding Remarks	248
12.6	References	249

CHAPTER 13**The Accumulation of Poly-(R)-3-hydroxybutyrate in *Alcaligenes eutrophus*****4. Influence of Granule Surface**

13.1	Introduction	251
13.2	Theory	252
13.2.1	Introduction	252
13.2.2	Introduction of Boundary Layers	255
13.2.3	Influence of the Boundary Layer on Polymerization Kinetics	258
13.2.4	Chain Transfer in the Cytoplasm vs. Chain Transfer in the Boundary Layer	260
13.3	Theory, Model and Experiment	261
13.3.1	Constant Surface Concentration of Polymer-Polymerase Conjugates	261
13.3.2	An Example: One step Batch Fermentation of PHB in <i>Alcaligenes eutrophus</i>	263
13.3.3	Influence of the Boundary Layer on the End of Polymerization	266
13.4	Conclusions	267
13.5	References	267

CHAPTER 14**The Accumulation of Poly-(R)-3-hydroxybutyrate in *Alcaligenes eutrophus*****5. *Model Calculations versus Experiments***

14.1	Introduction	269
14.2	Monomer and Polymerase Enzyme Concentration	270
	14.2.1 Monomer Concentration during the Accumulation Process	270
	14.2.2 Polymerase Enzyme Concentration	272
14.3	Estimation of Rate Coefficients	273
14.4	Estimation of Granule Formation Parameters	276
	14.4.1 Estimation of z from <i>in vivo</i> Polymerizations	276
	14.4.2 Estimation of j	277
14.5	Model Calculations	278
	14.5.1 Influence of Variations in Input Parameters on the Number of Granules	280
14.6	Experimental Results and Model Calculations	286
	14.6.1 Influence of Carbon Source Concentration	287
	14.6.2 Influence of pH	289
	14.6.3 Influence of Temperature	290
14.7	Concluding Remarks	292
14.8	References	293

CHAPTER 15**The Accumulation of Poly-(R)-3-hydroxybutyrate in *Alcaligenes eutrophus*****6. *On the Applicability of the Developed Model***

15.1	Introduction	295
15.2	Some Critical Comments on the Developed Model	296
	15.2.1 Enzyme Kinetics and the Biosynthesis of PHB	296
	15.2.2 Does the Biosynthesis of PHB exhibit Oscillatory Behavior ?	297
	15.2.3 The Granule Formation and Granule Growth Stage	299
15.3	Copolymers from Different Bacteria	304
	15.3.1 Copolymers from <i>Alcaligenes eutrophus</i>	304
	15.3.2 Copolymers from <i>Pseudomonas putida/oleovorans</i>	307
15.4	Genetic Engineering and the Biosynthesis of Polyhydroxyalkanoates	310
	15.4.1 Cloning of Genes Responsible for the Biosynthesis of PHB	310
	15.4.2 Towards the <i>in vitro</i> Synthesis of Polyhydroxyalkanoates	314
15.5	Concluding Remarks	315
15.6	References	316

Epilogue	319
-----------------	-----

Summary	323
----------------	-----

Samenvatting	327
---------------------	-----

Curriculum Vitae	331
-------------------------	-----

CHAPTER 1

General Introduction

1.1 Introduction

Macromolecules are an intrinsic part of our daily life, not only with respect to polymeric construction materials, but also as essential constituents of nature. When polymers are categorized according to their origin they can be divided into synthetic polymers (*Polymers of Commerce*) and natural polymers (*Polymers of Life*)¹. Examples of natural polymers are nucleic acids (DNA, RNA), polysaccharides (e.g. cellulose, starch), proteins (e.g. collagen, wool, silk), and polyisoprenes (e.g. natural rubber and gutta percha). Synthetic polymers are often subdivided into Commodity Plastics like polyethylene (PE), polypropylene (PP), polystyrene (PS), and polyvinylchloride (PVC), Engineering Plastics such as, for instance, polycarbonate (PC), polyphenylene ether (PPE), and nylon-6, and Specialty Polymers such as polyetherimide and liquid-crystalline polymers (LCPs). A more general classification can be made according to the presence of physical or chemical cross-links which are denoted then as thermoplastics, elastomers or thermosets, respectively.

If one considers the polymer industry from a historical point of view, its beginning can be traced back to the modification of natural polymers such as natural rubber, lac (shellac), gutta percha, and last but not least cellulose². The earliest written references to natural rubber were made by Spaniards following the voyages of Columbus in the late fifteenth century. Antonio de Herrera Tordesillas (1601) described a game (like pelota), using a rubber ball, which was played by the Mayans at the court of Aztec emperor Montezuma II and which, as a religious rite, could lead to the ritual slaughter of the losing team. Indians in South America used coagulated latex to make boots, liquid containers, and waterproofed clothing³. In order to tailor its properties, cellulose is chemically modified. These modifications are not

considered as the first synthetic polymer chemical reactions, but more as modifications of an already existing natural polymer.

Table 1.1 Classification of Polymerization Reactions ⁴

Classification	Mode
By Stoichiometry	A-polymers and C-polymers
By Mechanism of Polymerization	Chain and Step Polymerization
By Nature of Propagating Species	Anionic, Cationic, Zwitterionic, Insertion, Radical, Coordination, Charge-transfer complexes, and Group-transfer Polymerizations
By Method of Initiation	Thermal, Enzymatic, Electrochemical, Plasma, Mechanochemical, and Radiation-induced
By Medium of Reaction	Bulk (or Mass), Solution, Template, Gas phase, Emulsion (macro, micro, mini, and inverse), Interfacial, Solid-state, Template, Suspension, and Polymerization in Clathrates
By Structure of Product	Stereospecific, Isomerization, Crosslinking, Ring-opening, cyclo-, block and graftcopolymerizations, bead or pearl, and popcorn polymerizations
By Nature of Reactants	e.g. Vinyl, allyl, and diene polymerizations

Synthetic polymer chemistry, however, probably started when Leo Baekeland in 1910 at the University of Gent (Belgium) developed a method of controlling the reaction of phenol with formaldehyde. This reaction yielded a powder which could be processed into a useful material for electrical insulation (Bakelite). Herman Staudinger postulated in the 1920s that polymers were macromolecules, for which he received the Nobel prize in 1953 ⁵. A few years later, in 1929, Wallace H. Carothers (at E.I. du Pont de Nemours) started to synthesize polymers using well-established reactions from organic chemistry such as esterification and amidation and demonstrated beyond, any doubt, that Staudingers concept was correct ⁶. In 1937, this investigation resulted in the synthesis of the first synthetic fiber (nylon-6,6). Another important result of the above mentioned research project was that polymeric materials could be oriented by cold drawing to give greatly improved tensile strengths. Carothers did not only synthesize polymers, but he also defined important terms such as *end group* and *copolymer* ⁷. Further, he categorized synthetic polymers into two classes: **A-polymers**, produced by recurring addition of monomers, and **C-polymers**, produced by recurring condensation of monomers. Concomitantly, the molar mass of A-polymers is equal to the product of the

number and the molar mass of the monomer unit in the polymer chain. In *C*-polymers the molar mass of the polymer formed is less than the sum of the masses of the original monomer units which have been combined to form the polymer. After Carothers, numerous methods of classifying polymerization reactions were postulated which are summarized in *table 1.1*.

1.2 Classification of Polymerization Reactions

If one classifies polymerization reactions according to the medium of reaction, a more commonly used classification is preferred, i.e. classifying a polymerization reaction either being homogeneous or heterogeneous from a phase composition point of view. Bulk and solution polymerizations are often referred to as homogeneous polymerizations, and are mainly characterized by the fact that the concentration of the different species, e.g. polymer chains, monomer and solvent, is virtually the same throughout the whole system. Emulsion and suspension polymerization can be designated as heterogeneous polymerizations. In contrast with homogeneous polymerizations, the concentration of the different species during a heterogeneous polymerization can differ significantly throughout the system. Therefore, the exchange of for instance monomer, initiator and propagating polymer chains between the different phases which can have a profound effect on the kinetics of the polymerization and thus on the characteristics of the polymer formed during such processes, has to be taken into account. In the following section, different heterogeneous polymerization processes will be classified and discussed. In doing so, the differences between the emulsion and suspension polymerization process will be highlighted.

1.3 Heterogeneous Polymerization Processes

An excellent review exists on the classification of heterogeneous polymerizations⁸. Here, only a brief summary will be given of this classification, which does not include precipitation, emulsifier free polymerization and dispersion polymerization, since these polymerizations often start from a homogeneous system and the heterogeneity is introduced during polymerization. Heterogeneous polymerizations can be categorized according to the following two criteria: 1. surface tension driving force, which is the difference in the surface

tension between the aqueous phase and the hydrophilic part of the emulsifier and the organic phase and the hydrophobic part of the emulsifier, and 2. stability threshold, which represents a critical emulsifier concentration below which a kinetically stable macro-emulsion is formed. Under appropriate conditions these kinetically stable *macro-emulsion* can be transformed to thermodynamically stable *micro-emulsions* upon adding emulsifier above its critical concentration (see *figure 1.1*). As depicted in *figure 1.1*, four heterogeneous polymerization regions have been identified⁸: A. *Macro-emulsions*, B. *Micro-emulsions*, C. *Inverse-macro-emulsions*, and D. *Inverse-micro-emulsions*.

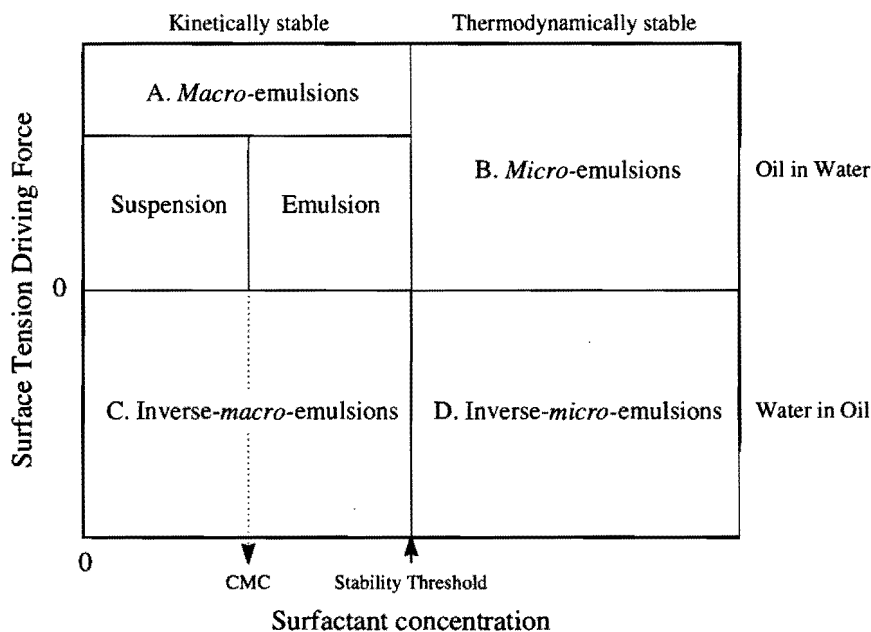


Figure 1.1 Heterogeneous polymerization regions⁸

We will focus now on the macro-emulsion regions. The discussion given below for macro-emulsions, however, also holds for inverse-macro-emulsions. Depending on the surfactant concentration in the system the macro-emulsion can be divided into two regimes, i.e. surfactant concentrations below and above the critical micelle concentration (CMC) of the added surfactant. At surfactant concentrations below the CMC a suspension of monomer in water is formed, where nucleation proceeds predominantly via the monomer droplets. The kinetics of these kind of polymerizations, i.e. *suspension* polymerizations, resemble bulk

kinetics (large number of radicals are present in the monomer droplets), and the continuous water phase lowers the viscosity of the reaction mixture and dissipates the heat of polymerization. However, when the surfactant concentrations exceed the CMC, micelles are present initially in the polymerization system, which is referred to as an *emulsion* polymerization. These micelles can act as sites for nucleation, and have a profound effect on the kinetics of the polymerization process. The average number of radicals present in these small colloidal particles is often not larger than one ⁹. The major difference between suspension and emulsion polymerizations is the mode of nucleation, monomer droplets (suspension) versus monomer swollen micelles (emulsion), and the kinetics of the polymerization, i.e. a pseudo-bulk system (suspension, average number of radicals in the monomer droplets is in the order of 10^4) versus a compartmentalized system (emulsion, where the average number of radicals per polymer particle is relatively low).

1.4 Emulsion Polymerization

Emulsion polymerization is often referred to as a particular case of free radical polymerization, although other types of polymerization reactions in emulsion are known ¹⁰, e.g. the emulsion polymerization of siloxanes ^{11,12,13} and the ring-opening metathesis polymerization of oxanorbornene derivatives ¹⁴. The kinetics and mechanisms involved in an emulsion polymerization are highly complicated, since events occur in several phases, and exchange of radicals and monomer between these phases needs to be taken into account. Models and theories dealing with these aspects of emulsion polymerization are numerous and excellent reviews are available ^{15,16,17}. Here, only an overview of the most important models and theories will be given.

1.4.1 Emulsion Polymerization Kinetics

In contrast to bulk and solution polymerization, emulsion polymerizations are heterogeneous reaction systems ¹⁸. Generally an emulsion polymerization system comprises of water, monomer, surfactant, initiator and additives such as chain transfer agents and buffers. A widely used and accepted mathematical model for the emulsion polymerization process is that of Smith and Ewart ¹⁹, which is based on the descriptive model of Harkins ²⁰. The Smith-Ewart model subdivides the emulsion polymerization process into three distinct intervals. A

typical conversion-time curve is shown in *figure 1.2*. For simplicity we will assume that the added surfactant is present at a concentration above the CMC (= critical micelle concentration), although this is not necessary since there are several examples of emulsifier free emulsion polymerizations described in the literature ^{e.g. 21}.

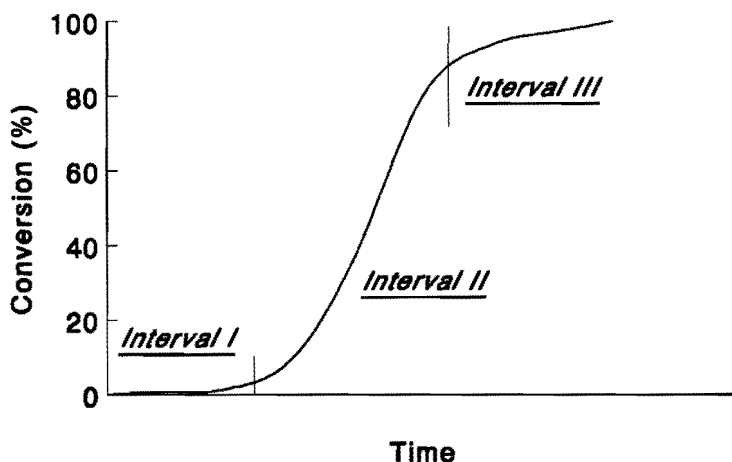


Figure 1.2 A typical conversion-time curve for an emulsion polymerization with the different intervals indicated.

Interval I is the initial stage where particle formation takes place via several possible mechanisms ^{15,18,22,23}. *Interval II* is entered when no new particles are being formed (no micelles are present anymore) and is characterized by the fact that the number of polymer particles reaches a constant value. *Interval III* begins with the disappearance of the monomer droplets, after which the monomer concentration in the polymer particles decreases continuously. Concomitantly, the rate of polymerization decreases. In the following sections the separate intervals of an emulsion polymerization will be discussed in more detail.

During the particle growth phase of an emulsion polymerization the polymerization reaction proceeds in the presence of a separate monomer phase, which ensure a constant transport of monomer to the growing polymer particles (no diffusion limitation), i.e. the rate of diffusion of monomer from the monomer droplets to the water phase and subsequently to the polymer particles is equal to the rate of consumption of the monomer in the polymerization

process. The monomer and radical concentration within the water phase and the polymer particles is constant during *interval II*, leading to a constant rate of polymerization. For clarity we would like to emphasize that during an conventional emulsion polymerization the polymerization reaction takes mainly place **inside** the growing polymer particles, although exceptions to this are known such as the emulsion polymerization of acrylonitrile and tetrafluoroethylene^{10,24}. In general, the rate of a free radical polymerization (R_p) is given by:

$$R_p = k_p * [M] * [R] \quad (1.1)$$

where k_p is the second order propagation rate coefficient, $[M]$ and $[R]$ the monomer and free radical concentrations, respectively. In emulsion polymerization the overall rate of polymerization can be taken as the summation of those in each individual polymer particle, leading to:

$$R_p = \frac{k_p * C_M * \bar{n} * N}{N_{Av.}} \quad (1.2)$$

where C_M is the monomer concentration within the polymer particles, \bar{n} the average number of radicals per particle, N the number of polymer particles per unit volume, and $N_{Av.}$ Avogadro's number. *Equation 1.2* is often written in terms of fractional conversion of monomer (x):

$$R_p = - \frac{dx}{dt} = \frac{k_p * C_M * \bar{n} * N}{n_{mo} * N_{Av.}} \quad (1.3)$$

where n_{mo} is the initial average concentration of monomer in the latex system. We now consider those factors which may affect the rate of emulsion polymerization at high conversions. In this chapter high conversion always applies to the so-called *interval III* of an emulsion polymerization, where there are no monomer droplets in the system and all the monomer is contained in the latex particle and aqueous phases. Note that, we are specifically interested in the latter part of *interval III*. There are four variables in the rate equation (*equations 1.2 or 1.3*) that can vary during the course of polymerization in *interval III*: 1. the

propagation rate coefficient, 2. the latex particle concentration, 3. the monomer concentration in the latex particles, and 4. the average number of free radicals per latex particle. The effect of these factors upon the rate of emulsion polymerization during *interval III* has been discussed elsewhere²⁵. Here, we will only discuss the influence of the monomer concentration on the rate of polymerization during *interval III*. As already stated the rate of emulsion polymerization depends directly upon the monomer concentration in the latex particles. Therefore, as monomer is consumed the rate decreases. In *interval III*, if it is assumed that all monomer is contained within the latex particles, the fractional conversion of monomer is given by:

$$x = \frac{C_{M_0} - C_M}{C_{M_0}} \quad (1.4)$$

where C_{M_0} is the saturation concentration of monomer in the latex particles (or that at the beginning of reaction in *Interval III*). Therefore, the emulsion polymerization rate equation (*equation 1.3*) can be written as⁵:

$$-\frac{d \ln(1-x)}{dt} = \frac{k_p * C_{M_0} * \bar{n} * N}{n_{mo} * N_{Av.}} \quad (1.5)$$

Since in *equation 1.5*, C_{M_0} is a constant, it is obvious that the consumption of monomer results in an exponentially decreasing rate of polymerization during *Interval III*. This is only true if monomer is contained mainly within the latex particles, a situation that arises only for very water insoluble monomers (e.g. styrene). Obviously for more water soluble monomers the effect of the monomer concentration upon the rate of polymerization is complicated by monomer partitioning between the latex particle and aqueous phases.

When copolymerizations are considered, however, the instantaneous composition of the copolymer formed depends on the ratio of monomers and the reactivity ratios of the different comonomers present, as depicted by *equation 1.6*, which is also known as the differential copolymer equation.

$$\frac{d[M_1]}{d[M_2]} = \frac{[M_1]}{[M_2]} * \left[\frac{r_1 * [M_1] + [M_2]}{r_2 * [M_2] + [M_1]} \right] \quad (1.6)$$

here $[M_1]$ and $[M_2]$ represent the concentration monomer 1 and 2, respectively. While r_1 and r_2 are the reactivity ratios of monomer 1 and 2, respectively, defined as the ratio of the homo-propagation rate coefficient and the hetero-propagation rate coefficient. Equation 1.7 gives the mole fraction of monomer 1 in the copolymer (F_1) formed as a function of the fraction of monomer 1 and 2 in the monomer feed, i.e. f_1 and f_2 , respectively:

$$F_1 = \frac{r_1 * f_1^2 + f_1 * f_2}{r_1 * f_1^2 + 2 * f_1 * f_2 + r_2 * f_2^2} \quad (1.7)$$

The reactivity ratios can differ in such a way that the chemical composition of the copolymer formed changes with conversion or reaction time. This is typically the case when the reactivity ratios strongly deviate from unity, i.e. one of the comonomers is consumed at a higher rate than the other.

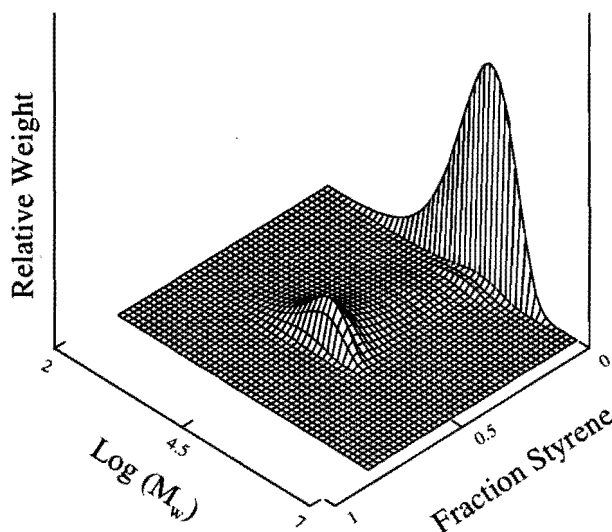


Figure 1.3 Model MMCCD of a high conversion S-MA emulsion copolymer. $(S/MA)_0 = 0.33$ (mole/mole), monomer over water ratio of 0.5 (g/g), 1 wt-% chain transfer agent, and $M_w = 110,000$ g/mole. Data taken from Van Doremalee²⁶.

In the case of the emulsion polymerization process where the continuous aqueous phase acts as a reservoir of monomer, differences in water solubility of the comonomers can magnify this effect. The phenomenon that the chemical composition of the copolymer formed changes as function of reaction time/conversion is also referred to as composition drift ²⁶. *Figure 1.3* gives a typical molar mass chemical composition distribution (MMCCD) of a styrene methyl acrylate (S-MA) copolymer prepared via an emulsion polymerization. Methyl acrylate is the more water soluble monomer, while styrene is built in the copolymer at a higher relative rate. As can be clearly seen from this figure, the chemical composition distribution (CCD) of the copolymer formed is extremely broad. In this particular case the chemical composition changes in such a way that at the end of the polymerization process only homopolymer, i.e. poly(methyl acrylate), is formed.

1.4.2 Monomer Partitioning during Emulsion Polymerization

Let us now look somewhat closer at the partitioning of monomer during an emulsion polymerization process, which consists initially of three phases, i.e. a monomer phase, monomer swollen micelles and a continuous water phase containing dissolved monomer (*interval I*). As initiation occurs, the monomer swollen micelles will be, to a great extent, converted into monomer swollen polymer particles. Once there are no monomer swollen micelles present anymore no new polymer particles will be formed and *interval II* of the emulsion polymerization process is entered. The polymerization system consists now of monomer swollen polymer particles, monomer droplets and a continuous water phase with monomer dissolved in it. During *interval II* monomer will diffuse from the monomer droplets to the monomer swollen polymer particles where the major part of the propagation process occurs. At some point the monomer phase will be depleted and the concentration in the polymer particles will drop as the propagation process continuous (*interval III*), monomer will be only diffusing from the continuous water phase to the polymer particles. The system comprises now monomer swollen polymer particles and the monomer containing water phase. Finally, all the monomer will be converted into polymer and the system consists then only of polymer particles and the continuous water phase also referred to as latex. It is clear from the above that during an emulsion polymerization the partitioning of monomer over the different phases present changes continuously (see *table 1.2*). An accurate knowledge of the concentration of the monomer in the different phases of the polymerization system is necessary to develop and test kinetic models for the emulsion polymerization process. These models can

be useful in the design of polymerization reactors, process control and product characteristics such as molar mass, molar mass distribution, chemical composition, and chemical composition distribution of the (co)polymers formed.

Table 1.2 *Partitioning of Monomer(s) during an Emulsion Polymerization*

	Micelles	Aqueous Phase	Latex Particles	Monomer Droplets
Interval I	Saturated <i>[M] decreases</i>	Saturated <i>[M] constant</i>	Saturated <i>[M] increases</i>	Saturated <i>[M] constant</i>
Interval II	Disappeared	Saturated <i>[M] constant</i>	Saturated <i>[M] is a function of particle size</i>	Saturated <i>[M] constant</i>
Interval III	Disappeared	Below Saturation <i>[M] decreases</i>	Below Saturation <i>[M] decreases</i>	Disappeared

1.5 Some Outstanding Problems in Emulsion Polymerization-like Systems

Due to the intrinsic heterogeneity of an emulsion polymerization, the kinetics and thermodynamics which control this polymerization process are difficult to describe since there is a continuous exchange of radicals and monomer between the different phases present. Below, three areas are identified that embody problems, thermodynamic and/or kinetic in nature, of which the solutions are of key importance for the further development of emulsion polymerization or emulsion polymerization-like processes.

1. Monomer Partitioning during Emulsion Polymerization

In order to get more insight in the kinetic processes involved in an emulsion polymerization a detailed knowledge of the partitioning of monomer(s) over the different phases present is necessary. The monomer concentration in the latex particles directly determines the rate of polymerization, while, during an emulsion copolymerization, the monomer ratio in the latex particles determines the chemical composition of the copolymer

formed. Concomitantly, if one wants to model the emulsion polymerization process, detailed knowledge of the partitioning of monomer over the different phases is of utmost importance.

2. Control of Latex Particle Morphology during Emulsion Polymerization

It has been known for some time that one can perform a free radical type of polymerization in micelles, i.e. an emulsion polymerization²⁷ and in inverse micelles, i.e. an inverse emulsion polymerization^{27,28}. The question arises if one can polymerize in other surfactant structures such as vesicles, i.e. performing a *Polymerization in Vesicles*. In order to be able to control this polymerization process, knowledge of the partitioning of monomer between the aqueous phase and the hydrophobic vesicle bilayer, and the polymerization kinetics are of crucial importance.

3. Kinetics of Unconventional Emulsion Polymerizations

Numerous publications have been devoted to the description of the kinetics of conventional, free-radical initiated, emulsion polymerization processes^{see e.g. 29}. Emulsion polymerizations which utilize other propagating species than radicals have not been the subject of in-depth kinetic studies¹⁰. An example of an unconventional emulsion polymerization is the biosynthesis of poly-(R)-3-hydroxybutyrate (PHB) in *Alcaligenes eutrophus*. The polymerization process, catalyzed by an enzyme, takes place mainly at the surface of latex particles which are formed at the earliest stage of the polymerization. This heterogeneous polymerization system exhibits, among others, two interesting features: First, the polymerization reaction is catalyzed by an enzyme, which shows some resemblance with the biosynthesis of natural rubber, and not via free-radicals. Second, the polymerization reaction occurs mainly at the granule surface. Therefore, the monomer partitioning between the aqueous phase (cytoplasm) and the granule surface has been taken into consideration.

1.6 Objective of the Thesis

The *first* objective of this thesis is to describe, explain and predict the partitioning of monomer(s) over the separate phases present during the course of an emulsion polymerization. Special attention will be paid to the partitioning of monomers during emulsion polymerizations where the monomer(s) present is (are) a poor solvent for the polymer in the latex particles.

Further, an attempt will be made to visualize the partitioning of monomer between the different phases present during an emulsion polymerization utilizing phase diagrams. At the same time, the monomer partitioning between vesicles and the aqueous phase will be studied and some guidelines for the polymerization of an unsaturated monomer(s) in the bilayer of these vesicles will be proposed. Polymerization in vesicles can be designated as an unconventional emulsion polymerization, due to the fact that this polymerization process differs, in terms of kinetic processes, from a conventional emulsion polymerization. This brings us to the *second* objective of this thesis, which deals with the applicability of the concepts known from conventional emulsion polymerizations, concerning for instance the processes of particle nucleation and growth and the exchange of monomer and active species between the different phases present, to polymerization processes that were, until recently, not recognized as emulsion polymerizations since they do not proceed through mechanisms involving propagating free-radicals, but other propagating species like for instance enzymes. The biosynthesis of poly-(R)-3-hydroxybutyrate (PHB) in *Alcaligenes eutrophus* will serve in this case as a model system.

1.7 Survey of the Thesis

In *Chapter 2* the basic aspects of the thermodynamics of polymer solutions will be discussed, thus creating a framework for *Chapters 3, 4, 5, 6, and 8* where the monomer partitioning for different emulsion polymerization systems is discussed.

Chapter 3 deals with the swelling of latex particles in the case where the aqueous phase and the latex particles are not saturated with monomer(s). The influence of different parameters, such as latex particle size, cross-link density, and water solubility of the monomer, are discussed with respect to the swelling of latex particles below saturation.

Chapter 4, on the other hand, deals with the situation in which the polymer phase and the aqueous phase are saturated with monomer(s), which results in the formation of a separate monomer phase, corresponding to Interval II of an emulsion polymerization.

The saturation swelling of latex particles with monomers which have different solvent qualities for the polymer in the latex particles, most notably the swelling of poly(styrene-co-acrylonitrile) latex particles by styrene and acrylonitrile or mixtures of both, will be investigated in *Chapter 5*.

In order to be able to visualize the thermodynamic model developed in *Chapters 3, 4, and 5*, *Chapter 6* deals with phase diagrams of emulsion polymerization systems. In doing so, not only the partitioning of monomer during an emulsion polymerization will be discussed using these phase diagrams but also, for instance, the (*ab initio*) emulsion homopolymerization process.

Guidelines for the *Polymerization in Vesicles* are presented in *Chapter 7*, together with a condensed discussion of the kinetic processes occurring during this novel polymerization process.

In *Chapter 8*, the swelling of vesicle bilayers by one solvent is discussed.

In *Chapter 9* an overview will be given of unconventional emulsion polymerizations. In doing so, it will be shown that only little is known about the kinetics and mechanism involved in unconventional emulsion polymerizations. The proceeding chapters will deal with the development of a kinetic model for the biosynthesis of poly-(R)-3-hydroxybutyrate in *Alcaligenes eutrophus*, which will be based on the concepts of particle formation and growth known from the conventional emulsion polymerizations process.

In *Chapter 10* a study of the kinetic and metabolic regulation of the biosynthesis of poly-(R)-3-hydroxybutyrate in *Alcaligenes eutrophus* is presented from an enzymological as well as polymer chemical point of view. This is done via *in vitro* experiments in which the purified PHB-synthase and a substrate, i.e. (R)-3-hydroxybutyryl-CoA, which is the actual monomer in the *in vivo* enzymatic polymerization, are incubated.

In *Chapter 11* the granule growth process of the PHB inclusions which are formed during the accumulation of PHB in *Alcaligenes eutrophus* will be discussed. *Chapter 11*

creates a framework for *Chapters 12, 13, and 14*, i.e. it contains the basic concepts of the granule growth process of the model presented in this thesis.

Chapter 12 mainly deals with granule formation stage of the accumulation process. A detailed kinetic model describing the granule formation process will be discussed and model calculations are compared with experimental data.

Chapter 13 deals with the kinetic processes occurring at the granule surface in much more detail. In particular, the influence of the granule surface and the intergranular distance are considered. Further, some comments are made concerning the partitioning of monomer and, especially, coenzyme-A between the aqueous phase and the granule surface.

In *Chapter 14* model calculations using the model developed in *Chapters 11, 12 and 13* are presented and compared with experimental data.

In *Chapter 15* the results from the model developed in the previous chapters will be placed in a broader perspective. In doing so, some critical comments will be made with respect to the model developed. After which, the use of genetic engineering in the biosynthesis of polyhydroxyalkanoates (PHAs) is considered. Finally, the *in vitro* synthesis of PHAs is thought over from the perspective of the developed model.

The intention of this thesis is that the different chapters can be read independently. Hence, this thesis contains an epilogue in which the results of the separate chapters will be summarized and evaluated with respect to the objectives of this thesis. This thesis is based on a collection of publications^{10,30,31,32,33,34,35,36,37,38}. Furthermore, the author has also contributed to other papers^{39,40,41,42}, not presented in this thesis.

1.8 References

- 1 Bolker, H.I., "*Natural and Synthetic Polymers : An Introduction*", M. Dekker, New York, (1974).
- 2 Utracki, L.A., *Polymer Eng. and Sci.*, 35, 2 (1995)

- 3 Paterson-Jones, J.C., Gilliland, M.G., and van Staden, J., *J. Plant Physiol.*, 136, 257 (1990).
- 4 Bikales, N.M., "Classification of Polymerization Reactions" in Encyclopedia of Polymer Science and Engineering, 2nd ed., Vol. 3, pp. 549 (1985)
- 5 Staudinger, H., and Fritschi, J., *Helv. Chim. Acta*, 5, 785 (1922)
- 6 Carothers, H.W., *J. Am. Chem. Soc.*, 51, 2548 (1929)
- 7 "Collected Papers of Wallace H. Carothers on Polymerization" edited by Mark, H., and Whitby, G.S., Interscience Publ., Inc., New York (1940)
- 8 Hunkeler, D., et al., *Adv. Pol. Sci.*, 112, 115 (1994)
- 9 Harkins, W.D., *J. Am. Chem. Soc.*, 69, 1428 (1947)
- 10 Kurja, J., Zirkzee, H.F., and Maxwell, I.A., "Unconventional Emulsion Polymerizations", in "Emulsion Polymers and Emulsion Polymerization", M.S. El-Aasser and P. Lovell (Eds.), Wiley, Chapter 23, 763 (1997)
- 11 Weyenberg, D.R., Findlay, D.E., Cekada, J., and Bey, A.E., *J. Pol. Sci., Part C*, 27, 27 (1969)
- 12 US 4,273,634 (1981), Dow Corning Corp., invs.: Saam, J.C., Wegener, R.L., *Chem Abstr.* 95, 82044r
- 13 Saam, J.C., and Huebner, D.J., *J. Pol. Sci., Polym Chem. Ed.*, 20(12), 3351 (1982)
- 14 Lu, S-Y, Quayle, P., Booth, C., Yeates, S.G., and Padget, J.C., *Polymer International*, 32, 1 (1993)
- 15 Maxwell, I.A., Morrison, B.R., Gilbert, R.G., and Napper, D.H., *Macromolecules*, 24, 1629 (1991)
- 16 Hansen, F.K., and Ugelstad, J., 'Particle Formation Mechanisms', in 'Emulsion Polymerization', Ed. I. Piirma, Academic Press, New York, (1982)
- 17 Gilbert, R.G., and Napper, D.H., *J. Macromol. Sci. - Rev. Macromol. Chem. Phys.*, C23, 127 (1983)
- 18 Blackley, D.C., 'Emulsion Polymerization', Applied Science Publishers LTD, London (1975)
- 19 Smith, W.V., and Ewart, R.H., *J. Chem. Phys.*, 16, 592 (1948)
- 20 Harkins, W.D., *J. Am. Chem. Soc.*, 69, 1428 (1947)
- 21 Goodwin, J.W., Hearn, J., Ho, C.C., and Ottewill, R.M., *Col. Polym. Sci.*, 252, 464 (1974)
- 22 Fitch, R.M., and Tsai, C.H., in 'Polymer Colloids', Ed. R.M. Fitch, Plenum, New York, (1971)
- 23 Ugelstad, J., and Hansen, F.K., *Rubber Chem. Technol.*, 49, 536 (1976)
- 24 McCarthy, S.J., Eibing, E.E., Wilson, I.R., Gilbert, R.G., Napper, D.H., and Sanger, D.F., *Macromolecules*, 19, 2440 (1986)
- 25 Maxwell, I.A., Verdurmen, E.M.F.J., and German, A.L., *Makromol. Chem.*, 193, 2677 (1992)
- 26 Van Doremale, G.H.J., "Model Prediction, Experimental Determination, and Control of Emulsion Copolymer Microstructure", PhD. Thesis, Eindhoven University of Technology, The Netherlands (1990)
- 27 J. Barton and I. Capek, *Radical Polymerization in Disperse Systems*, Ellis Horwood Limited, New York, 1994.
- 28 F. Candau, *Scientific Methods for the Study of Polymer Colloids and Their Applications*, F. Candau and R.H. Ottewill Ed., Kluwer Academic Publishers, Dordrecht, 1988.
- 29 Gilbert, R.G., *Emulsion Polymerization: A Mechanistic Approach* (1995)
- 30 Maxwell, I.A., Kurja, J., Van Doremale, G.H.J., German, A.L., and Morrison, B.R., *Makromol. Chem.*, 193, 2049 (1992)
- 31 Maxwell, I.A., Kurja, J., Van Doremale, G.H.J., and German, A.L., *Makromol. Chem.*, 193, 2065 (1992)
- 32 Maxwell, I.A., and Kurja, J., *Langmuir*, 11, 1987 (1995)
- 33 Kurja, J., Nolte, R.J.M., Maxwell, I.A., and German, A.L., *Polymer*, 34, 2045 (1993)

-
- 34 Kurja, J., Zirkzee, H.F., German, A.L., Nolte, R.J.M., and Maxwell, I.A., "Polymerization in Vesicles : Thermodynamics, Kinetics and Characterization", in : "The Polymeric Materials Encyclopedia : Synthesis, Properties and Applications", J.C. Salamone (Ed.), CRC Press, Inc., Vol. 11, 8550 (1996)
- 35 Kurja, J., Zirkzee, H.F., De Koning, G.J.M., Maxwell, I.A., A New Kinetic Model for the Accumulation of Poly-3-hydroxybutyrate in *Alcaligenes eutrophus*, in : " Biodegradable Plastics and Polymers ", Y. Doi and K. Fukuda (Eds.), Elsevier, Amsterdam, p. 379 (1994)
- 36 Kurja, J., Zirkzee, H.F., De Koning, G.J.M., and Maxwell, I.A., *Macromol. Theory and Sim.*, 4, 839 (1995)
- 37 Aerdts, A.M., Herk, van, A.M., Klumperman, B, Kurja, J., German, A.L., "Emulsion Polymerization" in: "Materials Science and Technology: A Comprehensive Treatment", R.W. Cahn and E.J. Kramer (Eds.), VCH Verlagsgesellschaft, Chapter 11, in press (1997)
- 38 Lemstra, P.J., Kurja, J., Meijer, H.E.H., "Processing of Polymers using Reactive Solvents" in: "Materials Science and Technology: A Comprehensive Treatment", R.W. Cahn and E.J. Kramer (Eds.), VCH Verlagsgesellschaft, Chapter 10, in press (1997)
- 39 Van Doremale, G.H.J., Kurja, J., Claessens, H.A., and German, A.L., *Chromatographia*, 31, 9/10 (1991)
- 40 Van Doremale, G.H.J., Schoonbrood, H., Kurja, J., and German, A.L., *J. Appl. Polym. Sci.*, 45, 957 (1992)
- 41 Van Doremale, G.H.J., Geerts, F., Schoonbrood, H., Kurja, J., and German, A.L., *Polymer*, 33, 1914 (1992)
- 42 Aerdts, A.M., Kreij de, J., Kurja, J., and German, A.L., *Polymer*, 35, 1636 (1994)

CHAPTER 2

Thermodynamics of Polymer Solutions

Synopsis: In this chapter, the thermodynamics of polymer solutions has been discussed. In doing so, a summary of the Flory-Huggins theory has been given and the solution behavior of amorphous and semi-crystalline polymers in solvents of different quality has been reviewed.

2.1 Introduction

In this chapter the solution behavior of polymers will be discussed. First, a short summary will be given of the Flory-Huggins lattice theory which is often used to describe polymer solutions. Second, the phase behavior of amorphous and semi-crystalline polymers in solution will be discussed. Finally, thermally and chemically induced phase separation are discussed.

2.2 Flory-Huggins Lattice Theory

The Flory-Huggins lattice theory is often used to describe the mixing of polymers with solvents^{1,2}. The Gibbs free energy of mixing a polymer and solvent (ΔG_{mix}) is given by:

$$\Delta G_{\text{mix}} = \Delta H_{\text{mix}} - T * \Delta S_{\text{mix}} \quad (2.1)$$

* In part reproduced from : Lemstra, P.J., Kurja, J., Meijer, H.E.H., "Processing of Polymers using Reactive Solvents" in : "Materials Science and Technology: A Comprehensive Treatment", R.W. Cahn and E.J. Kramer (Eds.), VCH Verlagsgesellschaft, Chapter 10, in press (1997)

Where T is the absolute temperature. ΔS_{mix} can be calculated using a lattice model, which takes into account the fact that the polymer molecules are much larger than the solvent molecules. Further, it is assumed that each space on the lattice is filled either by a solvent molecule or a segment of the polymer molecule. Moreover, the model of Flory and Huggins takes account for the fact that each side which is occupied by a segment of a polymer molecule must have two adjacent polymer sites so that there is a continuous path of polymer segments. The entropy of mixing is given by *equation 2.2*:

$$\Delta S_{\text{mix}} = -k [N_1 \ln \phi_1 + N_2 \ln \phi_2] \quad (2.2)$$

where N is the number of molecules, k is the Boltzmann constant, and ϕ denotes the volume fraction, respectively. The subscript 1 and 2 refer to solvent and polymer, respectively. The enthalpy of mixing, ΔH_{mix} , can also be taken into account using the Flory-Huggins theory. It is assumed that $\Delta H_{\text{mix}} \neq 0$, because the polymer-polymer and solvent-solvent interactions in the pure states are different from polymer-solvent interactions in solution. There are three kind of contacts in solution each with its own contact energy, i.e. the interaction between solvent-solvent (with interaction energy ω_{11}), polymer-polymer (with interaction energy ω_{22}), and polymer-solvent (with interaction energy ω_{12}). Since for every polymer-solvent interaction one solvent-solvent and one polymer-polymer contact have to be broken, the energy difference per polymer-solvent contact, $\Delta\omega$, between the mixed and unmixed states is given by *equation 2.3*.

$$\Delta\omega = \omega_{12} - \frac{1}{2} (\omega_{11} + \omega_{22}) \quad (2.3)$$

The number of lattice sites occupied by polymer is N_2 times the ratio of the size of the polymer chain to that of the solvent, i.e. V_2/V_1 . ΔH_{mix} is obtained by multiplying the energy of formation of a polymer-solvent contact, $\Delta\omega$, by the number of such contacts ³:

$$\Delta H_{\text{mix}} = \left(N_1 + \frac{N_2 * V_2}{V_1} \right) * z * \Delta\omega * \phi_1 * \phi_2 \quad (2.4)$$

here z is the lattice coordination number. Combining *equations 2.2 and 2.4*, the Gibbs free energy of mixing polymer with a solvent is obtained:

$$\Delta G_{\text{mix}} = kT \left(N_1 + \frac{N_2 * V_2}{V_1} \right) \left[\phi_1 \ln \phi_1 + \phi_2 \left(\frac{V_1}{V_2} \right) \ln \phi_2 + \chi_1 * \phi_1 * \phi_2 \right] \quad (2.5)$$

χ_1 is the polymer-solvent interaction parameter. The term in square brackets is identifiable with the free energy per lattice site, in which the entropic part decreases with V_2 while the enthalpic is virtually constant with molar mass. The free energy can be calculated on a volume basis by dividing both sides of *equation 2.5* by the total volume of the system, V . This results in *equation 2.6*:

$$\frac{\Delta G_{\text{mix}}}{V} = kT \left[\frac{\phi_1}{V_1} \ln \phi_1 + \frac{\phi_2}{V_2} \ln \phi_2 + \frac{\chi_1 * \phi_1 * \phi_2}{V_1} \right] \quad (2.6)$$

The Flory-Huggins interaction parameter is a function of temperature and composition, it has lost its simplistic classification of “parameter”. However, an estimation of the Flory-Huggins interaction parameter can be made utilizing the Hildebrand solubility parameter approach^{1,3}. In doing so, *equation 2.7* represents the Flory-Huggins interaction parameter between solvent and polymer, $\chi_{1,2}$:

$$\chi_1 = \left(\frac{V_1}{RT} \right) (\delta_{\text{solvent}} - \delta_{\text{polymer}})^2 \quad (2.7)$$

where δ_{solvent} and δ_{polymer} represent the Hildebrand solubility parameter for solvent and polymer, respectively. The molar volume of an interacting lattice segment is in this case equal to the molar volume of the solvent. The Flory-Huggins equation is widely used and has been largely successful in describing the behavior of polymer solutions. However, there are a number of important limitations of the Flory-Huggins equation that should be emphasized, of which the most important are:

1. The Flory-Huggins equation is only applicable to *concentrated* polymer solutions, thus having a uniform polymer segment density.
2. There is no volume change of mixing, although a negative volume change would be expected in the case of favorable interactions between polymer and solvent.
3. The arrangement of polymer-segments and solvent molecules on the lattice are pure statistical and have no energetically-preferred arrangements.

Although the Flory-Huggins approach is an important improvement upon ideal solution theory, it does not fit the behavior of *dilute* polymer solutions very well.

2.3 Thermodynamics of Polymer Solutions

2.3.1 Phase Separation Behavior of Polymer Solutions

The phase separation behavior of both amorphous and semi-crystalline polymer solutions can be described utilizing the Flory-Huggins theory. For a solution of an amorphous polymer in a solvent the Gibbs free energy of mixing polymer and solvent per mol of segments is given by *equation 2.8*, which is equivalent to *equation 2.6*.

$$\Delta G_{\text{mix}} = RT \left[\phi_1 \ln \phi_1 + \frac{\phi_2}{P_n} \ln \phi_2 + \chi_1 * \phi_1 * \phi_2 \right] \quad (2.8)$$

Utilizing this equation, the effect of the Flory-Huggins interaction parameter, temperature and degree of polymerization of the polymer on the phase behavior of the polymer solution can be investigated. If phase separation occurs, the Gibbs free energy change associated with the phase separation process should be negative. The curves in *figure 2.1* have two different forms: **1.** At χ_1 values below a certain critical value, the polymer and solvent are miscible over the entire composition range, i.e. the change in the Gibbs free energy is positive. **2.** At values of χ_1 above a certain critical value, the system can phase separate (either via a binodal or a spinodal phase separation process) depending on the overall composition, i.e. at a certain critical composition. It can be noticed that in these curves two minima are present which result from the contribution of the enthalpy of mixing, i.e. $\Delta H_{\text{mix}} \neq 0$, to the Gibbs free

energy of mixing (most notably for $\chi = 1.5$ in the case of $P_n = 5$, in *figure 2.1*). The binodal and spinodal points get closer together until at a critical temperature T_c they coincide at the critical composition ϕ_{2c} .

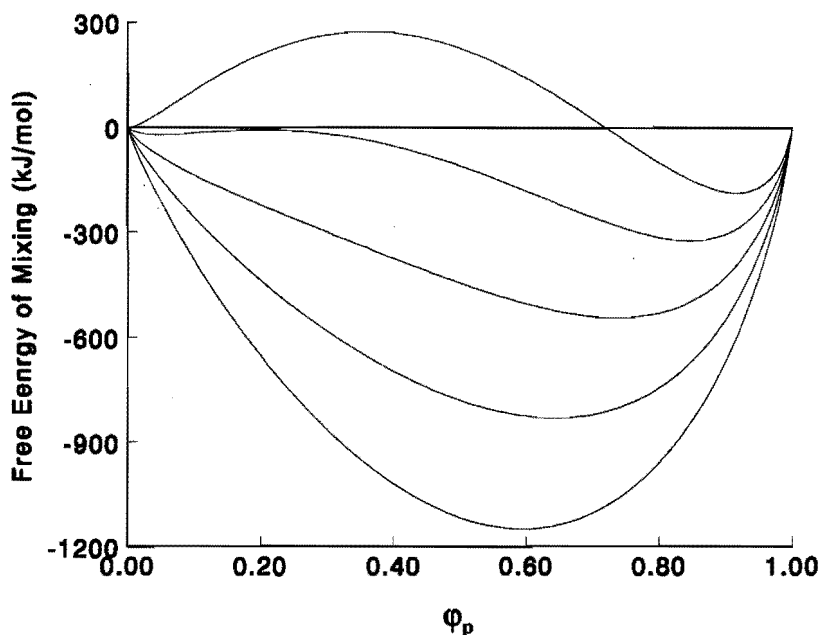


Figure 2.1 Free energy of mixing polymer and solvent as a function of the volume fraction of polymer (ϕ_p) at different values for χ , ranging from 0 (lower line) to 0.5, 1, 1.5, and 2 (upper line) at $P_n = 5$ and $T = 323$ K.

For polymer solutions where ΔH_{mix} is positive, T_c corresponds to the common maximum of the binodal and spinodal, the critical temperature is referred to as the *upper critical solution temperature* (UCST) above which polymer and solvent are completely miscible at all compositions. In the case where ΔH_{mix} is negative, the critical temperature corresponds to the common minimum of the binodal and spinodal, and is referred to as the *lower critical solution temperature* (LCST), below which polymer and solvent are completely miscible at all compositions. LCST solution behavior is often observed in systems where specific favorable polymer-solvent interactions (e.g. hydrogen bonding) are operative. From *equation 2.8*, the critical compositions (spinodal points: second derivative of *equation 2.8* with respect to ϕ_2 equals zero (*equation 2.9A*); critical composition (ϕ_{2c}): third derivative of

equation 2.8 with respect to ϕ_2 equals zero (equation 2.9B)) can be evaluated and the critical interaction parameter (substituting equation 2.9B in equation 2.9A, resulting in equation 2.9C) can be evaluated at which phase separation occurs.

$$\frac{1}{(1-\phi_2)} + \frac{1}{\bar{P}_n * \phi_2} - 2 * \chi = 0 \quad (2.9A)$$

$$\phi_{2c} = \frac{1}{(1+\sqrt{\bar{P}_n})} \quad (2.9B)$$

$$\chi_c = \frac{1}{2} \left[1 + \frac{2}{\sqrt{\bar{P}_n}} + \frac{1}{\bar{P}_n} \right] \quad (2.9C)$$

It is obvious from equation 2.9C, that for $\bar{P}_n \rightarrow \infty$, $\phi_{2c} \rightarrow 0$, and $\chi_c \rightarrow 0.5$. In the case of the example depicted in figure 2.1, $\bar{P}_n = 5$, from which it follows that $\phi_{2c} = 0.31$ and $\chi_c = 1.05$. For a mixture of two low molecular weight solvents the critical composition equals 0.5 and the critical interaction parameter equals 2, and the phase diagram is symmetrical.

2.3.2 Phase Behavior of Amorphous Polymers in Solution

In the case of an amorphous polymer the T_g will be lowered in the presence of a (good) solvent. The solvent acts as a plasticizer and the T_g decreases with increasing solvent content. Couchman ⁴ has developed a thermodynamic approach for predicting the glass transition temperature of polymer mixtures, but in actual practice the simpler Fox equation ⁵, (see equation 2.10) is often used to describe the T_g depression in the presence of a solvent. In equation 2.10, ϕ_2 represents the volume fraction of the polymer in the polymer-solvent mixture.

$$\frac{1}{T_g(\phi_2)} = \frac{(1-\phi_2)}{T_g^{\text{Solvent}}} + \frac{\phi_2}{T_g^{\text{Polymer}}} \quad (2.10)$$

Depending on the solvent quality, various situations can be encountered as shown schematically in Figure 2.2. In the case of a good solvent, the T_g will decrease with increasing solvent concentration and below ϕ_x a homogeneous solution will be obtained at room temperature,

T_R . Above ϕ_x , the solution will vitrify into a homogeneous glass upon cooling to room temperature. In the case of a poor solvent, the phase diagram can become more complex. The T_g curve often interferes with a liquid-liquid demixing curve as shown in *Figure 2.2*.

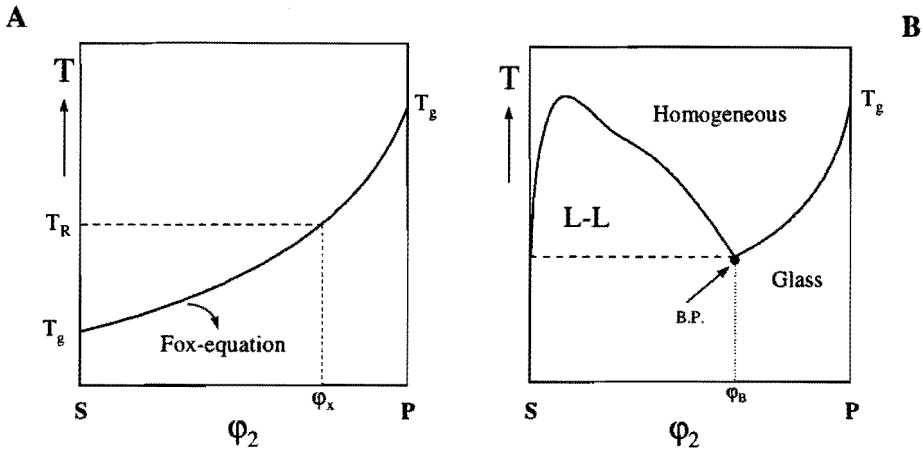


Figure 2.2 Phase diagrams of an amorphous polymer (P) and a solvent (S). A: represents a system with a polymer and a good solvent, and B: represents a system with a polymer and a poor solvent.

The intersection point where the T_g composition curve intersects with the L-L demixing or cloud point curve, is called the Berghmans point ⁶, B.P. in *Figure 2.2*. At a concentration ϕ_2 higher than ϕ_B , the homogeneous solution vitrifies upon cooling below the T_g -curve as discussed previously. At concentrations lower than ϕ_B , the homogeneous solution will become metastable upon cooling into the L-L demixing region. From a purely thermodynamic point of view, the most favorable and final equilibrium situation will be the separation into two coexistent macroscopic phases, respectively a dilute and concentrated polymer/solvent phase. This process, however, is rather slow in polymer systems. If the temperature, upon cooling, passes T_B (temperature corresponding to the Berghmans point) the metastable solution will vitrify if continuity of the glassy phases (domains) is present in the system, usually at higher polymer concentrations, or vitrified particles will separate from solution at lower concentrations. The formation of a vitrified gel or the precipitation of vitrified particles is, as mentioned above, dependent on the polymer concentration in solution. Although a detailed thermodynamic description is beyond the scope of the present Chapter, we will briefly address some details. In the case of thermally-induced phase separation, a

distinction must be made between binodal and spinodal decomposition. In practice, we are dealing with multi-component systems since polymers are usually polydisperse materials with a broad molar mass distribution. In these polydisperse systems, the critical point is not on the top of the cloud-point curve but shifted somewhat to the right and the cloud-point curve is usually indented ⁷.

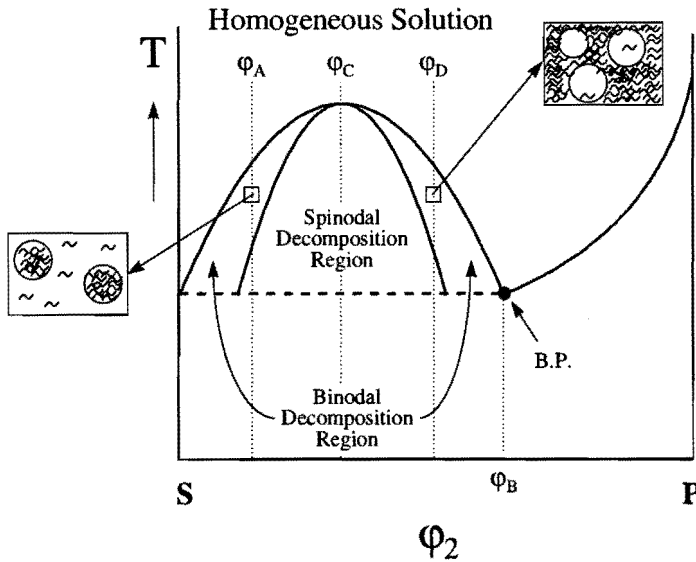


Figure 2.3 Illustration of the morphology development during different phase separation mechanisms.

In order to illustrate the morphology development and its dependence on the mechanism of phase separation, i.e. binodal vs. spinodal, it is shown in *Figure 2.3* that for the case of a binodal system (monodisperse polymer and solvent), the critical point is at the top of the cloud-point curve, where the binodal and spinodal curves meet. Upon cooling from the homogeneous solution, either spinodal (through the critical point) or binodal demixing occurs. In the case of binodal demixing, phase separation proceeds through nucleation and growth of the minor phase. Upon cooling, a solution with a polymer concentration ϕ_A into the binodal region will result in the precipitation of (spherical) particles. The overall polymer concentration is too low to provide material continuity. Upon cooling a solution with a polymer concentration ϕ_D , the concentrated polymer phase will form the continuous matrix which will then vitrify at the temperature corresponding to the Berghmans point, T_B . In the case of spinodal decomposition (ϕ_C), spontaneous phase separation

occurs via concentration fluctuations. The word spontaneous does not imply that phase separation via spinodal decomposition is an instantaneous process. According to the Cahn-Hilliard theory⁸, concentration fluctuations develop and the fluctuation length with the highest growth rate (the most dominant wavelength) results in the most frequently found domain size. At the start of the demixing process interconnectivity (co-continuous structure) prevails, but gradually the texture will coarsen, approaching an ultimate separation into two macroscopic phases⁹. However, this situation is not reached since the system vitrifies upon cooling below the temperature corresponding to the Berghmans point.

2.3.3 Phase Behavior of Semi-Crystalline Polymers in Solution

In the case of semi-crystalline polymers, we have to focus on the melting temperature T_m instead of T_g . The melting-point depression due to the presence of solvent(s) is usually described by the well-known melting-point depression relationship which reads for high molar mass polymers¹⁰:

$$\frac{1}{T_m} - \frac{1}{T_m^0} = \frac{R}{\Delta H_f} * \frac{V_u}{V_1} (\varphi_1 - \chi_1 \cdot \varphi_1^2) \quad (2.11)$$

In *equation 2.11*, T_m represents the melting temperature, or equivalently the dissolution temperature, of the crystals in the solvent, T_m^0 is the equilibrium melting point of the pure crystal. R is the gas constant, φ_1 the volume fraction of solvent, χ_1 the Flory-Huggins interaction parameter, V_u the molar volume of the monomer unit in the polymer chain, V_1 the molar volume of the solvent and ΔH_f is the heat of fusion per mole of repeating units. *Figure 2.4* shows the melting point depression of a polymer crystal in equilibrium with the surrounding solution for a poor and good solvent for the polymer. *Equation 2.11* is only applicable to concentrated and semi-dilute systems and, consequently, the very left part of the phase diagram is represented with a dotted line. The melting point of the polymer is lowered by the presence of a solvent, and vice versa, the melting point of the solvent is lowered by the presence of the polymer. Consequently, a eutectic point is to be expected. However, as shown by Smith¹¹, an eutectic point is not observed if the difference between the melting point of the polymer and the solvent exceeds 100 K. In *Figure 2.4*, the melting point of the solvent is not indicated in view of the fact that in the systems to be discussed below, the melting point of the solvent is far below room temperature and the difference between the melting point of the polymer and the solvent is larger than 100 K.

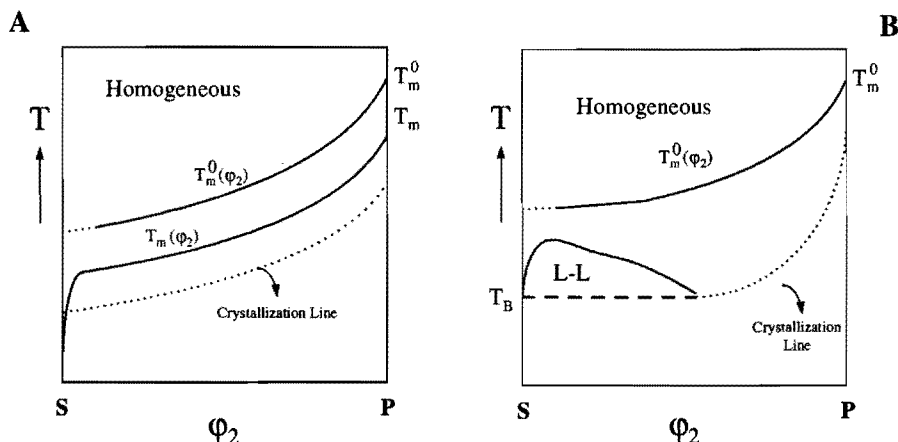


Figure 2.4 Phase diagram of a semi-crystalline polymer and a low molar mass solvent. A: represent a system in which the solvent is a good solvent for the polymer, and B: represent a system in which the solvent is a poor solvent for the polymer

It is important to note that the equilibrium curve $T_m^0(\phi_2)$ in Figure 2.4 is never obtained experimentally. Equilibrium refers to perfect, large crystals which implies for polymers the so-called extended-chain crystals. In practice, however, polymer crystals consist of folded-chain crystals and the fold length, or equivalently, the thickness of the folded-chain crystals is in the order of 10-30 nm. These imperfect and small crystals melt or dissolve at a lower temperature, as also indicated in Figure 2.3 by the curve $T_m(\phi_2)$, in literature the melting point is indicated with T_m , to distinguish from the equilibrium melting point T_m^0 . Melting (dissolution) of polymer crystals at low concentrations is currently a matter of debate again¹². When the polymer concentration approaches zero, the melting point T_m should approach the melting point of the solvent. However, it is measured in practice that the melting point T_m becomes independent of the polymer concentration when ϕ approaches zero. The reason is, probably, that upon melting (dissolution) of a polymer crystal, the polymer chain goes from a folded-chain conformation within the crystal into a random-coil chain in solution. The random-coil in solution has its own local concentration, i.e. upon dissolution the chain experiences a low but finite local concentration, in the order of a few percent, related to the coil dimensions. Consequently, the melting (dissolution) temperature remains constant at low ϕ , i.e. the local concentration of a random coil. Crystallization is a nucleation-controlled process and crystallization occurs only at a certain degree of super-cooling, indicated by the crystallization line in Figure 2.4. For crystallizable polymers in solution, crystallization can also interfere with liquid-liquid demixing. This is depicted schematically in Figure 2.4. The L-L

demixing curve can be located above or below the equilibrium melting curve- $T_m^0(\phi_2)$. This latter case is shown in *Figure 2.4*. Even if the L-L demixing curve is below the equilibrium melting curve $T_m^0(\phi_2)$, L-L demixing usually occurs before crystallization, since the crystallization process is a slower process and requires a certain degree of undercooling. Instead of vitrification, the concentrated domains will crystallize upon cooling below the temperature T_B .

2.4 Thermally vs. Chemically induced Phase Separation

As noted before, the morphology development during thermally-induced phase separation (TIPS) is very similar to the morphology development during chemically-induced phase separation (CIPS) (see *Figure 2.5*). The reason is that upon polymerizing a polymer/monomer system, the polymerized monomer will become immiscible with the dissolved polymer and phase separation should occur at some stage during the polymerization step. There is, however, one important difference between TIPS and CIPS. In the case of TIPS, a two phase system will be formed consisting of a dilute and concentrated polymer phase, either in the form of two separate macro-phases or in micro-domains if vitrification occurs, cooling below the Berghmans point. In the case of CIPS, liquid-liquid demixing will occur due to immiscibility of the originally dissolved polymer and the polymer which is formed during polymerization. Coarsening of the structure is strongly suppressed by the increase in viscosity, induced by phase separation and the polymerization reaction. Moreover, fixation of the structure via vitrification, crystallization, or crosslinking will prevent the formation of two macro-phases. Another important difference with TIPS is that phase separation is complete, not in the sense of the formation of two macro-phases but in terms of 100 % conversion of monomer into polymer. Considering the morphology development upon polymerization, an important distinction has to be made between *step-growth* and *chain-growth* polymerizations. In the case of *step-growth* polymerization, the molar mass of the polymerizing monomer changes continuously with conversion. At 50 % monomer conversion, the number average degree of polymerization is 2, i.e. the main product present are dimers. Suppose a polymer (P)/monomer (M) system with a UCST (Upper Critical Solution Temperature) phase behavior as depicted schematically in *Figure 2.5* is polymerized at temperature T_p . The phase behavior will change during the polymerization process due to the increasing molar mass of the polymerizing monomer, i.e. the formation of dimers, trimers etc. Concomitantly, the L-L demixing curve will shift upwards. Phase separation will occur when the L-L demixing curve shift to temperatures above T_p .

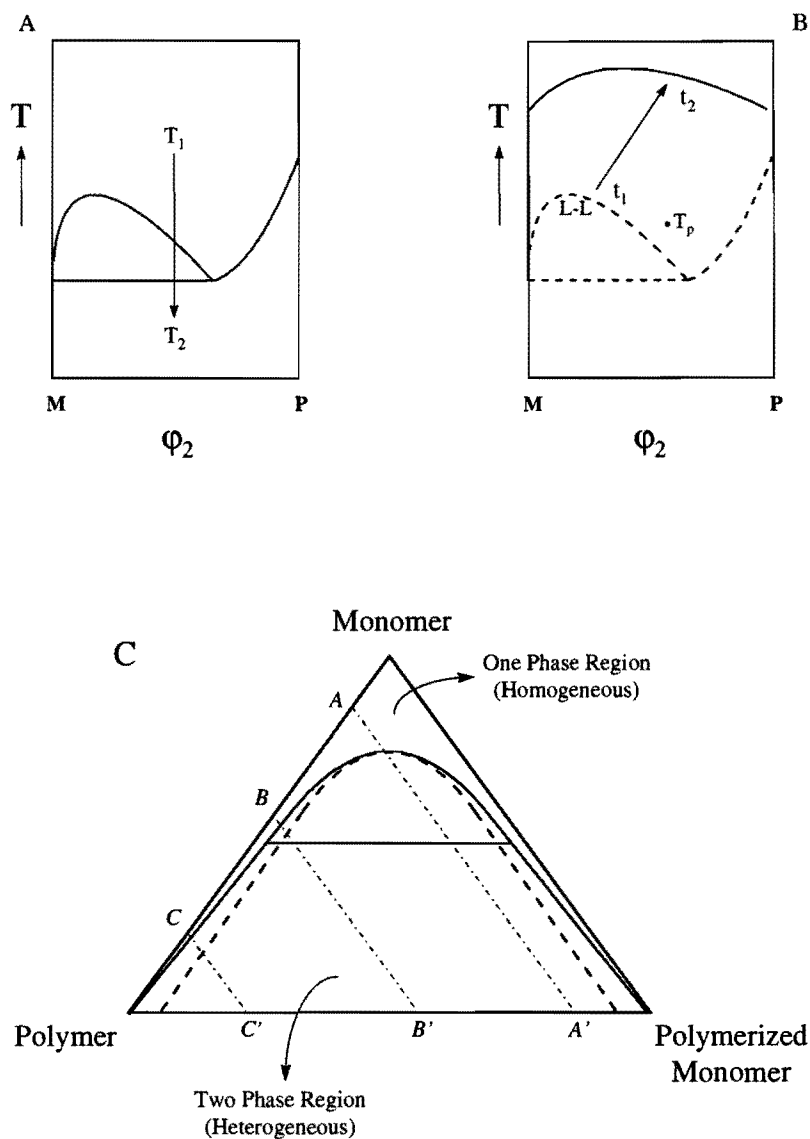


Figure 2.5 Schematic representation of the changes in miscibility of a polymer in a monomer which is a poor solvent in the case of: A: cooling from T_1 to T_2 (TIPS), B: isothermal polymerization of the monomer from t_1 to t_2 (CIPS), and C: a ternary phase diagram of the polymer-polymerizing monomer system. Lines A-A', B-B', and C-C' represent polymerization lines, and the horizontal line a tie line connecting the co-existing phases.

Let us consider now a polymer-monomer system of which the monomer is being polymerized via a *chain-growth* type of polymerization mechanism. Initially, the polymer-monomer

system can be considered as a binary system, with a phase diagram as presented by the dashed line in *Figure 2.5*. Upon polymerization of the monomer, a polymer is formed with a high molar mass, which will not change significantly during polymerization. Concomitantly, a ternary system is formed consisting of polymer-monomer-polymerized monomer (see *Figure 2.5*). Although the reacting system is not in equilibrium due to the continuous formation of polymer, and, moreover, that we are dealing with polydisperse polymers, the use of a simple (equilibrium) ternary phase diagram, as shown in *Figure 2.5*, might be useful for the discussion on the morphology development. The initial composition of the homogeneous solution is located on the polymer-monomer axis. Upon polymerization a reaction line is followed as indicated by the dashed lines in *Figure 2.5*. After low conversion of the monomer, the binodal line (solid line) is crossed and the system becomes metastable. This might lead to phase separation. However, when the spinodal line is crossed, the system will phase separate. The position of the binodal and spinodal curves depend on the molar mass of the polymer and polymerized monomers and the interaction parameters between the polymers and the monomer. Considering the case that the interaction between the solvent and both polymers are identical, the critical point is located at the maximum of the binodal and the corresponding tie lines are horizontal, when the polymers have equal molar masses. The examples given above show that for these reactive systems the morphology depends not only on thermodynamics, but more importantly on the relative rate of phase separation and rate of polymerization. In the case where the dissolved polymer is amorphous, vitrification can interfere with L-L demixing (see *Section 2.3.2*), while in the case of a semi-crystalline polymer crystallization can interfere with L-L demixing. The occurrence of vitrification/crystallization enables the fixation of the non-equilibrium morphologies. When all the monomer has been transformed into polymer the system can be considered as a binary system again, containing the polymer and the polymerized monomer.

2.5 References

- 1 Young, R.J., 'Introduction to Polymers', Chapman and Hall, London, (1987)
- 2 Fried, J.R., 'Polymer Science and Technology', Prentice Hall, New Jersey, (1995)
- 3 Olabisi, O., Robeson, L.M., and Shaw, M.T., "Polymer-Polymer Miscibility", Academic Press, New York (1979)
- 4 Couchman, P.R., *Macromolecules*, **16**, 1924 (1983)
- 5 Fox, T.G., *Bull. Am. Phys. Soc.*, **2**, 123 (1956)
- 6 Arnauts J., Berghmans H. and Koningsveld, R., *Makrom. Chemie*, **194**, 77 (1993)
- 7 Koningsveld R., Stockmayer W. and Nies E.L.F., *Thermodynamics of Polymer Systems*, Vol I, Phase Diagrams, Oxford University Press, UK, in press (1997)
- 8 Cahn, J.W., *J. Chem. Phys.*, **42**, 93 (1963)

- 9 Fujita, H., *Polymer Solutions in Studies in Polymer Science*, Vol. 9, Elsevier, Amsterdam (1990)
- 10 Flory, P.J., *Principles of Polymer Chemistry*, Cornell University Press, Ithaca (1956)
- 11 Smith, P., *Eutectic Solidification of Polymer Solutions*, PhD. Thesis, Groningen (1976)
- 12 Nies, E. and Berghmans, H., *private communications* (1996)

CHAPTER 3

Partial Swelling of Latex Particles

Synopsis: Two methods are described for experimentally determining the concentrations of monomer in both the aqueous phase and the latex particle phase during partial swelling, and therefore also during interval III of an emulsion polymerization. The ratio of the monomer concentrations in the aqueous phase, both below and at saturation, can be related to the volume fraction of polymer in the latex particles via the Vanzo equation. Comparison of theory and experiments for the methyl acrylate and poly(methyl acrylate-*co*-styrene) system shows that the monomer partitioning is insensitive to temperature, latex particle radius, polymer composition, polymer molecular weight and polymer cross-linking. Systems containing monomers either exhibiting a very high water solubilities, i.e. water miscible, or portraying strong interactions with the polymer in the latex particles, have shown to exhibit a deviate behavior from the earlier discussed ideal systems as could be anticipated. Thermodynamic treatment of these and previously published partitioning results shows, at higher volume fractions of polymer, that the combinatorial entropy of mixing polymer and monomer is the significant term determining the degree of partial swelling by monomer. Theoretical predictions of experimental results are quite insensitive to values of the Flory-Huggins interaction parameter and to the latex particle-water interfacial tension. A simple model is developed for the estimation of monomer partitioning which requires only the saturation monomer concentration in the latex particle and the aqueous phase.

In part reproduced from: Maxwell, I.A., Kurja, J., Van Doremale, G.H.J., German, A.L., and Morrison, B.R., *Makromol. Chem.*, **193**, 2049 (1992)

3.1 Introduction

The swelling of polymeric latex particles with solvents and monomers has long been a subject of interest. Early work by Morton *et al.*¹ dealt with *saturation* swelling of latex particles, primarily by monomers. However, the *partial* swelling of latex particles by monomers has received less attention. This fact is in contrast with the importance of the so-called interval III of emulsion polymerization, where there are no monomer droplets present, and all monomer is solubilized in both the particle and the aqueous phases. During interval III of an emulsion polymerization the partitioning of monomer between the particle and aqueous phases is a critical factor that may determine directly the rate of polymerization, the rate of free radical exit from latex particles, and the initiator efficiency: the last two also affecting the rate of polymerization. It should be noted that typical rates of emulsion polymerization are such that thermodynamic equilibrium of monomer between the phases during polymerization is usually achieved.

In this chapter early work on the partial swelling of latex particles by Vanzo *et al.*² and Gardon³ is reviewed. A series of experimental results on the partitioning of monomers between the aqueous and particle phases are discussed, in which the following variables are systematically changed: latex particle radius, temperature, monomer type, polymer cross-linking density, polymer molar mass, polymer type and polymer composition. The observed monomer partitioning results (and previously published results) are compared with predicted results. The purpose of this chapter is to determine which thermodynamic factors are important in determining the partitioning of monomer/solvent between the aqueous and latex particle phases when there is no separate monomer phase present.

3.2 Theory

Morton *et al.*¹ considered the saturation swelling of latex particles by solvent having limited solubility in the water phase. When the swollen latex particle is in equilibrium with the free monomer phase the partial molar Gibbs free energy of the monomer is given by:

$$\Delta G = \Delta G_{\text{mix}} + \Delta G_{\text{surf}} = 0 \quad (3.1)$$

where ΔG is the partial molar Gibbs free energy of monomer, ΔG_{mix} the contribution from the energy of mixing of monomer and polymer, and ΔG_{surf} the contribution from the particle-water interfacial energy. Morton *et al.*¹ expressed the free energy of mixing of monomer and polymer in terms of the classical Flory-Huggins theory⁴:

$$\frac{\Delta G_{\text{mix}}}{RT} = \ln(1 - v_p) + v_p \left[1 - \frac{1}{\bar{P}_n} \right] + \chi * v_p^2 \quad (3.2)$$

where v_p is the volume fraction of polymer in the latex particles, \bar{P}_n the number average degree of polymerization, R the gas constant, T the temperature and χ the Flory-Huggins interaction parameter. The interfacial free energy was given in terms of the Gibbs-Thomson equation^{1,5,6}:

$$\Delta G_{\text{surf}} = \frac{2 * V_m * \gamma * v_p^{1/3}}{R_0} \quad (3.3)$$

where V_m is the partial molar volume of the monomer, γ the particle-water interfacial tension and R_0 the unswollen radius of the latex particle. Combining equations 3.1, 3.2 and 3.3 gives the equation 3.4:

$$\ln(1 - v_p) + v_p \left[1 - \frac{1}{\bar{P}_n} \right] + \chi * v_p^2 = - \frac{2 * V_m * \gamma * v_p^{1/3}}{R_0 * RT} \quad (3.4)$$

In the case where there is no separate monomer phase present the partial molar free energy of the aqueous phase has to be taken into account. This can be done by a similar expression as derived for the polymer phase, i.e. via the Flory-Huggins theory. Equation 3.5 gives the partial molar free energy of monomer in the aqueous phase (ΔG_a):

$$\frac{\Delta G_a}{RT} = \ln \phi_{\text{mon}} + \phi_{\text{water}} * \left[1 - m_{\text{mon,water}} \right] + \chi_{\text{mon-water}} * \phi_{\text{water}}^2 \quad (3.5)$$

here ϕ_{mon} and ϕ_{water} represent the volume fraction of monomer and water in the aqueous phase, respectively. $\chi_{\text{mon-water}}$ is the Flory-Huggins interaction parameter between water and the monomer, while $m_{\text{mon,water}}$ is the ratio of the molar volumes of monomer and water.

Vanzo *et al.*² were the first to derive an analogue *equation 3.4* that dealt with partial swelling of latex particles utilizing a simpler equation for the partial molar free energy of the aqueous phase. In doing so, they assumed that the monomer containing aqueous phase could be considered as a dilute solution of monomer and water. Later, Gardon³ derived the same expression. If the latex particles are not saturated by monomer then there is no pure monomer phase present (i.e. no monomer droplets). The partial molar free energy of the monomer in the aqueous phase is then given by²:

$$\Delta G = RT * \ln a \quad (3.6)$$

where a is the activity of the monomer. Vanzo et al. pointed out that the monomer activity can be approximated by p/p_0 , i.e. the ratio of the vapor pressure of the monomer at a given volume fraction of polymer (p) to the vapor pressure at saturation swelling (p_0). Gardon³ showed that, since Henry's Law holds for latex free water, the ratio p/p_0 can be approximated by the ratio of the monomer concentration in the aqueous phase below and at saturation:

$$\frac{p}{p_0} = \frac{[M]_{\text{aq}}}{[M]_{\text{aq,sat}}} \quad (3.7)$$

where $[M]_{\text{aq}}$ is the concentration of monomer in the aqueous phase and $[M]_{\text{aq,sat}}$ is the saturation concentration of monomer in the aqueous phase. The final result for partial swelling of latex particles by monomer and solvents, hereafter called the Vanzo equation, is^{2,3}:

$$\begin{aligned} \ln(1 - v_p) + v_p * \left[1 - \frac{1}{P_n} \right] + \chi * v_p^2 + \frac{2 * V_m * \gamma * v_p^{1/3}}{R_0 * RT} \\ = \ln \left[\frac{[M]_{\text{aq}}}{[M]_{\text{aq,sat}}} \right] \end{aligned} \quad (3.8)$$

Gardon³ derived an expression for the saturation swelling of latex particles composed of densely cross-linked polymer. This theory was an adaptation of the Flory-Rehner theory⁴ which describes the free energy contribution of the elastic energy of the cross-linked polymer network as:

$$\Delta G_e = \frac{V_m * \rho_p}{M_c * RT} * \left[v_p^{1/3} - \frac{v_p}{2} \right] \quad (3.9)$$

where ρ_p is the density of the polymer, and M_c the mean molar mass between cross-links. Finally, for the case of partial swelling of latex particles composed of cross-linked polymer we find:

$$\begin{aligned} \ln(1 - v_p) + v_p * \left[1 - \frac{1}{P_n} \right] + \chi * v_p^2 + \frac{2 * V_m * \gamma * v_p^{1/3}}{R_0 * RT} \\ + \frac{V_m * \rho_p}{M_c * RT} * \left[v_p^{1/3} - \frac{v_p}{2} \right] = \ln \left[\frac{[M]_{aq}}{[M]_{aq,sat}} \right] \end{aligned} \quad (3.10)$$

3.3 Experimental

Reagents: Reagent grade styrene (S) and methyl acrylate (MA) (Merck) were distilled under reduced nitrogen pressure in order to remove inhibitor. The middle fraction was cut and stored at 4°C. Before use the cross-linking agent ethylene diacrylate (EDA) was washed with a NaOH solution in order to remove inhibitor. The water was distilled twice. Potassium persulfate (Merck p.a.), n-dodecyl mercaptan (Merck p.a.) and Aerosol MA80 (sodium dihexyl sulfosuccinate, Cyanamid) were used without further purification.

Seed latex preparation: The seed latices were prepared in a glass reactor under 1,7 atm. nitrogen pressure at 50°C for both MA and copolymerizations containing MA, and at 70°C for S. The recipes are given in *table 3.1*. After approximately 24 hours the temperature was increased to 90°C for 3 hours in order to dissociate the remainder of the initiator. After

polymerization initiator fragments, unreacted monomer and most of the free surfactant were removed by dialysis.

Particle sizing: Particle morphology and size were examined by means of transmission electron microscopy. UV hardening of the soft poly(methyl acrylate) particles prevented melting under the microscope beam. The sizes of the latex particles used in this study are listed in *Table 3.2*.

Table 3.1 Seed latex recipes (MA and copolymerizations at 50°C : S at 70°C)

	Non crosslinked (g)	Crosslinked (g)
MA and/or S	30 ^a	30 ^a
Water	750	750
Potassium persulfate	0.2	0.2
n-Dodecyl mercaptan	0.3 ^a	
EDA		1.5
Aerosol MA80	2.0	2.0

^a unless stated otherwise

Table 3.2 Seed latex composition, solid content (by weight-%), mean latex particle radius and number average degree of polymerization (\bar{P}_n).

Seed Latex	Copolymer Composition (mol/mol)	Solid Content (%)	Unswollen Radius (nm)	\bar{P}_n
SMA-1	S/MA, 25/75	16.9	61	15,000
SMA-2	S/MA, 25/75	17.3	96	87
SMA-3	S/MA, 50/50	14.7	63	
SMA-4	S/MA, 25/75	16.2	48	560
SMA-5	S/MA, 75/25	9.0	32	
SMA-6	S/MA, 25/75	16.5	32	
MA-1	MA	12.5	50	15,000
MA-2	MA + 5% EDA	4.3	65	∞
S-1	S	34.3	89	
VAc	VAc	-	~ 100	
MMA	MMA	2.6	65	
RGM-5	S	3.6	56	

Molar mass determination: The molar mass of the polymer in seed latices SMA1, SMA2 and SMA4 were controlled by added n-dodecyl mercaptan in the seed latex recipes (0, 9.6, and 0.3 g respectively). Molar mass determination of selected seed latices was carried out

by size exclusion chromatography utilizing polystyrene standards (this was found to be an adequate method for determining molar masses of polymers containing MA). The results are listed in *table 3.2*.

Monomer partitioning: centrifuge method: A latex of known solids content and polymer composition was mixed with known amounts of MA in the absence of initiator. The system was allowed to reach equilibrium by shaking (for at least 24 hours) while thermostated at the required temperature. The phases (swollen polymer particles and aqueous phases) were separated using an ultracentrifuge (Centrikon T-2060) thermostated to the same temperature as above. The concentration of MA in the aqueous phase was determined by gas liquid chromatography (GC) after adding a standard 2-propanol solution in water to a sample of the aqueous phase. The determination of monomer content in the polymer particles was then determined by mass balance. In order to calculate the monomer concentrations inside the particles, the volumes of all components within the particles (monomer and polymer) were assumed to be additive. Copolymer densities were calculated by the appropriate averaging of the densities of the homopolymers. All partitioning experiments were carried out at 45°C unless otherwise stated.

Monomer partitioning: dialysis method: The reliability of the above method was confirmed by means of additional monomer partitioning experiments using common dialysis tubing for the separation of the latex and aqueous phases. GC analysis of the aqueous phase was by the same method as described in the previous paragraph. The results obtained for the two methods were in excellent accord (data not shown). It was also noted that phase equilibrium was always achieved within 30 minutes.

Saturation concentration of MA in the aqueous phase: The effect of surfactant concentration upon the saturation concentration of MA in the aqueous phase at various temperatures was investigated. MA was mixed with water containing various concentrations of surfactant (sodium dodecylsulfate, SDS). GC analysis of the aqueous phase was carried out as above. It was found (*figure 3.1*) that the saturation concentration of MA in the aqueous phase was virtually independent of the SDS concentration. Further, the concentration of MA in water increased with decreasing temperature. This was subscribed to stronger hydrogen bonding at lower temperatures.

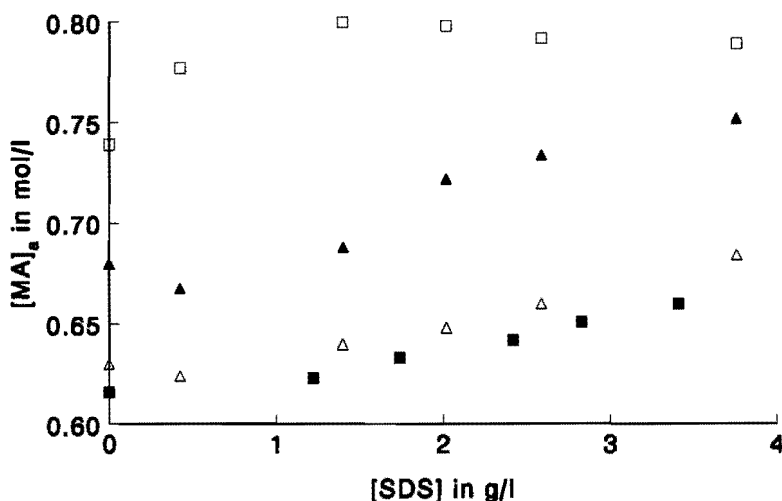


Figure 3.1 Experimentally determined saturation concentrations of MA in water as a function of SDS concentration at 4°C (open squares), 20°C (closed triangles), 35°C (open triangles) and 45°C (closed squares).

3.4 Results and Discussion

3.4.1 Influence of Temperature

Monomer partitioning experiments were undertaken with seed SMA-4 at two different temperatures (20°C and 45°C). The saturation concentrations of MA in the seed SMA-4 was found to be temperature independent at 20°C and 45°C (the error in these measurements was calculated to be approximately 3%). The saturated aqueous phase concentrations of MA were found to be 0.68 M (20°C) and 0.63 M (45°C). Within experimental error temperature had no effect upon the partitioning of MA (see *figure 3.2*). The temperature independence of the partitioning results can be partially understood since the partial molar free energy of the interface is unlikely to change considerably over the temperature range studied. However, it is not known how the Flory-Huggins interaction parameter would change with temperature for this monomer-polymer system, since χ , as defined, contains both temperature dependent enthalpic terms and temperature independent entropic terms. Despite this, the temperature independence of the partitioning results is expected since the major contribution to the partial

free energy of monomer is the combinatorial entropy term (denoted as the 'configurational entropy' by Flory⁴) of the free energy of mixing of monomer and polymer.

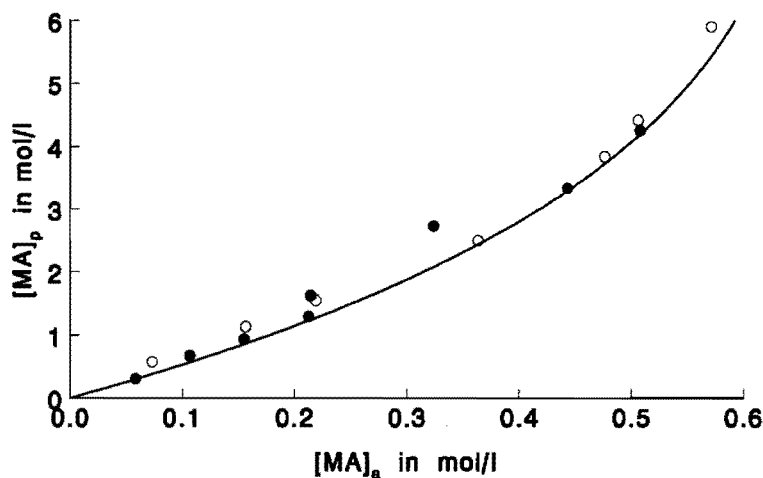


Figure 3.2 Comparison of the experimentally measured monomer partitioning of MA for seed latex SMA4 at 20°C (closed circles) and 45°C (open circles).

Accordingly, the Vanzo equation with a single value of the interaction parameter and of the interfacial tension provide excellent predictions of the results at 20°C and 45°C.

3.4.2 Influence of the Radius of the Latex Particles

Experiments were performed to determine the MA partitioning between the latex particle and aqueous phases for latex particles differing only by particle size. The three seed latices used (SMA-1, SMA-2, SMA-6) all have similar copolymer composition, polymer solids and surfactant type, although they differed in nominal polymeric molar mass (it will be shown in section 3.4.3 that this last point does not change the conclusions of this section). Further, each of the seeds was found to have less than 1 g/l free surfactant in the aqueous phase. It has been found that latices of differing sizes with similar polymer composition, surfactant, and surfactant coverages have similar interfacial tensions at a particular fraction polymer⁷. Hence, in the experiments described in this section it was thought that the interfacial tension at a particular fraction of polymer for all three latices would be approximately the same. The partitioning results for MA with the three different particle sizes are displayed in figure 3.3. The most significant result of these experiments is the small effect of the differing particle

sizes. It is apparent that the interfacial free energy has little effect upon the partitioning of monomer.

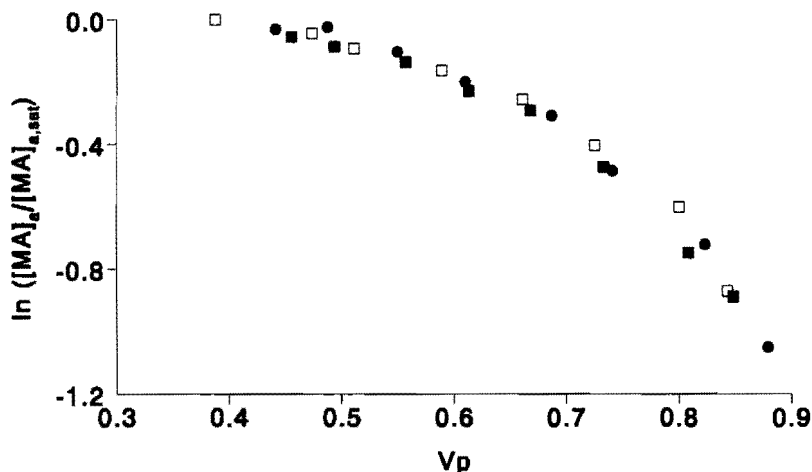


Figure 3.3 Comparison of the experimentally measured monomer partitioning of MA at 45°C for three seed latices differing only by their mean unswollen particle radii, $R_0 = 32$ nm (open squares), 61 nm (closed circles), and 96 nm (closed squares).

To emphasize this point, in *figure 3.4* the predicted contribution of all three terms in *equation 3.8* (the Vanzo equation) are displayed individually for seed SMA-6 ($R_0 = 32$ nm): these terms are the combinatorial entropy of mixing of polymer and solvent term ($\ln(1 - v_p) + v_p$, derived by considering the entropy of mixing of an assembly of random-flight chain molecules with solvent), the 'residual' free energy term ($\chi * v_p^2$, containing both enthalpic and entropic terms) and the interfacial free energy term ($\frac{2 * V_m * \gamma * v_p^{1/3}}{R_0}$)⁴. It is possible that both the interaction parameter and the interfacial tension change with volume fraction polymer. However, an estimate of the interaction parameter can be made from the high volume fraction polymer data, where the contribution to the degree of swelling of the interfacial free energy is least (this point is realized by the converging curves in *figure 3.4* at high volume fraction polymers). Assuming, at these high volume fractions of polymer, that $\gamma = 0$ mN/m for all three latices we find from fitting *equation 3.8* to the data that $\chi = 0.2$. Further, the *saturation* swelling of the latex particles is limited by the interfacial tension, and at these conditions the Morton equation (a limit of the Vanzo equation) is most sensitive to the value of the interfacial

tension. Assuming that the above calculated value of the interaction parameter is valid at lower volume fraction polymers, from the saturation swelling of seed SMA-6 we find from *equation 3.8*, $\gamma = 45 \text{ mN/m}$. Inserting these values for the interaction parameter and the interfacial tension into the Vanzo equation we find excellent agreement of theory and experiment (*figure 3.4*).

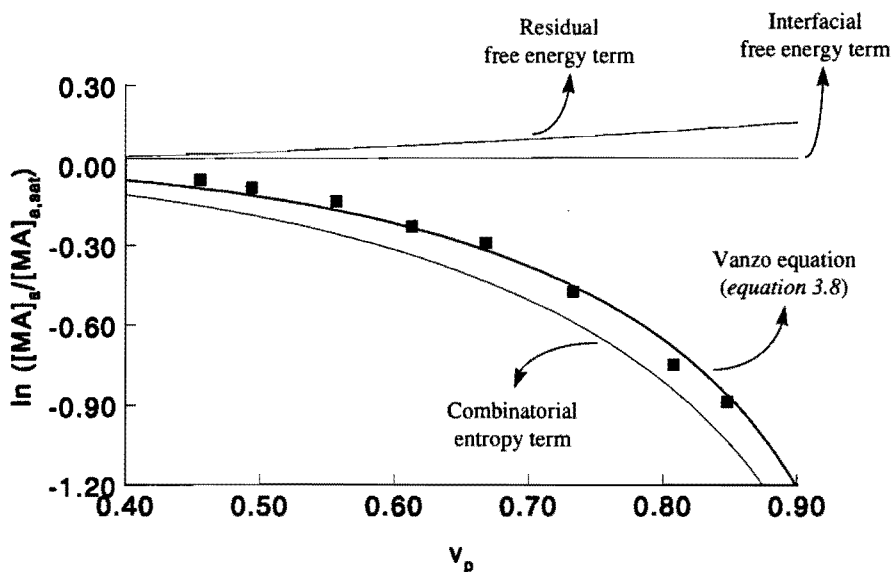


Figure 3.4 Comparison of theoretical predictions and experimental measurements (squares) of MA partitioning at 45°C for seed latex SMA-2 ($R_0 = 96 \text{ nm}$). Theoretical predictions: combinatorial entropy term given by $\ln(1 - v_p) + v_p$; residual free energy term given by $\chi * v_p^2$, with $\chi = 0.2$; interfacial free energy term given by $\frac{2 * V_m * \gamma * v_p^{1/3}}{R_0}$, with $\gamma = 45 \text{ mN/m}$; and Vanzo equation (equation 3.8) with $\chi = 0.2$ and $\gamma = 45 \text{ mN/m}$.

From this series of experiments we can state that the major contribution to the limit of partial swelling of latex particles by monomer is the partial free energy associated with the combinatorial entropy of mixing of monomer and polymer. The residual free energy of mixing (the term including the interaction parameter) and the partial molar free interfacial energy do not make a significant contribution at higher volume fractions of polymer in the latex particles. Of course, as saturation swelling is approached the contributions of both the latex particle interfacial free energy and the residual free energy become more important.

3.4.3 Influence of the Molar Mass of the Polymer

Three seed latices were prepared with significantly different average degrees of polymerization, $\bar{P}_n = 87$ (SMA-2), $\bar{P}_n = 560$ (SMA-4), and $\bar{P}_n = 15,000$ (SMA-1). The partitioning results for MA between the polymer and aqueous phases for these three latices are displayed in figure 3.5.

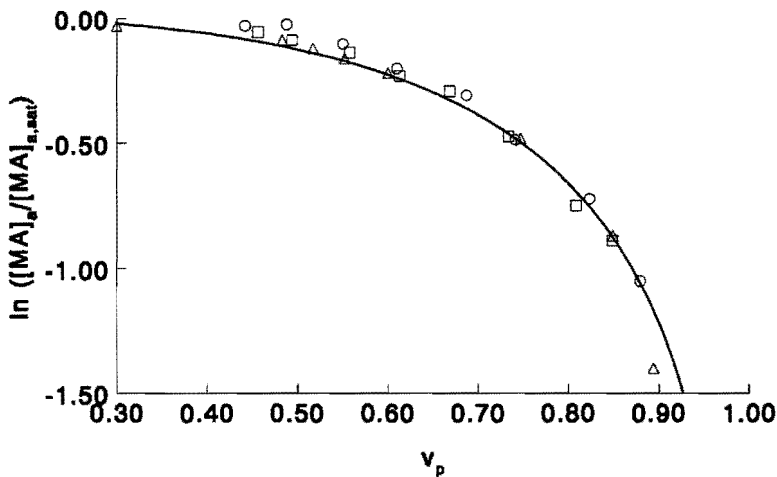


Figure 3.5 Comparison of the experimentally measured partitioning of MA at 45°C for three latices differing by their number average degree of polymerization: $\bar{P}_n = 87$ (SMA-2) (squares), 560 (SMA-4) (triangles), and 15,000 (SMA-1) (circles). Solid line represents the theoretical line constructed utilizing the Vanzo equation (equation 3.8) with $\bar{P}_n = 87$, $R_0 = 96$ nm, $\chi = 0.2$ and $\gamma = 45$ mN/m.

It is apparent that the partitioning of MA is not affected by the differing number average degree of polymerization. The reciprocal of the average degree of polymerization of the lowest molar mass polymer utilized, $\bar{P}_n = 87$, is considerably smaller than unity, and therefore has negligible effect upon the combinatorial entropy of mixing (i.e. $v_p * \left[1 - \frac{1}{\bar{P}_n} \right] \approx v_p$). These results are in accord with what would be expected from theoretical considerations (figure 3.4), since we have already found that the combinatorial entropy term dominates the partitioning, and that the combinatorial entropy free energy term

in the Vanzo equation does not predict change in the partitioning of MA over the range of molar mass of polymer utilized.

3.4.4 Influence of the Cross-link Density

The partitioning of MA between the particle and aqueous phases for a latex made with 5% EDA ($M_c \approx 1000$ g/mol) is compared with the MA partitioning in an uncross-linked latex (figure 3.6).

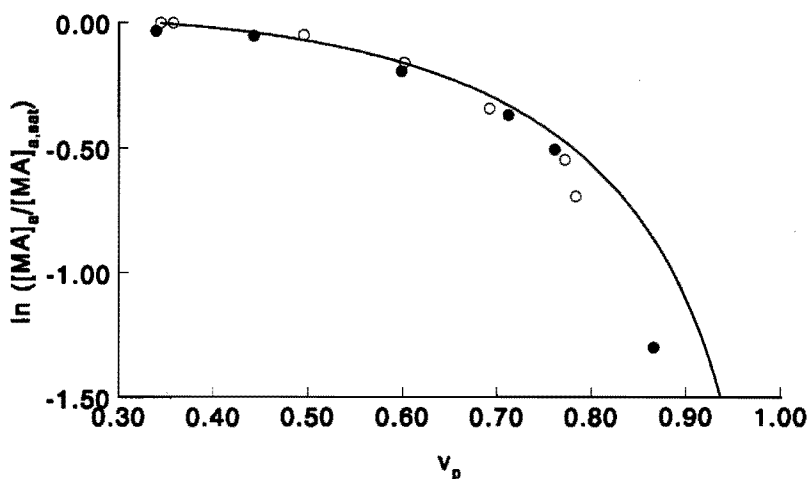


Figure 3.6 Comparison of the experimentally measured partitioning of MA at 45°C for two latices differing by their degree of cross-linking: uncross-linked (MA-1)(open circles) and 5% cross-linking agent (MA-2)(closed circles). Theoretical line: equation 3.10 with $M_c \approx 1000$ g/mol, $R_0 = 50$ nm, $\chi = 0.2$ and $\gamma = 45$ mN/m.

Again, there is no difference in the partitioning between these two polymer latices. This is simply because the free energy due to the combinatorial entropy of mixing of monomer and polymer dominates the thermodynamics of monomer partitioning. It was expected from numerical calculations utilizing equation 3.10 that the measured cross-linking density would have no effect upon the monomer partitioning (figure 3.6).

3.4.5 Influence of Copolymer Composition

In the previous section it was shown that temperature has little effect on monomer partitioning below saturation swelling. In this section the effect of the residual free energy of

mixing on the partitioning of MA is examined by swelling particles of different copolymer composition. It is thought that the interaction parameter for the MA-polymer systems will vary considerably for polystyrene and poly(methyl acrylate); and also for different compositions of copolymers containing these two polymers. The results of these experiments are displayed in *figure 3.7* together with the predictions of the Vanzo equation with values of the interaction parameter and interfacial tension fitted in *section 3.4.2*.

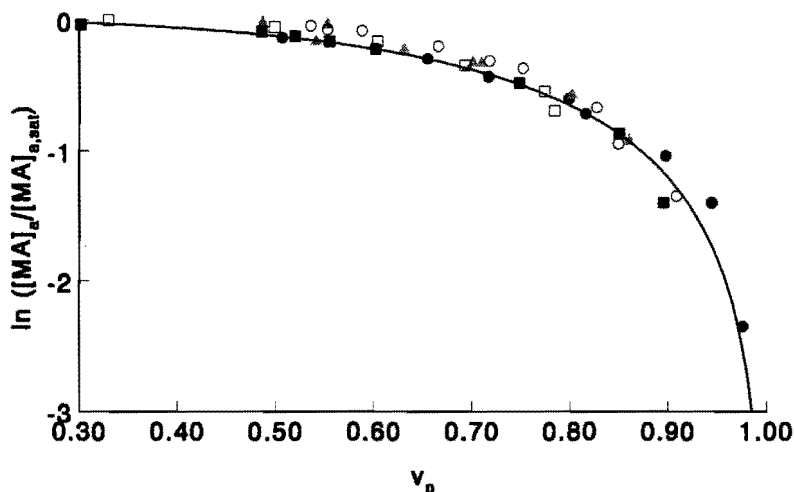


Figure 3.7 Comparison of the experimentally measured monomer partitioning of MA at 45°C for five seed latices differing by their polymer composition: S-1 (S:MA; 100:0)(open circles), SMA-5 (75:25)(closed circles), SMA-3 (50:50)(closed triangles), SMA-1 (25:75)(closed squares), MA-1 (0:100)(open squares). Theoretical line: Vanzo equation (equation 3.8) with $R_0 = 96$ nm, $\chi = 0.2$ and $\gamma = 45$ mN/m.

It is obvious that the polymer composition has little effect upon the partitioning of MA in these seed latices. Although we might expect the value of the interaction parameter to change in value for MA-polymer systems with differing polymer composition, the main contribution to the partitioning appears to be the combinatorial entropy of mixing of monomer and polymer, and hence we see little variation in the partial swelling of different seed latices with the one monomer.

3.4.6 Influence of Water Solubility of Monomer/Solvent

During conventional emulsion polymerizations numerous monomers are used to tailor the properties of the polymers produced. One of the most striking difference between these monomers is their difference in water solubility, ranging from e.g. a rather hydrophobic monomer as styrene (3 mM) to 2-hydroxyethylmethacrylate (HEMA) which is completely water miscible. Water miscible monomers often exhibit interesting functionalities, such as carboxylic and hydroxyl groups, which makes them interesting co-monomers during an emulsion polymerization thus introducing reactive groups into the polymer synthesized. Currently, there is quite some debate whether water miscible monomers are solely polymerized in the aqueous or also involved in the polymerization process inside the latex particles during an emulsion polymerization. Only little is known about the partitioning behavior of water miscible monomers during an emulsion polymerization.

Schoonbrood ⁸ investigated the partitioning of HEMA between water, the monomer droplet phase and polymer latex particles. Despite the experimental difficulties separating the different phases, it was observed that the concentration of MA in the water phase below saturation was independent of the amount of HEMA in the water phase which was comparable with the case where no latex particles were present. Popli *et al.* ^{9,10} studied the partitioning of several solvents, exhibiting different water solubilities, between the aqueous phase and latex particles, i.e. a polystyrene and a acrylate terpolymer (butyl methacrylate/butyl acrylate/methacrylic acid) latex. They measured that solvents with low water solubility preferably reside in the hydrophobic latex particles. With increasing water solubility the volume fraction solvent in the polymer phase decreased. The solubility of ethanol in the acrylate terpolymer latex was rather low as one would expect since ethanol is a non-solvent for the polymer in the latex particles. The volume fraction of ethanol in the acrylate terpolymer latex was approximately 0.05 while the volume fraction in the aqueous phase was 0.30. On the other hand, the volume fraction of ethanol in the polystyrene latex particles increased significantly when more ethanol was present in the aqueous phase despite the fact that ethanol is a non-solvent for polystyrene.

Two different situations can be encountered when latex particles are swollen by a water miscible monomer/solvent. Firstly, the water miscible monomer/solvent is a *poor* solvent for the polymer in the latex particles leading to phase separation and probably a low

solvent/monomer uptake by these particles if micro phase separation within the latex particles is ignored. Secondly, the water miscible monomer/solvent is a *good* solvent for the polymer in the latex particles. Concomitantly, the latex can lose its colloidal stability and a homogeneous solution is obtained, *viz.* adding a polystyrene latex to tetrahydrofuran yields ultimately a homogeneous solution. The solvent quality of the water miscible monomer/solvent can be expressed in the Flory-Huggins interaction parameter.

In the case of water miscible monomer/solvent the terms partial and saturation swelling of latex particles do not hold anymore since the monomer/solvent used to swell the latex particles is completely water miscible. The partitioning behavior of a water miscible monomer/solvent between the aqueous phase and the latex particles can not be predicted by utilizing *equation 3.6* for the free energy of the aqueous phase since the monomer/solvent is not partially but completely water miscible, in which case Henry's law does not hold anymore. Therefore, *equation 3.5* should be used to calculate the free energy of the aqueous phase. The partitioning of a water miscible monomer/solvent between the aqueous phase and the latex particles can be calculated using *equation 3.11*:

$$\begin{aligned} \ln(1-v_p) + v_p * \left[1 - \frac{1}{P_n} \right] + \chi * v_p^2 + \frac{2 * V_m * \gamma * v_p^{1/3}}{R_0 * RT} \\ = \ln \phi_{\text{ethanol}} + \phi_{\text{water}} * [1 - m_{\text{ethanol, water}}] + \chi_{\text{ethanol, water}} * \phi_{\text{water}}^2 \end{aligned} \quad (3.11)$$

here ϕ_{ethanol} and ϕ_{water} represent the volume fraction of ethanol and water in the aqueous phase, respectively. $\chi_{\text{ethanol-water}}$ is the Flory-Huggins interaction parameter between water and ethanol, while $m_{\text{ethanol, water}}$ is the ratio of the molar volumes of ethanol and water. *Figure 3.8* shows the partitioning of a water miscible monomer/solvent between the aqueous phase and latex particles for different values of the Flory-Huggins parameter expressing the solvent quality of water miscible monomer/solvent for the polymer present in the latex particles. *Table 3.3* shows the different input parameters used to for the calculations depicted in *Figure 3.8*.

Table 3.3 Input parameters for equation 3.11 which are shown in Figure 3.8

Input Parameter	Value
γ	45 mN/m
R_o	100 nm
V_m (ethanol)	58.4 ml/mol
\bar{P}_n	10,000
$\chi_{\text{ethanol-water}}$	3 ^a
$m_{\text{ethanol,water}}$	3.24

^a from solubility parameters, $\delta_{\text{ethanol}} = 26.5 \text{ MPa}^{1/2}$ and $\delta_{\text{water}} = 47.8 \text{ MPa}^{1/2}$, and $\chi = (V_m/R.T) * (\delta_{\text{ethanol}} - \delta_{\text{water}})^2$

As can be seen from Figure 3.8, increasing the Flory-Huggins interaction parameter results in a lower volume fraction of ethanol in the latex particles. This can be easily understood, since ethanol becomes a poorer solvent at higher values of χ for the polymer in the latex particles and, therefore, will reside preferentially in the aqueous phase.

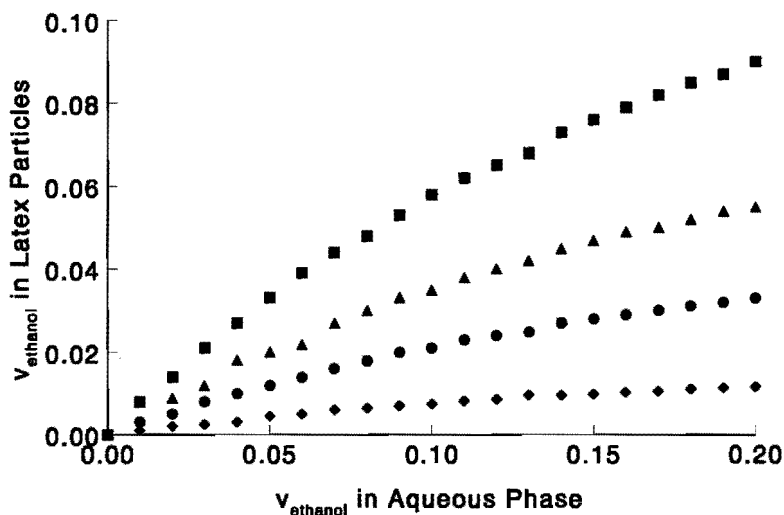


Figure 3.8 The volume fraction of ethanol in the aqueous phase as a function of the volume fraction of ethanol in the latex particles, indicating the influence of the solvent quality of ethanol for different polymer latex particles. The different Flory-Huggins parameters indicate the solvent quality of ethanol for the polymer in the latex particles. Squares: $\chi = 0$, triangles: $\chi = 0.5$, circles: $\chi = 1$, and diamonds: $\chi = 2$.

3.4.7 Influence of Specific Interactions between Solvent and Polymer

In the previous section monomers/solvents have been considered which are water miscible, therefore, are often poor solvents for the polymer in the latex particles. Concomitantly, the latex particles will only contain minor amounts of water miscible monomer/solvent, even at high volume fractions of the miscible component in the aqueous phase. In this section, monomers/solvents which can have strong interactions with the polymer in the latex particle but are only sparsely water soluble. Bindschaedler *et al.*¹¹¹² reported on the swelling of cellulose acetate (CA) latex particles with different organic solvent which are capable of forming hydrogen bonds with the polymer in the latex particles. *Figure 3.9* shows the partitioning behavior of different organic solvent between CA latex particles and the aqueous phase.

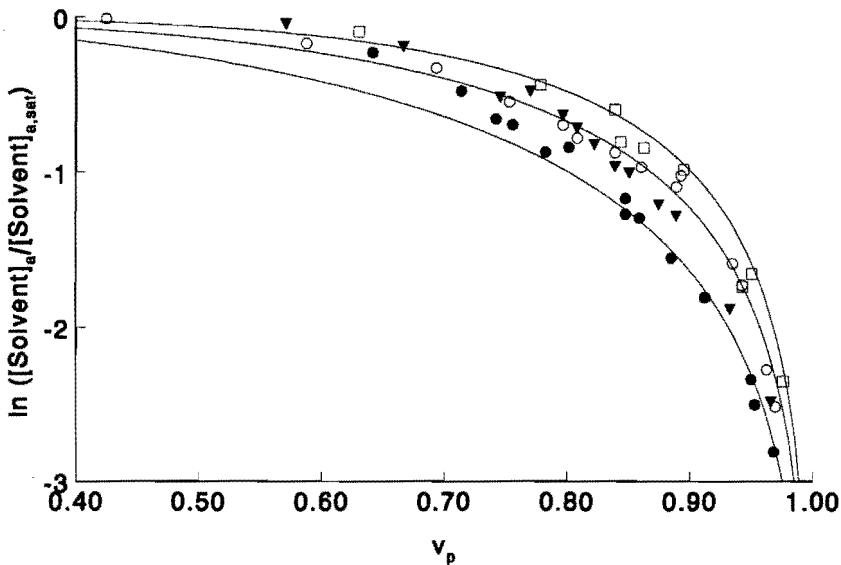


Figure 3.9 Swelling behavior of a cellulose acetate latex with different solvent which are capable of forming hydrogen bonds with the polymer in the latex particles but are sparsely water soluble. The different solvents are aniline (closed circles), furfural (closed triangles), nitromethane (open squares), and cyclohexanone (open circles). Lower solid line: Vanzo equation (equation 3.8) with $R_0 = 350 \text{ nm}$, $\chi = -0.2$ and $\gamma = 45 \text{ mN/m}$, middle solid line: Vanzo equation (equation 3.8) with $R_0 = 350 \text{ nm}$, $\chi = 0.2$ and $\gamma = 45 \text{ mN/m}$, and the upper solid line: Vanzo equation (equation 3.8) with $R_0 = 350 \text{ nm}$, $\chi = 0.5$ and $\gamma = 45 \text{ mN/m}$. Experimental data taken from Bindschaedler *et al.*¹².

From *Figure 3.9* it can be clearly seen that the partition behavior of nitromethane and cyclohexanone is similar as non interacting solvents/monomers partition between the aqueous phase and the latex particles (see previous sections) and can be easily described with the Vanzo equation. In the case of aniline and furfural, however, the partition behavior is quite different from conventional solvents/monomers and can not be described with the Vanzo equation. Here, the interaction between the solvent and the polymer is strong (hydrogen bonding), while the Vanzo equation only accounts for weak interactions between the monomer and polymer. Specific interactions between monomer/solvent and polymer can be dealt with in several different ways. Weak interactions are normally accounted for by the enthalpic term ($\chi^*v_p^2$) in the Flory-Huggins equation for mixing (*equation 3.2*). The more specific interactions, such as hydrogen bonding, can be accounted for by a separate term in *equation 3.2*, also referred to as the ΔG_H term. This ΔG_H term accounts for the free energy change that is a result of specific interactions^{4,13} and is implemented in *equation 3.2*. The resulting equation is shown below:

$$\frac{\Delta G_{mix}}{RT} = \ln(1-v_p) + v_p * \left[1 - \frac{1}{P_n} \right] + \chi^* v_p^2 + \frac{\Delta G_H}{RT} \quad (3.12)$$

It appears that the ΔG_H term is simply added to *equation 3.2* but in fact it stems from the formal application of a Flory type lattice model to a system in which specific interactions are operative. The parameters in the ΔG_H term can be measured spectroscopically¹³, and thus the partitioning of monomer/solvent between the aqueous phase and the latex particles can be predicted. It is outside the scope of this thesis to further evaluate the applicability of *equation 3.12* to the partitioning of monomers/solvent between the aqueous phase and the latex particles

Another approach to predict and describe the partitioning behavior in systems where there are strong interactions between the monomer/solvent and polymer in the latex particles is the use of *negative* Flory-Huggins interaction parameters between monomer/solvent and polymer. The lower line in *Figure 3.9* represents the Vanzo equation in which the χ -parameter was kept at -0.3. At high volume fractions of polymer in the latex particles, the negative χ -parameter can predict the partitioning reasonably well, but at lower volume fractions of

polymer large deviations between the experimental data and model prediction is observed. This can be attributed to the fact that at high volume fractions of polymer in the latex particles the inter-association of aniline and CA is predominant while at lower volume fractions of polymer in the latex particles self-association of aniline becomes more important (favorable) which leads to lower amounts of aniline in the latex particles than predicted by the Vanzo equation. In the case of furfural a similar explanation can be given as for aniline.

3.5 Estimation of Monomer Partitioning

The partitioning of monomer/solvent between the aqueous phase and the latex particle phase can be predicted/described from the complete Vanzo equation (*equation 3.8*). However, this requires that both the Flory-Huggins interaction parameter (c) and the interfacial tension (g) are known. A further complication already mentioned is that both these parameters may be volume fraction polymer dependent. Also, values of these parameters are difficult to determine by independent experiments. With these complications in mind there are at least two possible approaches for the estimation of monomer/solvent partitioning in latex systems: First, an estimate of the interaction parameter can be made from partitioning results at high volume fractions of polymer in the latex particles, since the contribution of the interfacial tension to the Vanzo equation is least at high fraction polymers. Then, from saturation swelling results a value of the interfacial tension which can be estimated by fitting of the Morton equation. For the MA-poly(methyl acrylate-co-styrene) systems discussed in the previous sections this technique provides excellent agreement between prediction and experiment (*Figures 3.4 - 3.7 and 3.9*). However, it requires that partitioning results be determined experimentally. Another, more empirical approach, is to estimate the value of the sum of the residual free energy and the particle-water interfacial free energy terms in the Vanzo equation from the saturation swelling volume fraction of polymer ($v_{p,sat}$). In doing so, a correction term can be calculated utilizing the Morton equation (*equation 3.4*), as is shown by *equation 3.13*:

$$\text{Corr.} = - [\ln(1 - v_{p,sat}) + v_{p,sat}] \quad (3.13)$$

This correction can be implemented in the Vanzo equation (*equation 3.8*):

$$\ln(1 - v_p) + v_p + \text{Corr.} = \ln \left[\frac{[M]_{\text{aq}}}{[M]_{\text{aq, sat}}} \right] \tag{3.14}$$

Note that, for simplicity, the contribution of the number average number degree of polymerization upon the partial molar free energy of mixing of monomer and polymer in equation 3.13 and 3.14 has been neglected (i.e. $\bar{P}_n \gg 1$). The approach used to derive equation 3.14 incorrectly assumes that the both the interfacial free energy and the residual free energy term are independent of the volume fraction of polymer. However, since the absolute values of these terms are small compared to the combinatorial entropy term, this approach, as a first estimate, gives quite good results for the MA-poly(methyl acrylate-co-styrene) system (see Figure 3.10).

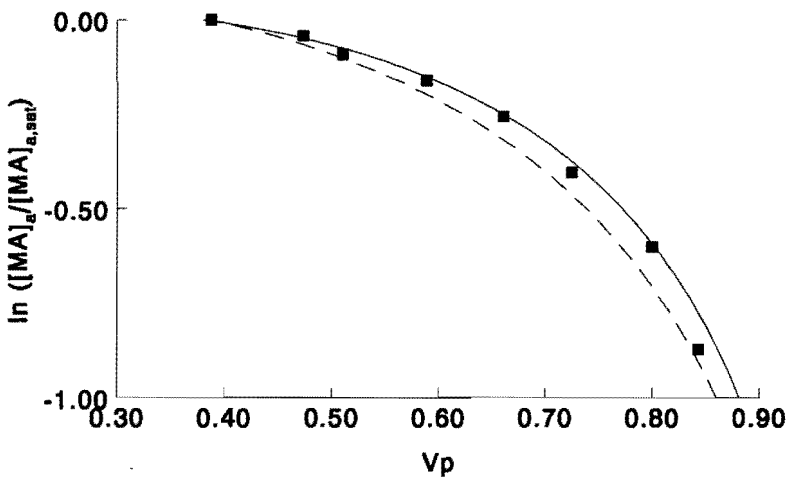


Figure 3.10 Comparison of the theoretical predictions (equation 3.14) experimentally measurements of MA partitioning at 45°C for latex SMA-6. Theoretical predictions with the Vanzo equation ($\chi = 0.2$ and $\gamma = 45 \text{ mN/m}$)(Solid line) and equation 3.14 (Corr. = 0.1)(Dashed line).

Before complete confidence can be expressed in the predictive capacity of equation 3.14, more experimental results are needed. It is important to note that the only parameters needed to predict the partial monomer partitioning between the latex particle and aqueous phases by this approach are the saturation concentrations of monomer in the latex particles and the aqueous phase.

3.6 Conclusions

For the partitioning of MA between the aqueous phase and the latex particle phase it was found that the following variables had little or no effect upon the experimental results: latex particle radius, temperature, polymer cross-linking density, polymer molar mass, polymer type and polymer composition. All these results agree well with theoretical predictions. Several authors have shown that the approach discussed in this chapter not only holds for other monomer-polymer systems¹⁴ but also for the partial swelling of latex particles with two or more monomers^{8,15,16}.

For those system which contained monomers/solvents which were water miscible a partition behavior was observed which was quite different from that of sparsely water soluble monomers/solvents. This is mainly due to the fact these water miscible monomers/solvents are often poor solvents for the polymer in the latex particles, therefore, only very small amounts were found in the latex particles at relatively high concentrations of the water miscible component in the aqueous phase.

Monomers/solvents capable of given strong interactions with the polymer in the latex particles, exhibit a partitioning behavior similar to the sparsely water soluble monomers/solvents which only have weak interactions with the polymer in the latex particles. The strong interactions between the monomer/solvent with the polymer can be accounted for by an extra energy term in the Flory-Huggins equation for mixing monomer and polymer with weak interactions. It was shown that an alternative approach utilizing a *negative* Flory-Huggins interaction parameter, which accounts for strong interactions, can predict the partition behavior of these strong interacting solvents/monomers in a qualitative way.

Finally, the following, more general, conclusions can be drawn from this chapter:

- a. The Vanzo equation successfully models the partitioning of monomer between the aqueous phase and the latex particle phase in the absence of a separate monomer phase.
- b. For the systems studied in this chapter, amongst others studied elsewhere, the contribution of the combinatorial entropy of mixing of monomer and polymer dominates the free energy of mixing at higher volume fraction of polymer which are typical within latex particles (i.e. approximately $v_p = 0.3 - 1$).

- c. The interfacial free energy does not contribute greatly to those parameters that determine the degree of *partial* latex particle swelling. This is in contrast to the *saturation* swelling of latex particles where the balance between the free energy associated with the mixing of monomer and polymer and the free energy of the particle-water interface determines the degree of latex particle swelling. It should be noted that as saturation swelling is approached both the residual free energy and interfacial free energy terms in the Vanzo equation become more important.
- d. The partitioning of monomer between the aqueous and latex particle phases when there is no separate monomer phase present can be predicted accurately if both the interaction parameter and interfacial tension are known. Both of these parameters are possibly polymer concentration dependent (in the case of the interfacial free energy this may be due to the monomer concentration at the interface). This fact, combined with the typical experimental uncertainties makes any prediction of these parameters from fits of the Vanzo equation to experimental data an unfavorable technique. However, if these parameters are not known, the partitioning can be well estimated by utilizing the entropy of mixing term in the Vanzo equation along with a correction term (*equations 3.13 and 3.14*) calculated from a fit of the Morton equation to saturation swelling data. In this case, prediction of the partial monomer swelling of latex particles requires only that the values of the saturation concentrations of the monomer in the particle and aqueous phases be known.

The Flory-Huggins theory for mixing monomer and polymer works very well for the partial swelling of latex particles for the following reasons:

- a. The polymer concentrations within latex particles are always relatively high. Therefore there should be an uniform density of Flory-Huggins segments.
- b. The residual free energy term (the χ -term) is not a major contributor to the thermodynamic problem at the higher volume fraction of polymers, when the monomer is a good solvent for the polymer present in the latex particles. Hence all the uncertainties associated with the measurement and interpretation of the interaction parameter are less consequential, again for systems in which the monomer is a good solvent for the polymer. The original derivation of the Flory-Huggins theory resulted in an interaction parameter that should be polymer concentration dependent at high volume fraction of polymer⁴. This is not a problem for most of the experimental systems studied in this work since within

experimental error the fit of the Vanzo equation to experimental data was insensitive to the value of the interaction parameter (within reasonable bounds), except for the systems in which strong interactions exist between the monomer/solvent and the polymer, in which case an extra term should be added accounting for these strong interactions (equation 3.12). The Flory-Huggins term that describes the combinatorial entropy of mixing of monomer and polymer is very successful at predicting the monomer partitioning (This entropic term was also derived by Hildebrand¹⁷ via a free volume approach and is probably quite general).

3.7 References

- 1 Morton, M., Kaizerman, S., Altier, M.W., *J. Colloid Sci.*, **9**, 300 (1954)
- 2 Vanzo, E., Marchessault, R.H., Stannett, V., *J. Colloid Sci.*, **20**, 65 (1965)
- 3 Gardon, J.L., *J. Polym. Sci., Polym. Chem. Ed.*, **6**, 2859 (1968)
- 4 Flory, P.J. in *Principles of Polymer Science*, Cornell University Press, Ithaca, New York 1953
- 5 Ugelstad, J. *et al.*, in *Science and Technology of Polymer Colloids*, NATO ASI Series E, Vol. 1, Plenum, New York (1983)
- 6 Johnson, C.A., *Surface Science*, **3**, 429 (1965)
- 7 Tseng, C.M., El-Aasser, M.S., Vanderhoff, J.W., *ACS, Div. of Org. Coatings Plastics Chem.*, **45**, 373 (1981)
- 8 Schoonbrood, H.A.S., *PhD. Thesis*, Eindhoven University of Technology (1994)
- 9 Popli, R., Luccas, M.H., Tsaur, S.L., *Langmuir*, **7**, 69 (1991)
- 10 Popli, R., *Langmuir*, **7**, 73 (1991)
- 11 Bindschaedler, C., Gurny, R., Doelker, E., Peppas, N.A., *J. Colloid Interface Sci.*, **108**, 75 (1985)
- 12 Bindschaedler, C., Gurny, R., Doelker, E., Peppas, N.A., *J. Colloid Interface Sci.*, **108**, 83 (1985)
- 13 Coleman, M.M., Painter, P.C., *Prog. Polym. Sci.*, **20**, 1 (1995)
- 14 Maxwell, I.A., Kurja, J., van Doremale, G.H.J., German, A.L., Morrisen, B.R., *Makromol. Chem.*, **193**, 2049 (1992)
- 15 Noël, L.F.J., Maxwell, I.A., German, A.L., *Macromolecules*, **26**, 2911 (1993)
- 16 Schoonbrood, H.A.S., Van den Boom, M.A.T., German, A.L., Hutovic, J., *J. Pol. Sci., Part A: Polymer Chemistry*, **32**, 2311 (1994)
- 17 Hildebrand, J.H., *J. Chem. Phys.*, **15**, 225 (1947)

CHAPTER 4[#]

Saturation Swelling of Latex Particles

1. *Ideal Systems*

Synopsis: The partitioning of two monomers between the latex particle, monomer droplet and aqueous phases of an emulsion polymer latex are measured at saturation swelling of the latex particle phase (corresponding to intervals I and II of an emulsion polymerization). The monomer and polymer types are varied systematically and the experiments are performed at two temperatures. In all the monomer-polymer systems studied, the monomer was a good solvent for the polymer. The results of these experiments correspond well to a simplified thermodynamic theory of the saturation swelling of an emulsion polymer with two monomers, in which it is realized that the fraction of one monomer is equivalent in the latex particle and monomer droplet phases. Further, it is shown that Henry's law holds for monomers, both in the absence and in the presence of swollen latex particles. A simple empirical relationship is developed whereby the concentration of the two monomers at any ratio can be calculated from the individual saturation concentration of the two monomers in the latex of interest.

4.1 Introduction

The swelling of polymeric latex particles with solvents and monomers is of great importance for the emulsion polymerization process. For example, consider the rate of an emulsion polymerization: the monomer concentrations in all of the latex particle, monomer droplet and aqueous phases can be critical factors that may determine the rate of polymerization directly. The monomer concentration in the particle phase may also determine the rate of free radical exit from latex particles ¹, and the initiator efficiency ²: these also influencing the rate of polymerization. It should also be noted that typical rates of emulsion

[#] Maxwell, I.A., Kurja, J., Van Doremale, G.H.J., and German, A.L., *Makromol. Chem.*, 193, 2065 (1992)

polymerization are such that thermodynamic equilibrium of monomer between the phases during polymerization is usually achieved.

The absolute concentrations and concentration ratios of monomers in the latex particles of an emulsion polymerization are also key parameters in understanding copolymer composition, and the inter- and intra-molecular polymer structure. The saturation swelling of latex particles by two monomers has been dealt with by various workers^{3,4,5}. In this chapter a simplified thermodynamic model that deals with saturation swelling of polymer latex by two monomers is developed. This model is based on experimental monomer partitioning data, in which the monomer concentrations in the latex particle, monomer droplet and aqueous phases are measured for a range of monomer and polymer types. This chapter will deal exclusively with swelling of latex particles by two monomers, but the considerations made are quite general and should apply to most solvents which are good solvents for the polymer present in the latex particles and show a low water solubility⁶. Furthermore, the approach developed in this study can be easily extended to deal with multi monomer/solvent systems^{7,8}.

4.2 Theory

Morton *et al.*⁹ considered the saturation swelling of latex particles by solvent having limited solubility in the water phase. When the swollen latex particle is in equilibrium with the free monomer phase the partial molar Gibbs free energy of the monomer is given by:

$$\Delta G = \Delta G_{\text{mix}} + \Delta G_{\text{surf}} = 0 \quad (4.1)$$

where ΔG is the partial molar Gibbs free energy of monomer, ΔG_{mix} the contribution from the energy of mixing of monomer and polymer, and ΔG_{surf} the contribution from the particle-water interfacial energy. Morton *et al.*⁹ expressed the free energy of mixing of monomer and polymer in terms of the classical Flory-Huggins theory¹⁰:

$$\frac{\Delta G_{\text{mix}}}{RT} = \ln(1 - v_p) + v_p \left[1 - \frac{1}{P_n} \right] + \chi * v_p^2 \quad (4.2)$$

where v_p is the volume fraction of polymer in the latex particles, \bar{P}_n the number average degree of polymerization, R the gas constant, T the temperature and χ the Flory-Huggins interaction parameter. The interfacial free energy was given in terms of the Gibbs-Thomson equation^{4,11}:

$$\Delta G_{\text{surf}} = \frac{2 * V_m * \gamma * v_p^{1/3}}{R_0} \quad (4.3)$$

where V_m is the partial molar volume of the monomer, γ the particle-water interfacial tension and R_0 the unswollen radius of the latex particle. Combining *equations 4.1, 4.2* and *4.3* gives the *equation 4.4*, which represent the saturation equilibrium swelling of a polymer latex with one monomer.

$$\ln(1 - v_p) + v_p * \left[1 - \frac{1}{\bar{P}_n} \right] + \chi * v_p^2 = - \frac{2 * V_m * \gamma * v_p^{1/3}}{R_0 * RT} \quad (4.4)$$

Since the number average degree of polymerization (\bar{P}_n) is often high for polymers produced via emulsion polymerization, the $v_p * \left[1 - \frac{1}{\bar{P}_n} \right]$ term in *equation 4.2* can be approximated by v_p . *Equation 4.4* shows that the saturation swelling of a polymer latex with one monomer is determined one side by the partial molar free energy of mixing monomer and polymer and the surface free energy of the monomer swollen latex particle on the side.

The partial molar free energy of mixing of monomer i with polymer ($\Delta G_{m,i}$) in the presence of a second monomer j is given by an equation^{4,5,10} analogous to *equation 4.2*:

$$\begin{aligned} \frac{\Delta G_{m,i}}{RT} = & \ln v_{p,i} + (1 - m_{ij}) * v_{p,j} + v_p + \chi_{ij} * v_{p,j}^2 + \chi_{ip} * v_p^2 \\ & + v_{p,j} * v_p * (\chi_{ij} + \chi_{ip} - \chi_{jp} * m_{ij}) \end{aligned} \quad (4.5)$$

where $v_{p,i}$ and $v_{p,j}$ are the volume fractions of monomer i and j in the latex particles, respectively. χ_{ij} the interaction parameter between monomers i and j , and χ_{ip} and χ_{jp} are the interaction parameters between each of the respective monomers i and j and polymer. The term m_{ij} is the ratio of the molar volumes of monomers i and j (i.e. $m_{ij} = V_{m,i} / V_{m,j}$, where $V_{m,i}$ and $V_{m,j}$ are the molar volumes of monomer i and j , respectively). The derivation of *equation 4.5* involves the reasonable assumption⁴ that $m_{i,p}$ and $m_{j,p}$, the ratio of the respective molar volumes of monomers i and j and the molar volume of polymer, are negligible as compared with all other terms.

The partial molar free energy of monomer i in the particle phase ($\Delta G_{p,i}$) is given by the sum of the contributions from both the mixing of monomer i and polymer, and the contribution of monomer i to the interfacial free energy ($\Delta G_{s,i}$):

$$\Delta G_{p,i} = \Delta G_{m,i} + \Delta G_{s,i} \quad (4.6)$$

The partial molar free energy of monomer i in the droplets ($\Delta G_{d,i}$) can also be calculated from the Flory-Huggins lattice theory⁴.

$$\frac{\Delta G_{d,i}}{RT} = \ln v_{d,i} + v_{d,j} * [1 - m_{ij}] + \chi_{ij} * v_{d,j}^2 \quad (4.7)$$

In this equation $v_{d,i}$ represents the volume fraction of monomer i in the droplets, and $v_{d,j}$ the volume fraction of monomer j in the droplets. The use of *equation 4.7* assumes that the lattice model is valid for mixtures of small molecules: this may be valid for two organic monomers. Note also, that due to the normally large size of monomer droplets, contributions from the monomer droplet-water interfacial free energy in *equation 4.7* have not been taken into account (this assumption may not be valid for a system containing very small monomer droplets).

Equation 4.8 gives the partial molar free energy of monomer i in the aqueous phase ($\Delta G_{a,i}$):

$$\frac{\Delta G_{a,j}}{RT} = \ln v_i + v_{\text{water}} * \left[1 - m_{i,\text{water}} \right] + \chi_{i-\text{water}} * v_{\text{water}}^2 \quad (4.8)$$

here v_i and v_{water} represent the volume fraction of monomer and water in the aqueous phase, respectively. $\chi_{i-\text{water}}$ is the Flory-Huggins interaction parameter between water and the monomer, while $m_{i,\text{water}}$ is the ratio of the molar volumes of monomer and water. Vanzo *et al.*¹² were the first to derive an analogue *equation 3.4* that dealt with partial swelling of latex particles utilizing a simpler equation for the partial molar free energy of the aqueous phase. In doing so, they assumed that the monomer containing aqueous phase could be considered as a dilute solution of monomer and water. Later, Gardon¹³ derived the same expression. If the latex particles are not saturated by monomer then there is no pure monomer phase present (i.e. no monomer droplets). The partial molar free energy of the monomer in the aqueous phase is then given by^{4,12,13,14}:

$$\Delta G = RT * \ln a \quad (4.9)$$

where a is the activity of the monomer. Vanzo *et al.*¹² pointed out that the monomer activity can be approximated by p/p_0 , i.e. the ratio of the vapor pressure of the monomer at a given volume fraction of polymer (p) to the vapor pressure at saturation swelling (p_0). Gardon¹³ showed that, since Henry's Law holds for latex free water, the ratio p/p_0 can be approximated by the ratio of the monomer concentration in the aqueous phase below and at saturation:

$$\frac{p}{p_0} = \frac{[M]_{\text{aq}}}{[M]_{\text{aq},\text{sat}}} \quad (4.10)$$

where $[M]_{\text{aq}}$ is the concentration of monomer in the aqueous phase and $[M]_{\text{aq},\text{sat}}$ is the saturation concentration of monomer in the aqueous phase.

$$\frac{\Delta G_{a,i}}{RT} = \ln \left[\frac{[M]_{\text{aq}}}{[M]_{\text{aq},\text{sat}}} \right] \quad (4.11)$$

At equilibrium the partial molar free energy (or the chemical potential) of each monomer will be equal in each of the three phases.

$$\Delta G_{p,i} = \Delta G_{d,i} = \Delta G_{a,i} \quad (4.12)$$

Applying this condition, from *equations 4.5, 4.7 and 4.11* the following equations for monomer *i* are found:

$$\begin{aligned} & \ln v_{p,i} + (1 - m_{ij}) * v_{p,j} + v_p + \chi_{ij} * v_{p,j}^2 + \chi_{ip} * v_p^2 \\ & + v_{p,j} * v_p * (\chi_{ij} + \chi_{ip} - \chi_{jp} * m_{ij}) + \frac{2 * V_{m,i} * \gamma * v_p^{1/3}}{R_0 * RT} = \end{aligned} \quad (4.13)$$

$$\ln v_{d,i} + (1 - m_{ij}) * v_{d,j} + \chi_{ij} * v_{d,j}^2 = \ln \left[\frac{[M_i]_{aq}}{[M_i]_{aq,sat}} \right]$$

Similarly, for monomer *j* *equation 4.14* can be found:

$$\begin{aligned} & \ln v_{p,j} + (1 - m_{ji}) * v_{p,i} + v_p + \chi_{ij} * v_{p,i}^2 + \chi_{jp} * v_p^2 \\ & + v_{p,i} * v_p * (\chi_{ij} + \chi_{jp} - \chi_{ip} * m_{ji}) + \frac{2 * V_{m,j} * \gamma * v_p^{1/3}}{R_0 * RT} = \end{aligned} \quad (4.14)$$

$$\ln v_{d,j} + (1 - m_{ji}) * v_{d,i} + \chi_{ij} * v_{d,i}^2 = \ln \left[\frac{[M_j]_{aq}}{[M_j]_{aq,sat}} \right]$$

Equations 4.13 and 4.14 can be used to predict and/or model partitioning data for latex systems with two monomers. There are, however, some difficulties associated with the use of these equations: First, the use of *equations 4.13 and 4.14* requires known values for the three interaction parameters. Flory¹⁰ pointed out two complications involved with the use of interaction parameters: (a) For systems with high volume fraction polymers (which is certainly the case for swollen latex particles) the interaction parameters cannot be independent of the volume fraction polymer. Hence, the original Flory-Huggins equation, and its two-monomer

analogue (*equation 4.5*) can only be used as useful semi-empirical relationships, where the terms containing an interaction parameter can be thought of as residual free energy terms, containing both temperature dependent enthalpic terms and temperature independent entropic terms. (b) The situation where the Flory-Huggins equation is used as a semi-empirical equation can be satisfactory for systems with one monomer, since there is only one adjustable parameter (χ). However, for two monomer systems there are at least three interaction parameters. These may be determined by fitting *equations 4.13* and *4.14* to experimental data, but often do not offer unique values for these fitted parameters. An alternative approach for estimating interaction parameters, the use of mutual solubility measurements, can be less than satisfactory¹. An extra difficulty for the polymer latex situation is that the value of the particle-water interfacial tension is difficult to determine experimentally. Therefore, in systems with one monomer the interfacial tension is often determined by fits to the Morton equation^{9,14}. However, it should be noted that the interfacial tension may change with the ratio of monomer i to j , and also with the total concentration of monomer at the interface, and hence also the volume fraction polymer in the latex particles. It should be noticed that, at saturation swelling of latex particles by two monomers, the variables of interest are the concentrations of monomer i and j in each of the three phases. The theory that describes this situation consists of two equations (*equations 4.13* and *4.14*) and at least four unknown parameters (χ_{ij} , χ_{ip} , χ_{jp} , γ) all of which may vary with the volume fraction polymer and/or the ratio of monomers within the latex particles, thereby introducing many more unknown variables. There are methods for estimating the values of these parameters (χ can be estimated from for instance solubility parameters), and hence predicting monomer concentrations in each phase.

4.3 Experimental

Materials: Reagent grade styrene (S), butyl acrylate (BA) and methyl acrylate (MA) (Merck) were distilled under reduced nitrogen pressure in order to remove inhibitor. The middle fraction was cut and stored at 4°C. The water was distilled twice. Potassium persulfate (Merck p.a.), n-dodecyl mercaptan (Merck p.a.) and sodium dodecyl sulfate (SDS, Fluka) were used without further purification.

Seed latex preparation: The seed latices were prepared in a glass reactor under 1.7 atmosphere. nitrogen pressure at 50°C for both MA and BA and also for copolymerizations containing these two monomers, and at 70°C for S. The recipes are given in *Table 4.1*. After approximately 24 hours the temperature was increased to 90°C for 3 hours in order to dissociate the remainder of the initiator. After polymerization initiator fragments, unreacted monomer and most of the free surfactant were removed by dialysis.

Table 4.1 *Seed latex recipes (MA, BA and copolymerizations at 50 °C; S at 70 °C)*

	mass (g)
MA, BA, S (total)	30
Water	750
Potassium persulfate	0.2
n-Dodecyl mercaptan	0.3
SDS	2.0

Particle Sizing: Particle morphology and size were examined by means of transmission electron microscopy and dynamic light scattering. UV hardening of the soft poly(methyl acrylate) particles prevented melting under the microscope beam. All the latex particles used in this study are listed in *Table 4.2*.

Table 4.2 *Seed latex compositions and mean radii*

Monomer System	Polymer Composition (mole/mole)	Unswollen Radius (nm)
S-MA	S	89
	S-MA, 50:50	63
S-BA	MA	50
	S	43
	S-BA, 25:75	50
MA-BA	BA	80
	MA	65
	MA-BA, 50:50	84
	BA	73

Monomer Partitioning: Monomer partitioning experiments were performed for three different pairs of monomers, S-MA, S-BA and MA-BA. Three polymer latices were used for the partitioning experiments for each monomer pair. In each experiment a latex of known

solids content and polymer composition (see *Table 4.2*) was mixed with known amounts of the two monomers in the absence of initiator. In all experiments sufficient water was added to ensure that the solids content in each experiment was approximately 5-10% (it was found that varying latex solids content had no influence on the partitioning results). The system was allowed to reach equilibrium by shaking (for at least 24 hours) while thermostated at the required temperature. The phases (swollen polymer particles, monomer droplet and aqueous phases) were separated using an ultracentrifuge (Centrikon T-2060, 55000 rpm) thermostated to the same temperature as above. The swollen particles could not be analyzed without some residual aqueous phase. Monomer concentrations in the particles were determined by gas chromatography (GC) after dissolving the monomer swollen polymer phase (with some aqueous phase content) in acetone with some toluene as an internal standard, or alternatively in the case of polystyrene latices, after dissolving in toluene with 2-propanol as internal standard. Determination of the dry solids content of the sample gave the polymer content. The concentration of MA in the aqueous phase was determined after adding a standard 2-propanol solution in water to a sample of the aqueous phase. For the determination of monomer content in the polymer particles appropriate corrections were made for the monomer contained in the residual aqueous phase. The monomer droplet phase was analyzed by GC in terms of the monomer ratios. In order to calculate the monomer concentrations inside the particles, the volumes of all components within the particles (monomer and polymer) were assumed to be additive. Copolymer densities were calculated by the appropriate averaging of the densities of the homopolymers. The partitioning experiments were carried out at 20°C for S-MA and S-BA, and at 35°C for MA-BA.

Saturation concentration of MA in aqueous phase: The effect of surfactant concentration upon the saturation concentration of MA in the aqueous phase at various temperatures was investigated. MA was mixed with water containing various concentrations of surfactant (SDS). GC analysis of the aqueous phase was carried out as above. It was found that the saturation concentration of MA in the aqueous phase was virtually independent of the SDS concentration¹⁴. Further, the concentration of MA in water increased with decreasing temperature. This was subscribed to stronger hydrogen bonding at lower temperatures. From these results we can be sure that the determination of concentrations of MA in the aqueous phase were free of artifactual effects arising from varying surfactant concentrations in the aqueous phase. All partitioning experiments were carried out with less than 0.5 g/l free SDS in

the aqueous phase: this value being well below the critical micelle concentration of SDS at the experimental temperatures.

4.4 Results and Discussion

4.4.1 Experimental Results

In *figures 4.1, 4.2, and 4.3* experimental data on the partitioning of MA, S and BA between the latex particle and monomer droplet phases for a variety of seed latices, with different (co)polymer compositions, are displayed. It is apparent that in every case the mole fraction of the monomer in the droplet and particle phases is, virtually, equal, and independent of (co)polymer composition, temperature and monomer type. In *figure 4.4* the partitioning of methyl methacrylate (MMA) between the droplet phase and S-MMA latex particles or S-MMA-graft-PB copolymer composite latex particles is displayed, as reported by Aerdts *et al.*¹⁵. As can be seen from this figure, the fraction of MMA in the droplet phase is equal to fraction of MMA in the latex particles irrespectively the copolymer composition and cross-link density (PB-phase).

It is the actual concentration of the monomers in the latex particles that is of interest, especially with respect to the kinetic of the polymerization, *viz.* the rate of polymerization and the chemical composition of the copolymer formed are directly related to the concentration of the different monomers in the latex particles. In *figures 4.5, 4.6, 4.7, and 4.8* the concentration of both monomers in various latex particle phases are plotted against the mole fraction of one the monomers in the droplet phase. From *figures 4.5 - 4.8* it is apparent that the absolute saturation concentration of monomer in the latex particles depends on monomer and polymer type. In general, the more water soluble monomer is, the higher the monomer (saturation) concentration in the latex particles, i.e. $[MA]_{\text{latex particles}} > [BA]_{\text{latex particles}} > [S]_{\text{latex particles}}$. Thus, it seem that the monomer concentration in the latex particles depends on the hydrophilicity of the monomer.

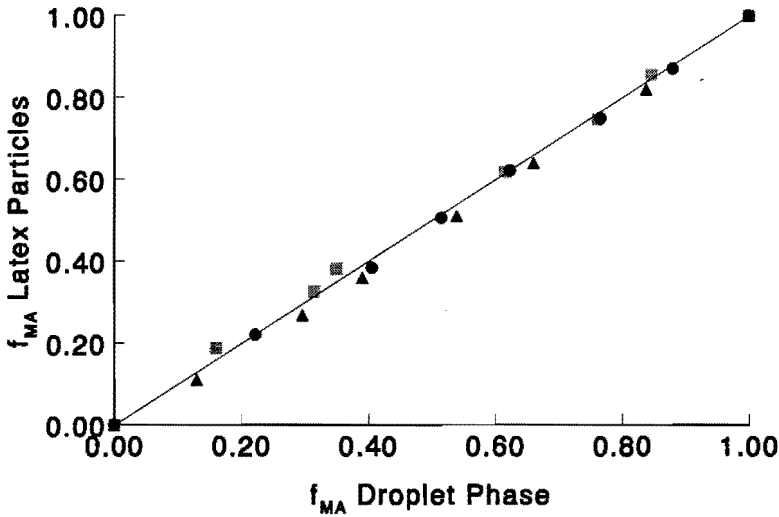


Figure 4.1 Experimentally determined mole fraction of MA in the latex particles as a function of the mole fraction of MA in the droplet phase. Polystyrene latex (triangles), poly(styrene-co-methyl acrylate) latex (circles), and poly(methyl acrylate) latex (squares) at 20 °C (for copolymer compositions see Table 4.2). Solid line: theoretical prediction according to equations 4.18/4.19.

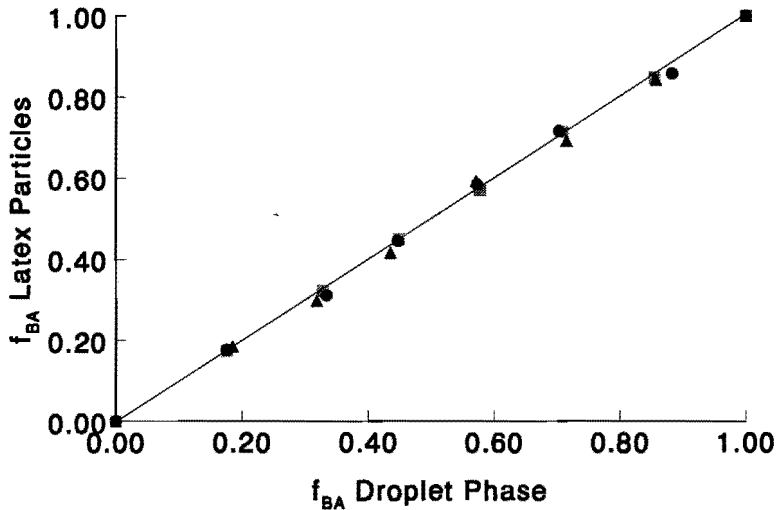


Figure 4.2 Experimentally determined mole fraction of BA in the latex particles as a function of the mole fraction of BA in the droplet phase. Polystyrene latex (triangles), poly(styrene-co-butyl acrylate) latex (circles), and poly(butyl acrylate) latex (squares) at 20 °C (for copolymer compositions see Table 4.2). Solid line: theoretical prediction according to equations 4.18/4.19.

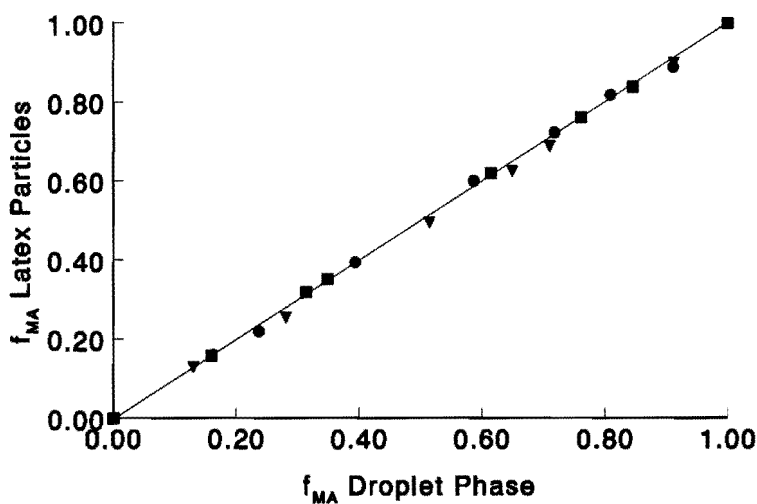


Figure 4.3 Experimentally determined mole fraction of BA in the latex particles as a function of the mole fraction of BA in the droplet phase. Poly(methyl acrylate) latex (squares), poly(methyl acrylate-co-butyl acrylate) latex (circles), and poly(butyl acrylate) latex (triangles) at 35 °C. (for copolymer compositions see Table 4.2). Solid line: theoretical prediction according to equations 4.18/4.19.

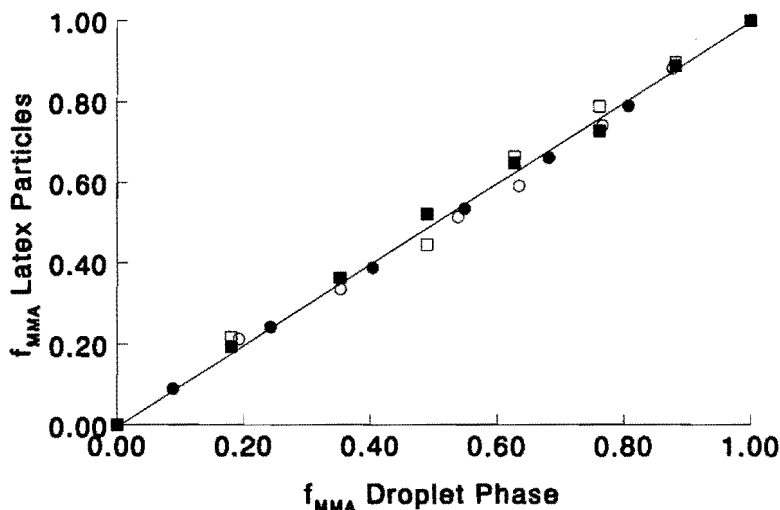


Figure 4.4 Experimentally determined mole fraction of MMA in the latex particles as a function of the mole fraction of MMA in the droplet phase. PB latex (closed circles), SMMA-f (open squares), SMMA-g (closed squares) from MBS latex particles, and the open circles a SMMA latex. The average composition of the S-MMA copolymer was 25 mole-% of S. Experimental data taken from Aerds et al.¹⁵. Solid line: theoretical prediction according to equations 4.18/4.19.

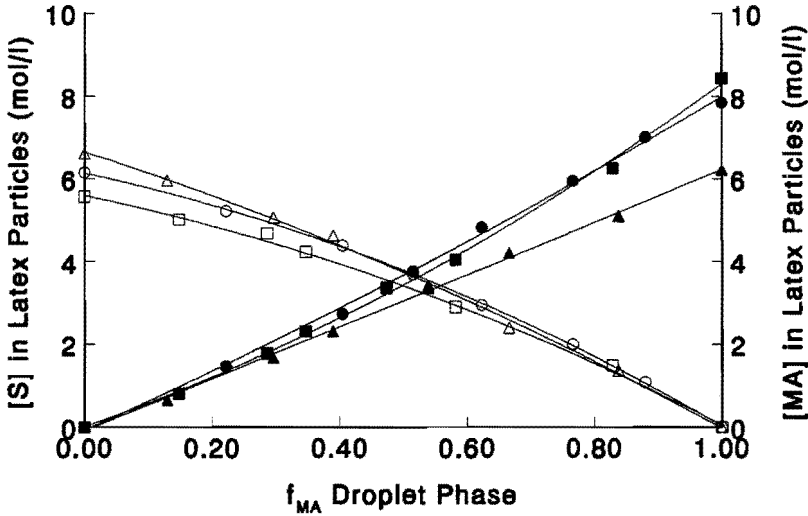


Figure 4.5 Experimentally determined monomer concentrations in the latex particles as a function of the mole fraction of monomer in the droplet phase. The open symbols represent the concentration of *S* in the latex particles and the closed symbols the concentration of *MA* in the latex particles. Polystyrene latex (triangles), poly(styrene-co-methyl acrylate) latex (circles), and poly(methyl acrylate) latex (squares) at 20 °C (for copolymer compositions see Table 4.2). Solid lines: theoretical prediction according to equations 4.21/4.22.

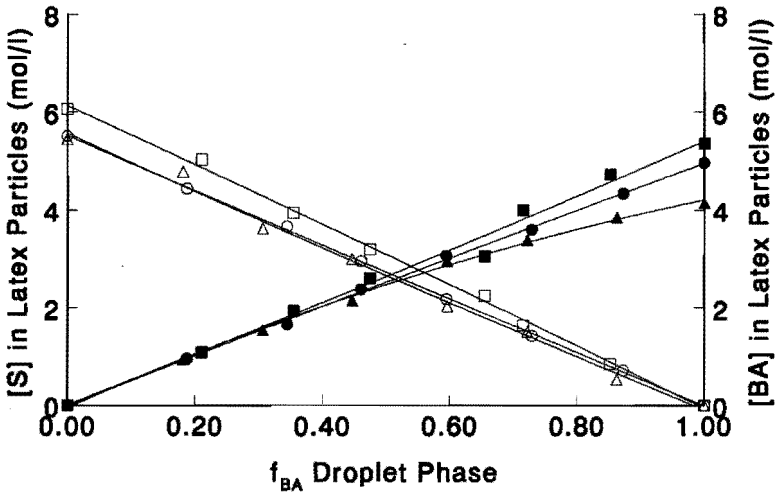


Figure 4.6 Experimentally determined monomer concentrations in the latex particles as a function of the mole fraction of monomer in the droplet phase. The open symbols represent the concentration of *S* in the latex particles and the closed symbols the concentration of *BA* in the latex particles. Polystyrene latex (triangles), poly(styrene-co-butyl acrylate) latex (circles), and poly(butyl acrylate) latex (squares) at 20 °C (for copolymer compositions see Table 4.2). Solid lines: theoretical prediction according to equations 4.21/4.22.

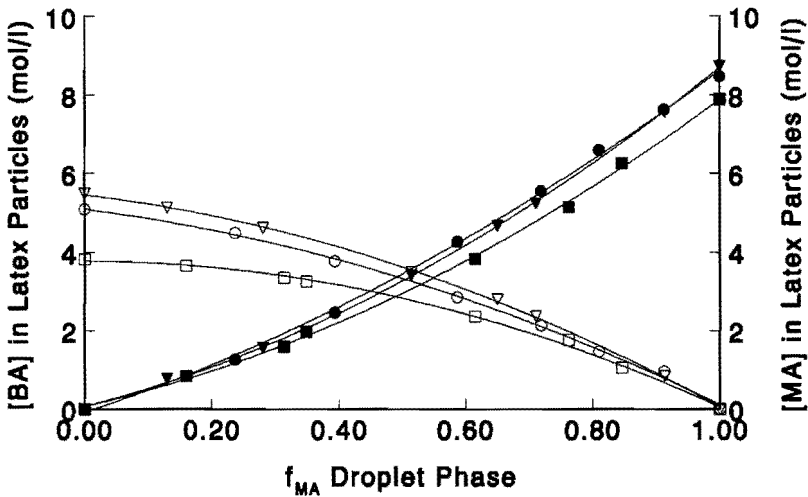


Figure 4.7 Experimentally determined monomer concentrations in the latex particles as a function of the mole fraction of monomer in the droplet phase. The open symbols represent the concentration of BA in the latex particles and the closed symbols the concentration of MA in the latex particles. Poly(methyl acrylate) latex (squares), poly(methyl acrylate-co-butyl acrylate) latex (circles), and poly(butyl acrylate) latex (triangles) at 35 °C. (for copolymer compositions see Table 4.2). Solid lines: theoretical prediction according to equations 4.21/4.22.

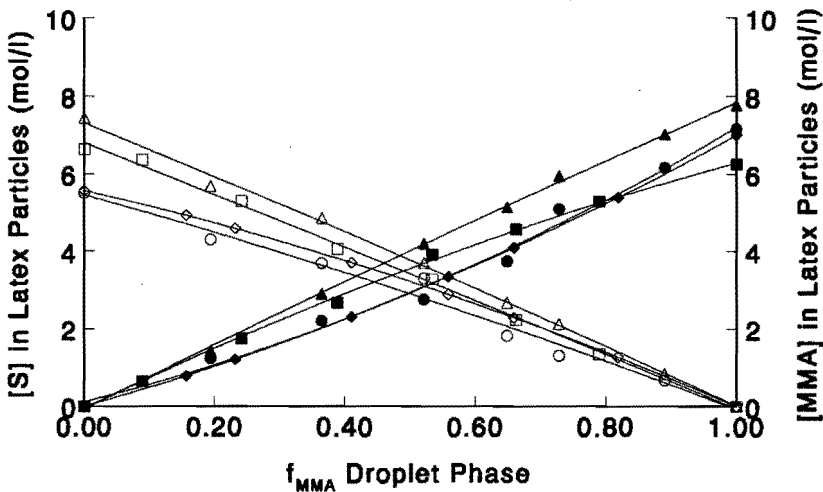


Figure 4.8 Experimentally determined monomer concentrations in the latex particles as a function of the mole fraction of monomer in the droplet phase. The open symbols represent the concentration of S in the latex particles and the closed symbols the concentration of MMA in the latex particles. PB latex (squares), SMMA-f (circles), SMMA-g (triangles) from MBS latex particles, and the diamonds a SMMA latex. The average composition of the S-MMA copolymer was 25 mole-% of S. Experimental data taken from Aerdt et al.¹⁵. Solid lines: theoretical prediction according to equations 4.21/4.22.

However, if the volume fraction of monomer in the latex particles is calculated, the degree of swelling is virtually independent of the monomer type, assuming that the monomer is a good solvent for the polymer and is sparsely water soluble. This is due to a difference in molar volume between the separate monomers.

4.4.2 Modeling of Saturation Swelling of Latex Particles

In this chapter an alternative approach for modeling monomer partitioning will be given: simplifications to theory of two monomer swelling of latex particles (*equations 4.13 and 4.14*) are described in the first part of this section. In the second part, a method will be presented for estimating/predicting the absolute monomer concentration in latex particles.

Part 1: Monomer fractions in the latex particle phase and droplet phase

In an attempt to simplify *equations 4.13 and 4.14* three assumptions are made:

1. For many pairs of monomer the differences between the molar volumes of the monomers is slight (see *Table 4.3*). If this is the case the ratio of the molar volumes of monomer i and j is well approximated by unity, i.e. $m_{ij} = m_{ji} = 1$. The molar volume of the three monomers used in this study are listed in *Table 4.3*. It is apparent that the ratio of the molar volumes of the monomers do not deviate far from unity. Hence this assumption appears valid for the systems under investigation.

Table 4.3 *Molar volumes and the ratio of molar volumes for different monomers*

Monomer System $i-j$	Temperature (°C)	$V_{m,i}$ (l/mole)	$V_{m,j}$ (l/mole)	m_{ij}
S-MA	20	0.115 (S)	0.090 (MA)	1.3
S-BA	20	0.115 (S)	0.140 (BA)	0.8
MA-BA	35	0.093 (MA)	0.142 (BA)	0.7

2. The contribution to the partial molar free energy arising from the residual (enthalpic and non-conformational entropic) partial molar free energy of the mixing of the two monomers is small relative to all other terms in the expressions describing the partial molar free energy of monomers in the droplet phase (see also *equation 4.7*).

By applying the above two assumptions to *equations 4.13 and 4.14*, the right hand equalities of these equation can be simplified:

$$v_{d,i} = \frac{[M_i]_{aq}}{[M_i]_{aq,sat}} \quad (4.15)$$

$$v_{d,j} = \frac{[M_j]_{aq}}{[M_j]_{aq,sat}} \quad (4.16)$$

Equations 4.15 and 4.16 are simply in the form of Henry's law, which has been shown to hold for partially water soluble organic solvents/monomers in the absence of latex particles^{13,14}. *Figure 4.9* clearly shows that *equations 4.15 and 4.16* also hold for partially water soluble monomers in the presence of latex particles.

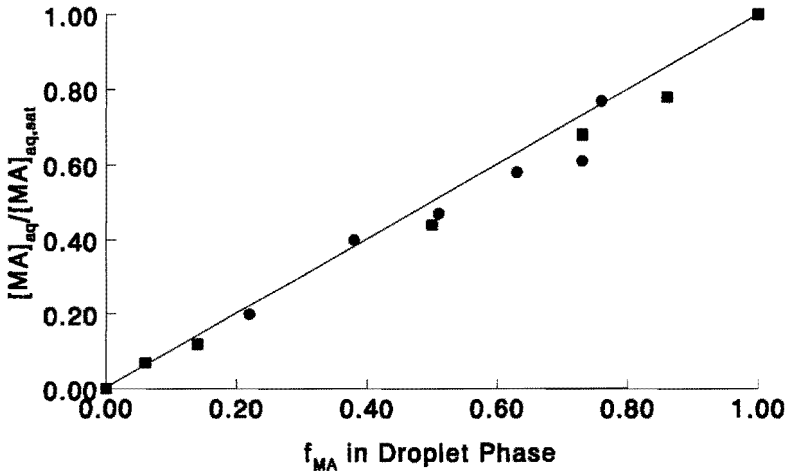


Figure 4.9 Experimentally determined MA concentration in the aqueous phase as a function of the mole fraction of MA in the droplet phase with S as the co-monomer at 20 °C in the presence of a poly(styrene-co-methyl acrylate) latex (squares) and in the absence of latex particles (circles). The solid line represents the theoretical prediction by equations 4.15/4.16.

3. The interaction parameter for each monomer with the same polymer is almost equal ($\chi_{ip} = \chi_{jp}$), while at the same time both monomers are good solvents for the polymer in

the latex particle phase. Applying assumptions 1, 2, and 3, to *equations 4.13* and *4.14*, the following simple equation is obtained:

$$\frac{v_{p,i}}{v_{p,j}} = \frac{v_{d,i}}{v_{d,j}} \quad (4.17)$$

Equation 4.17 relates the ratios of the volume fractions (or concentrations) of monomers *i* and *j* in the latex particles to those in the droplet phase. From *equation 4.17* the following equalities can be written:

$$f_{p,i} = f_{d,i} \quad (4.18)$$

$$f_{p,j} = f_{d,j} \quad (4.19)$$

where $f_{p,i}$, $f_{d,i}$, $f_{p,j}$, and $f_{d,j}$ represent the monomer volume fraction of monomers *i* and *j* in the droplet and particle phases, respectively.

Note that in the latex particle phase these monomer fractions relate only to the volume of one monomer as a fraction of the total volume of both monomers in the particles (i.e. the volume of the polymer in the latex particles is not included in these fractions). Via assumption 1, the monomer volume fractions also represent the monomer molar fractions. Ugelstad *et al.*⁴ incorrectly stated that the assumptions 1 and 3 are sufficient to show that the ratios of the volume fractions of monomer *i* to *j* are equal in both the latex particle and monomer droplet phases. In fact, the use of these two assumptions in *equations 4.13* and *4.14* gives:

$$\ln \left[\frac{v_{p,i}}{v_{p,j}} \right] - \ln \left[\frac{v_{d,i}}{v_{d,j}} \right] = \chi_{ij} \left[(v_{d,j} - v_{d,i}) - (v_{p,j} - v_{p,i}) \right] \quad (4.20)$$

Assumption 2 needs to be made to arrive at the situation where the ratios of the volume fractions of monomers *i* and *j* are equal in the particle and droplets phases, i.e. *equations 4.18* and *4.19*. The experimental verification/justification of/for the assumptions made above is given *figures 4.1 - 4.4*, which show that *equations 4.18* and *4.19* are valid. In

conclusion it can be said that the fraction of monomer i and j in the droplet phase is equal to the fraction of monomer i and j in the latex particle phase when the monomers are good solvents for the polymer in the latex particles, have virtually equal molar volumes, and at the same time the monomers mix well which is virtually always the case with organic solvent.

Equations 4.13 and 4.14 have been simplified such that the ratio of the concentrations of monomers i and j in the latex particle and monomer droplet phases can be equated. Given the fraction of each monomer in the droplet phase the simplified equations also allow the calculation of the concentration of each monomer in the aqueous phase. However, the aim of this thesis is also to present a method whereby the actual concentrations of two monomers in the particle phase can be calculated. It must be realized that, although the residual partial molar free energy (enthalpic and non-conformational entropic) and the free energy associated with the interface do not, in the simple theory described by *equations 4.17, 4.18, and 4.19*, influence the ratio of the concentration of the two monomers in the latex particles, they do influence the absolute values of the concentration of each monomer in the particles. This is simply because the total degree of swelling of latex particles is restricted by the surface free energy and the residual free energy.

Part 2: Monomer concentrations in the latex particles

The approach discussed here to predict the monomer concentration in the latex particles at saturation swelling makes use of the assumptions resulting in *equations 4.18 and 4.19* and the additional assumption that the total monomer concentration in the latex particles is just equal the sum of the concentrations of the individual monomers. The total monomer concentration is assumed to be a linear function of the fraction of the monomers in the droplet phase. The impetus for this assumption arose from the experimental observation that the total monomer concentration displays relatively linear behavior as a function of the fraction of one monomer in the droplet phase (see *figures 4.10, 4.11, and 4.12*). In this approach, all that is required to predict the concentration of the two monomers in a particular latex, at any ratio of these two monomers in the feed, is the concentrations of the two monomers when they exclusively swell the particular latex, i.e. during “homo-swelling”.

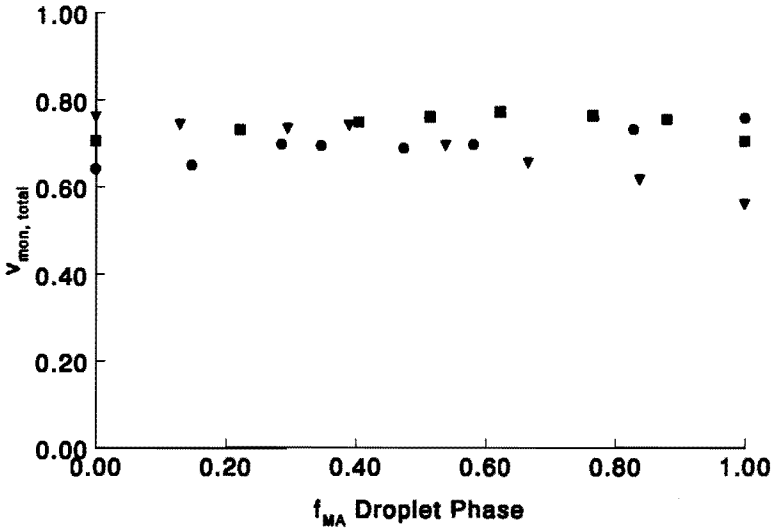


Figure 4.10 Experimentally determined total volume fraction of monomer in the monomer swollen latex particles as a function of the monomer fraction in the droplet phase. Triangles represent a polystyrene latex, squares a poly(styrene-co-methyl acrylate), and the circles a polymethyl acrylate all at 20 °C.

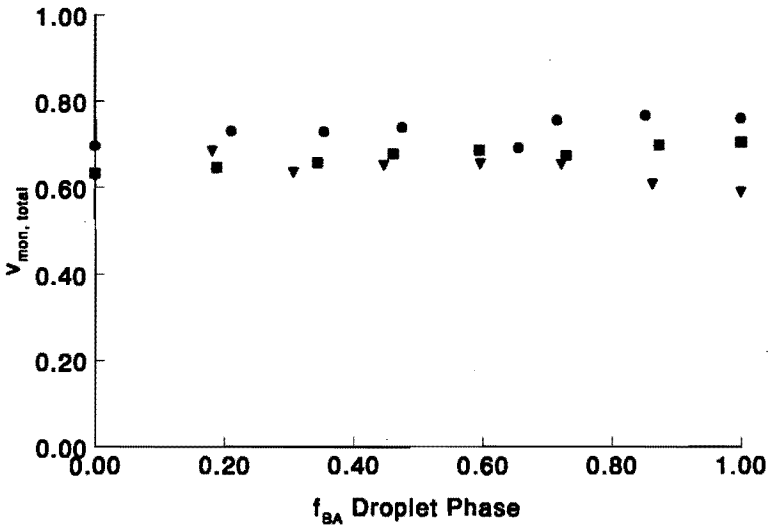


Figure 4.11 Experimentally determined total volume fraction of monomer in the monomer swollen latex particles as a function of the monomer fraction in the droplet phase. Triangles represent a polystyrene latex, squares a poly(styrene-co-butyl acrylate), and the circles a polybutyl acrylate all at 20 °C.

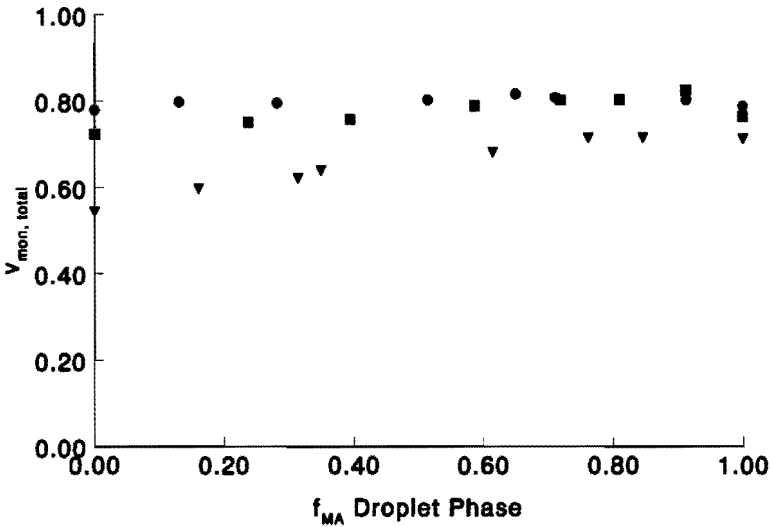


Figure 4.12 Experimentally determined total volume fraction of monomer in the monomer swollen latex particles as a function of the monomer fraction in the droplet phase. Triangles represent a polymethyl acrylate latex, squares a poly(methyl acrylate-co-butyl acrylate), and the circles a polybutyl acrylate all at 35 °C.

Hence, for a particular seed latex the concentration of monomer i within the particles (C_i) as a function of the fraction of monomer i in the droplets is given by:

$$C_i = f_{d,i} * [(C_{i,m} - C_{j,m}) * f_{d,i} + C_{j,m}] \quad (4.21)$$

Similarly, for monomer j the following expression is found:

$$C_j = f_{d,j} * [(C_{j,m} - C_{i,m}) * f_{d,j} + C_{i,m}] \quad (4.22)$$

where $C_{i,m}$ and $C_{j,m}$ are the maximum saturation concentrations of monomers i and j in the latex particles during homo-swelling, respectively. In figures 4.5 - 4.8 the predictions of equations 4.21 and 4.22 are compared to experiment. It can be seen that in all cases equations 4.21 and 4.22 provide adequate predictions of the experimental data. Therefore, for the systems studied, if the maximum saturation concentration of each monomer in the latex

particles of interest are known then the concentration of both monomers at different monomer ratios can be predicted by *equations 4.21 and 4.22*.

4.5 Concluding Remarks

For the systems studied the simplified equations (*equations 4.17, 4.18 and 4.19*) that describe the saturation partitioning of monomers between the latex particle and droplet phases adequately predict the fraction of each monomer in the two phases. These simplified equations state that the ratio of the two monomers, and also the fraction of each monomer, are equal in the droplet and latex particle phases. This result is based upon the following assumptions: **Assumption 1:** the molar volumes of the monomers are not too dissimilar, which is a reasonable assumption for most monomer pairs. **Assumption 2:** the contribution to the overall thermodynamic problem of the residual partial molar free energy of mixing of the two monomers within the latex particles is small compared to the contribution of the conformational entropy of mixing of the two monomers. The presence of the polymer has no significant effect upon the ratio of the two monomers since the entropy of mixing of the two monomers contributes the dominant thermodynamic effect. **Assumption 3:** The interaction parameters for each monomer with polymer are equal, or at least similar. This assumption seems reasonable since these interaction parameters describe the enthalpic and non-conformational entropic partial molar free energy of mixing of two small molecules with the one polymer.

The prediction of the concentration of two monomers in a single polymer latex phase is facilitated by the above result, namely that the fractions of each monomer in the particle and droplet phases are equal. Prediction of the concentration of each monomer in the latex particles requires the further experimentally observed result that the overall concentration of monomer in the latex particles is an approximate linear function of the fraction of each monomer in the particle and droplet phases. Given the values of the homo-monomer saturation concentrations of the two monomers in the latex of interest the individual monomer concentrations in the latex phase can be calculated from the fraction of monomer in the whole system (with mass balance considerations).

The relationship between the concentration of monomer in the aqueous phase and the droplet phase was shown to obey Henry's Law in the presence and absence of latex particles. This was as expected, since it has already been shown that Henry's Law is obeyed for monomers both in the absence¹³ and presence¹⁴ of latex particles. The presence of a swollen latex particle phase does not influence the monomer partitioning between the droplet and water phases since the monomer ratio in the particle phase is equal to that in the droplet phase for those systems studied in this paper.

Finally, the results of this chapter are of considerable importance for the emulsion polymerization field since, if general, they allow simple predictions of both the monomer ratio and concentrations in each of the three phases present during an emulsion polymerization. Although we have endeavored to utilize monomers with different water solubilities, and also in each case varying latex polymer composition, further experimental results are needed to test the limits of the theoretical assumptions utilized in this work. For example, assumption 1 requires that the molar volumes of the two monomers of interest be similar. Although this is usually the case, there are systems where this condition is not met (see *Chapter 5*). Further, it must be pointed out that the results of this chapter probably only apply to partially water soluble monomers and water insoluble polymers. More complicated expressions for special cases where these conditions are not met have been developed elsewhere^{1,5,3}, and will be tested in *Chapter 5* for the saturation swelling of polybutadiene and poly(styrene-co-acrylonitrile) latex particles by various monomers like styrene and acrylonitrile.

4.6 References

- 1 Ugelstad, J, Hansen, F.K., *Rubber Chem. Technol.*, **49**, 536 (1976)
- 2 Maxwell, I.A., Morrison, B.R., Gilbert, R.G., Napper, D.H., *Macromolecules*, **24**, 1629 (1991)
- 3 Tseng, C.M., El-Aasser, M.S., Vanderhoff, J.W., *ACS, Div. of Org. Coatings Plastics Chem.*, **45**, 373 (1981)
- 4 Ugelstad, J. *et al.*, in *Science and Technology of Polymer Colloids*, NATO ASI Series E, Vol. 1, Plenum, New York (1983)
- 5 Guillot, J., *Acta Polym*, **32**, 593 (1981)
- 6 Chapter 3 of this thesis
- 7 Schoonbrood, H.A.S., *PhD. Thesis*, Eindhoven University of Technology, 1994
- 8 Schoonbrood, H.A.S., Van den Boom, M.A.T., German, A.L., Hutovic, J., *J. Pol. Sci., Part A: Polymer Chemistry*, **32**, 2311 (1994)
- 9 Morton, M., Kaizerman, S., Altier, M.W., *J. Colloid Sci.*, **9**, 300 (1954)

-
- 10 Flory, P.J. in *Principles of Polymer Science*, Cornell University Press, Ithaca, New York 1953
 - 11 Johnson, C.A., *Surface Science*, 3, 429 (1965)
 - 12 Vanzo, E., Marchessault, R.H., Stannett, V., *J. Colloid Sci.*, 20, 65 (1965)
 - 13 Gardon, J.L., *J. Polym. Sci., Polym. Chem. Ed.*, 6, 2859 (1968)
 - 14 Maxwell, I.A., Kurja, J., van Doremale, G.H.J., German, A.L., Morrisen, B.R., *Makromol. Chem.*, 193, 2049 (1992)
 - 15 Aerdt, A.M., Boei, M.M.W.A., German, A.L., *Polymer*, 34, 574 (1993)

CHAPTER 5

Saturation Swelling of Latex Particles

2. Non-Ideal Systems: The Styrene-Acrylonitrile-Butadiene Case

Synopsis: The partitioning of several monomers between the latex particle, monomer droplet and aqueous phases of an emulsion polymer latex are discussed at partial and saturation swelling of the latex particle phase. The monomer and polymer types exhibit a special feature, i.e. the solvent quality of the monomer for the polymer varies. The major part of this chapter has dealt with the saturation swelling of poly(styrene-*co*-acrylonitrile) latex particles by styrene and acrylonitrile or mixtures of both. The experimental partitioning results can be described using the Flory-Huggins lattice theory, which was also successful in previous chapters in describing partial and saturation swelling of ideal systems. A simple empirical relationship is developed whereby the concentration of styrene and acrylonitrile at any ratio can be calculated from the individual saturation concentration of the two monomers in the latex of interest.

5.1 Introduction

Various industrially important and scientifically interesting systems consist of monomer-polymer mixtures which show a non-ideal behavior, i.e. monomer and polymer exhibit strong interactions or in other words the monomer is a non-solvent for the polymer. Industrially important systems which display such a behavior are for instance styrene-acrylonitrile-butadiene (ABS)¹, polyacrylonitrile (PAN)², and polytetrafluoroethylene homo- (PTFE) and copolymers^{3,4}. ABS graft copolymers are often used as impact modifiers in numerous polymer blends. During the preparation of ABS, via an emulsion polymerizations, polybutadiene (PB) seed latex particles are swollen by a mixture of styrene (S) and acrylonitrile (AN), which are subsequently polymerized. This results in a composite latex particle containing styrene-acrylonitrile (SAN) copolymer which is either grafted on PB or present as so-called free polymer. During the polymerization process two phase separation

processes will occur. Firstly, the phase separation between the PB polymer in the seed latex particles and the formed SAN copolymer. Secondly, due to composition drift, the phase separation between SAN copolymers which differ only little in overall chemical composition⁵. Due to the complex phase behavior of this emulsion polymerization process, it is of utmost importance to study and understand the monomer partitioning during the formation of ABS composite latex particles. Concomitantly, the knowledge of the composition of the different phases present during the emulsion polymerization of ABS enables one to develop an effective process control procedure, not only with respect to the rate of polymerization and the chemical composition of the graft and free copolymer formed but also with respect to the final ABS composite latex particle morphology which determines directly the performance of these latex particles in polymer blends.

In the previous chapters, the, saturation as well as partial, swelling behavior of latex particles with monomers has been considered for those systems in which the monomers are good solvents for the polymer in the latex particles and are sparsely water soluble. Some attention has been paid in *Chapter 3* to the partial swelling of latex particles by water miscible monomers and solvents which exhibit strong specific interactions with the polymer in the latex particles. Thus, the swelling of latex particles in these cases is not only determined, to a large extent, by the combinatorial entropy of mixing but also by the enthalpy of mixing. It has been already argued in *Chapter 2* that the Flory-Huggins interaction parameter depends on temperature and copolymer composition. This chapter will deal with the swelling behavior of PB/SAN latex particles mainly by S and AN and mixtures of both. It will be shown that the copolymer composition of the SAN latex particles has a profound effect on the saturation swelling of these particles with monomer(s). Before experimental results on the swelling of PB/SAN latex particles by monomer(s) is discussed, a theoretical frame work will be presented which is used to explain and understand the experimental partitioning results. After this, experimental results on the swelling of PB/SAN latex particles mainly by S and AN and mixtures of both, as reported in literature^{6,7,8,9,10}, will be discussed.

5.2 Theory

Morton *et al.*¹¹ considered the saturation swelling of latex particles by solvent having limited solubility in the water phase. When the swollen latex particle is in equilibrium with the free monomer phase the partial molar Gibbs free energy of the monomer is given by:

$$\Delta G = \Delta G_{\text{mix}} + \Delta G_{\text{surf}} = 0 \quad (5.1)$$

where ΔG is the partial molar Gibbs free energy of monomer, ΔG_{mix} the contribution from the energy of mixing of monomer and polymer, and ΔG_{surf} the contribution from the particle-water interfacial energy. Morton *et al.*¹¹ expressed the free energy of mixing of monomer and polymer in terms of the classical Flory-Huggins theory¹²:

$$\frac{\Delta G_{\text{mix}}}{RT} = \ln(1 - v_p) + v_p \left[1 - \frac{1}{\bar{P}_n} \right] + \chi * v_p^2 \quad (5.2)$$

where v_p is the volume fraction of polymer in the latex particles, \bar{P}_n the number average degree of polymerization, R the gas constant, T the temperature and χ the Flory-Huggins interaction parameter. The interfacial free energy was given in terms of the Gibbs-Thomson equation^{13,14}:

$$\Delta G_{\text{surf}} = \frac{2 * V_m * \gamma * v_p^{1/3}}{R_0} \quad (5.3)$$

where V_m is the partial molar volume of the monomer, γ the particle-water interfacial tension and R_0 the radius of the unswollen latex particle. Combining *equations 5.1, 5.2 and 5.3* gives *equation 5.4*:

$$\ln(1 - v_p) + v_p \left[1 - \frac{1}{\bar{P}_n} \right] + \chi * v_p^2 = - \frac{2 * V_m * \gamma * v_p^{1/3}}{R_0 * RT} \quad (5.4)$$

In the case where there is no separate monomer phase present the partial molar free energy of the aqueous phase has to be taken into account. This can be done by a similar expression as derived for the polymer phase, i.e. via the Flory-Huggins theory. *Equation 5.5* gives the partial molar free energy of monomer in the aqueous phase (ΔG_a):

$$\frac{\Delta G_a}{RT} = \ln \phi_{\text{mon}} + \phi_{\text{water}} * [1 - m_{\text{mon,water}}] + \chi_{\text{mon-water}} * \phi_{\text{water}}^2 \quad (5.5)$$

here ϕ_{mon} and ϕ_{water} represent the volume fraction of monomer and water in the aqueous phase, respectively. $\chi_{\text{mon-water}}$ is the Flory-Huggins interaction parameter between water and the monomer, while $m_{\text{mon,water}}$ is the ratio of the molar volumes of monomer and water.

Vanzo *et al.*¹⁵ were the first to derive an analogue *equation 5.4* that dealt with partial swelling of latex particles utilizing a simpler equation for the partial molar free energy of the aqueous phase. In doing so, they assumed that the monomer containing aqueous phase could be considered as a dilute solution of monomer and water. Later, Gardon¹⁶ derived the same expression. If the latex particles are not saturated by monomer then there is no pure monomer phase present (i.e. no monomer droplets). The partial molar free energy of the monomer in the aqueous phase is then given by:

$$\Delta G = RT * \ln a \quad (5.6)$$

where a is the activity of the monomer. Vanzo *et al.* pointed out that the monomer activity can be approximated by p/p_0 , i.e. the ratio of the vapor pressure of the monomer at a given volume fraction of polymer (p) to the vapor pressure at saturation swelling (p_0). Gardon showed that, since Henry's Law holds for latex free water, the ratio p/p_0 can be approximated by the ratio of the monomer concentration in the aqueous phase below and at saturation:

$$\frac{p}{p_0} = \frac{[M]_{\text{aq}}}{[M]_{\text{aq,sat}}} \quad (5.7)$$

where $[M]_{aq}$ is the concentration of monomer in the aqueous phase and $[M]_{aq,sat}$ is the saturation concentration of monomer in the aqueous phase. The final result for partial swelling of latex particles by monomer and solvents, hereafter called the Vanzo equation, is:

$$\ln(1 - v_p) + v_p \left[1 - \frac{1}{\bar{P}_n} \right] + \chi * v_p^2 + \frac{2 * V_m * \gamma * v_p^{1/3}}{R_0 * RT} = \ln \left[\frac{[M]_{aq}}{[M]_{aq,sat}} \right] \quad (5.8)$$

When the monomer swollen latex particle are swollen by two monomers, the partial molar free energy (or the chemical potential), of each of the monomers will be equal in each of the three phases.

$$\Delta G_{p,i} = \Delta G_{d,i} = \Delta G_{a,i} \quad (5.9)$$

where $\Delta G_{p,i}$, $\Delta G_{d,i}$, and $\Delta G_{a,i}$ represent the partial molar Gibbs free energy of monomer i in the latex particles, monomer droplet, and aqueous phase, respectively. The partial molar free energy of monomer i with polymer in the presence of a second monomer j is given by *equation 5.10*:

$$\begin{aligned} \frac{\Delta G_{p,i}}{RT} = & \ln v_{p,i} + (1 - m_{ij}) * v_{p,j} + v_p + \chi_{ij} * v_{p,j}^2 + \chi_{ip} * v_p^2 \\ & + v_{p,j} * v_p * (\chi_{ij} + \chi_{ip} - \chi_{jp} * m_{ij}) + \frac{2 * V_{m,i} * \gamma * v_p^{1/3}}{R_0 * RT} \end{aligned} \quad (5.10)$$

where $v_{p,i}$ and $v_{p,j}$ are the volume fractions of monomer i and j in the latex particles, respectively. χ_{ij} the interaction parameter between monomers i and j , and χ_{ip} and χ_{jp} are the interaction parameters between each of the respective monomers i and j and polymer. The term m_{ij} is the ratio of the molar volumes of monomers i and j (i.e. $m_{ij} = V_{m,i} / V_{m,j}$, where $V_{m,i}$ and $V_{m,j}$ are the molar volumes of monomer i and j , respectively). \bar{P}_n is the number average degree of polymerization, R the gas constant, T the temperature and χ the Flory-Huggins interaction parameter. V_m is the partial molar volume of the monomer, γ the particle-water interfacial tension and R_0 the unswollen radius of the latex particle. The partial molar free

energy of monomer i in the droplets ($\Delta G_{d,i}$) can also be calculated from the Flory-Huggins lattice theory.

$$\frac{\Delta G_{d,i}}{RT} = \ln v_{d,i} + v_{d,j} * [1 - m_{ij}] + \chi_{ij} * v_{d,j}^2 \quad (5.11)$$

In this equation $v_{d,i}$ represents the volume fraction of monomer i in the droplets, and $v_{d,j}$ the volume fraction of monomer j in the droplets. The use of *equation 5.11* assumes that the lattice model is valid for mixtures of small molecules: this may be valid for two organic monomers. Note also, that due to the normally large size of monomer droplets, contributions from the monomer droplet-water interfacial free energy in *equation 5.11* have not been taken into account (this assumption may not be valid for a system containing very small monomer droplets). The partial molar free energy of the monomer in the aqueous phase is given by ^{15,16,17,}

$$\frac{\Delta G_{a,i}}{RT} = \ln \left[\frac{[M_i]_{aq}}{[M_i]_{aq,sat}} \right] \quad (5.12)$$

where $[M_i]_{aq}$ is the concentration of monomer i in the aqueous phase and $[M_i]_{aq,sat}$ is the saturation concentration of monomer i in the aqueous phase. Combining *equations 5.9, 5.10, 5.11, and 5.12*, the following equation for monomer i is found:

$$\begin{aligned} & \ln v_{p,i} + (1 - m_{ij}) * v_{p,j} + v_p + \chi_{ij} * v_{p,j}^2 + \chi_{ip} * v_p^2 \\ & + v_{p,j} * v_p * (\chi_{ij} + \chi_{ip} - \chi_{jp} * m_{ij}) + \frac{2 * V_{m,i} * \gamma * v_p^{1/3}}{R_0 * RT} = \end{aligned} \quad (5.13)$$

$$\ln v_{d,i} + (1 - m_{ij}) * v_{d,j} + \chi_{ij} * v_{d,j}^2 = \ln \left[\frac{[M_i]_{aq}}{[M_i]_{aq,sat}} \right]$$

Similarly, for monomer j , *equation 5.14* can be found:

$$\ln v_{p,j} + (1 - m_{ji}) * v_{p,i} + v_p + \chi_{ji} * v_{p,i}^2 + \chi_{jp} * v_p^2 + v_{p,j} * v_p * (\chi_{ji} + \chi_{jp} - \chi_{ip} * m_{ji}) + \frac{2 * V_{m,j} * \gamma * v_p^{1/3}}{R_0 * RT} = \quad (5.14)$$

$$\ln v_{d,j} + (1 - m_{ji}) * v_{d,i} + \chi_{ji} * v_{d,i}^2 = \ln \left[\frac{[M_j]_{aq}}{[M_j]_{aq,sat}} \right]$$

Equations 5.13 and 5.14 can be used to predict and/or model partitioning data for latex systems with two monomers as discussed in the previous chapter¹⁸.

5.3 Experimental Partitioning Results and Discussion

The monomer partitioning during the preparation of ABS graft copolymers is a complex process which is governed by several phenomena such as the interaction between different monomer-polymer and monomer-monomer pairs. Especially, the occurrence of phase separation yields composite particles exhibiting good toughening properties. Due to the complexity of the swelling behavior of ABS latex particles, the swelling behavior of PB and SAN latex particles with S and AN and mixtures of both will be discussed below.

5.3.1 Partial Swelling of PB Particles by One Monomer

The partial swelling behavior of PB latices has not been studied extensively in literature. Hergeth and Cordella⁸ reported on the partial swelling of PB latex particles by AN as studied by Raman spectroscopy (see *figure 5.1*). The measurement of the partitioning behavior of acrylonitril between the aqueous phase and PB latex particles is based on the solvent-induced frequency shift of the nitrile stretching vibration in AN present in the aqueous phase and the polymer phase. Aerdtts *et al.*¹⁹, on the other hand, studied the partial swelling of PB particles by methyl methacrylate (*figure 5.1*), for different latex particle sizes and crosslinking densities (expressed as gel content). As can be seen from *figure 5.1*, AN swells PB latex particles to a lesser extent than methyl methacrylate does. This can be explained by the fact that AN is a poor solvent for PB, while methyl methacrylate can be designated as a

good solvent, which is reflected in the value of the Flory-Huggins interaction parameter between monomer and polymer, as will be discussed in *section 5.4.1*.

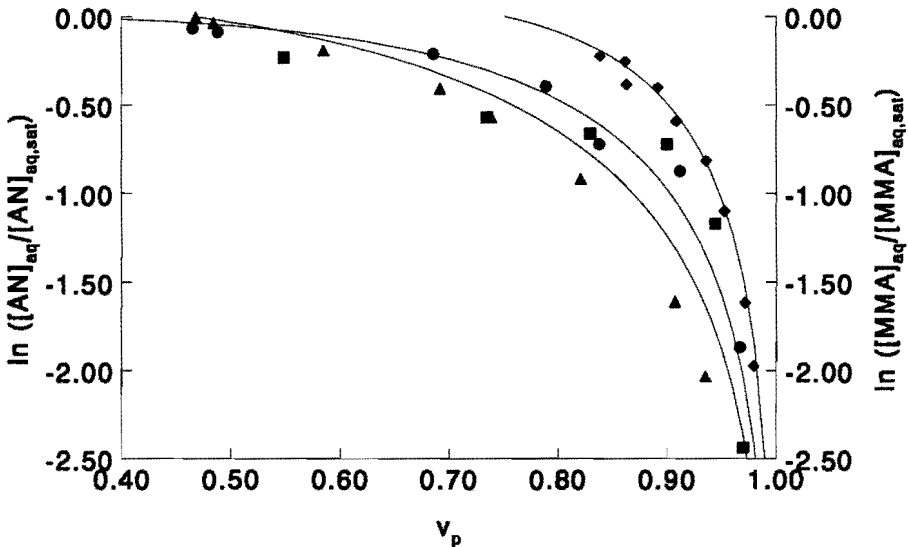


Figure 5.1 Comparison of experimentally measured monomer partitioning of AN and methyl methacrylate for PB latices differing only by their mean unswollen particle radii. The diamonds represent the swelling of a PB latex ($R_0 = 107$ nm) with AN as reported by Hergeth and Cordella⁸. The circles, squares, and triangles represent the swelling of PB latices with methyl methacrylate with a mean unswollen radius of 105 nm, 105 nm, and 150 nm, respectively, as reported by Aerdts et al.¹⁹. The upper solid line represent a fit of equation 5.8, with $\chi = 1.17$ and $\gamma = 45$ mN/m. The solid line in the middle represent a fit to the data of Aerdts et al. By equation 5.8 with $\chi = 0.53$ and $\gamma = 45$ mN/m. While the lower solid line utilized equation 5.15/5.16 with a corr. term = 0.163.

5.3.2 Saturation Swelling of PB and SAN Latex Particles by One Monomer

Figure 5.2 represents the saturation swelling of PB latices with different radii and by different monomers as reported in literature. As can be seen from this figure, the radius of the PB latex has a profound effect on the saturation concentration of monomer in the monomer swollen latex particles. The saturation concentration of styrene (S), methyl methacrylate as well as butadiene can be relatively well described by *equation 5.4* using a value of χ equal to 0.5 and a value of γ in the range of 20 to 45 mN/m. AN has a lower saturation concentration which can be attributed to a high Flory-Huggins interaction parameter with PB than the other three monomers (see also *figure 5.1* and *section 5.4.1*).

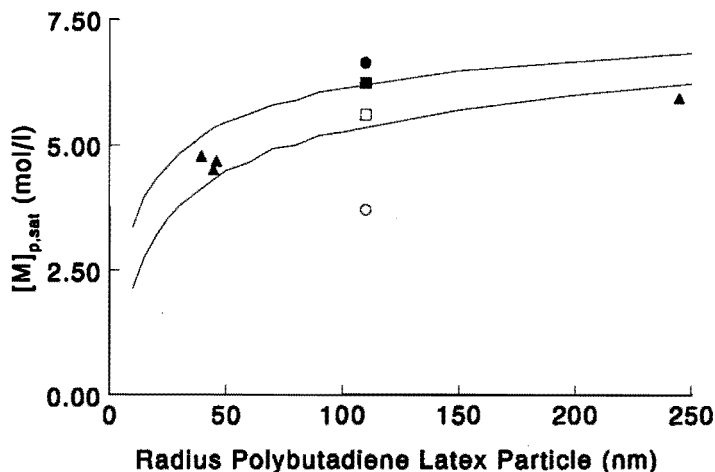


Figure 5.2 Comparison of experimentally measured saturation concentration of different monomers for polybutadiene (PB) latices differing only by their mean unswollen particle radii. The closed triangles represent the saturation concentration of S in different PB particles as reported by Mathey and Guillot⁹. The closed circle and closed square, the saturation concentration of S and methyl methacrylate, respectively, as reported by Aerdtz *et al.*¹⁹. The open square represents the saturation concentration of butadiene as reported by Maxwell *et al.*²⁰. While the open circle is the saturation concentration of AN in PB calculated from experimental data from Hergeth and Cordella⁸ using equation 5.4. The solid lines represent model calculation using equation 5.4, with $\chi = 0.5$ and $\gamma = 20$ mN/m (upper line) and $\gamma = 45$ mN (lower line)

Nomura *et al.*⁶ reported recently on the swelling behavior of SAN copolymer in the latex particles by S and AN and mixtures of both. In *figure 5.3*, the saturation concentration of S and AN in monomer swollen latex particles is shown as a function of the mole fraction of AN in the SAN copolymer in the latex particles. A remarkable observation is the fact that the saturation concentration of S and AN in the SAN latex particles depends strongly on the AN content in the SAN copolymer.

5.3.3 Saturation Swelling of SAN Latex Particles by Two Monomers

In this section the saturation swelling of latex particles, with different chemical compositions, by different monomers is considered. In *figure 5.4* experimental data on the partitioning of S and AN between the latex particle and monomer droplet phases for a variety of seed latices, with different (co)polymer compositions, are displayed.

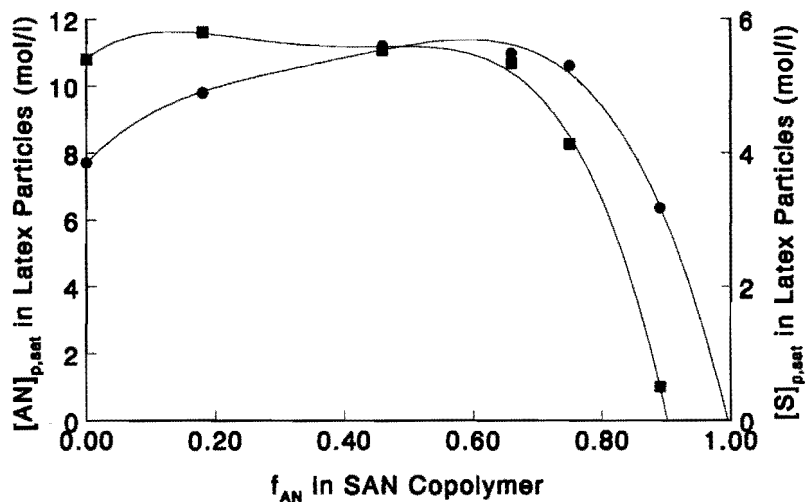


Figure 5.3 Saturation concentration of S (squares) and acrylonitrile (circles) in SAN latex particles versus the fraction of AN in the SAN copolymer. Lines are to guide the eye.

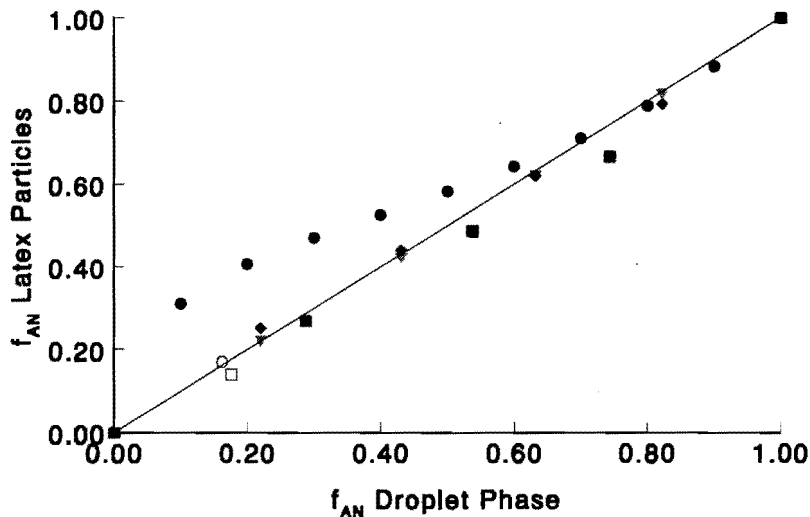


Figure 5.4 Experimentally determined mole fraction of AN in the latex particles as a function of the mole fraction of AN in the droplet phase. Polystyrene latex (squares), SAN (82, 54, and 34 mole-% S) (triangles), SAN (25 mole-% S) (diamonds), and SAN (11 mole-% S) (circles) at 50 °C. As reported by Nomura et al.⁶ The open circle and open square represent a SAN latex with a composition of 100 and 67 mole-% S, respectively, as reported by Dimonie et al.¹⁰ Solid line: theoretical prediction according to equations 5.18 and 5.19.

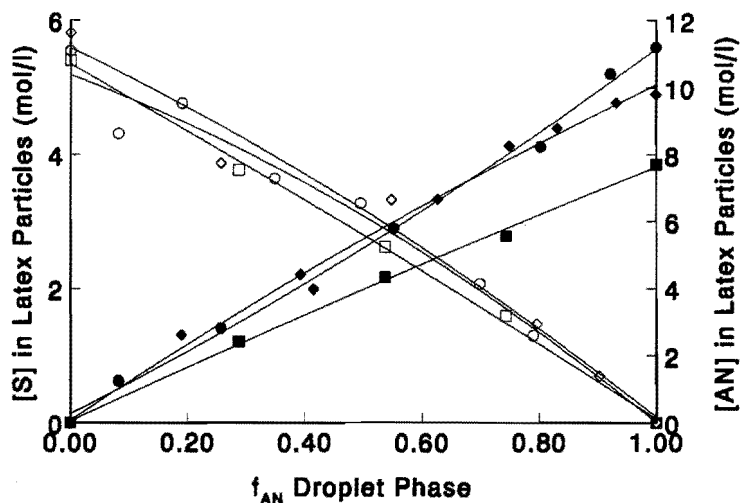


Figure 5.5 Experimentally determined monomer concentrations in the latex particles as a function of the volume fraction of AN in the droplet phase. The open symbols represent the concentration of S in the latex particles and the closed symbols the concentration of AN in the latex particles. Polystyrene latex (squares), SAN (18 mole-% AN) (diamonds) SAN (46 mole-% AN) (circles) at 50°C. Experimental data taken from Nomura et al. ⁶. Lines are to guide the eye.

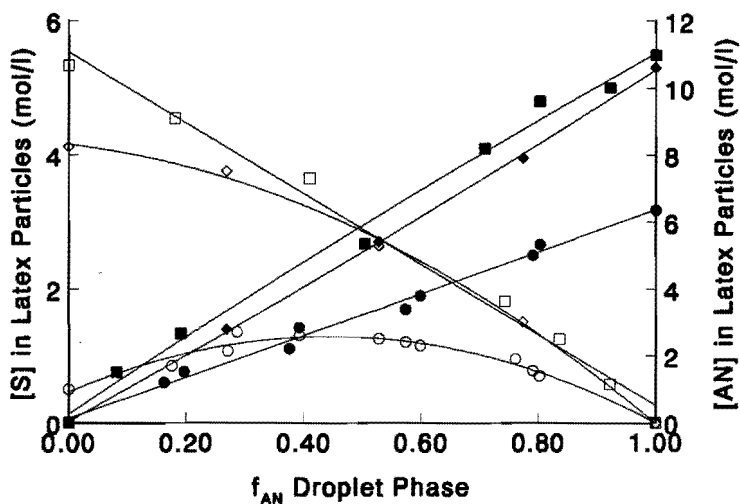


Figure 5.6 Experimentally determined monomer concentrations in the latex particles as a function of the volume fraction of AN in the droplet phase. The open symbols represent the concentration of S in the latex particles and the closed symbols the concentration of AN in the latex particles. SAN (66 mole-% AN) (squares), SAN (75 mole-% AN) (diamonds) SAN (89 mole-% AN) (circles) at 50°C. Experimental data taken from Nomura et al. ⁶. Lines are to guide the eye.

It is the actual concentration of the monomers in the latex particles that is of interest, especially with respect to the kinetics of the polymerization process, *viz.* the rate of polymerization and the chemical composition of the copolymer formed are directly related to the concentration of the different monomers in the latex particles. In *figures 5.5, 5.6, and 5.7*, the concentration of S and AN, in various latex particle phases are plotted versus the mole fraction of one of the monomers in the droplet phase.

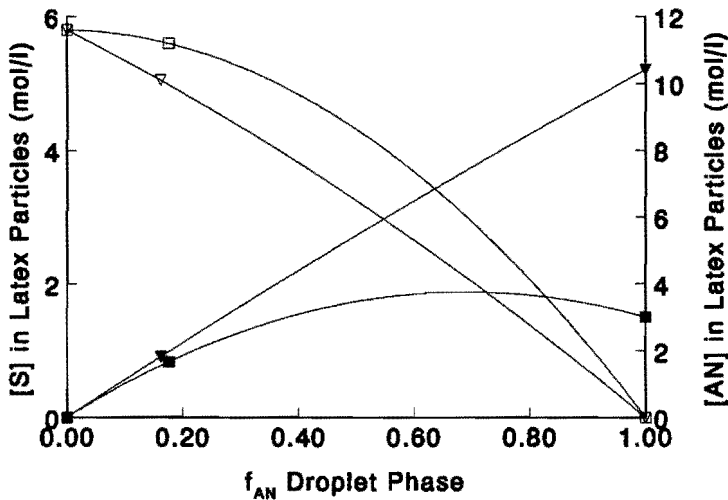


Figure 5.7 Experimentally determined monomer concentrations in the latex particles as a function of the volume fraction of AN in the droplet phase. The open symbols represent the concentration of S in the latex particles and the closed symbols the concentration of AN in the latex particles. Polystyrene (squares), and SAN (33 mole-% AN) (triangles) at 55 °C. Experimental data taken from Dimonie *et al.*¹⁰. Lines are to guide the eye.

From *figures 5.5, 5.6, and 5.7*, it is apparent that the absolute saturation concentration of S and AN in the latex particles depends not only on the copolymer composition but also on the composition of the monomer mixture. Upon increasing the AN content of the SAN copolymer, the saturation concentration of S and AN in the latex particles decreases, as is clearly shown in *figure 5.6*, but also in *figures 5.5 and 5.7* for polystyrene latex particles.

5.4 Modeling and Prediction of Monomer Partitioning in Non-Ideal Latex Systems

In this section an attempt will be made to explain and predict experimental partitioning data utilizing simple thermodynamic and semi-empirical relationships which were successful in the modeling and prediction the swelling behavior of ideal latex particles (see also *Chapters 3 and 4*)

5.4.1 Partial Swelling of PB Latices by One Monomer

The modeling and prediction of the partial swelling of latex particles by one monomer has been extensively discussed in *Chapter 3*. The partial swelling behavior of a latex can be considered in two ways. First, via the introduction of a correction term. This correction term embraces the enthalpy of mixing and the particle-water interfacial free energy terms in the Vanzo equation from the saturation swelling volume fraction of polymer ($v_{p,sat}$), as envisaged by *equations 5.15 and 5.16* utilizing the Morton equation (see also *Chapter 3*).

$$\text{Corr.} = - [\ln(1 - v_{p,sat}) + v_{p,sat}] \quad (5.15)$$

This correction can be implemented in the Vanzo equation (*equation 5.8*):

$$\ln(1 - v_p) + v_p + \text{Corr.} = \ln \left[\frac{[M]_{aq}}{[M]_{aq,sat}} \right] \quad (5.16)$$

Note that, for simplicity, the contribution of the number average number degree of polymerization upon the partial molar free energy of mixing of monomer and polymer in *equation 5.15 and 5.16* has been neglected (i.e. $\bar{P}_n \gg 1$). In *figure 5.1*, the lower solid line represent a fit of the partial swelling of a PB latex with methyl methacrylate as reported by Aerdts *et al.*¹⁹. Relatively good agreement is obtained between the experimental results and the model prediction according to *equations 5.15 and 5.16*. The discrepancy between experimental results and model prediction has been discussed in *Chapter 3*, and can be attributed to the fact that the dependency of the Flory-Huggins interaction parameter and the interfacial tension on the volume fraction of polymer in the monomer swollen latex particles is not taken into account. As has been shown in *Chapter 3*, crosslink density has only a minor

effect on the swelling behavior of latex particles unless the degree of polymerization between chemical crosslinks is very low typically in the order of 10. The only other difference in the monomer swollen PB latices is the particles size distribution. Since it is not known how the characteristics of the PB latex particles change with size it is hard to make a solid statement about the observed swelling behavior.

An alternative way of modeling/predicting the partial swelling behavior of latex particles is via *equation 5.8*. However, before *equation 5.8* can be used values for the Flory-Huggins interaction parameter and the particle-water interfacial tension have to be known or estimated. The Flory-Huggins interaction parameter may be evaluated from solubility parameters as discussed in *Chapter 2*, according to *equation 5.17*:

$$\chi_{1,2} = \left(\frac{V_1}{RT} \right) (\delta_{\text{monomer}} - \delta_{\text{polymer}})^2 \quad (5.17)$$

where $\chi_{1,2}$ represents the Flory-Huggins interaction parameter between monomer and polymer. δ_{monomer} and δ_{polymer} represent the Hildebrand solubility parameter for solvent and polymer, respectively. V_1 is the molar volume of a lattice segment, which in this case is equal to the molar volume of the monomer. Utilizing the method of group contributions²¹, solubility parameters of AN, methyl methacrylate and PB can be calculated. In doing so, values for the solubility parameter of 22.7, 19.2, and 17.1 (J/cm³)^{1/2} are obtained for AN, methyl methacrylate, and PB, respectively. This results in Flory-Huggins interactions parameters of 1.17 and 0.53 for AN-PB and methyl methacrylate-PB, respectively. In other words, AN is a poor solvent for PB which is expressed by a lower concentration of AN in the monomer swollen PB latex particles than one would expect when the swelling behavior would be governed solely by the entropy of mixing (see *figure 5.1*). Methyl methacrylate, on the other hand, is a relatively good solvent for PB, which is also observed experimentally. Using a value of 45 mN/m (see *Chapter 3*) for the interfacial tension between PB latex particles and water, the upper and middle solid line in *figure 5.1* are obtained which are in good agreement with experimental results. Please note that the particle-water interfacial free energy term has only little effect on the *partial* swelling of latex particles and a more profound effect on the *saturation* swelling (see also *Chapter 3*).

5.4.2 Saturation Swelling by One Monomer

The saturation swelling of PB latices by several monomers is depicted in *figure 5.2* as function of the radius of the PB latex particles. As is shown in this figure, the saturation concentration of monomer in the monomer swollen latex particles can be described using *equation 5.4*, for a given value of χ , i.e. 0.5, and two different values of the particle-water interfacial tension (γ), i.e. 20 (upper line) and 45 mN/m (lower line). The experimental data can be understood by utilizing *equation 5.4* and the previously mentioned values of χ and γ . In the case of acrylonitrile, a lower saturation concentration is obtained due to the higher value of χ between AN and PB.

The saturation swelling of SAN copolymer latices with S and AN strongly depends on the chemical composition of the SAN copolymer, i.e. on the fraction of AN in the copolymer. This can be related to the fact that the Flory-Huggins interaction parameter depends on the chemical composition of the copolymer present in the latex particles. The observed phenomenon can be related to polymer blends of a homopolymer and a statistical copolymer in which the internal copolymer segmental “repulsion” often influences the mixing of the homopolymer and the copolymer. Kambour *et al.*²² and Ten Brinke *et al.*²³ have derived an expression for the Flory-Huggins interaction parameter (χ) of a polymer blend containing a homopolymer A and a copolymer BC, as is shown by *equation 5.18*:

$$\chi = v_B * \chi_{AB} + (1 - v_B) * \chi_{AC} - v_B * (1 - v_B) * \chi_{BC} \quad (5.18)$$

where v_B is the volume fraction of monomer B in the pure copolymer BC, and χ_{AB} , χ_{AC} , and χ_{BC} the Flory-Huggins interaction parameters between the different segments. The presence of a miscibility window in certain blends of homopolymers and copolymers follows simply from *equation 5.18*. It results from the fact that the net Flory-Huggins interaction parameter is a quadratic function of the copolymer composition. The shape and location of the miscibility window are determined by the difference in interaction strength between the segments in the homopolymer and the two different segments in the copolymer as denoted by the different Flory-Huggins interaction parameters in *equation 5.18*. By assuming now that the degree of polymerization of homopolymer A is one, while at the same time $A = C$, a model is obtained for the Flory-Huggins interaction parameter of a copolymer AB which is mixed with

one of its monomers (A or B). For solutions of monomer A or B with copolymer AB to be homogeneous, χ has to smaller than 0.5 (see also *Chapter 2*). This simplification leads for the system SAN-S-AN to *equation 5.19* for SAN-S and *equation 5.20* for SAN-S.

$$\chi_{S-SAN} = v_S * \chi_{S-PS} + (1-v_S) * \chi_{S-PAN} - v_S * (1-v_S) * \chi_{PS-PAN} \quad (5.19)$$

$$\chi_{AN-SAN} = v_S * \chi_{AN-PS} + (1-v_S) * \chi_{AN-PAN} - v_S * (1-v_S) * \chi_{PS-PAN} \quad (5.20)$$

The definition of the different Flory-Huggins interaction parameters is obvious from their subscripts.

Table 5.1 Values for different Flory-Huggins interaction parameter

	χ_{S-PS}	0.47 ^a		
	χ_{S-PAN}	2.11 ^a		
	χ_{AN-PAN}	1.50 ^a		
	χ_{AN-PS}	0.65 ^a		
	χ_{PS-PAN}	2.87 ^a		
			Styrene	Acrylonitrile
v_S in SAN	χ^b	χ^c	χ^b	χ^c
1	0.47	0.47	0.68	0.68
0.88	0.39	0.36	0.52	0.55
0.66	0.44	0.38	0.38	0.53
0.56	0.48	0.48	0.41	0.61
0.36	0.67	0.86	0.45	0.94
0.17	2.11	1.43	0.79	1.47

a calculated from solubility parameters as reported by van Krevelen²¹

χ^b calculated utilizing *equation 5.4*, with $\gamma = 45$ mN/m, from experimental data as reported by Nomura *et al.*⁶

χ^c calculated utilizing *equation 5.19* and *5.20*, from experimental data as reported by Nomura *et al.*⁶

By calculating χ_{S-PS} , χ_{S-PAN} , and χ_{PS-PAN} using solubility parameters²¹, the Flory-Huggins interaction parameter of styrene-SAN copolymer (χ_{S-SAN}) can be determined and compared with the value obtained from fitting *equation 5.4* (with $\gamma = 45$ mN/m) to experimental data (see *figure 5.8*).

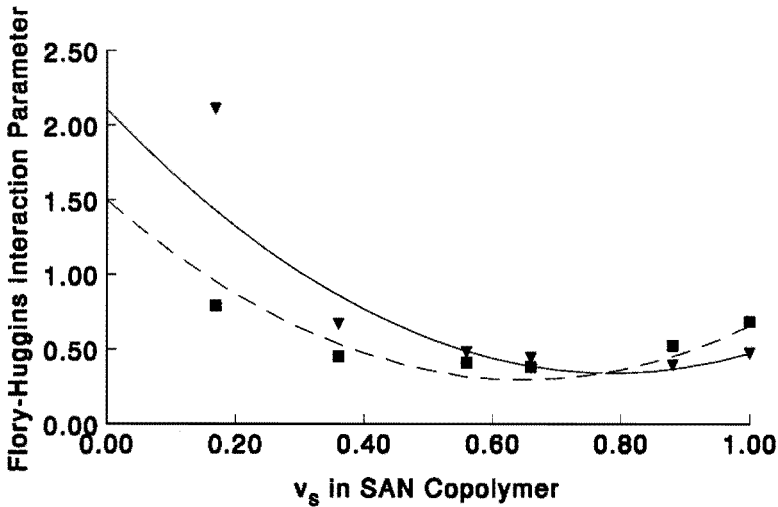


Figure 5.8 Flory-Huggins interaction parameter as function of the volume fraction styrene in the SAN copolymer. The squares represent χ obtained from experimental data (calculated via equation 5.4, with $\gamma = 45$ mN/m) for the saturation swelling of SAN copolymer latices by AN. The dashed line is the theoretical prediction according to equation 5.18. The triangles represent χ obtained from experimental data (calculated via equation 5.4, with $\gamma = 45$ mN/m) for the saturation swelling of SAN copolymer latices by S. The solid line is the theoretical prediction according to equation 5.18. Experimental data taken from Nomura et al. ⁶.

The same can be done for acrylonitrile. Table 5.1 contains the values of the different Flory-Huggins interaction parameters as calculated via equations 5.19 and 5.20 and obtained by fitting equation 5.4 to the experimental data shown in figure 5.3. Excellent agreement is obtained between the values of the Flory-Huggins interaction parameter calculated by equations 5.19 and 5.20 and the values derived from experimental results using equation 5.4. This result is indicative for the occurrence of “repulsion” between styrene and acrylonitrile segments in the copolymer and styrene or acrylonitrile monomer segments during the saturation swelling of SAN copolymer latices with styrene or acrylonitrile.

5.4.3 Saturation Swelling by Two Monomers

In this section an approach for the swelling of SAN latex particles by S and AN will be given. In doing so, a comparison will be made with the saturation swelling of ideal latices by two monomers (see Chapter 4). Further, a method will be presented for the

estimation/prediction of the absolute monomer concentration in latex particles which resembles the method for the saturation swelling of ideal systems.

Part 1: Monomer fractions in the latex particle phase and droplet phase

In this part the assumptions made to simplify *equations 5.13* and *5.14* for ideal latex systems (see *Chapter 4*) will be tested for the system currently under investigation, i.e. the saturation swelling of SAN latex particles by S and AN:

1. For many pairs of monomer, the difference between the molar volumes of the monomers is small, as in the case of the systems studied in *Chapter 4*. However, in the case of S (monomer *i*) and AN (monomer *j*), m_{ij} is equal to 1.75. Therefore this assumption becomes questionable for the current system.

2. The contribution to the partial molar free energy arising from the residual (enthalpic and non-conformational entropic) partial molar free energy of the mixing of the two monomers is small relative to all other terms in the expressions describing the partial molar free energy of monomers in the droplet phase (see *equation 5.11*). This is due to fact that the Flory-Huggins interaction parameter between monomer *i* and *j* is relatively small in the case of many pairs of monomer (see *table 5.2*).

Table 5.2 *Flory-Huggins interaction parameters for different pairs of monomer^a*

χ Styrene-Methyl Acrylate	0.35
χ Styrene-Methyl Methacrylate	0.34
χ Styrene-Butyl Methacrylate	0.34
χ Styrene-Acrylonitrile	1.05
χ Acrylonitrile-Styrene	0.73

^a calculated from solubility parameters as reported by van Krevelen²¹

Again, in the case of S and AN deviation from this behavior is observed. Please note that for two low molar mass components to become immiscible, $\chi \geq 2$ (see also *Chapter 2*).

If the above two assumption are valid and applied to *equations 5.21* and *5.22*, the right hand equalities of these equation can be simplified:

$$v_{d,i} = \frac{[M_i]_{aq}}{[M_i]_{aq,sat}} \quad (5.21)$$

$$v_{d,j} = \frac{[M_j]_{aq}}{[M_j]_{aq,sat}} \quad (5.22)$$

Equations 5.21 and 5.22 are simply in the form of Henry's law, which has been shown to hold for partially water soluble organic solvents/monomers in the absence of latex particles^{16,17} for pairs of monomer for which assumption 1 and 2 hold (see Chapter 4). Figure 5.9 clearly shows that equations 5.21 and 5.22 do not hold for the system currently under investigation, as already could be anticipated from the fact that assumptions 1 and 2 are not valid for the monomer pair styrene-acrylonitrile. In figure 5.9, the experimental partitioning data of S and AN between the aqueous phase and the monomer droplet phase are fitted by the right hand equalities in equation 5.13 and 5.14, utilizing values for the different parameters as mentioned in the legend of figure 5.9. As can be seen from this figure, the experimental partitioning data of AN can be predicted by equation 5.13/5.14. The S partitioning data, on the other hand, is relatively well described for the data of Dimonie *et al.* but poorly for the data of Nomura *et al.* This can be due to the fact that in the case of Dimonie *et al.* latex particles were present while in the case of Nomura *et al.* latex particles were not present. For the systems discussed in Chapter 4 the presence of latex particles did not influence the partitioning behavior of the monomers between the aqueous phase and the monomer droplet phase. The difference could be attributed to the fact that the Flory-Huggins interaction parameter for S-AN is rather high compared with many other pairs of monomer, indicating the existence of strong interactions between these monomers. In which case the Flory-Huggins theory is not that convenient anymore for describing this particular system. The exact reason for this difference in partition behavior, however, is yet unknown. Further, it could be argued whether equation 5.12 can describe the partial molar free energy of AN in the aqueous phase in a satisfactory way like it can for sparingly water soluble monomers, since AN exhibits a relatively high water solubility, but is not completely water miscible, while at the same time it can also form hydrogen bonds with water. Finally, the interaction parameter between S and AN probably depends on the volume fraction of S or AN in the monomer droplet phase and is not evaluated as such.

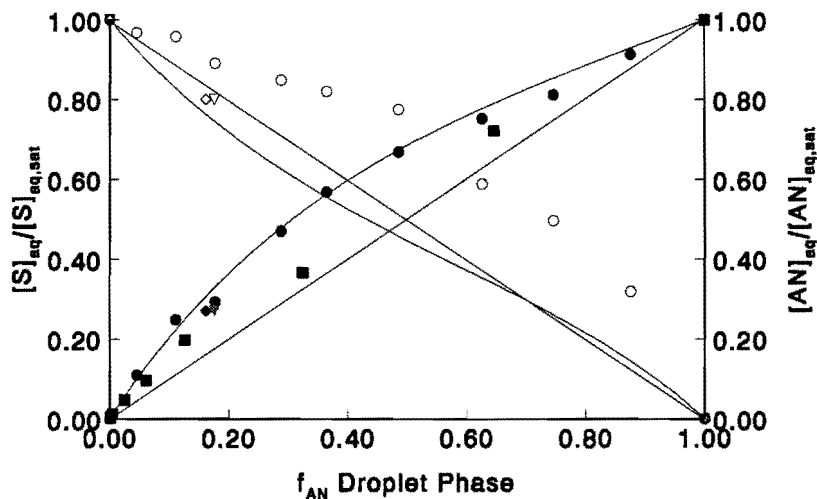


Figure 5.9 Experimentally determined S (open symbols) and AN (closed symbols) concentration in the aqueous phase as a function of the volume fraction of AN in the droplet phase with S as the comonomer. Circles as reported by Nomura et al. ⁶ in the absence of latex particles, squares as reported by Guillot ⁷ unknown whether latex particles were present, and diamonds and triangles reported by Dimonie et al. ¹⁰ in the presence of latex particles. The solid lines represent a fit according to equations 5.21 and 5.22. The curved lines represent a fit of right hand equalities of equation 5.13 and 5.14, with $m_{ij} = 1.75$, $m_{ji} = 0.57$, $\chi_{ij} = 1.05$, and $\chi_{ji} = 0.40$.

In the case of the saturation swelling of ideal latex systems a third assumption was made to model the partition behavior of the two monomers between the different phases:

3. The Flory-Huggins interaction parameter for each monomer with the same polymer was assumed almost equal, while at the same time both monomers are good solvents for the polymer in the latex particles. In the current case, the solvent quality of S and AN depends on the copolymer composition of the SAN copolymer in the latex particles. For SAN copolymers with low AN content *both* S and AN are good solvents, while for SAN copolymer with AN content, S and AN are *both* poor solvents for the polymer in the latex particles (see also *table 5.1*).

Applying assumptions 1, 2, and 3, to equations 5.13 and 5.14, the following simple equation is obtained:

$$\frac{v_{p,i}}{v_{p,j}} = \frac{v_{d,i}}{v_{d,j}} \quad (5.23)$$

Equation 5.23 relates the ratios of the volume fractions (or concentrations) of monomers i and j in the latex particles to those in the droplet phase. From *equation 5.23* the following equalities can be written:

$$f_{p,i} = f_{d,i} \quad (5.24)$$

$$f_{p,j} = f_{d,j} \quad (5.25)$$

where $f_{p,i}$, $f_{d,i}$, $f_{p,j}$, and $f_{d,j}$ represent the monomer volume fraction of monomers i and j in the droplet and particle phases, respectively. Note that in the latex particle phase these monomer fractions relate only to the volume of one monomer as a fraction of the total volume of both monomers in the particles (i.e. the volume of the polymer in the latex particles is not included in these fractions). When assumption 1 is valid, the monomer volume fractions also represent the monomer molar fractions.

In *figure 5.4* experimental data on the partitioning of S and AN between the latex particle and monomer droplet phases for a variety of seed latices, with different (co)polymer compositions, are displayed. As can be seen clearly from this picture, the partitioning of S and AN between the SAN copolymer latices and the monomer droplet phase can be accurately described by *equations 5.24* and *5.25* for SAN copolymers with an AN content ranging from 18 to 66 mole-% AN. In the case of a polystyrene and, especially, SAN (89 mole-% AN) copolymer latex, *equations 5.24* and *5.25* are not so successful in describing the partitioning of S and AN between the latex particle and monomer phase. As already discussed in *section 5.4.2*, the dependency of the swelling of SAN copolymer latices on the chemical composition of the copolymer is indicative for the occurrence of “repulsion” between the different monomer segments in the copolymer and different monomers. Especially, the swelling of the SAN copolymer latex with a high AN content (89 mole-% AN) exhibits the features of preferential solvation as discussed by Locatelli and Riess²⁴, i.e. the presence of styrene in the SAN latex particles promotes the solubility of AN in these monomer swollen latex particles

and vice versa. This preferential solvation itself is probably due to the dependency of the different Flory-Huggins interaction parameters on the volume fraction of copolymer in the latex particles, chemical composition of the copolymer in the latex particle, as well as on the composition of the monomer mixture in the same latex particles.

In an attempt to quantify to what extent the different assumptions discussed above contribute to the deviation from pseudo-ideal behavior, i.e. fulfillment of *equations 5.24* and *5.25*, the same approach will be used as by Maxwell *et al.*²⁵, who performed a sensitivity analysis with respect to the earlier mentioned assumptions. In doing so, every assumptions will be dealt with separately in such a way that the other assumptions are assumed to be valid. At the same time the experimental data represented in *figure 5.4*, more specifically in the case of polystyrene and SAN copolymer (89 mole-% AN), will be modeled.

Assumption 3: Let us assume that assumptions **1** and **2** are valid and that assumption **3** does not hold. This is the case in the current system as has been shown in this section for the polystyrene and SAN copolymer (89 mole-% AN) latices swollen by S and AN. For the intermediate compositions, assumption **3** seemed to be valid as discussed above. If assumption **3** is not made, *equations 5.13* and *5.14* reduce to *equation 5.26*:

$$\ln \left[\frac{v_{p,i}}{v_{p,j}} \right] - \ln \left[\frac{v_{d,i}}{v_{d,j}} \right] = v_p * [\chi_{jp} - \chi_{ip}] \quad (5.26)$$

In *figures 5.10* and *5.11*, the solution of *equation 5.26* is shown for a given set of values for the different parameters, for a polystyrene and SAN copolymer (89 mole-% AN) latex, respectively (see *Table 5.3*).

In the case of the swelling of the polystyrene latex (see *figure 5.10*), assumption **3** causes only a small concave deviation from the ideal behavior. While for the SAN copolymer latex (see *figure 5.11*), assumption **3** gives a large convex deviation from the ideal behavior. Both cases can be easily understood, since the difference between χ_{ip} and χ_{jp} is small in the case of polystyrene and large for the SAN copolymer.

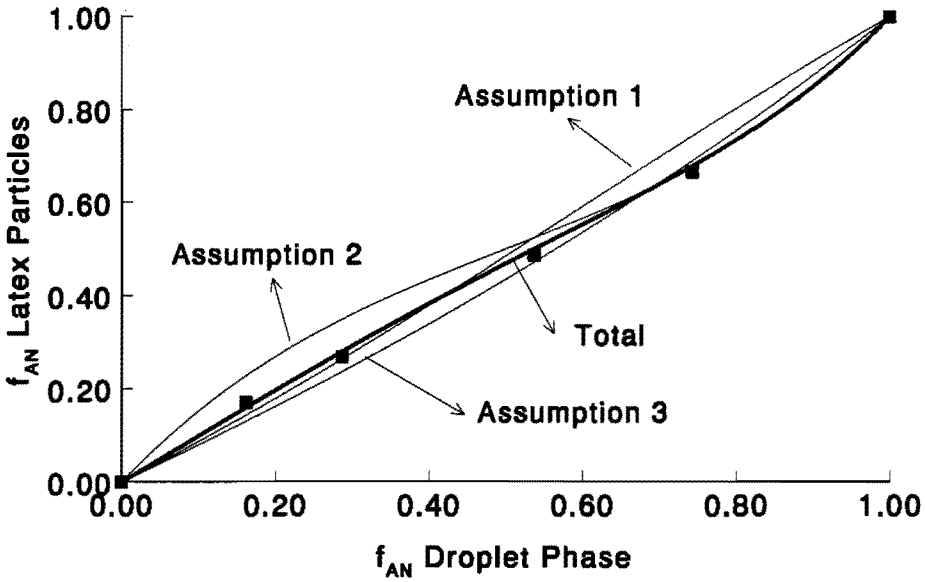


Figure 5.10 Modeling of the partitioning of AN between the monomer droplet phase and the monomer swollen polystyrene latex particles, with S as the co-monomer. Symbols represent experimental data taken from Nomura et al. ⁶.

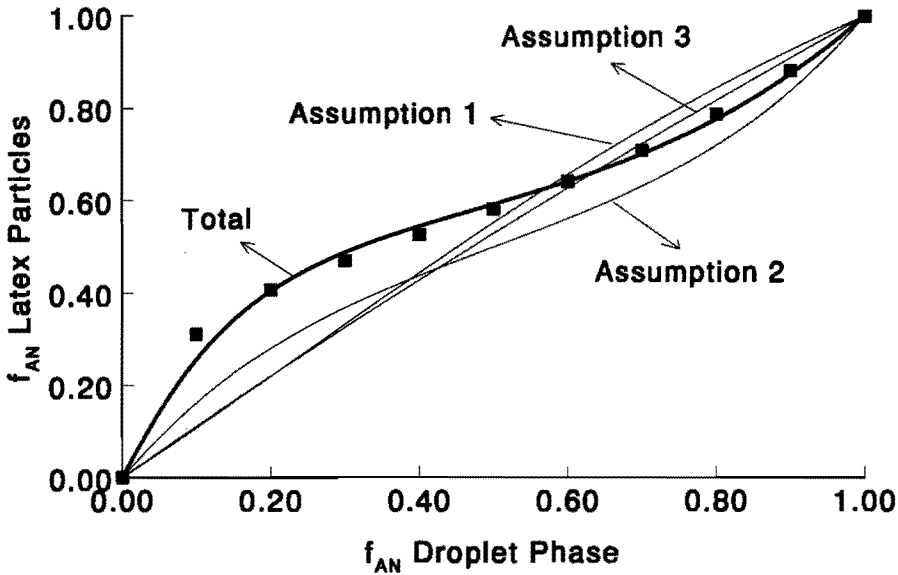


Figure 5.11 Modeling of the partitioning of AN between the monomer droplet phase and the monomer swollen SAN (89 mole-% AN) copolymer latex particles, with S as the co-monomer. Symbols represent experimental data taken from Nomura et al. ⁶.

Assumption 2: Let us assume that assumptions 1 and 3 are valid and that assumption 2 is not. In other words, the mixing of the monomers is not only governed by the configurational entropy of mixing but also by the enthalpy of mixing. On the basis of solubility parameters, the interaction parameter between styrene (monomer i) and acrylonitrile (monomer j), and vice versa, can be calculated (see section 5.4.2). This results in a value for χ_{ij} of 1.05 (see table 5.3).

Table 5.3 Parameters used in equations 5.26, 5.27, and 5.28

	Polystyrene latex	SAN (89 mole-% AN) latex
χ_{ij}	1.05	1.05
χ_{ip}	0.47	0.8
χ_{jp}	1.0	0.9
χ_{ji}	0.40	1.8
v_p	0.41	0.59
.....		
m_{ij}		1.75
m_{ji}		0.57
R_0	100	nm
$V_{m,i}$	115	ml/mole
$V_{m,j}$	65.8	ml/mole
γ	45	mN/m
T	293	K

By accepting assumptions 1 and 3, equations 5.13 and 5.14 give equation 5.27:

$$\ln \left[\frac{v_{p,i}}{v_{p,j}} \right] - \ln \left[\frac{v_{d,i}}{v_{d,j}} \right] = \chi_{ij} \left[(v_{d,j} - v_{d,i}) - (v_{p,j} - v_{p,i}) \right] \quad (5.27)$$

In figures 5.10 and 5.11, the solution of equation 5.27 is shown for a given set of values for the different parameters, for a polystyrene and SAN copolymer (89 mole-% AN) latex, respectively (see table 5.3 for the value of the different parameters used for the calculation). For both, the polystyrene as well as the SAN copolymer latex, assumption 2 gives a strong deviation from the ideal behavior. At low volume fractions AN in the droplet phase this deviation is concave with respect to the ideal behavior, while at higher fractions AN the deviation is concave.

Assumption 1: This assumption states that the molar volumes of the monomers are equal, which is definitely not the case for styrene and acrylonitrile (see *table 5.3*). Therefore, assumption 1 is not accepted here and assumptions 2 and 3 are. In doing so, *equation 5.28* is obtained.

$$\ln \left[\frac{v_{p,i}}{v_{p,j}} \right] - \ln \left[\frac{v_{d,i}}{v_{d,j}} \right] =$$

$$(1-m_{ij})(v_{d,j} - v_{p,j} - v_p * v_{p,j} * \chi_{ip}) - (1-m_{ji})(v_{d,i} - v_{p,i} - v_p * v_{p,i} * \chi_{ip}) \quad (5.28)$$

$$+ \frac{2 * (V_{m,j} - V_{m,i}) * \gamma * v_p^{1/3}}{R_o * RT}$$

Again in *figures 5.10* and *5.11*, the solution of *equation 5.28* is shown for a given set of values for the different parameters, for a polystyrene and SAN copolymer (89 mole-% AN) latex, respectively. As is observed for assumption 3, assumption 1 gives a small concave deviation from ideal behavior in the case of the polystyrene latex (see *figure 5.10*) and a larger convex deviation for the SAN copolymer latex (see *figure 5.11*).

Both, in *figure 5.10* as in *figure 5.11*, the fraction of AN in the monomer swollen latex particles ($f_{AN,part}$) as a function of the fraction of AN in the monomer droplet phase ($f_{AN,drop}$) (note that these fractions are taken on monomer basis) has been modeled without taken assumption 1, 2, and 3 into account, i.e. by simply calculating $f_{AN,part}$ and $f_{AN,drop}$ from *equations 5.13* and *5.14*, for the given set of parameters shown in *table 5.3* (denoted as *Total* in *figures 5.10* and *5.11*). Excellent agreement between experiment and theory is obtained. It should be emphasized that the solution to *equations 5.13* and *5.14*, as depicted in *figures 5.10* and *5.11*, are **not** super-positions of *equations 5.26*, *5.27*, and *5.28*.

In conclusion, it can be said that the deviation from ideal swelling behavior is mainly caused by the invalidity of assumption 2. Again it is shown that a simple model based on the classical Flory-Huggins theory is capable of describing not only the saturation swelling behavior of ideal latex systems, but also the saturation swelling behavior of non-ideal latex systems, like the SAN-S-AN system. Further, it has been shown that via *equations 5.13* and

5.14, the fraction of monomer i and j in the monomer droplet phase and the fraction of monomer i and j in the latex particle phase can be determined/calculated. However, the calculation/prediction of the monomer concentration in the aqueous phase is not possible, using *equations 5.13* and *5.14*, as discussed.

Part 2: Monomer concentrations in the latex particles

In *Chapter 4* a method was discussed via which the concentration of monomer i in the latex particles could be predict as a function of the fraction of monomer i in the monomer droplet phase. The basis of this approach are the following experimental observations: **1.** The total monomer concentration in the monomer swollen latex particles is just equal to the sum of the concentrations of the individual monomers. **2.** The total monomer concentration is a virtually linear function of the fraction of the monomers in the droplet phase. The two experimental observations are a result of the fact that the fraction of monomer i in the monomer droplet phase is equal to the fraction of monomer i in the monomer swollen latex particles, which are implemented in *equations 5.13* and *5.14* via assumption **1**, **2**, and **3**, made in the previous part of this section, and result in *equation 5.23*, *5.24*, and *5.25* (see also *Chapter 4*). All that is required to predict the concentration of monomer i and j in the latex particles is the saturation concentrations of monomer i and j in the latex particles when they exclusively swell the particular latex, i.e. during “homo-swelling”. Hence, for a particular seed latex the concentration of monomer i within the particles (C_i) as a function of the fraction of monomer i in the droplets is given by:

$$C_i = f_{d,i} * [(C_{i,m} - C_{j,m}) * f_{d,i} + C_{j,m}] \quad (5.29)$$

Similarly, for monomer j the following expression is found:

$$C_j = f_{d,j} * [(C_{j,m} - C_{i,m}) * f_{d,j} + C_{i,m}] \quad (5.30)$$

where $C_{i,m}$ and $C_{j,m}$ are the maximum saturation concentrations of monomers i and j in the latex particles during homo-swelling, respectively. The assumptions made to arrive at *equations 5.29* and *5.30* are not applicable to the system currently under investigation (see

previous part of this section). The linear relationship between the volume fraction of AN in the monomer droplet phase and the monomer swollen latex particles for SAN copolymers with AN contents of 18, 46, 66, and 75 mole-% AN, does not originate from the validity of assumptions 1, 2, and 3, but probable more from a coincidental cancellation of different effects. Further, the polystyrene latex and the SAN copolymer latex with a AN content of 89 mole-% exhibit a strong deviation from equations 5.23, 5.24, and 5.25 as discussed in the previous part of this section. However, in figures 5.12 and 5.13, predictions of equations 5.29 and 5.30 are compared with experimental data as presented in figures 5.5 and 5.6. Poor agreement is obtained between prediction and experimental results.

In figures 5.14 and 5.15, on the other hand, the monomer concentration in the latex particles is not plotted as a function of the volume fraction of AN in the droplet phase (f_{AN}) but as a function of the mole fraction of AN in the droplet phase (n_{AN}).

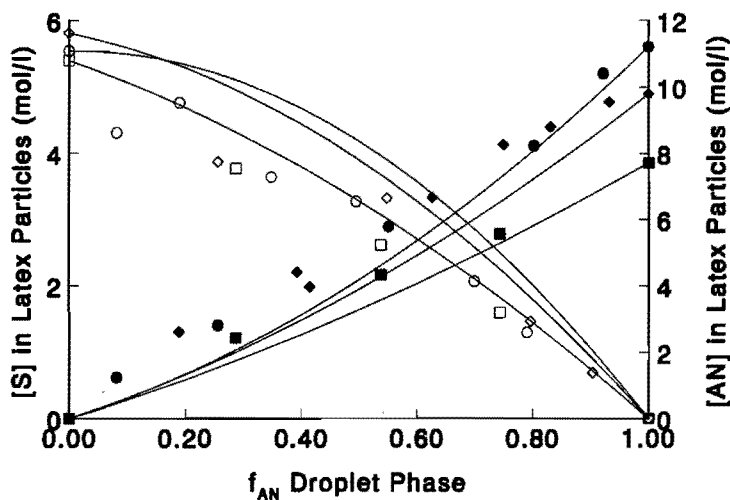


Figure 5.12 Experimentally determined monomer concentrations in the latex particles as a function of the volume fraction of AN in the droplet phase. The open symbols represent the concentration of S in the latex particles and the closed symbols the concentration of AN in the latex particles. Polystyrene latex (squares), SAN (18 mole-% AN) (diamonds) SAN (46 mole-% AN) (circles) at 50 °C. Solid lines are predictions according to equations 5.29 and 5.30. Experimental data taken from Nomura et al. ⁶.

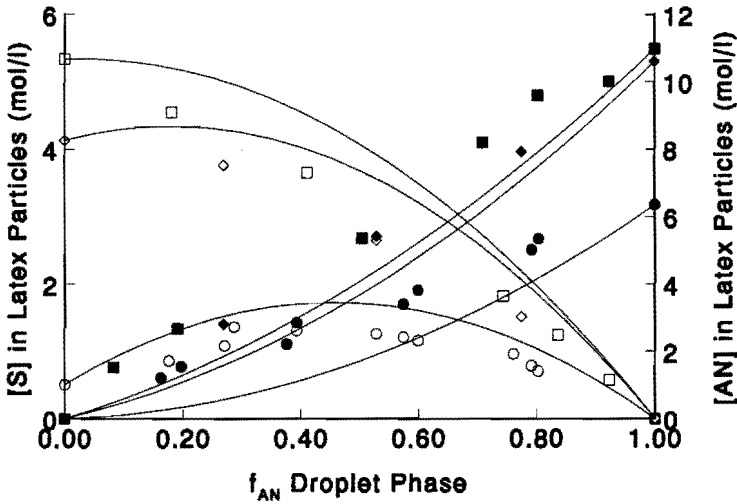


Figure 5.13 Experimentally determined monomer concentrations in the latex particles as a function of the volume fraction of AN in the droplet phase. The open symbols represent the concentration of S in the latex particles and the closed symbols the concentration of AN in the latex particles. SAN (66 mole-% AN) (squares), SAN (75 mole-% AN) (diamonds) SAN (89 mole-% AN) (circles) at 50 °C. Solid lines are predictions according to equations 5.29 and 5.30. Experimental data taken from Nomura et al. ⁶.

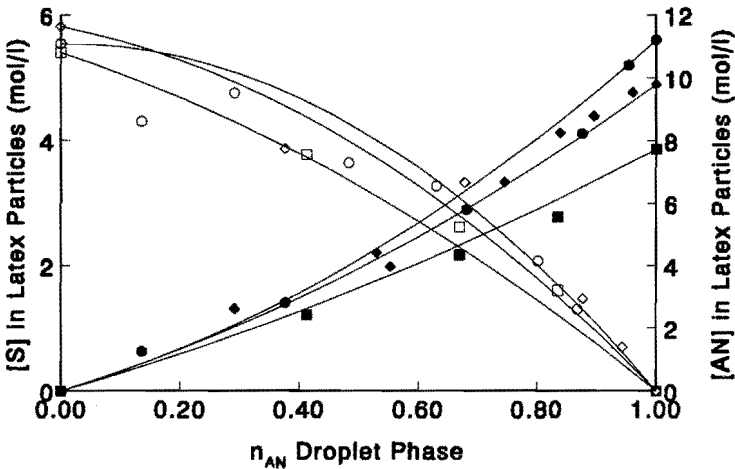


Figure 5.14 Experimentally determined monomer concentrations in the latex particles as a function of the mole fraction of AN in the droplet phase. The open symbols represent the concentration of S in the latex particles and the closed symbols the concentration of AN in the latex particles. Polystyrene latex (squares), SAN (18 mole-% AN) (diamonds) SAN (46 mole-% AN) (circles) at 50 °C. Solid lines are predictions according to equations 5.31 and 5.32. Experimental data taken from Nomura et al. ⁶.

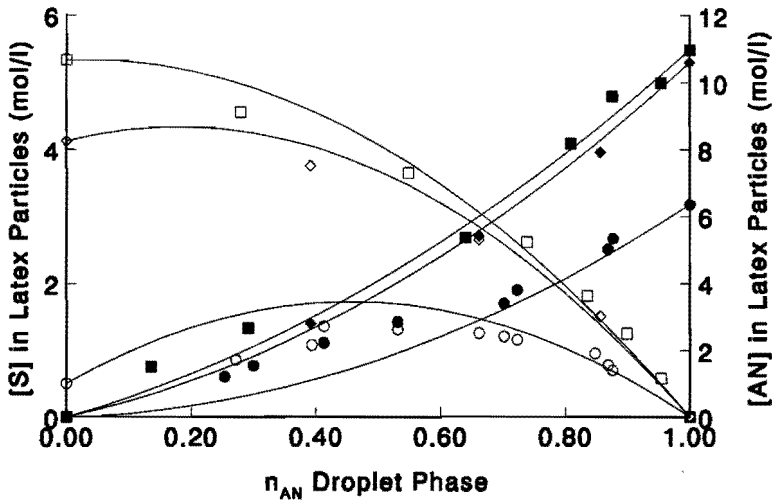


Figure 5.15 Experimentally determined monomer concentrations in the latex particles as a function of the mole fraction of AN in the droplet phase. The open symbols represent the concentration of S in the latex particles and the closed symbols the concentration of AN in the latex particles. SAN (66 mole-% AN) (squares), SAN (75 mole-% AN) (diamonds) SAN (89 mole-% AN) (circles) at 50 °C. Solid lines are predictions according to equations 5.31 and 5.32. Experimental data taken from Nomura et al. ⁶.

By substituting f_{AN} by n_{AN} , equations 5.31 and 5.32 are obtained for AN and S, respectively.

$$[AN] = n_{AN} * \left[([AN]_m - [S]_m) * n_{AN} + [S]_m \right] \tag{5.31}$$

$$[S] = (1 - n_{AN}) * \left[([S]_m - [AN]_m) * (1 - n_{AN}) + [AN]_m \right] \tag{5.32}$$

Therefore, if the maximum saturation concentrations of S ($[S]_m$) and AN ($[AN]_m$) in the latex particles during homo-swelling are known the S and AN concentration in the latex particles can be calculated as a function of the mole fraction of AN or S in the monomer droplet phase utilizing equations 5.31 and 5.32.

5.5 Concluding Remarks

It has been shown in this chapter that the Flory-Huggins lattice theory is not only successful in the description and prediction of the saturation swelling of ideal systems, i.e. latex systems in which the monomer is a good solvent for the polymer and has only a limited water solubility (see *Chapter 4*), but also for systems in which the monomer is a poor(er) solvent for the polymer. In the case of the ideal systems several assumption were made to simplify the expressions for the chemical potential of the monomer(s) in the different phases. In doing so, it was shown that the mixing of polymer and monomer(s) in these systems is mainly governed by the entropy of mixing. In the non-ideal systems studied in this chapter, the assumptions made in the case of the ideal systems are not valid any more as has been shown extensively in *section 5.4*. Further, it has been shown that the swelling of non-ideal systems is not only determined by the entropy of mixing but also by the enthalpy of mixing. Another important factor is the non-athermal mixing of styrene and acrylonitrile. Finally, the results of this chapter are of considerable importance for the emulsion polymerization field since, if general, they allow simple predictions of both the monomer ratio and concentrations in each of the three phases present during an emulsion polymerization.

5.6 References

- 1 Utracki, L.A., *Polymer Eng. and Sci.*, **35**, 2 (1995)
- 2 McCarthy, S.J., Elbing, E.E., Wilson, I.R., Gilbert, R.G., Napper, D.H., and Sangster, D.F., *Macromolecules*, **19**, 2440 (1986)
- 3 Putnam, R.E., in "Comprehensive Polymer Science", Edited by G.C. Eastmond, A. Ledwith, S. Russo and P. Sigwalt, Vol. 3, pp 321-326, Pergamon Press, Oxford (1989)
- 4 Murray, D.L., and Piirma, I., *Macromolecules*, **26**, 5577 (1993)
- 5 Molau, G.E., *J. Pol. Sci.*, **A3**, 4235, (1965)
- 6 Nomura, M., Liu, X., Ishitani, K., and Fujita, K., *J. Pol. Sci.*, **32**, 2491 (1994)
- 7 Guillot, J., *Makromol. Chemie, Suppl.*, **10/11**, 165 (1985)
- 8 Hergeth, W.D., and Codella, P.J., *Appl. Spectroscopy*, **48(7)**, 900 (1994)
- 9 Mathey, P, and Guillot, J., *Polymer*, **32**, 934 (1991)
- 10 Dimonie, V., El-Aasser, M.S., Klein, A., and Vanderhoff, J.W., *J. Pol. Sci.*, **22**, 2197 (1984)
- 11 Morton, M., Kaizerman, S., Altier, M.W., *J. Colloid Sci.*, **9**, 300 (1954)
- 12 Flory, P.J. in *Principles of Polymer Science*, Cornell University Press, Ithaca, New York 1953
- 13 Ugelstad, J. *et al.*, in *Science and Technology of Polymer Colloids*, NATO ASI Series E, Vol. 1, Plenum, New York (1983)
- 14 Johnson, C.A., *Surface Science*, **3**, 429 (1965)

-
- 15 Vanzo, E., Marchessault, R.H., Stannett, V., *J. Colloid Sci.*, 20, 65 (1965)
 - 16 Gardon, J.L., *J. Polym. Sci., Polym. Chem. Ed.*, 6, 2859 (1968)
 - 17 Maxwell, I.A., Kurja, J., van Doremaele, G.H.J., German, A.L., Morrisen, B.R., *Makromol. Chem.*, 193, 2049 (1992)
 - 18 Chapter 4 of this thesis
 - 19 Aerdt, A.M., Boei, M.M.W.A., and German, A.L., *Polymer*, 34, 574 (1993)
 - 20 Maxwell, I.A., Verdurmen, E.M.F.J., and German, A.L., *Makromol. Chem.*, 193, 2677 (1992)
 - 21 Krevelen van, D.W., "*Properties of Polymers: Their Estimation and Correlation with Chemical Structure*", Elsevier, New York (1976)
 - 22 Kambour, R.P., Bendler, J.T., and Bopp, R.C., *Macromolecules*, 16, 753 (1983)
 - 23 Ten Brinke, G., Karasz, F.E., and MacKnight, W.J., *Macromolecules*, 16, 1827 (1983)
 - 24 Locatelli, J.L., and Riess, G., *Polymer Lett.*, 11, 257 (1973)
 - 25 Maxwell, I.A., Noel, L.F.J., Schoonbrood, H.A.S., and German, A.L., *Makromol. Chem., Theory Simul.*, 2, 269 (1993)

CHAPTER 6

Phase Diagrams of Emulsion Polymerization Systems

Synopsis: In this chapter phase diagrams have been constructed for the visualization of the partial and saturation swelling of emulsion polymer latices by one or two monomers. The influence of different factors such as the latex particle radius, Flory-Huggins interaction parameter, and the saturation concentration of the monomer in the aqueous phase have been considered. Further, it has been shown that these phase diagrams can also be used in the visualization of seeded as well as *ab initio* emulsion homopolymerization. Finally, the phase rule has been revisited with respect to the heterogeneous systems containing curved phases (latices) as discussed in this chapter.

6.1 Introduction

A convenient way of representing the phase behavior of multi-component systems is via phase diagrams. In the case of binary phase diagrams the x-axis represents the composition of the binary mixture while the y-axis gives for instance the absolute temperature. In *Chapter 2*, various binary phase diagrams have been discussed for amorphous and semi-crystalline polymers with solvents of different solvent quality. In this chapter, the main focus will be on ternary and quaternary phase diagrams which are of interest in visualizing the phase behavior of emulsion homo- and copolymerizations. In literature, to the best of our knowledge, no attempts have been made to construct phase diagrams of emulsion polymerization systems. One of the major advantages of using phase diagrams is the fact that the phase behavior of the emulsion polymerization process, i.e. monomer partitioning during an emulsion polymerization, is visualized, rather than only being represented by equations as has been done in *Chapters 3, 4, and 5*, which are often not easily accessible.

An approach introduced by Scott ¹ to visualize phase equilibria in ternary systems containing at least one polymer will be used to construct phase diagrams of the swelling behavior of latices by one or two monomers. First, the ternary phase diagram for the swelling of a seed latex by one monomer (static system) will be discussed. After this, the swelling of a seed latex by two monomers (static system) will be described using quaternary phase diagrams. Finally, the phase behavior of a seeded and *ab initio* emulsion homopolymerization (dynamic system) will be discussed utilizing the previously developed ternary phase diagrams. It could be argued whether latices and monomer containing latices are thermodynamically (meta)stable phases. However, it is not the objective of this chapter to elucidate whether this is the case. Therefore, the term phase diagram, or maybe more conveniently phase maps, is used here merely as a synonym for the visualization of the phase behavior of latices swollen by one or two monomers. Nevertheless, in *appendix A (section 6.7)* a rationalization is given for the phase rule for systems containing curved phases, showing that the phase diagrams constructed in this chapter obey this rule.

6.2 Ternary Phase Diagrams

When the phase behavior of a Polymer (P)-Liquid 1 (L1)-Liquid 2 (L2) system is considered ¹, several different situations can be encountered depending on the compatibility of the different components, i.e. the binary systems P-L1, P-L2, and L1-L2 and the ternary system P-L1-L2. This compatibility can be expressed via the Flory-Huggins interaction parameters χ_{P-L1} , χ_{P-L2} , and χ_{L1-L2} . In principle it is possible that a polymer that is insoluble in L1 and L2, dissolves in a mixture of L1-L2. The partial molar free energy of L1, L2, and P are given by *equation 6.1, 6.2, and 6.3, respectively.*

$$\frac{\Delta G_{L1}}{RT} = \ln v_{L1} + (1 - m_{L1-L2}) * v_{L2} + v_P + \chi_{L1-L2} * v_{L2}^2 + \chi_{L1-P} * v_P^2 + v_{L2} * v_P * (\chi_{L1-L2} + \chi_{L1-P} - \chi_{L2-P} * m_{L1-L2}) \quad (6.1)$$

$$\frac{\Delta G_{L2}}{RT} = \ln v_{L2} + (1 - m_{L2-L1}) * v_{L1} + v_P + \chi_{L2-L1} * v_{L1}^2 \quad (6.2)$$

$$+ \chi_{L2-P} * v_P^2 + v_{L1} * v_P * (\chi_{L2-L1} + \chi_{L2-P} - \chi_{L1-P} * m_{L2-L1})$$

$$\frac{\Delta G_P}{RT} = \ln v_P - (\bar{P}_n - 1)(v_{L1} + v_{L2}) + \bar{P}_n * \chi_{L1-P} * v_{L1}^2 \quad (6.3)$$

$$+ \bar{P}_n * \chi_{L2-P} * v_{L2}^2 + \bar{P}_n * (\chi_{L1-P} + \chi_{L2-P} - \chi_{L1-L2} * v_{L1} * v_{L2})$$

where v represent the volume fraction of either component L1, L2, or P as indicated by the subscript. \bar{P}_n is the number average degree of polymerization of the polymer, while m gives the ratio of the molar volumes of the components indicated in the subscript. The equilibrium ternary phase diagrams can be calculated utilizing equations 6.1, 6.2, and 6.3. In any two-phase system, the thermodynamic condition for equilibrium requires that the partial molar free energy (chemical potential) of each component should be equal in both phases. As already stated before, the interaction between the different components in the ternary system determine the phase behavior of the total system. Scott¹ discussed extensively the phase behavior for various situations and calculated the corresponding ternary phase diagrams. In order to simplify the calculation of the phase diagrams, it was assumed that one phase did not contain any polymer. Concomitantly, the tie lines end on the L1-L2 edge of the triangle (for more details see Scott¹).

6.3 Ternary Phase Diagrams of Emulsion Polymerization Systems:

The Swelling of Latex Particles by One Monomer

Systems which resemble the phase behavior as discussed in the previous section are emulsion homopolymerizations. In which case the monomer and water are sparsely miscible, polymer and water are immiscible, while, at the same time, there is no polymer dissolved in the aqueous phase. However, a major difficulty in using phase diagrams for the visualization of emulsion polymerization systems is the fact that the polymer is present as latex particles of a certain dimension, which results in a limited solubility of the monomer in the polymer phase

although the Flory-Huggins interaction parameter is often smaller than 0.5. This is caused by the contribution of the interfacial free energy to the residual free energy of mixing, which has to equal the conformational entropy of mixing to attain thermodynamic equilibrium during swelling (see also *Chapters 3 and 4*). By taking the interfacial free energy of the polymer phase into account, the partial molar free energy of L1 and L2 in the polymer phase can be expressed by *equations 6.4 and 6.5*.

$$\frac{\Delta G_{L1}}{RT} = \ln v_{L1} + (1 - m_{L1-L2}) * v_{L2} + v_P + \chi_{L1-L2} * v_{L2}^2 + \chi_{L1-P} * v_P^2 + \quad (6.4)$$

$$v_{L2} * v_P * (\chi_{L1-L2} + \chi_{L1-P} - \chi_{L2-P} * m_{L1-L2}) + \frac{2 * V_{m,L1} * \gamma * v_P^{1/3}}{R_0 * RT}$$

$$\frac{\Delta G_{L2}}{RT} = \ln v_{L2} + (1 - m_{L2-L1}) * v_{L1} + v_P + \chi_{L2-L1} * v_{L1}^2 + \chi_{L2-P} * v_P^2 + \quad (6.5)$$

$$v_{L1} * v_P * (\chi_{L2-L1} + \chi_{L2-P} - \chi_{L1-P} * m_{L2-L1}) + \frac{2 * V_{m,L2} * \gamma * v_P^{1/3}}{R_0 * RT}$$

where, $V_{m,L1}$ and $V_{m,L2}$ represent the molar volumes of L1 and L2, respectively. R_0 and γ are the radius of the unswollen latex particle and the particle-water interfacial tension, respectively. It is obvious that in latex systems not only the enthalpy of mixing restricts the miscibility of polymer and solvents, but also the interfacial free energy of the particle-water interface.

6.3.1 Definition of Edges and Axis in Ternary Phase Diagrams of Latices Swollen by One Monomer

As already pointed out in the introductory section, ternary phase diagrams of emulsion polymerization systems are very uncommon. In order to create a framework for the development of phase diagrams for emulsion polymerization systems, the phase behavior of a latex swollen by one monomer will be discussed. In doing so, first, the different axes of such ternary phase diagrams will be discussed (see *figure 6.1*). Second, the different coexisting phases will be considered (see *figure 6.2*).

Water-Monomer axis (line A): This axis represents in fact the aqueous phase. In conventional emulsion polymerization systems, the monomers used have low water solubilities. In that case, phase separation will occur at a certain overall composition. A' on line A represents an aqueous phase saturated with monomer. Systems exhibiting overall compositions between A' and *Monomer* will phase separate in two separate phases, i.e. a pure monomer phase and a monomer saturated aqueous phase (A'). For overall compositions between *Water* and A' no phase separation will occur.

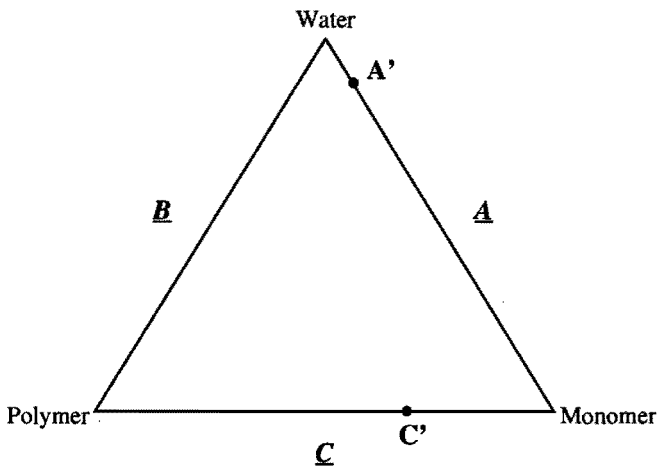


Figure 6.1 Schematic ternary phase diagram of a latex swollen by one monomer: definition of axes and edges

Polymer-Water axis (line B): Line B in figure 6.1 represents a system in which complete phase separation occurs in pure polymer and water. Which, in fact, is the case for a latex.

Polymer-Monomer axis (line C): As has been shown in the previous chapters, latex particles do not swell infinitely with monomer, but at a certain point equilibrium will be reached where the free energy of mixing polymer and monomer in the latex particle is equal to the surface free energy of the monomer swollen latex particle (see equations 6.4 and 6.5), for sparsely water soluble monomers. Upon adding more monomer a separate, a pure monomer phase will be formed. The composition of the *Monomer-Polymer* is restricted by two factors.

First, the interaction between monomer and polymer expressed via the Flory-Huggins interaction parameter. Second, the interfacial free energy of the monomer swollen polymer phase has to be taken into account via the radius of the polymer particle and the latex particle-water interfacial tension. In *figure 6.1* this situation is represented by C' . Systems with an overall composition between C' and *Polymer* will be homogeneous, i.e. the monomer concentration in the latex particle is below its saturation value. However, for compositions between C' and *Monomer*, phase separation will occur in a pure monomer phase and a phase C' consisting of a latex particle saturated with monomer.

Let us consider now the simple case of a polymer latex swollen by one sparingly water soluble monomer. When a latex is swollen by one monomer two regions can be distinguished with respect to the monomer content in the particle and aqueous phase, i.e. partial and saturation swelling (see also *Chapters 3* and *4*, respectively). During partial swelling, the ternary system consists of a monomer swollen polymer phase and a monomer containing aqueous phase, which are the coexisting phases. It has been shown in *Chapter 3* that at thermodynamic equilibrium the partial molar free energy of the monomer in the latex particle phase is equal to the partial molar free energy of the monomer in the aqueous phase, and is represented by *equation 6.6*. In fact, the left hand side of *equation 6.6* represents the composition of the *Polymer-Monomer* phase and the right hand side the composition of the *Monomer-Water* phase.

$$\ln(1-v_p) + v_p \left[1 - \frac{1}{P_n} \right] + \chi^* v_p^2 + \frac{2 * V_{m,L2} * \gamma^* v_p^{1/3}}{R_0 * RT} = \ln \left[\frac{[L2]_{L1}}{[L2]_{L1,sat}} \right] \quad (6.6)$$

where $[L2]_{L1}$ is the concentration of L2 (monomer) in L1 (water) and $[L2]_{L1,sat}$ is the saturation concentration of L2 in L1. During saturation swelling, there are three phases present, i.e. latex particles saturated with monomer, the monomer saturated aqueous phase, and a separate pure monomer phase. It has been shown in *Chapter 4* that in the case of thermodynamic equilibrium the partial molar free energy of the monomer is equal in all phases and is represented by *equation 6.7*.

$$\ln(1 - v_p) + v_p \left[1 - \frac{1}{P_n} \right] + \chi * v_p^2 = - \frac{2 * V_{m,L2} * \gamma * v_p^{1/3}}{R_0 * RT} \quad (6.7)$$

In figure 6.2, the results of equation 6.6 and 6.7 are schematically represented. Let us consider a latex to which a certain amount of monomer is being added, i.e. we are following the line *Latex-Monomer* in figure 6.2.

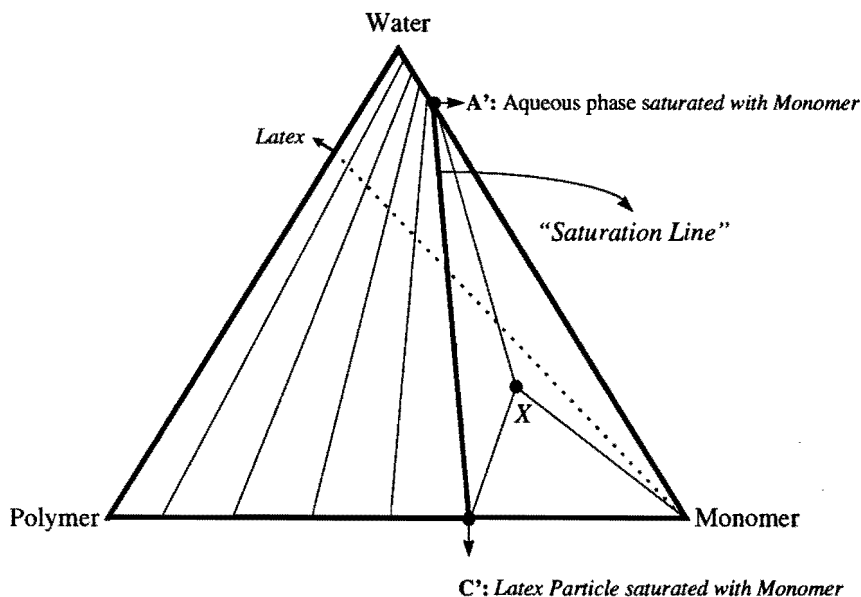


Figure 6.2 Schematic ternary phase diagram of a latex swollen by one monomer: The dashed line represents the saturation line and the solid lines the tie lines connecting the coexisting phases.

Depending on the amount of monomer added three situations can be distinguished. In all situations, below, at, and above saturation, the ratio of the different phases present can be calculated utilizing the lever rule. When the amount of monomer added is such that no separate monomer phase is formed, equation 6.6 can be used to calculate the composition of the two coexisting phases, i.e. only a monomer containing polymer phase and a monomer containing aqueous phase are present. The monomer containing polymer phase is represented by a point on the *Polymer-Monomer* axis, between *Polymer* and *C'*, while the monomer containing aqueous phase is represented by a point on the *Water-Monomer* axis, between *Water* and *A'*. If two such phases are in equilibrium they can be connected by tie-lines as has

been done in *figure 6.2*. When more monomer is added, i.e. moving on the line *Latex-Monomer* in the direction of *Monomer*, the polymer and aqueous phase become saturated with monomer. This point of saturation is indicated in *figure 6.2* by point *A'* and *C'* and the tie line (dashed line: *Saturation Line*) connecting them. Upon increasing the amount of monomer beyond this *Saturation Line*, a separate pure monomer phase will be formed. Using *equation 6.7*, the composition of the monomer containing aqueous and polymer phase can be calculated, which are equal to *A'* and *C'*, respectively. There are now three coexisting phases: 1. the monomer saturated aqueous phase, 2. the monomer saturated polymer phase and 3. a pure monomer phase. These three phases are connected by tie lines in *figure 6.2* as indicated for a certain composition *X*.

6.3.2 The Different Factors influencing the Ternary Phase Diagram of Latices Swollen by One Monomer

In this section the effect of the different parameters in *equations 6.6* and *6.7* on the ternary phase diagram (*figure 6.2*) will be discussed. From *equations 6.6* and *6.7* it can be easily seen that different factors affect the swelling behavior of latex particles by one monomer such as the Flory-Huggins interaction parameter, the latex particle radius, saturation concentration of L2 in L1, the particle-water interfacial tension, temperature, and the molar volume of the monomer. The effect of the first three of these factors will be discussed in somewhat more detail below.

The Flory-Huggins interaction parameter (χ): The interaction between monomer and polymer is accounted for by χ . For a low molar mass solvent and a high molar mass polymer the critical χ for phase separation is 0.5, i.e. below this value the system will be miscible as for values larger than 0.5 the system can phase separate. χ can vary over a large range. In the case of $\chi = 0$, the residual free energy of mixing is solely determined by the interfacial free energy term (see *Chapter 3* and *4*). In other words, the saturation concentration of monomer in the latex particles is determined by the size of the latex particle and the particle-water interfacial tension (see also *figure 6.3*).

The radius of the latex particles (R_0): In *Chapter 3*, the influence of the radius of the latex particles on the swelling behavior has been discussed. For very small values of R_0 ,

typically in the range of 5 nm (radius of micelles), the swelling is restricted due to the large value of the interfacial free energy term. As R_0 increases the influence of the interfacial free energy term becomes smaller. For large values of R_0 , the system behaves as a bulk phase and the interfacial free energy term becomes very small and negligible. In the latter case the residual free energy term is mainly determined by the enthalpy of mixing (see *Chapter 3* and *4*) (see also *figure 6.3*).

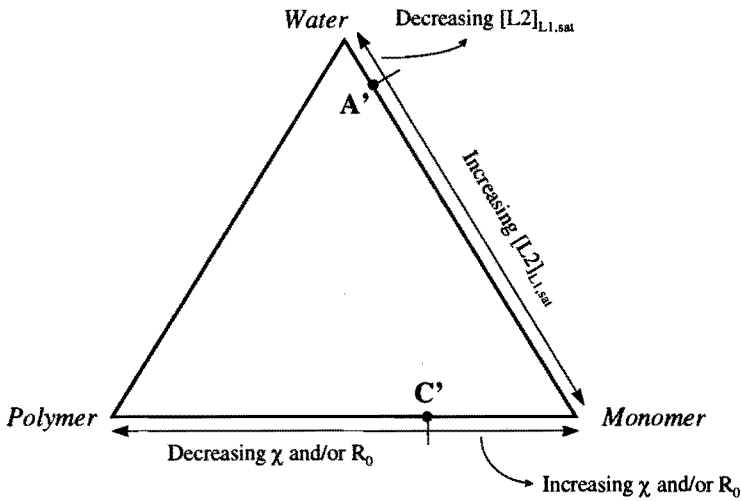


Figure 6.3 Schematic ternary phase diagram of a latex swollen by one monomer: the influence of χ , R_0 , and $[L2]_{L1,sat}$ on the position of A' and C'

The saturation concentration of monomer in the aqueous phase ($[L2]_{L1,sat}$): The water solubility of most of the monomers used in an emulsion polymerization is very low typically in the range of 3-300 mM. However, more and more monomers exhibiting interesting functionalities are used in emulsion polymerization which often exhibit a high water solubility or are even completely miscible with water (see also *figure 6.3*).

In *figure 6.3*, the effect of the above discussed factors is depicted. As can be seen from this figure, variation in χ and/or R_0 shifts point C' along the *Polymer-Monomer* axis. An increase in χ and R_0 shifts C' towards the *Monomer* vertex. On the other hand, changing the water solubility of the monomer causes A' to shift along the *Water-Monomer* axis. Increasing $[L2]_{L1,sat}$ causes A' to move towards the *Monomer* vertex. Summarizing, changing χ , R_0 ,

and/or $[L2]_{L,sat}$ causes a change in the size of the two or three phase region, i.e. the position of the saturation line changes depending on the value of the discussed parameters. *Figure 6.4* clearly shows that for a monomer which is sparsely water soluble and a poor solvent for the polymer (high χ) or relatively small latex particles (small R_0) the saturation line (line *K* in *figure 6.4*) is situated in the left part of the ternary phase diagram. In the case of a monomer which has a high water solubility and is a good solvent for the polymer or relatively large latex particles, the saturation line (line *L* in *figure 6.4*) is situated in the lower right part of the ternary phase diagram. In the first case the two phase region is rather small while in the latter case the two phase region is rather large.

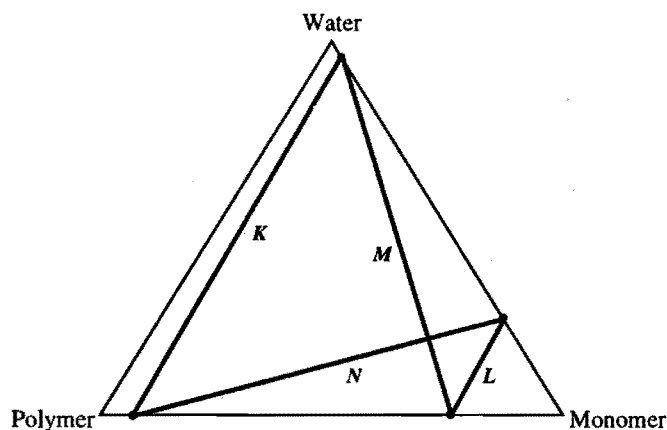


Figure 6.4 Schematic ternary phase diagram of a latex swollen by one monomer: the position of the saturation line depending on the water solubility of the monomer and the solvent quality of the monomer for the polymer, and the latex particle size.

Intermediate cases, i.e. a monomer that has a low water solubility and is a good solvent for the polymer or relatively large latex particles and a monomer which has a high water solubility and is a poor solvent for the polymer or relatively small latex particles, are indicated in *figure 6.4* by line *M* and *N*, respectively. One of the major advantages of phase diagrams is that for a given systems with a certain overall composition it is relatively easy to evaluate whether a separate monomer phase is present.

6.4 Quaternary Phase Diagrams of Emulsion Polymerization Systems: The Swelling of Latex Particles by Two Monomers

In the previous section ternary phase diagrams have been constructed for the swelling of seed latices by one monomer and the influence of different parameters has been addressed. In this section the swelling of seed latices by two monomers will be discussed. Since these systems consist of four components, i.e. polymer (P), water (L1), monomer A (L2), and monomer B (L3), quaternary phase diagrams have to be constructed. Every overall composition of the quaternary system is situated in the interior of the tetrahedral phase diagram. One difficulty in constructing such phase diagrams is their three-dimensional nature, making the interpretation of these phase diagrams extremely difficult. A simplification that can be applied is the division of the quaternary phase diagram in four ternary phase diagrams which form the sides of the tetrahedron². In order to be able to construct a quaternary phase diagram representing the swelling of a seed latex by two monomer, similar assumptions are made as in the case of the ternary phase diagrams in the previous section with respect to the composition of the different phases. First, there is no water (L1) present in the polymer (P) as well as the monomer (containing L2 and L3) phase. Second, there is no polymer dissolved in either the aqueous phase or the monomer phase. Again, two regions can be recognized, a region characterizing partial swelling and a region characterizing saturation swelling of latex particles. At equilibrium the partial molar free energy (or the chemical potential) of each monomer will be equal in each of the phases, at partial as well as saturation swelling. After applying this condition the composition of the different phases can be calculated utilizing *equations 6.8 and 6.9* for monomer A and B, respectively.

$$\ln v_{P,L2} + (1 - m_{L2-L3}) * v_{P,L3} + v_P + \chi_{L2-L3} * v_{P,L3}^2 + \chi_{L3-P} * v_P^2 + v_{P,L3} * v_P * (\chi_{L2-L3} + \chi_{L2-P} - \chi_{L3-P} * m_{L2-L3}) + \frac{2 * v_{m,L2} * \gamma * v_P^{1/3}}{R_0 * RT} = \quad (6.8)$$

$$\ln v_{d,L2} + (1 - m_{L2-L3}) * v_{d,L3} + \chi_{L2-L3} * v_{d,L3}^2 = \ln \left[\frac{[M_{L2}]_{L1}}{[M_{L2}]_{L1,sat}} \right]$$

$$\ln v_{P,L3} + (1 - m_{L3-L2}) * v_{P,L2} + v_P + \chi_{L3-L2} * v_{P,L2}^2 + \chi_{L2-P} * v_P^2$$

$$+ v_{P,L2} * v_P * (\chi_{L3-L2} + \chi_{L3-P} - \chi_{L2-P} * m_{L3-L2}) + \frac{2 * V_{m,L3} * \gamma * v_P^{1/3}}{R_0 * RT} = \quad (6.9)$$

$$\ln v_{d,L3} + (1 - m_{L3-L2}) * v_{d,L2} + \chi_{L3-L2} * v_{d,L2}^2 = \ln \left[\frac{[M_{L3}]_{L1}}{[M_{L3}]_{L1,sat}} \right]$$

the subscripts P, L1, L2, and L3, refer to polymer, water, monomer A, and monomer B, respectively. All the parameters have their normal meaning. In *figure 6.5*, the results of *equations 6.8* and *6.9* are represented schematically for sparingly water soluble monomers which are good solvents for the polymer.

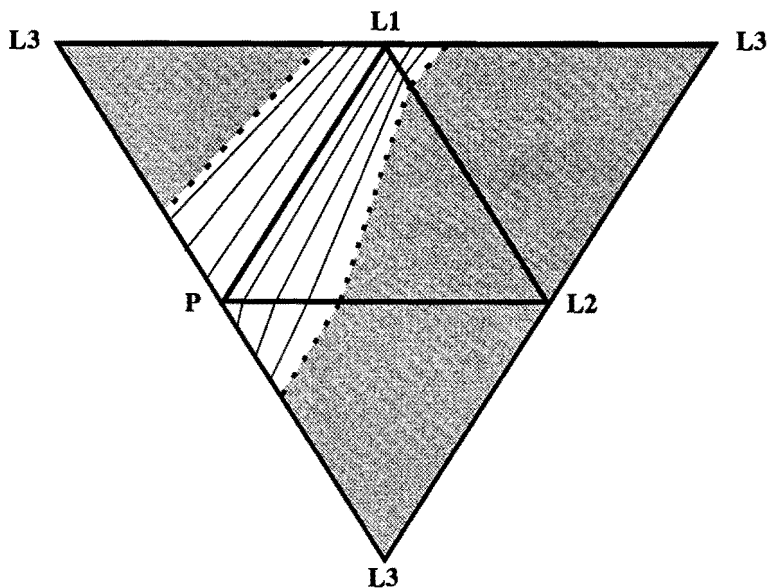


Figure 6.5 Schematic quaternary phase diagram of a latex swollen by two monomers. The dashed lines represent the saturation lines and the solid lines the tie-lines connecting the coexisting phases. The shaded areas indicate the three phase region.

The ternary diagrams P-L1-L2 and P-L1-L3 can be evaluated, in fact, in the same manner as the ternary diagrams for the swelling of a seed latex by one monomer as discussed

in the previous section. The ternary systems L1-L2-L3 and P-L2-L3 represent the monomer containing aqueous phase and polymer phase, respectively. Any quaternary overall composition can be divided into four ternary compositions of which the coexisting phases can be evaluated from *figure 6.5* in a relatively straightforward way. The location of the saturation lines in *figure 6.5* can be evaluated in ways similar to those followed in the ternary phase diagram discussed in the previous section.

6.5 The Use of Phase Diagrams in Emulsion Polymerization Processes

The major reason for the construction of phase diagrams of emulsion polymerizations systems is to use them in the visualization of the complex heterogeneous emulsion polymerization process. In the previous sections only static systems have been considered, i.e. monomer was added to an already existing latex. However, during the emulsion polymerization monomer (L2) is converted into polymer (P) (dynamic system) thus changing the overall composition of the system and consequently the composition of the different phases continuously.

6.5.1 Seeded Emulsion Polymerization

Seeded emulsion polymerizations are not only performed in kinetic studies which are focused on the latex particle growth process, but also in the preparation of for instance acrylonitrile-butadiene-styrene graft copolymers. *Figure 6.6* represent the ternary phase diagram of a seed latex (solid content X) swollen by one monomer. The initial situation (t_0) is represented by the left hand side ternary phase diagram in *figure 6.6*, where Y gives the overall composition of the monomer swollen seed latex. In the initial situation (t_0), the latex particles present are rather small as indicated by the position of the saturation line in the left part of the phase diagram. The phase diagram changes when monomer is converted into polymer in several ways. First, the size of the latex increases due to polymer formation (coagulation is excluded), concomitantly the saturation line shifts towards the *Monomer* (L2) vertex. Second, the overall composition of the ternary system (Y) changes since polymer is being formed as monomer is consumed which is indicated by the arrow in *figure 6.6*, thus the system becomes richer in polymer and poorer in monomer, while the water content is unchanged. Third, the

solid content of the latex increases of course when polymer is formed (indicated by X' in figure 6.6). At the end of the polymerization process (t_{end}), the solid content of the latex is equal to the monomer plus polymer content of the initial situation (indicated by Z in figure 6.6).

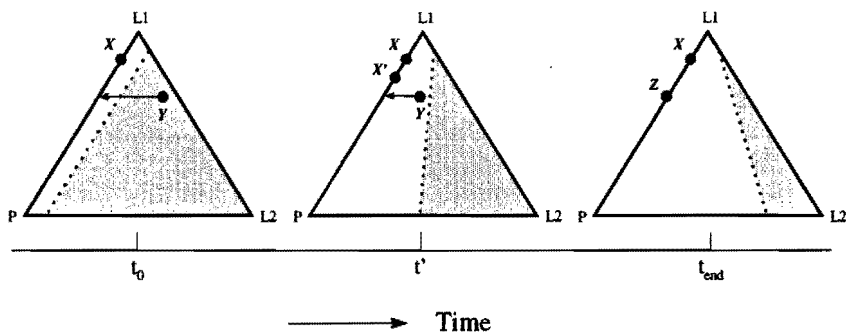


Figure 6.6 Schematic ternary phase diagram of a seeded emulsion homopolymerization. The region at the left hand side of the saturation line (dashed line) is the two phase region and the right hand side the three phase region

Please note that during the whole polymerization the ratio (*Monomer + Polymer*)/*Water* is constant (as indicated by the horizontal arrow in figure 6.6). The saturation line has moved more to the L2 vertex, since the latex particles have increased in size due to the conversion of monomer into polymer. A similar, although more complex, treatment can be given for a seeded emulsion copolymerization.

6.5.2 *Ab initio* Emulsion Homopolymerization

When one wants to use ternary phase diagram in the visualization of *ab initio* emulsion homopolymerizations some additional assumption have to be made in order to prevent the phase diagram from becoming too complex. Let us consider an emulsifier free emulsion homopolymerization. The formation of latex particles during this polymerization can be fully described by the homogeneous nucleation model followed by growth³ (see figure 6.7). In figure 6.7 two situations are depicted. In the first case a large number of latex particles (case *A* in figure 6.7) are formed, while in the second case less latex particles are formed (case *B* in figure 6.7). However, the total solid content of these systems is identical, i.e. the initial *Monomer/Water* ratio is equal in both situations. The latex particles formed are considered to be monodisperse, in other words the interval of latex particle formation is extremely short.

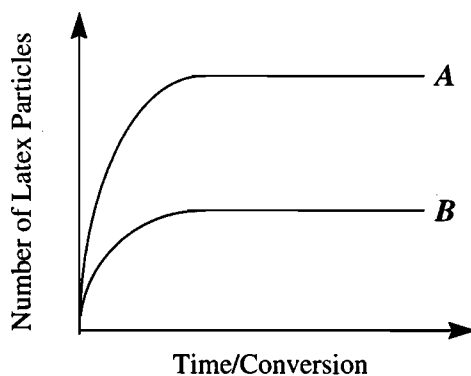


Figure 6.7 Schematic representation of the number of latex particles as a function of time/conversion for the homogeneous nucleation of latex particles followed by growth.

Further, it is assumed that the initiator and other additives (buffer) have no influence on the phase behavior of the polymerizing system. When these assumption are made, *ab initio* emulsion homopolymerizations can be treated in the same way as seeded emulsion homopolymerizations in the previous section yielding the same result. The only difference between these two situations is the fact that in the case of the seeded emulsion homopolymerization the initial systems is a ternary system while in the case of the *ab initio* emulsion polymerization this is a binary system.

6.6 Concluding Remarks

In this chapter, phase diagrams have been constructed for emulsion polymerization systems. In doing so, ternary phase diagrams become available capable of describing the swelling of latex particles by one monomer, in seeded emulsion homopolymerizations and in *ab initio* emulsion homopolymerizations. Quaternary phase diagrams have been shown to be very useful in the visualization of the swelling of a latex by two monomers. Although these phase diagrams result in a more than satisfactory graphical representation of emulsion polymerization systems some critical comments have to be made. First, the fact that in the discussion of the phase diagrams phase inversion phenomena have not been included. At high polymer and monomer content, the aqueous phase may no longer remain the continuous phase and the system may phase invert. Second, when the assumption made for the construction of the phase diagrams are not met, the tie lines and the saturation line in the ternary as well as

quaternary phase diagrams will not be linear but curved (Please note that this does not change the basic nature of the concept of phase diagrams describing emulsion polymerization systems). Third, the fact that the quaternary phase diagrams are only represented by the walls of the tetrahedron could cause a potential loss of valuable information concerning the phase behavior of these systems, although it is probably not a large source of deviation from the actual practical situation. Nevertheless, it can be concluded that the phase diagrams constructed in this chapter for various emulsion polymerization systems can be of great help in the visualization of the complex phase behavior of emulsion polymerization systems.

6.7 Appendix A: The Gibbs Phase Rule

The Gibbs phase rule is the relation employed to determine the number of thermodynamic degrees of freedom, or the number of independent, intensive variables for a multi-component, multi-phase system. The number of degrees of freedom of any composite system is evaluated by subtracting the number of equilibrium constraints equations from the number of intensive variables used to describe the composite system. For a multi-component systems there are n bulk or volume phases and each phase has C independent chemical components. In order to describe the state of a particular phase α for this heterogeneous system $C+1$ variables are required, temperature (T^α), pressure (P^α), and $\sum_{i=1}^{C+1} x_i^\alpha$ which is the mol fraction of component i in phase α . If all n phases are enumerated, the required number of intensive variables will be $P(C+1)$. Further, since these phases are in equilibrium, the intensive variables are constrained to satisfy thermal, mechanical, and chemical equilibrium conditions. These equilibrium conditions give a total of $(C+2)(P-1)$ constraints equations among the $P(C+1)$ intensive variables. The number of independent, intensive variables or the number of degrees of freedom, F , is equal to:

$$F = P(C+1) - (C+2)(P-1) = C - P + 2 \quad (\text{A.1})$$

Equation A.1 represents the standard Gibbs phase rule. It simply states that in a system with C independent chemical components and P coexisting phases the maximum number of independent, intensive variables that may be used to describe the state of the system. *Equation A.1* is deduced for a system satisfying the following conditions: First, boundary surface effects are neglected; and second, volume is the only work coordinate.

Let us consider now a latex prepared via emulsifier free emulsion polymerization, which consists only of water and polymer, i.e. $C = 2$ and $P = 3$ (two bulk phases and one liquid-liquid interface). Concomitantly, the number of degrees of freedom F is equal to 1. This is obviously unreasonable since it is well-known from experimental work that both temperature and pressure can be chosen as independent variables in open systems. Therefore, the number of degrees of freedom should be at least one. The reason why *equation A.1* is not applicable to latex systems is the fact that the previously stated conditions are not fulfilled. The phase rule for curved surface systems, as lattices are, has been deduced by several authors (see for instance Li et al. ⁴). For curved surfaces the pressures cannot be equal in all phases, i.e. $P^\alpha \neq P^\beta$. The equilibrium conditions in these kind of systems are given in *equation A.2*.

$$\begin{aligned} T^\alpha &= T^\beta = T^{\alpha-\beta} && \text{(thermal equilibrium)} \\ \mu^\alpha &= \mu^\beta = \mu^{\alpha-\beta} && \text{(chemical equilibrium)} \\ P^\alpha - P^\beta &= \gamma^{\alpha-\beta} J^{\alpha-\beta} && \text{(mechanical equilibrium)} \end{aligned} \quad (\text{A.2})$$

where the superscripts α and β denoted the different phases, and $\alpha-\beta$ the interface. γ is the interfacial tension and J is the mean curvature. By defining N as the total number of distinct $P^\alpha = P^\beta$ type relations among the mechanical equilibrium conditions, then for a curved, capillary, system with C chemical components and P phases, the total number of constraint equations is given by *equation A.3*.

$$\begin{array}{llll} P - 1 & + & C(P - 1) & + & N \\ \textit{thermal} & & \textit{chemical} & & \textit{mechanical} \\ \textit{equilibrium} & & \textit{equilibrium} & & \textit{equilibrium} \end{array} \quad (\text{A.3})$$

Since the number of intensive variables in the system is $P(C+1)$, the number of degrees of freedom, F , is readily obtained (see *equation A.4*).

$$F = P(C+1) - [(P-1) + C(P-1) + N] = C + 1 - N \quad (\text{A.4})$$

For a detailed derivation of *equation A.4* see Li et al. ⁴. If we consider now the same latex as above, the total number of degrees of freedom is now equal to 3 ($C = 2$ and $N = 0$). By choosing temperature, pressure and interfacial tension the system is determined, as can be observed also experimentally.

6.8 References

- 1 Scott, R.L., *J. Chem. Phys.*, 17, 268 (1949)
- 2 Novak, J.P., Matous, J., and Pick, J., in "*Liquid-liquid Equilibria*", *Studies in Modern Thermodynamics 7*, Elsevier (1987)
- 3 *Chapter 12* of this thesis
- 4 Li, D., Gaydos, J., and Neumann, A.W., *Langmuir*, 5, 1133 (1989)

CHAPTER 7

Polymerization in Vesicles

Synopsis: This chapter mainly dealt with the guidelines for the polymerization of an unsaturated monomer in the hydrophobic bilayer of vesicles.

7.1 Introduction

Polymerization processes can be subdivided in two ways. First, according to the polymerization mechanism by which the polymer is being formed, i.e. anionic, cationic, free radical or a coordination type of mechanism. Secondly, the physical system for polymerization, e.g. homogeneous or heterogeneous. It has been known for some time that one can perform a free radical type of polymerization in micelles, i.e. an emulsion polymerization^{1,2} and in inverse micelles, i.e. an inverse emulsion polymerization^{3,2}. Concomitantly, the question arises if one can polymerize in other surfactant structures such as vesicles, i.e. performing a *Polymerization in Vesicles*^{4,5}. Before we will discuss the different aspects of *Polymerization in Vesicles*, we have to distinguish between *Polymerization in Vesicles* and *Polymerizable Vesicles*.

Polymerizable Vesicles versus Polymerization in Vesicles

Polymerizable Vesicles are defined here as vesicles in which the surfactant molecules are polymerized. There exists an excellent overview of possible *Polymerizable Vesicles*⁶, here we will only give a summary of the possibilities:

In part reproduced from: Kurja, J., Zirkzee, H.F., German, A.L., Nolte, R.J.M., and Maxwell, I.A., "Polymerization in Vesicles: Thermodynamics, Kinetics and Characterization", in: "The Polymeric Materials Encyclopedia: Synthesis, Properties and Applications", J.C. Salamone (Ed.), CRC Press, Inc., Vol. 11, 8550 (1996), and Kurja, J., Nolte, R.J.M., Maxwell, I.A., and German, A.L., *Polymer*, **34**, 2045 (1993)

a. Counterion polymerization, here the counterion of the surfactant molecule can be polymerized. This polymerization results in so-called polymer-encased vesicles ⁷.

b. Head group polymerization, here a polymerizable moiety is attached to the hydrophilic head group of the surfactant ^{8,9}.

c. Chain polymerization, here the polymerizable group is present in the hydrophobic tail of the surfactant molecule and can be polymerized in different ways ^{10,11,12}. This kind of polymerization is also referred to as 2-D polymerization.

Polymerization in Vesicles is defined as the polymerization of a monomer in the hydrophobic vesicle bilayer, with the restriction that the monomer is not the original surfactant molecule ^{4,13}. The primary goal of performing a *Polymerization in Vesicles* is to use the vesicle structure in order to obtain a morphology which is similar to that of hollow latex particles. The major advantage of *Polymerization in Vesicles* over the conventional route for preparation of hollow latex particles ¹⁴ is that the *Polymerization in Vesicles* can be performed in an one-step process, whereas the conventional route consists of several, typically three or four, steps. Hollow latex particles find a broad field of application, as encapsulating species, opacifiers, fillers in composite materials and paper industry ^{15,16}.

7.2 Guidelines for the *Polymerization in Vesicles*

The theoretical guidelines for the *Polymerization in Vesicles* must address at least two critical variables, i.e. the monomer concentrations in the system, and the initiator system.

Monomer concentrations in the system: The total monomer content in the vesicle-system prior to polymerization is a very crucial parameter. We distinguish two cases. (a) In the first case the monomer partitions between the aggregates (vesicles) and the water phase. The monomer concentration in both phases is smaller than the saturation value of the monomer concentration in these two phases, therefore no separate monomer phase is present. (b) A second possibility is that the monomer concentrations in both the water phase and the vesicles exceed the saturation value, resulting in the formation of a separate monomer phase. Vesicle structures normally can swell with monomer to some saturation value and remain stable.

However, during an emulsion polymerization the reaction mixture is stirred to maintain thermal equilibrium, and hence any free monomer phase is dispersed as droplets. The surface area of the droplet phase will compete with vesicles for surfactant, and hence cause, to some extent, the break up of the vesicle structures. Of the above two cases the first, (a), is desirable since the vesicle structure is maintained while the monomer concentration in the vesicles is close to its saturation value. The saturation value of styrene in the water phase at different temperatures is well documented in the literature¹⁷. The saturation value of a solvent, e.g. styrene, in any vesicle system, e.g. DODAB vesicles, can be evaluated experimentally as well as theoretically as will be discussed later.

The initiator system: The initiators used in a conventional emulsion polymerization can be divided into three groups: dissociation, redox, and photoinitiators. The *dissociative initiators* can be divided into water soluble initiators, such as peroxyulfates and ammonium peroxyulfate, and oil-soluble dissociative initiators, such as benzoyl peroxide and 2-2'-azobisisobutyronitrile (AIBN). A major part of the initiator may be inactive because the cage effect can play an important role in the deactivation of radicals². On the other hand, a fraction of the above mentioned initiators may dissolve in the aqueous phase and cause secondary nucleation, i.e. the formation of latex particles, during the *Polymerization in Vesicles*. *Redox initiating systems* typically consists of a peroxide or a peroxyulfate combined with metal salt compounds (Fe^{2+}). The reaction scheme of these redox systems is very complex. The decomposition of peroxide or peroxyulfate is catalyzed by Fe^{2+} ions. These redox systems may be suitable for *Polymerization in Vesicles* because redox systems are capable of creating many radicals in a short period of time. Concomitantly, all monomer swollen vesicles can be initiated to form polymer-containing vesicles. However, a check on the vesicle stability after polymerization is very important since it is known that metal salts can change the vesicle structure and even can cause vesicle breakup¹⁸. *Photoinitiating systems*, such as Ultraviolet and g-radiation, have rarely been used in emulsion polymerization. The reason for this lies in the demands of the experimental technique and the purity of the reagents used. Also the limited penetration of radiation throughout the disperse medium in emulsion polymerization is a disadvantage. However, for *Polymerization in Vesicles* this technique may be suitable since the vesicle solution may be optically transparent. Incorporating photoinitiators such as benzophenone and phenylacetophenone into the vesicle bilayer followed by pulsed laser polymerizations may be an interesting approach¹³. The choice of the initiator system is

restricted because of the requirement that during the polymerization process the monomer swollen vesicle structure is retained and the formation of new particles is prevented, i.e. only vesicular nucleation occurs. This means that all the monomer swollen vesicles should be polymerized 'simultaneously' resulting in polymer containing vesicles. If this is not the case, monomer and surfactant from non reacting monomer swollen vesicles will diffuse to polymerizing vesicles.

Summarizing, in order to perform a real *Polymerization in Vesicles* a swelling technique for the incorporation of monomer in the vesicles bilayer combined with characterization procedures for vesicle stability are required. The type and amount of initiator is critical in ensuring vesicular nucleation and that polymerization takes place in the vesicle bilayer. In the following we will focus on the thermodynamics of vesicle bilayer swelling with organic solvents and the kinetic processes occurring during the *Polymerization in Vesicles*.

7.3 Kinetic Processes during the *Polymerization in Vesicles*

Radical polymerizations of unsaturated monomers in host systems such as vesicles have some similarities with a conventional emulsion polymerization, where traditional surfactants are used. These surfactants can form micelles which will act as loci (host system) for polymerization. Therefore, we will describe the characteristics of the *Polymerization in Vesicles* from an emulsion polymerization point of view. The important parameter in these type of radical polymerizations is the rate of polymerization (R_p), which is given for any radical polymerization as:

$$R_p = k_p * [M] * [R] \quad (7.1)$$

where k_p is the second order propagation rate coefficient, $[M]$ and $[R]$ the monomer and free radical concentrations, respectively. When the polymerization proceeds in compartmentalized species such as polymer particles in an emulsion polymerization or in vesicles as in the present case, the rate of polymerization can be depicted as:

$$R_p = \frac{k_p * C_{M,ves} * \bar{n} * N_v}{N_{Av.}} \tag{7.2}$$

where $C_{M,ves}$ is the monomer concentration within the polymer particles, \bar{n} the average number of radicals in the vesicle bilayer, N_v the number of vesicles per unit volume, and $N_{Av.}$ Avogadro's number. The procedure for polymerization in vesicles is that initially monomer is incorporated into the vesicle bilayer by bilayer swelling. After swelling, polymerization is performed by adding a free radical initiator or a photo initiating system. The procedure for the *Polymerization in Vesicles* is presented schematically in *figure 7.1*.

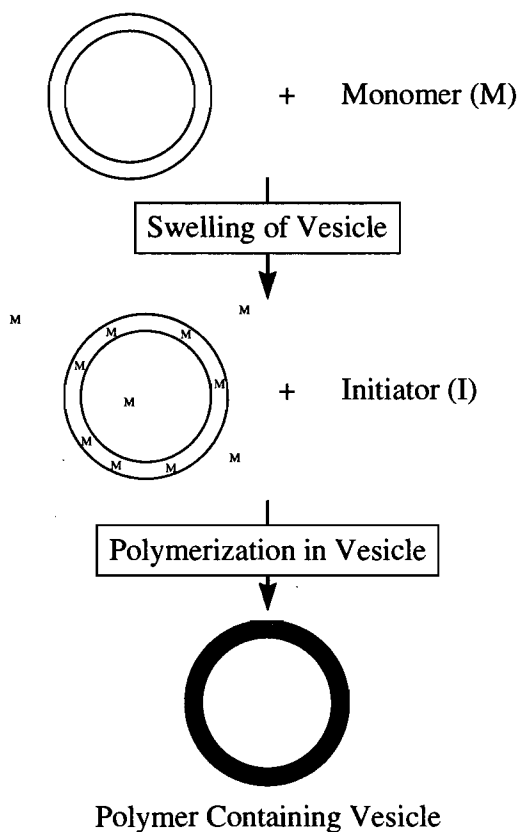


Figure 7.1 The schematic route for the *Polymerization in Vesicles*.

In the next section we will discuss some general emulsion polymerization kinetics which may also be applicable to the process of polymerization in vesicles. In emulsion polymerization the molecular weight of the polymer formed is affected by the processes of propagation, termination and chain transfer. These processes will dominate the kinetic chain length (\bar{v}), and hence the molecular weight of the polymer formed, according to ¹⁹ :

$$\bar{v} = \frac{R_p}{(R_t + R_{ct})} \quad (7.3)$$

where R_t is the rate of termination and R_{ct} the rate of chain transfer. Emulsion polymerization is a very complex process because the kinetic events occur in two different phases, i.e. the aqueous phase and the polymer particles. It is now generally accepted that when an initiator is used which is (partly) water soluble, the reaction starts in the aqueous phase by the formation of oligomeric radicals. These oligomeric radicals grow by monomer addition until they reach a critical chain length at which they become surface active and will be captured by already existing polymer particles. This process of radical capture by polymer particles is referred to as *entry* and is responsible for transferring the radical activity from the aqueous phase to the polymer phase. Assuming that the major part of the polymerization process occurs in the polymer particles, it is obvious that entry is a radical gaining process that will increase the rate of polymerization, and therefore, increase the kinetic chain length if no radical loss mechanisms are operative. Termination and chain transfer are radical loss mechanisms which will generally decrease the kinetic chain length of the polymer formed. In emulsion polymerization two termination processes can be operative, i.e. termination by combination and termination by disproportionation. Generally, the termination process depends upon the type of monomer. It is known that the mode of termination for styrene polymerization is by combination while for methylmethacrylate the termination is mainly determined by disproportionation ¹. However, when *Polymerization in Vesicles* is performed the termination process may be not only affected by the type of monomer but also by the two dimensional nature of the bilayer of the vesicles. It is expected that this nature may reduce the translational mobility of the growing polymer chains. On the other hand, chain transfer to monomer, polymer and/or a chain transfer agent can also influence the kinetic chain length of the polymer formed. When no chain transfer agents are added, however, chain transfer to

monomer is the most dominant event. If chain transfer to monomer occurs, the monomeric radical can propagate in the polymer particles. When propagation is not fast enough, however, the monomeric radical may diffuse away and escape from the polymer particle. This process is usually referred to as *exit*. It is obvious that exit from polymer particles is an important phenomenon which depends on the diffusion of monomeric radicals in the polymer phase and the surface-to-volume ratio of the polymer particle. The general observation is that the rate of exit decreases with decrease in the surface-to-volume ratio of the polymer phase. Translating the above event of exit to the process of *Polymerization in Vesicles*, we observe that the volume of the bilayer is rather low as compared with its surface area. Therefore, when chain transfer is occurring exit mechanisms may be dominant in vesicle systems. Concomitantly, the kinetic chain length of the polymer formed will decrease. Another item that should be considered when one wants to perform a *Polymerization in Vesicles* is the total amount of vesicle surface offered. If the vesicle surface is not sufficiently large, radicals formed in the aqueous phase can cause secondary nucleation leading to the formation of unwanted latex particles. In order to avoid secondary nucleation the total vesicle surface in the polymerization mixture has to be high and known. The number of vesicles in the system depends upon the vesicle formation process. The formation of vesicles is governed by the self-organization of the amphiphilic molecules in water²⁰. The number of vesicles (N_v) can be calculated if the vesicle size distribution is known, **assuming** perfectly spherical vesicles, according to:

$$N_v = \frac{6 * M_0}{\pi * \rho * d^3} \quad (7.4)$$

M_0 is the amount of surfactant, ρ is the density of the vesicle system and d is the average diameter of the vesicle system. It is obvious that the determination of the vesicle size distribution is difficult and requires proper characterization procedures. The monomer concentration in the vesicle bilayer, $C_{M,ves}$ is another very crucial parameter. The thermodynamics of vesicle bilayer swelling with monomers is described in the previous section. In order to determine the saturation value of monomer in the vesicle bilayer without vesicle breakup, a sophisticated swelling technique is required. In addition, characterization procedures to check the vesicle stability, and to visualize the swelling process should be available. The characterization procedures will be described in the next section. For proper

swelling the direct contact of vesicles with excess monomer should be avoided. Swelling of phospholipid vesicles with hexane and decane has been performed by Young and Dill^{21,22}, who used the gas phase as intermediate phase. Another swelling process where the aqueous phase serves as the transport medium for monomer was performed by Zirkzee *et al.*²³.

7.4 Concluding Remarks

Reliable swelling experiments are required to adjust the monomer concentration in the vesicle bilayer before *Polymerization in Vesicles* can be performed. In the foregoing we have presented an experimental method for determining the monomer concentration in the bilayer while also a theoretical framework is given from which the monomer concentration in the different phases present can be calculated and compared with experimental values. Furthermore, it is recognized that the choice of the initiator system is a very crucial parameter to ensure exclusively *Polymerization in Vesicles*, i.e. avoiding secondary nucleation at all times. Also the characterization of the vesicle system is very important. At each point during the swelling and polymerization process proper control of the vesicle structure is crucial to ensure *Polymerization in Vesicles*. It has become obvious that in order to perform a successful *Polymerization in Vesicles* the chain of knowledge between thermodynamics, i.e. vesicle bilayer swelling, polymerization kinetics, characterization of the vesicle system and the process control of the polymerization process, has to be closed. The concepts and experiments presented here and elsewhere show good perspectives for the *Polymerization in Vesicles* which may lead to new polymeric materials based on *Polymerization in Vesicles*.

7.5 References

- 1 Blackley, D.C., *Emulsion Polymerization*, Applied Science Publishers LTD, London, 1975.
- 2 Barton, J. and Capek, I., *Radical Polymerization in Disperse Systems*, Ellis Horwood Limited, New York, 1994.
- 3 Candau, F., *Scientific Methods for the Study of Polymer Colloids and Their Applications*, F. Candau and R.H. Ottewill Ed., Kluwer Academic Publishers, Dordrecht, 1988.
- 4 Kurja, J., Nolte, R.J.M., Maxwell, I.A., and German, A.L., *Polymer*, **34**, 2045 (1993)

- 5 Kurja, J., Zirkzee, H.F., German, A.L., Nolte, R.J.M., and Maxwell, I.A., "Polymerization in Vesicles: Thermodynamics, Kinetics and Characterization", in: "The Polymeric Materials Encyclopedia: Synthesis, Properties and Applications", J.C. Salamone (Ed.), CRC Press, Inc., Vol. 11, 8550 (1996)
- 6 Ringsdorf, H., Schlarb, B., and Venzmer, J., *Angew. Chem.*, **100**, 117 (1988).
- 7 Fukuda, H., Diem, T., Stefely, J., Kezdy, F.J., and Regen, S.L., *J. Am. Chem. Soc.*, **108**, 2321 (1986).
- 8 Iino, Y., Ogata, Y., Shigehara K. and Tsuchida, E., *Makromol. Chem.*, **186**, 923 (1985).
- 9 Dorn, K., Patton, E.V., Klingbiel, R.T., O'Brien, D.F., and Ringsdorf, H., *Makromol. Chem., Rapid Commun.*, **4**, 513 (1983).
- 10 Roks, M.F.M., Visser, H.G.J., Zwikker, J.W., Verkleij, A.J., and Nolte, R.J.M., *J. Am. Chem. Soc.*, **105**, 4507 (1983).
- 11 Sells, T.D. and O'Brien, D.F., *Macromolecules*, **27**, 226 (1994).
- 12 Fendler, J.H., *Science*, **223**, 888, (1984).
- 13 Murtagh, J. and Thomas, J.K., *Faraday Discuss. Chem. Soc.*, **81**, 127 (1986).
- 14 Okubo, M., Ichikawa, K., and Fujimura, K., *Col. Pol. Sci.*, **269**, 1257 (1991).
- 15 Kowalski, A., *et al.*, *US Patent*, Patent No. 4.468.498, Aug. 28 (1984).
Kowalski, A., *et al.*, *US Patent*, Patent No. 4.469.825, Sep. 4 (1984).
- 16 Blankenship, R.M., *et al.*, *US Patent*, Patent No. 4.594.363, Jun. 10 (1986).
- 17 Lane, W.H., *Ind. Eng. Chem. Anal. Ed.*, **18**, 295 (1946).
- 18 Rupert, L.A.M., PhD thesis, University of Groningen, (1988).
- 19 Young, R.J., *Introduction to Polymers*, Chapman & Hall, London, 1987.
- 20 Israelachvili, J.N., Mitchell, D.J., and Ninham, B.W., *J. of Chem. Soc. Faraday Trans.*, **72**, 1525, (1976).
- 21 De Young, L.R. and Dill, K.A., *Biochemistry*, **27**, 5281 (1988).
- 22 De Young, L.R. and Dill, K.A., *J Phys. Chem.*, **94**, 801 (1990).
- 23 Zirkzee, H.F., Kurja, J., Rietjens, G.H., and German, A.L., *Polymerization in Vesicles: The Mechanistics of Vesicle Bilayer Swelling*, in preparation (1997).

CHAPTER 8

Swelling and Vesicles

Synopsis: The equilibrium partitioning of solvent between water and phospholipid vesicles above the phase transition temperature of the vesicles is treated in a manner similar to that previously successful in describing solvent partitioning between water and emulsion polymer latex particles. The mixing of solvent and the alkane part of the phospholipid vesicles is described by the classical Flory-Huggins lattice theory. The vesicle surface free energy is described by the Gibbs-Thomson equation. The subsequent model has one adjustable parameter that is restricted within physical limits. Comparison of theory and experiment shows good agreement, and allows calculations of vesicle interfacial tensions.

8.1 Introduction

The swelling of vesicles and surfactant or phospholipid bilayers with solvents has been the subject of sporadic interest ^{1,2,3} despite the fact that it is a subject that possibly holds the key to the nature of vesicles. Surfactant and phospholipid bilayers are often used as model systems in biological studies and also in surfactant and colloidal studies. These species have also been studied because of their ability to absorb and release drugs in medical applications. Recently, we have performed a free radical polymerization of unsaturated oil soluble monomer within the interior of vesicles in order to make hollow polymer (latex) particles ⁴. Many of the above listed studies require a knowledge of how solvents are absorbed into vesicles, and how these solvents partition between the bilayer (vesicle) and aqueous phases.

In part reproduced from: Maxwell, I.A., and Kurja, J., *Langmuir*, **11**, 1987 (1995), and Kurja, J., Zirkzee, H.F., German, A.L., Nolte, R.J.M., and Maxwell, I.A., "Polymerization in Vesicles: Thermodynamics, Kinetics and Characterization", in: "The Polymeric Materials Encyclopedia: Synthesis, Properties and Applications", J.C. Salamone (Ed.), CRC Press, Inc., Vol. 11, 8550 (1996)

It has often been stated that the swelling of phospholipid bilayers and vesicles cannot be explained in terms of bulk thermodynamic models^{5,6}. There are at least two reasons for these statements. Firstly, bilayers have high surface to volume ratios, and are therefore often thought of as interfacial phases of matter rather than bulk phases. Secondly, bilayers are considered to have non-uniform structure, which is not the case for bulk phases. For these and other reasons much effort has been expended in modeling the swelling of surfactant bilayers by solvents in a manner that ignores bulk thermodynamics. Statistical mechanical approaches to the problem have been most common^{7,8}. These often have good success, but may suffer from being somewhat qualitative in nature, or by requiring the evaluation of unmeasured parameters. These facts limit the predictive power of these models.

In this chapter analogies are drawn between the swelling of latex particles by solvents and the swelling of phospholipid vesicles by solvents. The saturation swelling of latex particles by solvents is admirably described by the Morton equation^{9,10} and the partial swelling of latex particles is described by simple adaptation of this equation^{10,11,12}. The basis of these equations is that the mixing of solvents and polymer is readily described by Flory-Huggins theory. In this paper we extend this approach to phospholipid vesicles, and develop analogues to expressions previously described for the latex particle situation. The mixing of solvent and the alkane part of phospholipid in vesicle bilayers is thought of in bulk thermodynamic terms. Obviously this does not allow us to consider the microstructure of the swelling phenomena within vesicle bilayers. But we state from the outset that our primary goal is to develop a model that predicts only the absolute concentration of solvent within a vesicle bilayer, both at partial and at saturation swelling, and therefore, also the solvent partition coefficient.

Finally, listed below are the limitations of the systems that we are interested in. **1.** We consider only swelling of vesicles by a single solvent. Trivial extensions can be made to deal with two or more solvents. These extensions are analogous to theories previously developed for the swelling of latex particles by two or more solvents^{13,14}. **2.** We consider only partially water soluble solvents that are good solvents for the alkane part of the phospholipid vesicles. **3.** All work in this paper is for phospholipid vesicles, but the considerations are quite general and can be applied to all bilayer structures with simple modifications. **4.** Finally, only phospholipid vesicles above the phase transition of the phospholipid chains are considered.

Hence the mixing of the alkane part of the phospholipid chains and solvents results in a single phase.

8.2 Theory

In this section we first consider the swelling of latex particles by solvent and then derive analogous expressions for phospholipid vesicles.

Morton *et al.*⁹ considered the saturation swelling of latex particles by solvent having limited solubility in the water phase. When the swollen latex particle is in equilibrium with the free monomer phase the partial molar Gibbs free energy of the monomer is given by:

$$\Delta G = \Delta G_{\text{mix}} + \Delta G_{\text{surf}} = 0 \quad (8.1)$$

where ΔG is the partial molar Gibbs free energy of monomer, ΔG_{mix} the contribution from the energy of mixing of monomer and polymer, and ΔG_{surf} the contribution from the particle-water interfacial energy. Morton *et al.*⁹ expressed the free energy of mixing of monomer and polymer in terms of the classical Flory-Huggins theory¹⁵:

$$\frac{\Delta G_{\text{mix}}}{RT} = \ln(1 - v_p) + v_p \left[1 - \frac{1}{\bar{P}_n} \right] + \chi * v_p^2 \quad (8.2)$$

where v_p is the volume fraction of polymer in the latex particles, \bar{P}_n the number average degree of polymerization, R the gas constant, T the temperature and χ the Flory-Huggins interaction parameter. The interfacial free energy was given in terms of the Gibbs-Thomson equation^{16,17}:

$$\Delta G_{\text{surf}} = \frac{2 * V_m * \gamma * v_p^{1/3}}{R_0} \quad (8.3)$$

where V_m is the partial molar volume of the monomer, γ the particle-water interfacial tension and R_0 the unswollen radius of the latex particle. Combining *equations 8.1, 8.2 and 8.3* gives the *equation 8.4*:

$$\ln(1-v_p) + v_p \left[1 - \frac{1}{P_n} \right] + \chi^* v_p^2 = -\frac{2 * V_m * \gamma * v_p^{1/3}}{R_0 * RT} \quad (8.4)$$

In the case where there is no separate monomer phase present the partial molar free energy of the aqueous phase has to be taken into account. Vanzo *et al.* were the first to derive an analogue *equation 8.4* that dealt with partial swelling of latex particles utilizing a simpler equation for the partial molar free energy of the aqueous phase. In doing so, they assumed that the monomer containing aqueous phase could be considered as a dilute solution of monomer and water. Later, Gardon ¹⁰ derived the same expression. If the latex particles are not saturated by monomer then there is no pure monomer phase present (i.e. no monomer droplets). The partial molar free energy of the monomer in the aqueous phase is then given by ¹²:

$$\Delta G = RT * \ln a \quad (8.5)$$

where a is the activity of the monomer. Vanzo *et al.* pointed out that the monomer activity can be approximated by p/p_0 , i.e. the ratio of the vapor pressure of the monomer at a given volume fraction of polymer (p) to the vapor pressure at saturation swelling (p_0). Gardon ¹⁰ showed that, since Henry's Law holds for latex free water, the ratio p/p_0 can be approximated by the ratio of the monomer concentration in the aqueous phase below and at saturation:

$$\frac{p}{p_0} = \frac{[M]_{aq}}{[M]_{aq,sat}} \quad (8.6)$$

where $[M]_{aq}$ is the concentration of monomer in the aqueous phase and $[M]_{aq,sat}$ is the saturation concentration of monomer in the aqueous phase. The final result for partial swelling of latex particles by monomer, hereafter called the Vanzo equation ¹², is:

$$\ln(1 - v_p) + v_p \left[1 - \frac{1}{P_n} \right] + \chi * v_p^2 + \frac{2 * V_m * \gamma * v_p^{1/3}}{R_0 * RT} = \ln \left[\frac{[M]_{aq}}{[M]_{aq,sat}} \right] \quad (8.7)$$

The solvent partitioning between the aqueous and latex particle phases can be predicted from equation 8.7. However, this requires that both the interaction parameter and the interfacial tension be known. A further complication is that both these parameters may be volume fraction polymer dependent. Also, values of these parameters are difficult to determine by independent experiments.

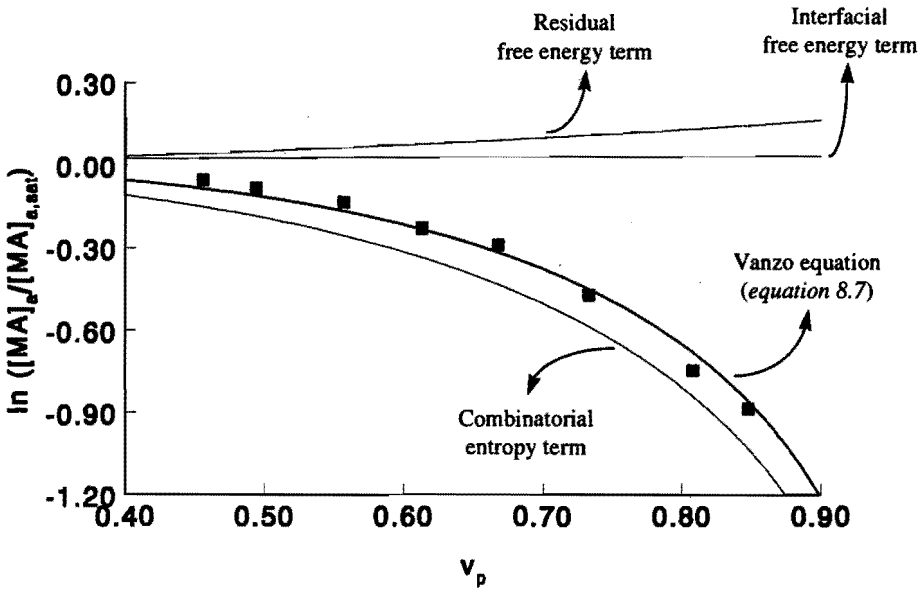


Figure 8.1 Comparison of theoretical predictions and experimental measurements (squares) of MA partitioning at 45°C for seed latex SMA-2 ($R_0 = 96 \text{ nm}$, see for further details Chapter 3). Theoretical predictions: combinatorial entropy term given by $\ln(1 - v_p) + v_p$; residual free energy term given by $\chi * v_p^2$, with $\chi = 0.2$; interfacial free energy term given by $\frac{2 * V_m * \gamma * v_p^{1/3}}{R_0}$, with $\gamma = 45 \text{ mN/m}$; and Vanzo equation (equation 8.7) with $\chi = 0.2$ and $\gamma = 45 \text{ mN/m}$.

Partitioning results for solvents at partial swelling of latex particles show that the interfacial free energy has little effect upon the changes in partitioning of solvent. To emphasize this point, in figure 8.1 the predicted contribution of all three terms in equation 8.7 are displayed individually for partial swelling of a latex particle by solvent. These terms are the

combinatorial entropy of mixing of polymer and solvent term $(\ln(1-v_p) + v_p * \left[1 - \frac{1}{P_n}\right])$, derived by considering the entropy of mixing of an assembly of random-flight chain molecules with solvent), the 'residual' free energy term ($\chi * v_p^2$, containing both enthalpic and entropic terms) and the interfacial free energy term ($\frac{2 * V_m * \gamma * v_p^{1/3}}{R_0 * RT}$). It is immediately obvious from these results that at high volume fractions of polymer the dominant contribution to equilibrium is the combinatorial entropy of mixing of solvent and polymer. The sum of all terms admirably reproduces experimental data (see *figure 8.1*).

Realizing the above result, a semi-empirical approach was developed¹¹ in which the sum of the residual free energy and the particle-water interfacial free energy terms in *equation 8.7* are considered approximately constant at high volume fractions of polymer (i.e. at partial swelling). These terms are incorporated into a correction term and calculated from saturation swelling data using the Morton equation¹¹.

$$\text{Corr.} = \chi * v_{p,\text{sat}}^2 + \frac{2 * V_m * \gamma * v_{p,\text{sat}}^{1/3}}{R_0 * RT} =$$

$$- [\ln(1 - v_{p,\text{sat}}) + v_{p,\text{sat}} * \left(1 - \frac{1}{P_n}\right)] \quad (8.8)$$

This correction can be implemented in the Vanzo equation (*equation 8.7*):

$$\ln(1 - v_p) + v_p * \left[1 - \frac{1}{P_n}\right] + \text{corr} = \ln \left[\frac{[M]_{\text{aq}}}{[M]_{\text{aq},\text{sat}}} \right] \quad (8.9)$$

The approach used to derive *equations 8.8* and *8.9* incorrectly assumes that the both the interfacial free energy and the residual free energy term are independent of the volume fraction of polymer. However in the latex particle situation, since the absolute values of these terms are small compared to the combinatorial entropy term (*figure 8.1*), this approach, as a first estimate, gives quite good results (*figure 8.2*)¹¹. Note that this approach requires no

knowledge of interfacial free energy or the free energy associated with the residual interactions between the solvent and polymer, the correction term can be calculated solely from a knowledge of the saturation concentration of solvent in the latex particles. This latter quantity can be simply determined by experiment ¹¹.

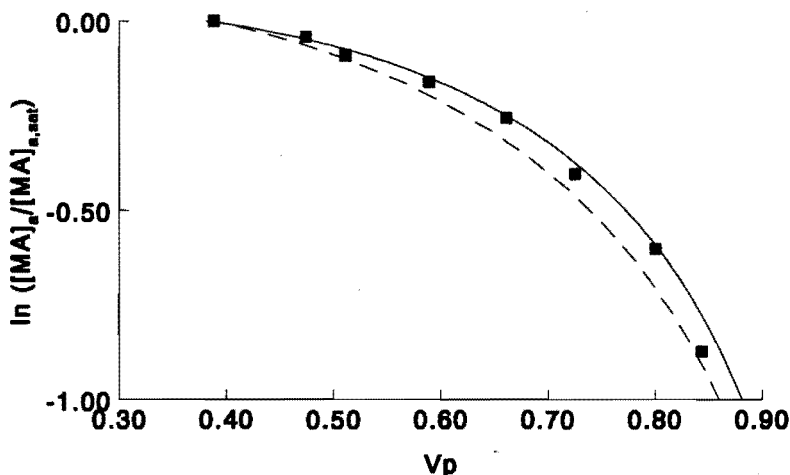


Figure 8.2 Comparison of the theoretical predictions (equation 8.8) experimentally measurements of MA partitioning at 45°C for latex SMA-6 (see for more details Chapter 3). Theoretical predictions with the Vanzo equation ($\chi = 0.2$ and $\gamma = 45$ mN/m)(Solid line) and equation 8.8 (Corr. = 0.1)(Dashed line).

We now turn to phospholipid vesicles. It is our assertion that simple concepts, similar to those used in the derivation of equations 8.7, 8.8, and 8.9 can be utilized to describe the partial swelling of phospholipid vesicles by solvents. One assumption used here is that the mixing of solvent and the alkane part of the phospholipid molecules is well described by Flory-Huggins theory. That is, we treat the alkane part of the phospholipid molecules as polymer. This will be valid if the alkane chains are immobile relative to the solvent mobility - this ensures that the mixing of the alkane part of the phospholipid chains and solvent can be considered as a volume- or space-filling exercise. This criteria will probably be satisfied since the phospholipid chains will be confined by the head group immobility in the hydrophobic part of the bilayers ¹⁸. Note that many statistical mechanical models derived for this problem assume that the alkane part of the phospholipid chains are fixed at the bilayer interface ⁷, which, ironically, is the one condition that allows the simple Flory-Huggins theory to be used.

Obviously the degree of saturation swelling of vesicles is limited compared to say a bulk phase. This limitation is due to the free energy associated with the vesicle-water interface, and also, in common with swelling in the bulk phase, by the residual free energy of mixing of the solvent and alkane part of the phospholipid bilayer. An equation, analogous to the Morton equation can be developed for vesicles so long as an expression for the vesicle-water interfacial free energy is available. This is not as simple as it may seem since instead of one interface in the latex particle case, there are two interfaces in the vesicle situation. Further, these two interfaces have different curvatures. The nature of the surface free energy of vesicles has been discussed in depth by Tanford¹⁹ and also by White²⁰. One result that follows from the considerations of White²⁰ is that we cannot discern between the contributions from the two interfaces. Tanford¹⁹ asserted that since vesicles are permeable to water the inside and outside pressures of a vesicle must be equal. Tanford then went on to state that this fact causes the macroscopic interfacial tension of a vesicle to be equal to zero. White pointed out that this was not the case: in fact the surface of a vesicle can be at equilibrium while having a non-zero interfacial tension. White gave the following equations for the macroscopic interfacial tension of a vesicle²⁰:

$$\gamma = \int_{Z_1}^{Z_2} [P_N(Z) - P_T(Z)] dZ \quad (8.10)$$

where the Z axis is normal to the surface layer, and the integration limits Z_1 and Z_2 include the entire bilayer. The interfacial tension, γ , arises from the anisotropy of the bilayer, and the pressure within the bilayer is then a tensor. This pressure has been resolved into two components, $P_N(Z)$ normal to the surface and $P_T(Z)$ tangential to the surface. Note that γ is an integrated property of the interface.

For the vesicle structure there is no single or simple solution for *equation 8.10*, hence it is difficult to consider the interfacial tension of the individual monolayers of a bilayer. Therefore, in what follows we have taken one step back in our considerations (see also *Appendix A, section 8.5*). Since we are dealing with large vesicles we can use the Laplace equation to describe the macroscopic surface free energy of vesicles^{19,20}:

$$P_0 - P_i = \frac{2 * \gamma}{R_0} \quad (8.11)$$

where $P_0 - P_i$ is the pressure difference across the vesicle, γ is now the macroscopic surface tension of the vesicle, and R_0 is the radius of curvature of the vesicle. The use of this equation runs contrary to the statements of White who states that this equation cannot be used since the radii of the vesicles is similar in size to the vesicle wall thickness. This is not strictly the case for the vesicles discussed in this work. Further, the sizes of the vesicles considered in this work are similar to latex particles previously studied in which we have shown that the radii is indeed large enough to use the Laplace equation^{9,10,11,12,13,14}. Most importantly, it is the use of the Laplace equation for vesicles which is being tested in this work - the validity of this will be assessed in the light of comparison of theory and experiment, especially in regard to the meaning of the interfacial tension for a bilayer system. In summary we are going to adopt the form of Laplace equation for vesicles. The equivalent surface free energy term to *equation 8.3* for vesicles is given by Gibbs-Thomson equation:

$$\Delta G_{\text{surf}} = \frac{2 * V_m * \gamma * v_{\text{pv}}^{1/3}}{R_0} \quad (8.12)$$

where R_0 is the macroscopic outer radius of the vesicle, V_m is the molar volume of the solvent, γ the macroscopic surface tension of the vesicle, and v_{pv} is the volume fraction of the alkane part of the phospholipid molecules in the whole swollen vesicle. Note that this fraction includes the volume of water in the interior of the vesicle, i.e.:

$$v_{\text{pv}} = \frac{V_p}{V_p + V_s + V_w} \quad (8.13)$$

where V is the absolute volume, and the subscripts p , s and w represent, respectively, the alkane part of the phospholipids in the bilayer, the solvent part in the bilayer and interior water²¹. The use of this fraction (*equation 8.13*) was rationalized by the desire to keep the form of the equations for vesicles and latex particles the same. The inclusion of water in

equation 8.13 above accounts for the total volume of the sphere that is described by the vesicle.

Note that as a vesicle bilayer is swollen by solvent any change in vesicle radius is due to expansion of the bilayer only, and there is assumed to be no change in volume of the water interior. Hence, the use of above form of Gibbs-Thomson equation can be justified since the only change in radius of a vesicle upon swelling results from the absorption of solvent into the bilayer, the change of radius is simply encapsulated in the $v_{pv}^{1/3}$ term. The full equation describing the swelling of vesicles by solvent is then just given by:

$$\ln(1-v_p) + v_p \left[1 - \frac{1}{\bar{P}_n} \right] + \chi * v_p^2 + \frac{2 * V_m * \gamma * v_{pv}^{1/3}}{R_0 * RT} = \ln \left[\frac{[M]_{aq}}{[M]_{aq,sat}} \right] \quad (8.14)$$

where v_p is redefined here as the volume fraction of phospholipid alkane in the vesicle bilayers, and \bar{P}_n is the number average degree of polymerization of half the number of carbon chains in the alkane backbone of a single phospholipid chain (this ensures that this term is consistent with the use of a interaction parameter, χ , from polymer type systems). These re-definitions hold for the rest of this chapter. Note that, at saturation the left-hand side of *equation 8.14* is equal to zero. The saturation concentration of solvent in a vesicle bilayer can be simply calculated if values for χ and γ are known or can be estimated. Arguments similar to those used in the derivation of *equations 8.8* and *8.9* can be developed for the vesicle situation. At the high volume fractions of the alkane in the vesicle interior (this just replaces the polymer component in the latex particles), if the dominant contribution to swelling is just given by the combinatorial entropy of mixing of solvent and the alkane part of the phospholipid, *equation 8.9* can be used to model partial swelling of vesicles, where the correction factor is just given by:

$$\text{Corr.} = \chi * v_{p,sat}^2 + \frac{2 * V_m * \gamma * v_{pv}^{1/3}}{R_0 * RT} = \quad (8.15)$$

$$- \left[\ln(1-v_{p,sat}) + v_{p,sat} \left(1 - \frac{1}{\bar{P}_n} \right) \right]$$

where $v_{p,sat}$ is the volume fraction of phospholipid alkane in the vesicle at saturation swelling by the solvent (redefined for the rest of this paper). Note that *equation 8.8* and *equation 8.15* are identical if the second definition of the correction factor is used, i.e. if "corr" is a function of $v_{p,sat}$ and \bar{P}_n .

8.3 Results and Discussions

Experimental results on the partial swelling of multilamellar vesicles by hexane and benzene have been reported by Young and Dill^{1,2}. The phospholipids utilized by these workers are dimyristoylphosphatidylcholine (DMPC) and protiated egg phosphatidylcholine (egg PC). The phospholipid main phase transition temperatures, T_c , of these phospholipid species are: $T_c = 23$ °C (DMPC), and $T_c = -10$ °C (egg PC). In what follows we utilize these reported experimental results of multilamellar partial swelling by the solvents hexane and benzene. Note that we only utilize data that are above the phase transition temperature of the phospholipids (swelling below the phase transition temperature is more complex since a ternary solvent system is described up to a solvent fraction of solvent in the vesicles that allows 'plasticisation' of the phospholipid alkane phase). These data were reported as solvent partition coefficients and as a function of mole fraction of the solvent in the lipid. For comparison of the data with *equation 8.14*, we have converted this data to the form shown in *figures 8.3* and *8.4*, i.e. the natural log of the ratio of the observed aqueous phase concentration of the solvent and the saturation concentration of that solvent in water at the experimental temperature versus the volume fraction of phospholipid alkane in the vesicles.

Dill *et al.* also reported data^{1,2} in which cholesterol was used as a co-solvent in bilayer swelling experiments. Cholesterol acts as a co-solvent (and possibly also as a co-surfactant), and the thermodynamic equations derived specifically for the single solvent case as described in the theory section of this paper no longer apply. Recently we have considered swelling of latex particles by two solvents¹³, including the partial swelling situation¹⁴. The application of these equations to bilayer swelling data with more than one solvent will be published separately.

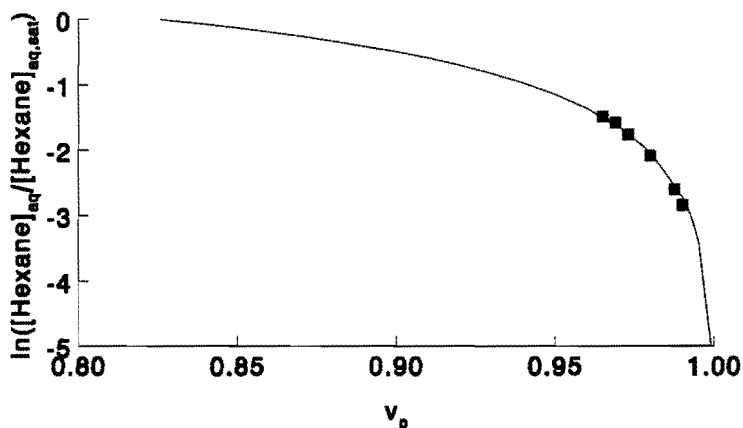


Figure 8.3 Partial swelling of hexane between the vesicle phase and aqueous phase. Experimental values of $\ln([Hexane]_{aq}/[Hexane]_{aq,sat})$ versus volume fraction of phospholipid alkane in the vesicles for DMPC at 25 °C. The lines represents the fit of equation 8.9 to experiment with values of $v_{p,sat}$ (in equation 8.15) as given in table 8.2.

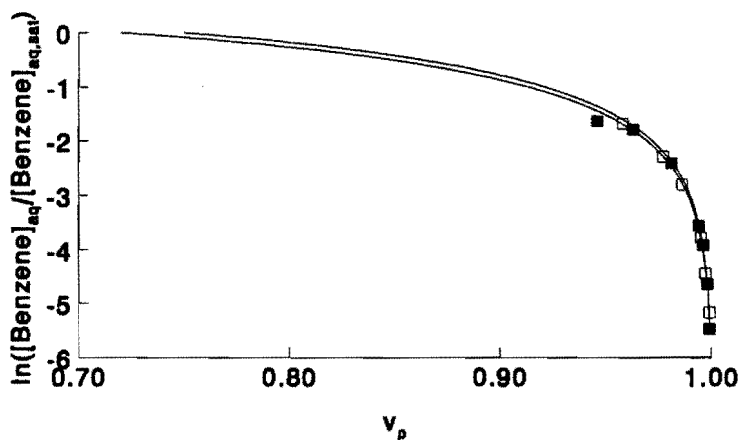


Figure 8.4 Partial swelling of benzene between the lipid phase and aqueous phase. Experimental values of $\ln([Benzene]_{aq}/[Benzene]_{aq,sat})$ versus volume fraction of phospholipid alkane in the vesicles for DMPC at 30 °C (full squares) and egg PC at 25 °C (empty squares). The lines are fits of equation 8.9 to experiment for DMPC at 30 °C (lower solid line) and egg PC at 25 °C (upper solid line) with values of $v_{p,sat}$ (in equation 8.15) as given in table 8.2.

The use of equation 8.9 in comparing theory with experiment requires the values of three parameters: the average degree of 'polymerization' of the alkane part of the phospholipid

chains and the saturation concentrations of the solvent in both the bilayer and aqueous phases. In what follows we discuss each of these parameters separately:

1. The average degree of 'polymerization' of the alkane part of the phospholipid chains, \bar{P}_n , is defined as half the number of backbone carbon atoms in the chain. As stated in the previous section this is simply to make this term consistent with the use of an interaction parameter, χ , in polymer type systems. In most cases it will be shown that these considerations are of little importance since the combinatorial entropy term containing \bar{P}_n contributes negligibly to the thermodynamic equilibrium at the higher values of v_p typically found in vesicles. The values of \bar{P}_n used in these calculations are listed in *table 8.1*.

Table 8.1. Parameters utilized in the fitting equations 8.10, 8.15 and 8.16 to experimental partitioning data.

Parameter	value	reference
[Benzene] _{aq,sat} at 20°C	2.28×10^{-2} mole/l	27
[Hexane] _{aq,sat} at 20°C	1.28×10^{-4} mole/l	27
molar volume of benzene at 20°C	88.7 ml/mole	27
molar volume of hexane at 20°C	130.7 ml/mole	27
molar volume of water	18.07 ml/mole at 25°C 18.10 ml/mole at 30°C	22
specific volume of DMPC	0.933 ml/g at 10°C 0.970 ml/g at 25°C 0.973 ml/g at 30°C	23
specific volume of egg PC	0.970 ml/g at 25°C	estimated from 24
molecular mass of DMPC	707 g/mole	
molecular mass of egg PC	733 g/mole	
\bar{P}_n of DMPC	7	
\bar{P}_n of egg PC	7	
χ benzene-polyisoprene 25-50°C	0.45	25
χ hexane-polyisoprene 25-50°C	0.52	
R_0	50, 400 nm	
thickness of vesicle bilayer	3 nm	

2. The saturation concentration of the solvent in the lipid phase is a difficult parameter to measure directly since saturation of a phospholipid system with solvent may lead to solvent droplet formation, especially when the mixture is stirred. Therefore in the absence of measured saturation concentration of solvent in the vesicles, in comparing *equation 8.9* with

experimental results we treat the correction term (*equation 8.15*) as an adjustable parameter, or more properly, the saturation volume fraction of phospholipid alkane in the vesicles, $v_{p,sat}$, is treated as an adjustable parameter. The ramifications of this will be discussed below.

3. The water solubilities of the solvents are readily found in the literature. Note that at all temperatures, single values of the water solubilities were utilized in the calculations. This was shown to introduce an imperceptible error over the small temperature range at which the experiments were carried out.

Table 8.2 *Fitted values of: the correction factor in equation 8.16, the volume fraction of alkane in the vesicles at saturation, the concentration of solvent in the vesicles at saturation, solvent partition coefficient at saturation, solvent partition coefficient at infinite dilution, and the vesicle interfacial tension at saturation.*

Parameter	Vesicle type		
	DMPC	DMPC	egg PC
solvent	hexane	benzene	benzene
T (°C)	25	30	25
corr	1.04	0.65	0.60
$v_{p,sat}$	0.82	0.72	0.70
$[M]_{v,sat}$ (mole/l)	1.4	3.2	3.4
k_{∞}	$3.4 * 10^5$	$4.1 * 10^5$	$4.5 * 10^5$
K_{sat}	$2.3 * 10^5$	$1.8 * 10^5$	$1.9 * 10^5$
γ (mN/m)	25-50	25-50	18-37

In figures 8.3 and 8.4 the fits of *equation 8.9* to experiment are displayed. In all cases a very good fit is observed. The only adjustable parameter in these fits is the volume fraction of phospholipid alkane at saturation swelling by the solvent ($v_{p,sat}$), which arises from the use of *equation 8.15* with *equation 8.9*. The value of this parameter is constrained by two factors. First, $v_{p,sat}$ must be less than all the partial saturation volume fractions, and, secondly, $v_{p,sat}$ must be greater than zero, probably with a value typical for micelles and very small latex particles. It cannot be too small nor too large. The fitted values of $v_{p,sat}$ are shown in *table 8.2*. From the values of $v_{p,sat}$ the saturation partition coefficients, K_{sat} , can be calculated from:

$$K_{sat} = \frac{[M]_{v,sat}}{[M]_{aq,sat}} \quad (8.16)$$

where $[M]_{v,sat}$ is the saturated concentration of solvent in the vesicles. Values of $[M]_{v,sat}$ and K_{sat} are displayed in *table 8.2*. Values for maximum solvent uptake by other surfactant structures, e.g. benzene into sodium dodecyl sulfate micelles ($[M]_{micelle,sat} = 2.5$ M, $K_{sat} = 1.6 \cdot 10^3$)²⁶, are about the same order of magnitude. Similar values are found for small (radii < 20nm) latex particles¹⁰. Values of K_{sat} are all less than the bulk values (at 25°C $K_{sat,hexane} = 4.5 \cdot 10^5$ and $K_{sat,benzene} = 2.4 \cdot 10^3$)²⁷. This is expected since the degree of solvent uptake by vesicles is restricted by the interfacial free energy. The fitted values of $[M]_{v,sat}$ and K_{sat} all compare well with expectations. In *figures 8.5* and *8.6* the raw partitioning data are compared to the fits of *equation 8.9*, i.e. partition coefficient versus mole fraction solvent in lipid. In all case a good fit is achieved. Notice that the fitted curves are not exactly linear, as has often been assumed. The value of the solvent partition coefficient at infinite dilution, K_{∞} , was calculated from extrapolation of the fitted lines in *figures 8.5* and *8.6* to zero mole fraction of solvent.

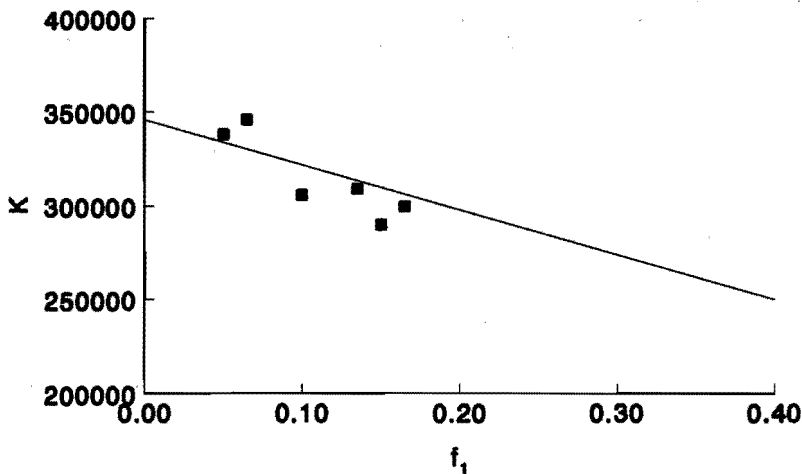


Figure 8.5 Partial swelling of hexane between the vesicle phase and aqueous phase. Experimental values of partition coefficient versus fraction of hexane in the lipid phase for DMPC at 25°C. The line represents the fit of *equation 8.9* to experiment with values of $v_{p,sat}$ (in *equation 8.15*) as given in *table 8.2*.

The excellent agreement between theory and experiment for a range of solvents, phospholipid types and temperatures suggests that the mixing of solvent and the alkane part of phospholipid chains is adequately described by the Flory-Huggins theory. It is known¹¹ that,

at high volume fractions of the polymer in latex systems, the dominant free energy contribution to the equilibrium situation is the combinatorial entropy of mixing of solvent and the alkane chains. The good agreement between theory and experiment in this work implies that at partial swelling the non-combinatorial and enthalpic terms are small compared to the combinatorial entropy term.

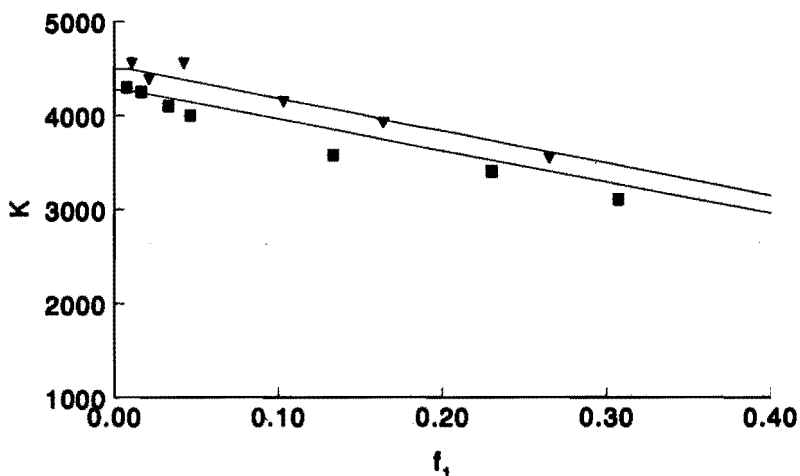


Figure 8.6 Partial swelling of benzene between the lipid phase and aqueous phase. Experimental values of partition coefficient versus fraction of benzene in the lipid phase for DMPC at 30 °C (squares) and egg PC at 25 °C (triangles). The lines are fits of equation 8.9 to experiment for DMPC at 30 °C (full line) and egg PC at 25 °C (dashed line) with values of $v_{p,sol}$ (in equation 8.15) as given in table 8.2.

More surprising, since vesicles are considered as interfacial phases of matter, is that the interfacial free energy is relatively small and constant (with respect to the combinatorial entropy free energy term) at partial swelling. Upon further reflection the cause for this result can be easily explained: the changes of the surface area with swelling over the full range of swelling is small. This is simply because the vesicles do not swell to a very large extent. Hence, relative to the combinatorial entropy of mixing, the interfacial free energy at partial swelling does not contribute significantly to changes in the thermodynamic equilibrium attained at various degrees of swelling by solvent. This is displayed in figure 8.7.

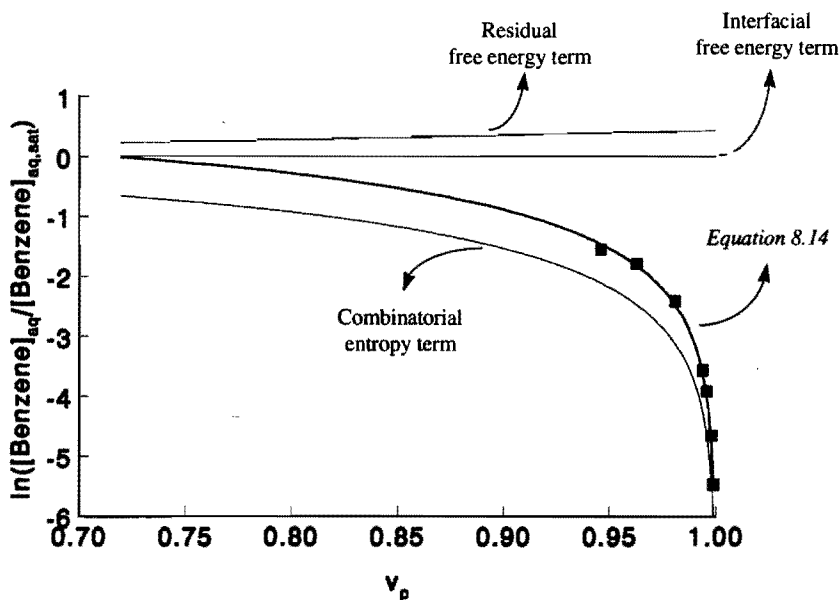


Figure 8.7 Comparison of theoretical predictions (assuming χ and γ independent of v_p) and experimental measurements of benzene partitioning between water and DMPC vesicles at 30 °C. Theoretical predictions: combinatorial entropy term; residual free energy term given with $\chi = 0.45$; interfacial free energy term given with $\gamma = 13.4$ mN/m and $R_0 = 50$ nm; and equation 8.14 with $\chi = 0.45$, $\gamma = 25$ mN/m, and $R_0 = 50$ nm.

It has been noted that the solvent partition coefficient changes with the surface density of phospholipid in the vesicles (i.e. the area per phospholipid molecule on the surface of the vesicles)². Obviously, as more solvent is imbibed by the vesicles the surface density will decrease, simply because the phospholipid head groups are slightly further apart. This correlation does not necessarily imply that surface density is the dominating factor that limits the degree of swelling. The combinatorial entropy, and not the surface free energy, appears to dominate the changes in the swelling behaviour at various degrees of saturation of vesicles by solvent.

At saturation swelling it is true that the degree of swelling is limited, to a large degree by the interfacial free energy. It was shown above that the values for saturation swelling of vesicles by solvents can be compared to micelles, or to very small latex particles, where the large surface area to volume ratio restricts swelling to far below the bulk value. It must be noted that this does not imply that mixing of alkane part of the phospholipids and solvent

cannot be described by bulk thermodynamic expressions: to the contrary, the latter must only combined with the appropriate interfacial free energy terms.

Note that, if vesicles are swollen to a degree greater than the 'saturation' values described in this work, it is likely that the phospholipid molecules on either side of a single bilayer will be separated, either in full or in part, by a region of pure solvent. In these cases the theory developed in this work does not apply, and the vesicle should properly be considered as a type of complex solvent droplet. Whether there is a true thermodynamic 'saturation' concentration of solvent in vesicle bilayers is a complex issue which may be confused by kinetic effects in experiments. We will discuss this issue in a future publication.

If we know the vesicle thickness, vesicle radius and the interaction parameter between the solvent and alkane chains of the phospholipid molecules then, from the experimentally fitted values of $v_{p,sat}$ and *equation 8.15*, the value of the vesicle-water interfacial tension can be determined. However, the former three parameters warrant further comment:

1. Bilayers of the type in this work are known to have a thickness of between 2 and 4 nm. This is related to the length of the phospholipid molecules. In this work we utilize a mean thickness of 3 nm.

2. Multilamellar vesicles are known to be from 50-400 nm in radius. In this work we have calculated values at both 50 nm and 400 nm.

3. The interaction parameter of the solvents with the alkane chain of the phospholipids can be approximated by the interaction parameter between the solvent and polyisoprene. These interaction parameters measured between the solvents and polyisoprene represent the most similar (measured) system to the vesicle situation at hand, namely alkyl tails of surfactants mixing with the same solvents. Polyisoprene is an alkyl polymer with some degree of unsaturation, and a methyl side group on the main chain, whereas the alkyl chains of the phospholipid molecules are generally unsubstituted and contain a small degree of unsaturation. It should be noted that these differences in structure are unlikely to significantly affect the value of the interaction parameter. Using this approximation for the interaction parameters ignores the possible interactions of solvent molecules with the head groups of the phospholipids (this is consistent with the approach of this work). At 25 - 50 °C the measured

interaction parameters between polyisoprene and benzene and hexane, respectively, are $\chi = 0.45$ and $\chi = 0.52$.

Utilizing the above values of the bilayer thickness, χ and R_0 , from the values of $v_{p,sat}$ calculated by fits of *equation 8.9* to experimental data, it is possible, via *equation 8.15*, to estimate the interfacial tension of the vesicles. These interfacial tensions are given in *table 8.2*. The range of interfacial tensions are those expected, and are well below the water-solvent interfacial tensions (of course the exact values of the interfacial tension rely upon better values for the interaction parameters). Of greater interest is that the interfacial tension of the hexane-DMPC and benzene-DMPC data are very similar despite the large differences in their swelling behavior. This is encouraging since if the interfacial tension is truly a interfacial phenomena then solvent should have little effect on this value since the surface is mainly characterized by surfactant (this is because of the low solvent concentrations in vesicles). This appears to be the case.

Utilizing the above calculated interfacial tensions, in *figure 8.7* the contributions of all terms in *equation 8.14* to the equilibrium partitioning of benzene in DMPC vesicles are displayed. In accord with the assumptions made, it can be clearly seen that, at partial swelling, the dominant contribution to the changing thermodynamic equilibrium is the combinatorial entropy of mixing of solvent and the alkane part of the phospholipid molecules.

8.4 Conclusions

Comparison of theory and experiment suggests that the swelling of vesicles by solvents can be modeled in a manner similar to that for the swelling of polymer latex particles by solvent. Data for the swelling of various bilayers by two solvent at two temperatures were all adequately fitted by the model. The only 'adjustable' parameter in this model, the volume fraction of solvent or alkyl chain in the vesicle at saturation is in fact limited by considerable physical understanding: the fitted values of this parameter compare well to values for similar systems.

The basis of the equations utilized in this paper is the consideration that the mixing of the alkyl part of the vesicles and solvent can be considered in terms of Flory-Huggins theory. The Flory-Huggins theory works very well for the partial swelling of vesicles with solvent for the following reasons:

1. The alkane concentrations within the vesicles are always relatively high. Therefore there should be a uniform density of Flory-Huggins segments.

2. The residual free energy term (the χ -term) is not a major contributor to the thermodynamic problem at the higher volume fraction of alkane. Hence all the uncertainties associated with the measurement and interpretation of the interaction parameter are less consequential. As pointed out by Flory the original derivation of the Flory-Huggins theory resulted in an interaction parameter that should be polymer (phospholipid alkane) concentration dependent at high volume fraction of polymer (phospholipid alkane). This is not a problem for the experimental systems studied in this work since within experimental error the fit of *equation 8.9* to experimental data was insensitive to the value of the interaction parameter (within reasonable bounds). The Flory-Huggins term that describes the combinatorial entropy of mixing of solvent and polymer is very successful at predicting the solvent partitioning. This entropic term was also derived by Hildebrand via a free volume approach and is quite general.

3. The alkyl tails of the phospholipid chains are relatively immobile compared to solvent molecules, and therefore the phospholipid molecules can be considered as fixed in space. In this case the placement of solvent molecules in the vesicles becomes a free volume problem, which is that which the Flory-Huggins approach addresses.

The interfacial free energy of vesicles was modeled with the Gibbs-Thomson equation, utilizing a single macroscopic interfacial tension. From the fit of the model to the experimental data, and specifically from the fitted value of the saturation concentration of solvent in the vesicles (here both γ and χ are important), a range of values of the interfacial tension of the vesicles were calculated. These values are similar to those expected for small latex particles and micelles. Unfortunately, the use of a single interfacial tension tells us very little about the individual interfaces of the bilayer, except that, being non-zero it confirms White's assertion that a vesicle can be at equilibrium even if the interfacial tension is non-zero: this just arises from the proper definition of the interfacial tension (*equation 8.10*). The use of a

macroscopic interfacial tension is consistent with the use of bulk thermodynamic expressions for the hydrophobic part of the bilayers. Now that we have shown that these equations can indeed describe certain vesicle behavior the next challenge will be to relate these macroscopic properties to the microscopic.

Finally, it was the original aim of this work to develop a relationship that could model the swelling of vesicle bilayers by solvent. The equations that are developed here can be used to predict the swelling of vesicles by solvent, and require that only the saturation concentration of the solvent in the vesicle be known. If this is known an estimate of the interfacial tension of the vesicle can also be calculated (or vice versa). The success of this work may allow for the modeling of solvent uptake by other types of bilayers (e.g. extended sheets), and even other surfactant structure (e.g. micelles), since the mixing of the solvent and surfactant within the interior of the vesicles can be easily modeled by macroscopic thermodynamic theory. This latter point may have farther reaching ramifications.

8.5 Appendix A: Surface Phenomena in Vesicle Bilayers and the Gibbs Phase Rule

It is a fundamental principle of surface chemistry that the hydrostatic pressure on the two sides of a curved surface between two homogeneous fluids is different (Laplace's Law). For a spherical surface of radius R , the relation between the equilibrium pressure P^α on the concave side and the pressure P^β on the convex side is given by *equation A.1*.

$$P^\alpha - P^\beta = \frac{2 * \gamma}{R} \quad (\text{A.1})$$

where γ is the surface tension. Since the value of surface tensions is positive, the pressure on the concave side is normally higher than at the convex side. One of the major questions concerning the physical chemistry of vesicles is whether the surface tension of vesicles is zero, since the chemical potential of the water in the interior of a vesicle is equal to the bulk chemical potential, or that one must be positive and the other negative as pointed out by Tanford¹⁹. White²⁰, on the other hand, pointed out that this was not the case: in fact the

surface of a vesicle can be at equilibrium while having a non-zero interfacial tension. White gave the following equations for the macroscopic interfacial tension of a vesicle:

$$\gamma = \int_{z_1}^{z_2} [P_N(Z) - P_T(Z)] dZ \quad (\text{A.2})$$

where the Z axis is normal to the surface layer, and the integration limits Z_1 and Z_2 include the entire bilayer. The interfacial tension, γ , arises from the anisotropy of the bilayer, and the pressure within the bilayer is then a tensor. This pressure has been resolved into two components, $P_N(Z)$ normal to the surface and $P_T(Z)$ tangential to the surface. Note that γ is an integrated property of the interface.

In this section we would like to use an approach based on the modified Gibbs phase rule to show that vesicles have a net surface tension. Let us consider a vesicle of 50 nm diameter and a bilayer thickness of 5 nm, in a bulk water phase. The classical phase rule states that in a system with C independent chemical components and P coexisting phases the maximum number of independent, intensive variables that may be used to describe the state of the system. The number of independent, intensive variables or the number of degrees of freedom, F , is equal to:

$$F = C - P + 2 \quad (\text{A.3})$$

Equation A.3 represents the standard Gibbs phase rule. *Equation A.3* is deduced for a system satisfying the following conditions: First, boundary surface effects are neglected; and second, volume is the only work coordinate. A vesicle can be considered in two different ways: First, C is equal to 2 and $P = 5$ (three bulk phases (one interior water phase, one exterior water phase, and one bilayer phase) and two liquid-liquid interfaces) thus $F = -1$ which is clearly unrealistic. The second way is by not counting the two water phases separately and only considering one liquid-liquid interface (the vesicle is equivalent now to an extended bilayer), i.e. $P = 3$, which yields $F = 1$, which is still unrealistic.

If one takes into consideration that the system contains curved surfaces *equation A.3* changes to *equation A.4*^{28,29}

$$F = C + 1 - N \quad (\text{A.4})$$

where N denotes the total number of distinct $P^\alpha = P^\beta$ type relations among the mechanical equilibrium conditions. In the case of the earlier mentioned vesicle, two situations can be encountered: First, the case where the vesicle has no net surface tension as stated by Tanford¹⁹. Concomitantly, $N = 2$ (since there are two liquid-liquid interfaces which fulfill the requirement that $P^\alpha = P^\beta$), with $C = 2$, the number of degrees of freedom F is equal to 1, which again is unrealistic. Second, the system has a net surface tension, thus $N = 0$, together with $C = 2$, resulting in $F = 3$. This results in the only physical realistic number of degrees of freedom being temperature, pressure and interfacial tension. In conclusion, it can be said that the vesicles need to have a net surface tension in order to fulfill the modified Gibbs phase rule, which not only holds for thermodynamically stable but also thermodynamically meta-stable systems.

8.6 References

- 1 De Young, L. R.; Dill, K. A. *Biochemistry*, 27, 5281(1988)
- 2 De Young, L. R.; Dill, K. A. *J. Phys. Chem.*, 94, 801 (1990)
- 3 Simon, S. A.; McDaniel, R. V.; McIntosh, T. J. *J. Phys. Chem.*, 86, 1449(1982)
- 4 Kurja, J.; Nolte, R.; Maxwell, I. A.; German, A. L. *Polymer*, 34, 2045. (1993)
- 5 Simon, S. A.; Stone, W. L.; Bennett, P. B. *Biochimica et Biophysica Acta*, 550, 38 (1979)
- 6 Simon, S. A.; Stone, W. L.; Busto-Latorre, P. *Biochimica et Biophysica Acta*, 468, 378 (1977)
- 7 Gruen, D. W. R. *Biophysics J.*, 33, 149 (1981)
- 8 Gruen, D. W. R.; Haydon, D. A. *Pure & Appl. Chem.*, 52, 1229 (1980)
- 9 Morton, M.; Kaizerman, S.; Altier, M. W. *J. Colloid Sci.*, 9, 300 (1954)
- 10 Gardon, J. L. *J. Polymer Science: Part A-1*, 6, 2859 (1968).
- 11 Maxwell, I. A.; Kurja, J.; van Doremaele, G. H. J.; German, A. L.; Morrison, B. R. *Makromol. Chem.*, 193, 2049 (1992).
- 12 Vanzo, E.; Marchessault, R. H.; Stannet, V. *J. Colloid Sci.*, 20, 62 (1965)
- 13 Maxwell, I. A.; Kurja, J.; van Doremaele, G. H. J.; German, A. L. *Makromol. Chem.*, 193, 2064 (1992)
- 14 Noel, L. F. J.; Maxwell, I. A.; German, A. L. *Macromolecules*, 26, 2911 (1993)
- 15 Flory, P.J. in *Principles of Polymer Science*, Cornell University Press, Ithaca, New York 1953
- 16 Ugelstad, J. *et al.*, in *Science and Technology of Polymer Colloids*, NATO ASI Series E, Vol. 1, Plenum, New York (1983)
- 17 Johnson, C.A., *Surface Science*, 3, 429 (1965)
- 18 The lateral diffusion coefficient of a C12 surfactant in a vesicle bilayer as measured by Pulsed Field Gradient NMR is an order of magnitude less than the mobility of a solvent molecule in the vesicle (Piton, M., Personal Communication). A phospholipid molecule has much greater steric hindrance than a C12 species, therefore it is considered that the lateral

diffusion coefficient of phospholipid species in bilayers will be at least two orders of magnitude less than that of a solvent molecule.

19 Tanford, C. *Proc. Natl. Acad. Sci., USA*, 76, 3318 (1979)

20 White, W. H. *Proc. Natl. Acad. Sci., USA*, 77, 4048 (1980)

21 For the purpose of calculations V_p is given by $V_p = \frac{4}{3} * \pi * (R_o^3 - R_i^3) * v_p$, where R_o is the outer radius of the vesicle bilayer, R_i the inner radius of the vesicle bilayer and v_p the fraction of phospholipid alkane on the bilayer. V_s is similarly given by

$$V_s = \frac{4}{3} * \pi * (R_o^3 - R_i^3) * (1 - v_p). \text{ The volume of the water interior of the vesicle, } V_w,$$

is simply given by $V_w = \frac{4}{3} * \pi * R_i^3$.

22 Weast, R. C., Ed. *CRC Handbook of Chemistry and Physics*; CRC Press: Florida, 1986.

23 Watts, A.; Marsh, D.; Knowles, P. F. *J. Am. Chem. Soc.*, 100, 1792 (1978)

24 Nagle, J. F.; Wilkinson, D. A. *Biophysical J.*, 23, 159 (1978)

25 Brandrup, J., Immergut, E.H., *Polymer Handbook*, 3rd ed., Wiley (1989)

26 Almgren, M.; Grieser, F.; Thomas, J. K. *J. Amer. Chem. Soc.*, 101, 279 (1979)

27 McAuliffe, C. *J. Phys. Chem.*, 70, 1267 (1966)

28 Chapter 6 of this thesis

29 Li, D., Gaydos, J., and Neumann, A.W., *Langmuir*, 5, 1133 (1989)

CHAPTER 9 [#]

Unconventional Emulsion Polymerizations

Synopsis: In this chapter, a brief survey of those heterogeneous polymerization process that can be considered as unconventional emulsion polymerizations has been given. It is likely that many other unconventional emulsion polymerizations exist, and as such it has been the purpose of this review only to give an introduction into this field. The polymerizations described have, in the main, not been the subject of in-depth kinetic studies, and this is reflected in the summaries of these processes.

9.1 Introduction

One difficulty in defining *unconventional* emulsion polymerizations is first defining emulsion polymerization. One can of course describe an emulsion polymerization by what it is *not*; it is not a suspension, dispersion, bulk or solution polymerization. On the other hand an emulsion polymerization *is* that category of heterogeneous polymerizations that results in 'latex' particles: so called because of the resemblance to natural rubber latex particles. Further, the title 'emulsion polymerization' has really been developed to describe the free-radical polymerization of sparingly water-soluble monomers, by which synthetic latex particles are formed. The title 'emulsion polymerization' is really a misnomer since the polymerization generally does not occur, as implied, in emulsion droplets of monomer, but rather in newly-generated latex particles for which the emulsion droplets act as reservoirs of monomer. The boundaries of the emulsion polymerization process are blurred, and can be indistinguishable from many other types of heterogeneous polymerizations. Two typical examples of such 'indistinguishable' processes are: First, the anionic dispersion polymerization of styrene

[#] In part reproduced from: Kurja, J., Zirkzee, H.F., and Maxwell, I.A., "*Unconventional Emulsion Polymerizations*", in "*Emulsion Polymers and Emulsion Polymerization*", M.S. El-Aasser and P.A. Lovell (Eds.), Wiley, Chapter 23, 763 (1997)

leading to the formation of uniform micron-size particles of polystyrene with a narrow molecular weight distribution ¹. Secondly, the preparation of polyphenol particles by an aqueous dispersion polymerization using horseradish peroxidase and hydrogen peroxide as catalysts ².

There are many unique polymerization processes which share a common heritage with emulsion polymerization, but which often are unrecognized as such. It is the purpose of this review to describe some of these emulsion polymerization-like processes and their products. Some further definition is in order; unconventional emulsion polymerizations can be described as those processes whereby the product is polymer latex that physically resembles latex from emulsion polymerization *and* cannot be grouped into any other recognized form of heterogeneous polymerization. In many cases the reasons why a process is not recognized as an emulsion polymerization is that the polymerization is not via a free-radical process. This review discusses four distinct types of polymerization processes, all of which have examples that produce latex particles and in many ways can be described as unconventional emulsion polymerizations. These are free-radical polymerization, ionic polymerization, transition metal catalyzed polymerization and enzyme-catalyzed polymerization. The precise systems discussed in this review are described in *Table 9.1*.

The recording and reviewing of these unconventional emulsion polymerizations is motivated by both academic and industrial aims. In many cases an understanding of the chemistry of emulsion polymerization can enable advances in a previously unrelated unconventional emulsion polymerization. By describing some of these processes that show resemblance to emulsion polymerization, substantial cross-fertilizations may occur, allowing the borders and influences of the science of emulsion polymerization to be broadened, whilst also providing fresh ground for new polymer products or processes.

Table 8.1: Unconventional emulsion polymerizations^a

Polymerization Mechanism	Monomer	Initiator (I), Catalyst (C), Enzyme (E) or Oxid. Agent (OA)	Polymer	Surfactant	Latex Particle Size (nm)	Ref.
Radical Polymerization						
Chemically-Initiated Vinyl Polymerization	Tetrafluoroethylene (TFE)	I: (NH ₄) ₂ S ₂ O ₈ , K ₂ S ₂ O ₈ , gamma-irradiation	PTFE	NH ₄ -perF-oct.	60 - 150	1 - 4
Ultrasound	Acrylonitrile (AN) Butyl acrylate (BA) Vinyl acetate (Vac)	H [•] /OH [•] radicals via Ultrasound	PAN PBA PVAc	SDS SDS	< 100	5
Conducting Polymers	Aniline (ANI) Pyrrole (Py)	OA : (NH ₄) ₂ S ₂ O ₈ , K ₂ S ₂ O ₈ , FeCl ₃ or electrochemically	PANI PPy	DBSA, PEO PVP	30 - 500	10 - 18
Ionic Polymerization	Permethylsiloxane (PMSi)	C : DBSA, R _n NOH	P(PMSi)	DBSA, R _n NOH	50 - 500	19 - 23
Transition-Metal catalyzed Polymerization						
Vinyl Polymerization	Norbornene (Nor) Butadiene (B) <i>cis/trans</i> -Pentadiene (Pent)	C : PdCl ₂ RhCl ₃ RhCl ₃	PNor PB <i>cis/trans</i> -PPent.	SDS DBS-Na DBS-Na	10 - ^b - ^b	27 28 - 29 30
Ring-Opening Metathesis Polymerization	Ethylene and Carbonmonoxide Norbornene-derivative. (Nor-der.) Oxanorbornene-derivative (BMM-7-ON)	Pd based catalyst Ir/Ru based catalyst Ru based catalyst	"Polyketone" P(Nor-der.) P(BMM-7-ON)	- ^b - ^b Synperonic F127	- ^b - ^b 40 - 60	26 32 - 35 36
Enzyme catalyzed Polymerization						
Bacterial PHAs	Hydroxybutyryl-CoA	E : PHB-synthase	PHB	Phospholipids	20 - 1000	37
Natural Rubber	Isopentenylphosphate	E : Rubber Transferase	<i>cis</i> -polyisoprene	Phospholipids	10 - 2000	46
Cellulose	Uridine diphosphoglucose	E : Cellulase	Cellulose	Phospholipids	- ^b	51

^a : acronyms are defined in the appropriate sections of this chapter^b : not mentioned in original reference

9.2 Unconventional Free-radical Emulsion Polymerizations

9.2.1 Chemically-Initiated Vinyl Polymerizations

There is an important category of free-radical emulsion polymerizations where the hydrophobic polymer does not dissolve in its own monomer^{3,4,5,6} or is only sparingly soluble in its own monomer³. Some examples of these kinds of polymerizations are the emulsion polymerization of fluorinated monomers (e.g. tetrafluoroethylene (TFE), chlorotrifluoroethylene (CTFE), 1,2-difluoroethylene)^{4,5}, and acrylonitrile⁶. The polymers formed by these polymerizations all have significant industrial importance, particularly as engineering polymers (e.g. Teflon, Acrylonitrile-Butadiene-Styrene rubber (ABS)). As a result much of the research into these processes remains outside the public domain. The fact that these polymers do not dissolve in their own monomers leads to complex phase separation at very low conversions during the polymerization process. The phase separation is even more complex than in a conventional emulsion polymerization since, not only is there phase separation between the newly-formed polymer and the continuous water phase, but also between the polymer and monomer present. Due to this phase separation the locus of polymerization is not the interior of the polymer particles, simply because there is no monomer in the interiors. Free-radicals formed in the water phase tend to precipitate or adsorb at the surface of existing particles rapidly after their formation. Thus the major part of the propagation process will take place at the surface of the polymer latex particles^{5,6}. Evidence for this is that the rate of polymerization is proportional to the total surface area of the latex particles; this trend has been determined by varying both the latex particle concentration and size and observing the polymerization rate⁵.

A kinetic treatment of these polymerization processes necessarily considers the surface area of the latex particles rather than the latex particle volume, as is usually the case in emulsion polymerization. Note that special cases of these polymerizations exist where a non-polymerizing solvent is added to change (normally increase) the solvency of the monomer in the latex particles, thereby modifying the polymer properties.

9.2.2 Ultrasound Polymerizations

An unusual free-radical polymerization of vinyl monomers utilizes ultrasound to both emulsify monomer, and to create free-radicals⁷. The ultrasound (at 20 kHz) acts on water to create hydrogen and hydroxyl initiating radicals, an initiating system that bears resemblance to many

radiation-induced polymerizations. The first claimed emulsion polymerizations by ultrasound were those of butyl acrylate and vinyl acetate ⁷. In most cases it was observed that the particle sizes obtained by ultrasound initiation are smaller than those of equivalent chemically-initiated polymerizations, although they may be dependent upon the energy input. It is interesting to note that this approach to initiation is a possible alternative to radiation-induced initiation in (pulsed) kinetic studies of (emulsion) polymerization mechanisms.

9.2.3 Polymerization in Vesicles

There are various morphologies of latex particles available; these include core-shell and other complex morphologies within the latex particles, and also hollow latex particles. The traditional route to hollow latex particles is the production of core-shell latexes where the inner core of the latex particles can be removed in a post-polymerization process ⁸. These hollow latex particles have a variety of uses in surface coatings, controlled release technologies and opacifiers. Recently a new approach to the production of hollow latex particles has been developed ⁹. In this approach a surfactant structure is stabilized by the polymerization of a vinyl monomer via free-radicals in the walls of the vesicles. A vesicle, which is usually a meta-stable structure is converted into a hollow 'latex particle'. This process, while not strictly an emulsion polymerization, has been optimized by use of emulsion polymerization procedures ¹⁰. In the future it is possible that many other unique surfactant structures may be maintained by the *in situ* introduction of polymer.

9.2.4 Conducting Polymer Latices

The preparation of conducting polymers in emulsion is generally via an oxidative coupling mechanism in which the active polymerizing species are free-radicals. In *figure 9.1* the polymerization scheme for formation of polyaniline is shown ¹¹. This polymerization process, which is distinct from vinyl chain polymerization, is described in detail elsewhere ¹¹. Because of their conjugated backbones, conducting polymers are intrinsically intractable polymers, making them very hard to process. Preparing these polymers in an emulsion overcomes many of these processing problems. Examples of conducting polymers which have been produced in an emulsion are polyacetylene, polypyrrole (PPy) and polyaniline (PANI) ^{12,13,14,15}. The latter two are discussed below.

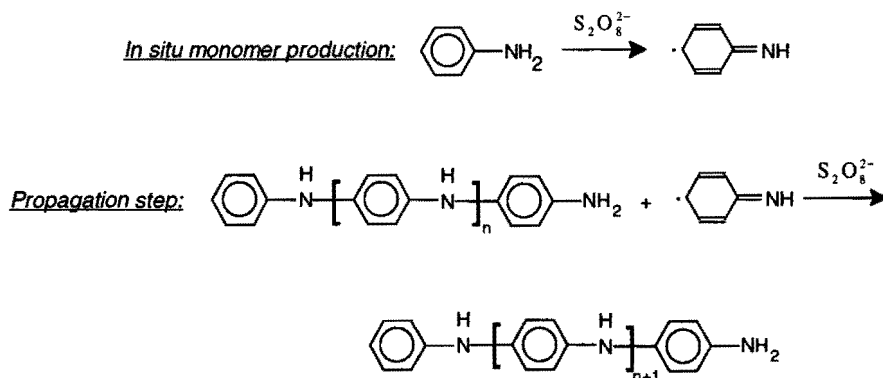


Figure 9.1 The polymerization scheme for formation of polyaniline¹⁶

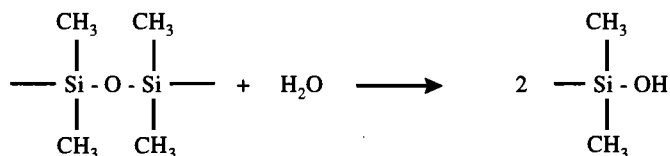
The literature of the oxidative polymerization of aniline in an aqueous medium describes both dispersion and emulsion types of polymerizations, each with differing types of stabilizers^{15,17,18}. In the case of dispersion polymerization a polymeric stabilizer is used, and rather large polymer (latex) particles are typically obtained, e.g. in the order of 300 - 400 nm diameter. However, there is also an example of an emulsion polymerization of aniline using dodecylbenzenesulfonic acid (DBSA) as a surfactant^{15,19}. The DBSA also acts as a doping agent for the PANI, while at the same time it makes the PANI easier to process.

The polymerization of pyrrole in water using a polymeric stabilizer (high molecular weight poly(ethylene oxide)) and potassium persulfate as an oxidising agent results in very small polypyrrole latex particles with diameters of approximately 30 nm²⁰. Using a polymeric stabilizer (e.g. partially hydrolyzed poly(vinyl acetate)) and FeCl₃ as an oxidizing agent, latex particles were obtained with mean diameters ranging from 50 - 250 nm¹⁴. Very recently polypyrrole latex particles have been created by an electrochemical route²¹, latex particles in the order of 10-200 nm diameter were produced.

9.3 Ionic Emulsion Polymerizations

Numerous studies have been conducted concerning the polymerization of siloxanes^{22,23,24}, but have focused mainly on bulk polymerization. Emulsions of polysiloxanes have attracted great

attention since the 1980's due to the fact that these emulsions can be utilized in surface coatings. Hyde and Wehrly²⁵ described the emulsion polymerization of permethylcyclsiloxanes which proceeds via an anionic polymerization mechanism involving a basic catalyst with a cationic surfactant. Weyenberg *et al.*²⁶ developed an analogous acid-catalyzed anionic emulsion polymerization which employs dodecylbenzenesulfonic acid (DBSA) as the catalyst and surfactant. The cationic polymerization can be compared with a conventional free-radical emulsion polymerization; the cationic polymerization involves monomer, water, surfactant, and catalyst and the particle size of the resulting polymer dispersion is normally much smaller than that of the initial monomer droplets. There are two major differences between cationic polymerizations of siloxane and conventional emulsion polymerizations. Firstly, there is a distinct difference between the catalyst used, i.e. cationic catalyst instead of a free-radical one. Secondly, there is a differing role of water in the polymerization mechanism. In the case of the free-radical emulsion polymerization water serves as an inert suspending medium. However, in the siloxane polymerization, water serves as a reactant and consequently affects the molar mass of the polymer, as follows :



Because of this well-known hydration of siloxane bonds, the molar mass of the polymer is influenced both by the polymerization temperature and the nature of the substituents attached to the silicon atoms. Polydimethylsiloxane emulsions with particle diameters of 50 - 500 nm can be obtained on heating aqueous dispersions of permethylcyclsiloxanes with dodecylbenzenesulfonic acid at 50 - 100 °C.

9.4 Transition Metal Catalyzed Emulsion Polymerizations

Generally speaking, transition metal catalyzed polymerization cannot be performed in aqueous media since water destroys active catalyst complexes. However, there are a few monomers which have been polymerized in pure water via transition metal catalyzed reactions. The

following discussion of these polymerizations have been divided into vinyl polymerizations and ring-opening metathesis polymerizations (ROMP).

9.4.1 Transition Metal Catalyzed Vinyl Polymerizations

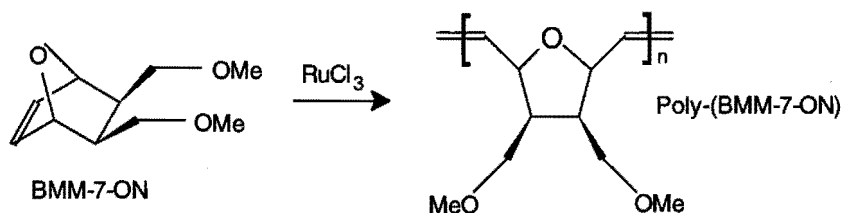
Palladium-based catalysts can be used for the polymerization of norbornene ²⁷ and the copolymerization of ethylene and carbon monoxide ^{28,29}. However, there are only two reports of these polymerizations in aqueous media, namely the oligomerization of norbornene ³⁰ and the alternating copolymerization of ethylene and carbon monoxide ²⁹. In the case of the oligomerization of norbornene a 'micro-latex' was obtained with an average particle diameter of approximately 10 nm. These authors claimed to have performed the first latex synthesis by a non-radical organometallic olefin polymerization, using PdCl₂ as a catalyst and sodium dodecylsulfate as a surfactant. In the case of the alternating copolymerization of ethylene and carbon monoxide it is not clear if a polymer latex was obtained. Since no surfactant was added to the initial reaction mixture it can be assumed that the polymer precipitated from the solution.

In 1962 Rinehart ³¹ and Canale ³² independently reported on the rhodium-catalyzed emulsion polymerization of butadiene to a high *trans*-1,4 polymer utilizing sodium dodecylbenzenesulfonate as an emulsifier. Almost ten years later Entezami *et al.* ³³ showed that *trans*- and *cis*-1,3-pentadiene can be polymerized in emulsion using RhCl₃ as a catalyst and sodium dodecylbenzenesulfonate as a surfactant. Unfortunately, these authors did not mention latex particle sizes. Finally, ethylene can also be polymerized in an emulsion using a rhodium-based catalyst ³⁴.

9.4.2 Ring-Opening Metathesis Polymerization (ROMP)

The first true emulsion polymerization of different norbornenes using transition metals as catalysts were reported by Rinehart and Smith ³⁵. These ROMP polymerizations utilized (NH₄)₂IrCl₆ and RuCl₃ as catalysts, plus a reducing agent, and different surfactants depending on the monomer polymerized. One of the major problems encountered with these polymerizations were the low yields of polymer. Several years ago Novak and Grubbs ^{36,37} reported on the ROMP of certain heteropolycyclic alkenes (7-oxanorbornene derivatives) in pure water using ruthenium salts. Feast and Harrison ³⁸ investigated the aqueous emulsion ROMP of *exo,exo*-2,3-bis(methoxymethyl)-7-oxanorbornene (BMM-7-ON) using ruthenium, iridium and osmium chloride as the precursors of the active catalysts. Only very recently Lu *et al.* ³⁹ were the first to report the aqueous dispersion (emulsion) polymerization of BMM-7-ON, using RuCl₃ as a catalyst

and a polyethylene oxide-polypropylene oxide tri-block surfactant. The polymerization is as follows:



As the surfactant concentration was increased the diameter of the latex particles became smaller, which is a general observation in emulsion polymerization. Depending upon the surfactant concentration, the latex particle diameters were typically in the range 40-60 nm .

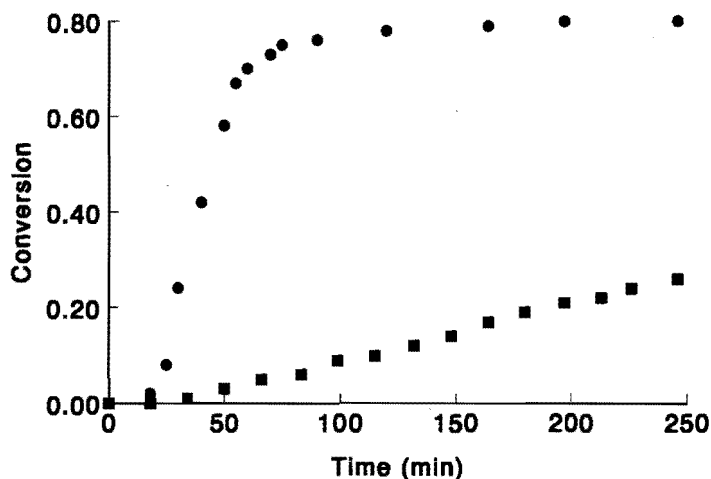


Figure 9.2 Conversion versus time plot for ROMP of BMM-7-ON (Circles: no surfactant added, 10 vol-% H₂O in C₂H₅OH), and ROMEP of BMM-7-ON (Squares: [Antarox-CO-990] = 31 g/l, pure H₂O). Overall [RuCl₃] = 0.048 mol/l, and [BMM-7-ON] = 0.862 mol/l.

In figure 9.2 a comparison is made between a homogeneous, polymer produced dissolves in reaction medium (ROMP), and heterogeneous polymerization system, polymer is present in latex particles which are stabilized by added surfactant (ROMEP: Ring-opening metathesis emulsion polymerization), containing RuCl₃ and BMM-7-ON. Due to the heterogeneous character of the ROMEP process, the rate of polymerization is orders of magnitude higher than in the case of the

ROMP process at equal monomer and catalyst concentration⁴⁰. This indicates that the ROMEPE process exhibits one of the major features of a conventional emulsion polymerization process, i.e. its compartmentalization.

9.5 Enzyme-Catalyzed Emulsion Polymerizations

The initial motivation behind the emulsion polymerization of butadiene in the late 1920's was the search for a substitute to natural rubber. The appellation "latex" is used for the extract which is tapped from the rubber tree. This also is used to describe the product of a synthetic emulsion polymerization. Natural rubber is one of three biopolymers formed by an enzyme-catalyzed polymerization which is recognizable as an emulsion polymerization. Bacterial polyhydroxyalkanoates and cellulose are the other two. A very important aspect of these biological emulsion polymerizations is the fact that they produce unique and different polymers latexes, i.e. a polyolefin, a polyether and a polyester, all from renewable resources. This may become of interest in polymer science in the future, especially as oil reserves are depleted.

In this section the biosynthesis of bacterial polyhydroxyalkanoates, natural rubber and cellulose is discussed, whilst simultaneously describing analogies with conventional (synthetic) emulsion polymerization processes.

9.5.1 Bacterial Polyhydroxyalkanoates

Poly-(R)-3-hydroxyalkanoates (PHAs) are linear biopolyesters produced by a wide variety of bacteria as a reserve of carbon and energy⁴¹. Very recently De Koning and Maxwell⁴² drew an analogy between the conventional emulsion polymerization process and the biosynthesis of PHAs. Based on this Kurja *et al.*^{43,44} made a more quantitative description of the accumulation of poly-(R)-3-hydroxybutyrate (PHB) in *Alcaligenes eutrophus*. PHAs are synthesized via a polycondensation reaction⁴¹. However, the molar mass of the polymer formed during the early stages (low conversions) of the accumulation process is high (typically in the order of $10^5 \text{ g}\cdot\text{mol}^{-1}$)⁴¹ indicating a chain mechanism of polymerization^{43,44}. Initially the polymerase enzyme, which is responsible for the polymerization of the 'monomer', hydroxybutyryl-coenzyme-A, into poly-(R)-3-hydroxybutyrate⁴¹, is present in the cytoplasm of the bacterium, which is the water phase^{45,46}. Once the bacterium is stimulated to accumulate PHB, monomer reacts with the polymerase enzyme in the water phase, and hence initiation has occurred. During the propagation process the

polymerase enzyme is bound to the growing polymer chain. This polymerase enzyme molecule propagates in the cytoplasm until it reaches some degree of polymerization whereby it presumably precipitates, since it exceeds its water solubility. In other words, a latex particle is formed so that the oligomeric polymerase enzyme molecule may minimize its hydrophobic surface area. The so-formed hydrophobic surface will attract phospholipids and other polymerizing species. The latex formation stage ends when there is sufficient hydrophobic surface available for the adsorption/precipitation of all oligomeric polymerase enzyme molecules. The latex formation stage of the PHB accumulation is similar to interval I in the conventional emulsion polymerization process⁴⁷. Once the stage of latex formation is complete the bacteria enter the stage of latex particle growth. Here, monomer diffuses to the surface of the particles where it is converted into polymer by the granule-associated polymerase enzyme. Alternatively an oligomeric polymerase enzyme formed in the cytoplasm precipitates or adsorbs onto the granule surface. At a volume fraction of PHA in the bacterium of approximately 0.58 the latex particles reach a close-packing density and coagulation between latex particles occurs, which is accompanied by a decrease in both the rate of polymerization and molar mass of the polymer formed^{43,44,48}.

Summarizing, the biosynthesis of PHB can be understood in terms of the kinetic processes of initiation, propagation and chain transfer and the affect of latex particle size on these. Further, the colloidal aspects of the formation of PHB latex particles can be explained by the homogeneous nucleation mechanism, well-known in conventional emulsion polymerization processes.

9.5.2 Natural Rubber

Natural rubber is synthesized by a wide variety of plants. The botanic rationale for this synthesis is still a mystery. The biosynthesis of natural rubber has been studied extensively in the past^{49,50,51,52}, and the basic polymerization reactions have been defined. However, the full mechanism of formation of the rubber particles has still not been elucidated, although some suggestions have been made^{50,52,53}. The formation of *cis*-poly-1,4-isoprene is a heterogeneous polymerization where the polymerization mainly occurs at the surface of the rubber particles. The propagating rubber transferase molecule is mainly situated at the surface of a rubber latex particle^{54,55}. The sizes of rubber latex particles can vary from 10 nm to several microns⁵². The outer layer of these latex particles mainly consists of phospholipids and proteins. Archer and Audley⁵⁰ suggested that the rubber particles are formed via a micellar nucleation mechanism, where the micelles consist of geranylgeranyl diphosphate (GGDP), rubber transferase and, possibly, other

molecules. These micelles are either dispersed in the cytoplasm or attached to some surface. Paterson-Jones *et al.*⁵² assumed that, initially, rubber transferase acts on a molecule of farnesyl diphosphate (FDP) or GGDP at some site in a suitable cell membrane. Via a complicated mechanism it is assumed that at a critical chain length the polymer chain, together with both a portion of the membrane and the rubber transferase, detaches to form a separate entity. This is a latex particle composed of a coiled rubber molecule, stabilized by phospholipid chains containing the rubber transferase, through which protrude the active growing ends of the rubber molecule. These authors also stated that the existence of rubber latex particles in the cell is a simple reflection of their chemical incompatibility with either the cytoplasm or the cell membranes.

Hager *et al.*⁵³ proposed another mechanism for rubber particle formation that suggests that the low molar mass rubber formed during the biosynthesis represents the first stable rubber particles that can exist as stable latex particles. These precursor particles can further polymerize until their large size hinders the geometrical positioning required for further polymerization. The precursor particles can also coagulate to form larger particles. A similarity of this process to the synthetic emulsion polymerization process of particle growth is the repeated initiation, propagation and termination of rubber transferase at the particle surfaces.

It is apparent that the mechanism for formation of rubber displays similarities to that of PHB. For this reason it is likely that useful comparisons can be made between the mechanisms of conventional emulsion polymerization and the emulsion polymerization producing natural rubber, particularly in a fashion as already applied to PHB.

9.5.3 Cellulose

Cellulose is the most abundant biopolymer and is produced by nearly all green plants and some fungi and bacteria in order to strengthen cell walls. The enzyme responsible for the formation of cellulose is cellulase, and it is active on the monomer, uridine diphosphoglucose⁵⁶. Under normal circumstances the cellulose is formed as microfibrils on the exterior of the cell walls. Initially the cellulase enzyme molecule is active within the cell, but the oligomeric cellulase chains are adsorbed onto the cell wall, and further polymerization occurs through and beyond the cell walls, forming microfibrils. In a sense the polymer is 'extruded' through the cell walls by the cellulase, and the polymer chains external to the cell walls crystallize, thus giving their strengthening properties. If the cellulose biosynthesis outside the cell walls is

delayed or repressed, the polymer can accumulate as latex particles within the cells. This supports the association-crystallization hypothesis⁵⁷ for cellulose biosynthesis. According to this model the cellulose is synthesized as individual chains within the cytoplasm, which then adsorb onto the cell walls. This is in contrast to other models where it is presumed that the enzyme is only active at the microfibril ends embedded in cell walls. If the former model is correct, and it is supported by experimental evidence, then the biosynthesis of cellulose can be considered, in part, as an emulsion polymerization.

9.6 Concluding Remarks

If the product of a polymerization is a latex then the process of polymerization can be considered, either in part or in full, as an emulsion polymerization. The advantage of doing so is that the physical chemistry of emulsion polymerization, combined with the appropriate polymer chemistry allows, in many cases, fuller understanding of the *unconventional* emulsion polymerization.

In this chapter, a brief survey of those heterogeneous polymerization process that can be considered as unconventional emulsion polymerizations has been given. It is likely that many other unconventional emulsion polymerizations exist, and as such it has been the purpose of this review only to give an introduction into this field. The polymerizations described have, in the main, not been the subject of in-depth kinetic studies, and this is reflected in the summaries of these processes. However, in the following chapters the kinetics and mechanisms involved in the biosynthesis of PHAs, more specifically poly-(R)-3-hydroxybutyrate, will be investigated. In doing so, concepts known from the conventional emulsion polymerization process will be used to describe the phenomena observed during the biological emulsion polymerization of bacterial polyesters.

Although we have drawn analogies between unconventional and conventional emulsion polymerizations there are still many features of the former that cannot be understood by such analogies. There is clearly scope for much work in this field. Finally, since the need for new polymeric materials is growing daily, the field of polymer science must anticipate this phenomenon. Of particular importance are the polymerization processes by which new

polymers or polymeric materials are developed. The study of *unconventional* emulsion polymerization processes, whether 'new' or 'old', will undoubtedly lead to new or improved polymer products or processes.

9.7 References

- 1 Awan, M.A., Dimonie, V.L., and El-Aasser, M.S., *Polymer Prepr*, **35**(2), 551 (1994)
- 2 Uyama, H., Kurioka, H., and Kobayashi, S., *Chemistry Lett*, 795 (1995)
- 3 Guyot, A., in "*Comprehensive Polymer Science*", Edited by G.C. Eastmond, A. Ledwith, S. Russo and P. Sigwalt, Vol. 4, pp 261-273, Pergamon Press, Oxford (1989)
- 4 Putnam, R.E., in "*Comprehensive Polymer Science*", Edited by G.C. Eastmond, A. Ledwith, S. Russo and P. Sigwalt, Vol. 3, pp 321-326, Pergamon Press, Oxford (1989)
- 5 Murray, D.L., and Piirma, I., *Macromolecules*, **26**, 5577 (1993)
- 6 McCarthy, S.J., Elbing, E.E., Wilson, I.R., Gilbert, R.G., Napper, D.H., and Sangster, D.F., *Macromolecules*, **19**, 2440 (1986)
- 7 Cooper, G., Grieser, F., and Biggs, S., *Chemistry in Australia*, **26**, 22 (1995)
- 8 Okubo, M., Ichikawa, K., and Fujimura, M., *Coll. Pol. Sci.*, **269**, 1257 (1991)
- 9 Kurja, J., Nolte, R.J.M., Maxwell, I.A., and German, A.L., *Polymer*, **34**, 2045 (1993)
- 10 Kurja, J., Zirkzee, H.F., German, A.L., Nolte, R.J.M., and Maxwell, I.A., in "*The Polymeric Materials Encyclopedia : Synthesis, Properties and Applications*", Edited by J.C. Salamone, CRC Press, Boca Raton, Vol. 11, 8550 (1996)
- 11 Lux, F., *Polymer*, **35**, 2915 (1994)
- 12 Edwards, J., Fisher, R., and Vincent, B., *Makromol. Chem. Rapid Commun.*, **4**, 393 (1983)
- 13 Armes, S.P., and Vincent, B., *Synth. Metals*, **25**, 171 (1988)
- 14 Armes, S.P., Miller, J.F., and Vincent, B., *J. Coll. Int. Sci.*, **118**, 410 (1987)
- 15 Österholm, J.E., Cao, Y., Klavetter, F., and Smith, P., *Synth. Metals*, **55-57**, 1034 (1993)
- 16 Lux, F., *Polymer*, **35**, 2915 (1994)
- 17 Banerjee, P., Digar, M.L., Bhattacharyya, S.N., and Mandal, B.M., *Eur. Polym. J.*, **30**, 499 (1994)
- 18 Stejskal, J., Kratochvil, P., Gospodinova, N., Terlemezyan, L., and Mokreva, P., *Polym. Int.*, **32**, 401 (1993)
- 19 Österholm, J.E., Cao, Y., Klavetter, F., and Smith, P., *Polymer*, **35**, 2902 (1994)
- 20 Cawdery, N., Obey, T.M., and Vincent, B., *J. Chem. Soc. Commun.*, 1189 (1988)
- 21 Eisazadeh, H., Spinks, G., and Wallace, G.G., *Polymer*, **35**, 3801 (1994)
- 22 Andranov, K.A., Zavin, B.G., and Sablina, G.F., *Polym. Sci. USSR (Eng. Ed.)*, **20**, 1240 (1979)
- 23 Sigwalt, P., and Stannett, V., *Makromol. Chem., Macromol. Symp.*, **32**, 217 (1990)
- 24 Andrianov, K.A., and Dabagora, A.K., *Polym. Sci. (Eng. Ed.)*, **1**, 313 (1960)
- 25 Hyde, J.F., and Wehrly, J.R., *US Patent*; 2,891,920 (1959)
- 26 Weyenberg, D.R., Findlay, D.E., Cekada Jr., J., and Bey, A.E., *J. Polym. Sci., Part C*, **27**, 27 (1969)
- 27 Mehler, C., and Risse, W., *Macromolecules*, **25**, 4226 (1992)
- 28 Drent, E., Van Broekhoven, J.A.M., Doyle, M.J., *J. Organomet. Chem.*, **417**, 235 (1991)
- 29 Jiang, Z., and Sen, A., *Macromolecules*, **27**, 7215 (1994)
- 30 Eychenne, P., Perez, E., Rico, I., Bon, M., Lattes, A., and Moisand, A., *Coll. Pol. Sci.*, **271**, 1049 (1993)
- 31 Rinehart, R.E., Smith, H.P., Witt, H.S., and Romeyn Jr., H., *J. Am. Chem. Soc.*, **84**, 4145 (1962)

- 32 Canale, A.J., Hewett, W.A., Shryne, T.M., and Youngman, A.E., *Chem. & Ind.*, 1054 (1962)
- 33 Entezami, A.A., Mechin, R., Schué, F., Collet, A., and Kaempf, B., *Eur. Pol. J.*, 13, 193 (1977)
- 34 Stryker, H.K., Mantell, G.J., and Helin, A.F., *J. Pol. Sci., Part C*, 27, 35 (1969)
- 35 Rinehart, R.E., and Smith, H.P., *Polymer Lett.*, 3, 1049 (1965)
- 36 Novak, B.M., and Grubbs, R.H., *J. Am. Chem. Soc.*, 110, 960 (1988)
- 37 Novak, B.M., and Grubbs, R.H., *J. Am. Chem. Soc.*, 110, 7542 (1988)
- 38 Feast, W.J., and Harrison, D.B., *J. Mol. Cat.*, 65, 63 (1991)
- 39 Lu, S-Y., Quayle, P., Booth, C., Yeates, S.G., and Padget, J.C., *Polymer Int.*, 32, 1, (1993)
- 40 Kurja, J., Wouters, M.E.L., Van Hamersveld, E, and Jacobs, E., *unpublished results.*
- 41 Anderson, A.J., and Dawes, E.A., *Microbiol. Rev.*, 54, 450 (1990)
- 42 De Koning, G.J.M., and Maxwell, I.A., *J. Environ. Pol. Degr.*, 3, 223 (1993)
- 43 Kurja, J., Zirkzee, H.F., De Koning, G.J.M., and Maxwell, I.A., in "Biodegradable Plastics and Polymers", Edited by Y. Doi and K. Fukuda, pp 379-386, Elsevier, Amsterdam (1994)
- 44 Kurja, J., Zirkzee, H.F., De Koning, G.J.M., and Maxwell, I.A., *Macromol. Theory Simulation*, 4, 839 (1995)
- 45 Griebel, R., Smith, Z., and Merrick, J.M., *Biochemistry*, 7, 3676 (1968)
- 46 Haywood, G.W., Anderson, A.J., and Dawes, E.A., *FEMS Microbiol. Lett.* 57, 1 (1989)
- 47 Blackley, D.C., *Emulsion Polymerization*, Applied Science, London (1975)
- 48 Ballard, D.G.H., Holmes, P.A., and Senior, P.J., *Recent Adv. Mech. Synth. Aspects Polym.*, 215, 293 (1987)
- 49 Backhaus, R.A., *Isr. J. Bot.*, 34, 283 (1985)
- 50 Archer, B.L., and Audley, B.G., *Bot. J. Lin. Soc.*, 94, 181 (1987)
- 51 Tanaka, Y., *Prog. Polym. Sci.*, 14, 339 (1989)
- 52 Paterson-Jones, J.C., Gilliland, M.G., and van Staden, J., *J. Plant Physiol.*, 136, 257 (1990)
- 53 Hager, T., MacArthur, A., McIntyre, D., and Seeger, R., *Rubb. Chem. Tech.*, 52, 693 (1979)
- 54 Cornish, K., *Eur. J. Biochem.*, 218, 267 (1993)
- 55 Lynen, F., *J. Rubb. Res. Inst. Malaya*, 21, 389 (1969)
- 56 Colvin, J.R., in "Encyclopedia of Polymer Science and Engineering", Edited by J.I. Krischwitz, A. Klingsberg, J. Muldoon and A.Salvatore, Vol. 3, 60, John Wiley & Sons, New York (1985)
- 57 Grout, B.W.W., *Planta*, 123, 275 (1975)

CHAPTER 10

The Accumulation of Poly-(R)-3-hydroxybutyrate in *Alcaligenes eutrophus*

1. Kinetics and Metabolic Regulation

Synopsis: In this chapter the regulation of the biosynthesis of PHB in *Alcaligenes eutrophus* has been discussed from an enzymological as well as polymer chemical point of view. The analysis of kinetic data obtained from the *in vitro* conversion of (R)-3-hydroxybutyryl-CoA, via two different enzymological approaches, revealed a K_M of 0.12 mM, which is in good agreement with values reported in literature. At the same time it was found that PHB synthase was inhibited by coenzyme-A, a product of the conversion of the substrate. The inhibition constant K_i for the inhibition of PHB synthase by coenzyme-A was found to be 17 μM which is comparable with the value found in literature for the inhibition of 3-ketothiolase by coenzyme-A, i.e. 16 μM . This result indicated that the biosynthesis of PHB in *Alcaligenes eutrophus* is not only regulated by coenzyme-A the level of 3-ketothiolase but also at the level of PHB synthase. From a polymer chemical point of view the conversion of (R)-3-hydroxybutyryl-CoA has been considered as a classical polycondensation in a closed system at equilibrium. The equilibrium constant found for this polycondensation was equal to 4.4 which is in the same range as found for synthetic polyestifications. In the polymer chemical view the PHB synthase has been considered as a catalyst thus not influencing the equilibrium.

10.1 Introduction

Bacterial polyhydroxyalkanoates (*b*-PHAs) are produced by a wide variety of microorganisms. They are linear aliphatic polyesters first discovered in bacteria by Lemoigne ¹ in 1925. Nowadays, these *b*-PHAs receive a lot of attention because of their biodegradability ². The kinetics and mechanisms involved in the biosynthesis of PHAs have been studied in the past. Griebel and Merrick ³ proposed a two-stage polymerization reaction which involved an acyl-S-enzyme intermediate. Ballard *et al.* ⁴ suggested that there are two thiol groups of the

PHB synthase involved in the polymerization process. One locating the incoming monomer and the other the growing polymer chain. The polymerization proceeds via a concerted insertion condensation. Presumably, this reaction involves a simple transthioesterification between the thioester bond of the polymer-enzyme complex and the bond in the (R)-3-hydroxybutyryl-CoA molecule. The molar mass of the polymer formed is controlled by some form of chain transfer reaction. Kawaguchi and Doi ⁵ discussed the kinetics and mechanisms involved in the synthesis and degradation of poly-3-hydroxybutyrate (PHB) in *Alcaligenes eutrophus*. They defined the principle steps of polymerization, i.e. initiation, propagation and chain transfer to water. The number of polymer chains produced during the accumulation stage of PHB in the presence of a carbon source increased with accumulation time suggesting that a chain transfer reaction, i.e. chain transfer to water, occurs which controls the molar mass of the polymer formed ⁶. Polymer degradation is caused by the intracellular PHA depolymerase enzyme which is supposed to be an *exo*-type of hydrolase. The PHA depolymerase is assumed to be a serine esterase with a hydroxy group as the active site ⁵. De Koning and Maxwell ⁷ drew an analogy between the conventional emulsion polymerization process and the biosynthesis of PHB. Kurja *et al.* ⁸ quantified this model and showed that the kinetics of the polymerization process are affected by the intrinsic heterogeneity of the polymerization system. Further, they showed that the molar mass of the polymer formed during the accumulation process was inversely proportional to the total surface area of the PHB granules present. However, these studies were not concerned with the mechanisms of the biosynthesis of PHAs but more with the kinetics of the polymerization process.

During World War I **synthetic** glycerol phthalate, its **natural** analogue was discovered 80 years earlier, was used for impregnating materials and as a coating ⁹. The chemistry of polyester formation was developed much later by Kienly and Carothers, who also defined the kinetics of polycondensations. After this pioneering study numerous papers have been published on the kinetics and mechanisms of polycondensations ¹⁰.

In comparing *b*-PHAs with synthetic linear aliphatic polyesters (*s*-PHAs) there are several remarkable differences between these polymers not only from a synthetic but also from a topological point of view. The aim of the current chapter is to show, nevertheless, how the

biosynthesis of *b*-PHAs can be understood in terms of *classical* polymerization/enzyme kinetics and mechanisms.

10.2 Theory

In this section we will discuss some basic concepts of polycondensations, synthetic as well as biosynthetic. Further, the biochemical regulation of the biosynthesis of PHB in *Alcaligenes eutrophus* will be summarized. Finally, a small overview of enzyme kinetics will be given.

10.2.1 Synthetic Polycondensations versus the Biosynthesis of *b*-PHAs

Before the synthesis of *b*-PHAs and *s*-PHAs are compared, the mechanistic aspects of these processes will be discussed separately.

10.2.1.1 Synthetic Polycondensations

Extensive literature exists on the mechanistic and synthetic aspects of polycondensations, therefore, in this thesis only the major phenomena which are important in the comparison with *b*-PHAs will be discussed. Two types of reactions are used to prepare polyesters, i.e. step-growth polyesterification (condensation polymerization) and ring-opening polymerization of lactones. Step-growth polyesterifications can be subdivided into (a) direct polyesterifications and (b) ester exchange (transesterification) reactions (also acylation and related reactions)¹¹.

(a) *Direct polyesterification*: In the synthesis of linear aliphatic polyesters, a stoichiometric amount of monomers, i.e. equimolar quantities of reactive groups, should be maintained at all stages of reaction. High molar mass polymers can be obtained only when the low molar mass by-products (often H₂O) are removed from the reaction mixture. Direct polyesterifications can be generalized by the following reaction:

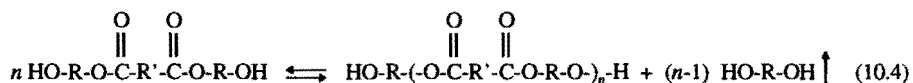
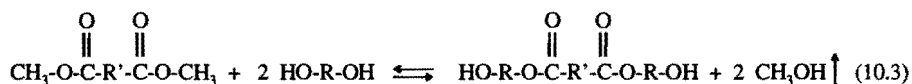


The equilibrium constant K for this reaction is:

$$K = \frac{[-O-R-CO-][H_2O]}{[-OH][COOH]} \quad (10.2)$$

where $[-O-R-CO-]$, $[-OH]$, and $[-COOH]$ denote the concentration of ester, hydroxyl, and acid groups in the reaction mixture, respectively.

(b) *Ester exchange reactions*: These reactions serve for the preparation of polyesters from diols and dicarboxylic acid. However, instead of using pure dicarboxylic acid mostly the dimethyl ester of the carboxylic acid is used for the formation of the polyester with the diol. This transesterification process yields a hydroxy terminated ester and an alcohol. Next, the intermediate ester is subjected to polycondensation, and the final polyester and a diol are formed (see *equations 10.3 and 10.4*).



Both reactions described in *equations 10.3 and 10.4* are reversible, but the proper reaction conditions ensure completion of the reaction. In *reaction 10.3* methanol is distilled off to ensure high yields of the methyl ester. In the next step (*reaction 10.4*) the product of *reaction 10.3* is heated in the molten state and under reduced pressure. Here, again the diol liberated during the condensation should be removed to ensure high yields and molar mass of the polyester formed.

The major requirement to perform a successful polycondensation is that the low molar mass product of the esterification (H_2O , CH_3OH and/or $HO-R-OH$) should be removed from the reaction mixture to ensure that high conversion is reached which, concomitantly, will lead to high molar mass polymers. This can be envisaged by the following equation, also known as

the Carothers equation¹², which relates the average degree of polymerization of the polymer formed with the extent of the reaction:

$$\bar{x}_n = 1 / (1 + p) \quad (10.5)$$

where \bar{x}_n denotes the number average degree of polymerization and p the extent of the reaction, i.e. the conversion.

10.2.1.2 Biosynthesis of *b*-PHAs

The availability of nutrients is a key factor in regulating the PHB metabolism in *Alcaligenes eutrophus*. Under balanced growth conditions, coenzyme-A (HS-CoA) levels are high and the synthesis of PHB is inhibited, so that acetyl-CoA is merely metabolized in the tricarboxylic acid cycle (see also figure 10.1).

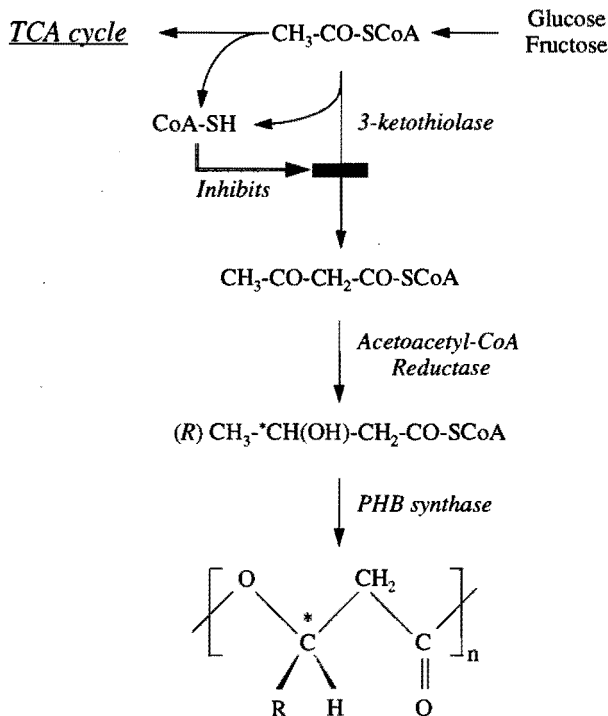


Figure 10.1 Schematic representation of the metabolic pathway of the biosynthesis of PHB in *Alcaligenes eutrophus*⁵.

In nutrient limitation but carbon excess, however, proteins can no longer be synthesized and the built up of NAD(P)H inhibits citrate synthase and consequently acetyl-CoA is no longer able to be oxidized at a high rate via the tricarboxylic acid cycle and therefore it accumulates. Although the equilibrium constant of the reversible condensation reaction of acetyl-CoA does not favor acetoacetyl-CoA formation, under these conditions, i.e. high concentrations of NAD(P)H and acetyl-CoA and low concentrations of coenzyme-A, the equilibrium is displaced in favor of PHB biosynthesis. Simultaneously, these conditions inhibit the degradation of PHB and prevent unrestricted recycling of polymer¹⁵. In summary, the biosynthesis of PHB in *Alcaligenes eutrophus* is regulated at the enzyme level. 3-Ketothiolase, which catalyses the condensation of acetyl-CoA into acetoacetyl-CoA, shows a strong competitive inhibition by coenzyme-A, i.e. competitive product inhibition with an inhibition constant K_i of 16 μM ^{13,14}.

Before, discussing the polymerization mechanism, several experimental observations will be summarized with respect to the characteristics of the polymerization process: Firstly, the molar mass of the polymer formed during the early stage of the accumulation process is high and typically in the order of 10^6 g/mol^{4,5,15}. Secondly, Ballard *et al.*⁴ and Kawaguchi and Doi⁵ stated that the polymerization of PHA is a chain type of polymerization. Further, the polymerization starts initially in the cytoplasm of the bacterium and is transferred to the surface of the granules formed during the early stage of the accumulation process^{8,16}, i.e. the polymerization process proceeds in an aqueous environment and has a heterogeneous character.

Let us turn back now to the actual mechanism, i.e. the formation of PHB via the condensation reaction of (R)-3-hydroxybutyryl-CoA (M-SCoA) and a polymer chain which is attached to the PHB synthase (E-SH) via a thioester bond (enzyme-acyl complex)^{e.g. 3,5}. This is in principle an equilibrium reaction and is depicted in *equation 10.6*. Please note that an enzyme **does not** affect the equilibrium since it only catalyses a reaction.



where $E-S-M_n$ is a polymer-enzyme complex with a degree of polymerization of n and HS-CoA is coenzyme-A which is comparable to the low molar mass product of the synthetic polycondensation described earlier. The major question that arises is: how can the experimentally observed characteristics of the polymerization process be explained by the polymerization mechanism depicted above?

(A) In the case of the biosynthesis of *b*-PHAs the enzyme which catalyzed the polymerization remains attached to the growing polymer chain during the chain growth process^{3,4,5}. This means that once the polymerization is initiated the polymer can grow by addition of new monomer units via the active site of the enzyme which is attached to the growing polymer chain (enzyme-acyl complex). A chain transfer reaction will cause the cleavage of the enzyme-polymer complex leading to a free PHB synthase molecule and a dead polymer chain. The fact that *b*-PHAs which are formed at the earliest stage of the accumulation process have a high molar mass is a consequence of the fact that the biosynthesis of these polymers is a chain type of polymerization. This is in contrast with *s*-PHAs where the molar mass increases with conversion.

(B) The bacterial polymerization process can be entitled as a transthioesterification. It is well known that thioesters, enol esters, oxime esters etc. make transesterification reactions kinetically irreversible¹⁷. The reaction rate of thioesters is about one to two orders of magnitude faster than transesterification of for instance methyl or ethyl esters. One major requirement for these activated esters to be effective is that the formed nucleophile should be removed from the reaction mixture one way or the other. The fact that the biosynthesis of PHAs does not reach equilibrium under accumulation conditions is probably due to the fact that the polymer accumulating micro-organism very efficiently recycles the low molar mass product of the condensation reaction, i.e. coenzyme-A (Under balanced growth conditions coenzyme-A levels are a factor three higher than under polymer accumulation conditions)¹⁵. The bacterium controls the biosynthesis via the kinetics of the polymerization, i.e. the use of fast reacting thioesters, as well as via the thermodynamics of the process (equilibrium), i.e. it recycles coenzyme-A in such a way that under accumulation conditions the concentration of coenzyme-A is low and equilibrium is not reached.

The differences in polymerization characteristics between the synthesis of *b*-PHAs and *s*-PHAs can be explained by the difference in polymerization mechanism of the separate polymerization reactions, i.e. chain polymerization (*b*-PHAs) versus step-growth polymerization (*s*-PHAs).

10.2.2 Enzyme kinetics: Analyzing Enzyme Rate Data

10.2.2.1 Initial Rate Method

In the study of enzyme catalyzed reactions the initial-rate method is often used, i.e. the initial velocity of product formation or substrate conversion is plotted versus the substrate concentration (= Michaelis-Menten curve (= M-M-curve))^{18,19}. In order to obtain an accurate M-M-curve a relatively large number of progress curves have to be measured. This approach, however, has several disadvantages of which the major one is that the initial and final part of the progress curve are the most difficult parts of the progress curve to measure. This often leaves the data between these two regions, i.e. the intermediate region, unused. In the following we will show that this intermediate region can be elegantly used in the study of the *in vitro* kinetics of the action of PHB synthase on (R)-3-hydroxybutyryl-CoA.

If one incubates an enzyme with a substrate the decrease of the substrate concentration can be monitored as a function of time. This is called the progress-curve. In *figure 10.2* three typical courses of a progress curve are depicted. Curve *A* represents a reaction in which the substrate is fully converted into product. The initial velocity of this reaction is equal to the slope of the initial part of the progress curve. Curve *B* is the progress curve for a reaction in which the enzyme concentration is half that of the reaction represented by curve *A*. The slope of the initial part of this curve is smaller by a factor of two compared with curve *A*. Finally, curve *C* represents a reaction in which not all the substrate is converted. This can be due to several factors such as: (1) a decrease in the substrate concentration (i.e. the rate of substrate conversion becomes very low), (2) an increase in product concentration (i.e. product inhibition or an increase in the rate of the reverse reaction), or (3) deactivation of the enzyme. If one wants to determine the kinetic parameters of an enzyme catalyzed reaction from the progress curve some assumptions have to be made concerning the cause of the decrease in the rate of substrate conversion.

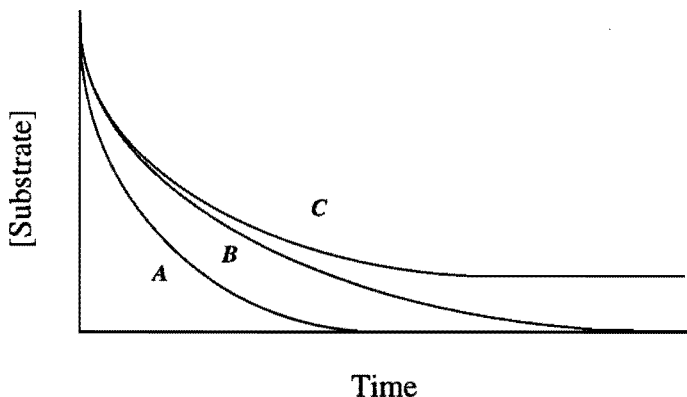
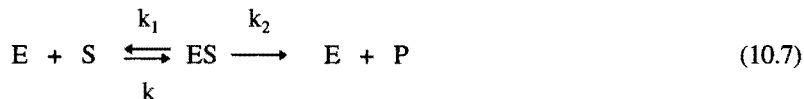


Figure 10.2 Substrate concentration as a function of time for various enzyme catalyzed reactions. Curve A represents a reaction in which the substrate is fully converted. Curve B represents a reaction in which the enzyme concentration was half the value of that in the reaction depicted by curve A. Curve C represents a reaction in which the substrate is not fully converted.

If an enzyme is incubated with substrate two regimes concerning the rate of substrate conversion can be observed: (a) the enzyme is saturated with substrate and will operate at its maximum velocity, (b) the enzyme is not saturated with substrate and will operate at a velocity lower than its maximum velocity.

In the following discussion we assume that the enzyme system can be described with Michaelis-Menten kinetics¹⁸ (see equation 10.7).



where E, S, ES, and P denote an enzyme, substrate, enzyme-substrate complex, and product, respectively. k is the rate coefficient for the formation of the substrate-enzyme complex, k_1 is the rate coefficient for the dissociation of the substrate-enzyme complex, while k_2 denotes the dissociation coefficient of the enzyme-product complex.

In figure 10.3 the velocity of product formation as a function of the ratio of substrate and enzyme concentration ($= [S]/[E]$) is depicted. If $[S]/[E]$ is high, i.e. the enzyme is

saturated with substrate, the rate of substrate conversion is maximum. In *figure 10.3* this is denoted by the horizontal line.

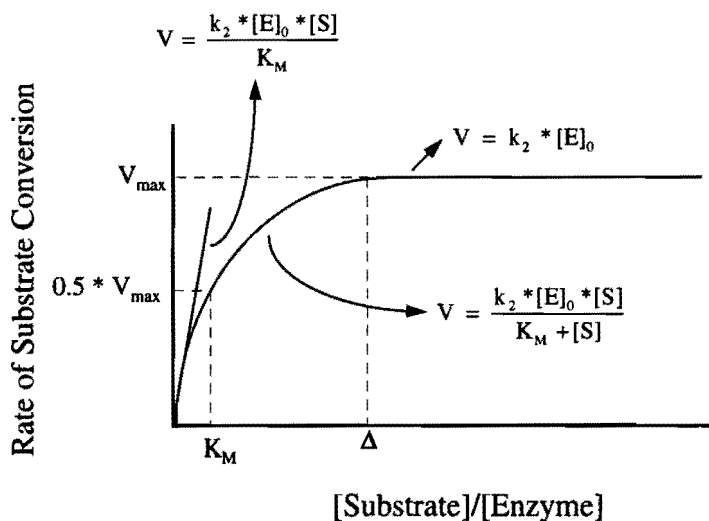


Figure 10.3 Initial rate of substrate conversion as a function of the ratio of the substrate and enzyme concentration (assuming Michaelis-Menten kinetics).

The rate of substrate conversion ($= V = -\frac{d[S]}{dt}$) is given by *equation 10.8*¹⁸:

$$V = k_2 * [E]_0 = V_{\max} \quad (10.8)$$

where k_2 denotes the dissociation coefficient of the enzyme-product complex and $[E]_0$ the total enzyme concentration. V_{\max} is the maximum rate of substrate conversion. *Equation 10.8* is zero order in substrate concentration. At some intermediate $[S]/[E]$, the enzyme is not saturated with substrate anymore. The rate of substrate conversion¹⁸ can then be expressed by *equation 10.9*:

$$V = \frac{k_2 * [E]_0 * [S]}{K_M + [S]} \quad (10.9)$$

where $[S]$ and K_M denote the substrate concentration and the Michaelis-Menten constant, respectively. By substituting V_{max} , which is equal to $k_2 * [E]_0$, into *equation 10.9* the well-known Michaelis-Menten equation is obtained^{18,19}.

At low substrate concentrations¹⁸, i.e. $[S] \ll K_M$, the rate of substrate conversion can be approximated by *equation 10.10*.

$$V = \frac{k_2 * [E]_0 * [S]}{K_M} \quad (10.10)$$

It is shown by *equation 10.10* that at low $[S]$ the rate of substrate conversion is first order in substrate concentration. The above discussion of *figure 10.3* holds for M-M-curves constructed via the initial rate method, i.e. the M-M-curve is composed of initial velocities from different progress curves.

During an enzyme catalyzed reaction $[S]/[E]$ changes from a relatively high value (maximum rate of substrate conversion) to virtually zero if the substrate is fully converted by the enzyme and no kind of enzyme deactivation or inhibition occurs, i.e. a reaction which follows curve *A* or *B* in *figure 10.2*.

10.2.2.2 Kinetic Analysis of Progress Curves

The analysis of the whole progress curve of enzyme-catalyzed reactions can be a very attractive alternative to the initial-rate method discussed in *section 10.2.2.1* for the determination of kinetic parameters. The use of the full progress curve in kinetic studies has several advantages, such as all data available from the progress curve are used and kinetic parameters can be determined from the results of a single experiment. However, there are also disadvantages, i.e. the decrease in the rate of substrate conversion can be due to several factors which are often not known. In the following we will discuss the use of the full progress curve in kinetic studies of enzyme-catalyzed reactions. If it is assumed that the decrease in the rate of substrate conversion is caused only by a decrease in substrate concentration in the reaction mixture, it should be possible to determine the rate of substrate conversion at different stages of the reaction. However, this method needs simplifying assumptions which are statistically not valid¹⁹.

An alternative procedure is to integrate the initial-rate equation that describes the entire progress curve. The initial-rate equation, which is equal to *equation 10.9*, for a single-substrate reaction can be written as:

$$V = \frac{V_{\max} * [S]}{K_M + [S]} \quad (10.11)$$

where V_{\max} is the maximum velocity. If the decrease of V is only caused by depletion of substrate, *equation 10.11* can be integrated and after some rearrangements *equation 10.12* is obtained ²⁰:

$$\frac{(S_0 - S)}{t} = V_{\max} - \frac{K_M * (\ln \frac{S_0}{S})}{t} \quad (10.12)$$

Plotting $\frac{(S_0 - S)}{t}$ against $\frac{(\ln \frac{S_0}{S})}{t}$ results in a straight line with a slope of $-K_M$,

intercept on the vertical axis of V_{\max} , and on the horizontal axis of V_{\max}/K_M . As stated previously *equation 10.12* represents a situation in which the decrease in substrate conversion is caused by the depletion of substrate. If a reaction is considered in which the rate of substrate conversion goes to zero while there is still substrate present, and the assumption is made that no enzyme deactivation occurs, then the observed decrease is either caused by product inhibition or by an increase of the rate of the reverse reaction. If product inhibition occurs and no product is present at the beginning of the reaction the simplest model to describe this phenomenon would be competitive product inhibition. This can be implemented in *equation 10.12* and after some algebra *equation 10.13* can be obtained ²⁰:

$$\frac{(S_0 - S)}{t} = \frac{V_{\max}}{(1 - (\frac{K_M}{K_i}))} - K_M * \frac{(K_i + S_0)}{(K_i - K_M)} * \frac{(\ln \frac{S_0}{S})}{t} \quad (10.13)$$

where K_i is the inhibitor constant. By plotting $\frac{(S_0 - S)}{t}$ against $\frac{(\ln \frac{S_0}{S})}{t}$ a straight line is obtained with a slope of $-K_M * \frac{(K_i + S_0)}{(K_i - K_M)}$ and intercept on the vertical axis of $\frac{V_{max}}{(1 - (\frac{K_M}{K_i}))}$. The slope of the curve obtained by equation 10.13 will be positive and the

intercept negative if $K_i < K_M$. The opposite effect will be observed if $K_i > K_M$. This is schematically represented in figure 10.4. If a series of plots are obtained from different progress curves with initially different substrate concentrations a family of lines are obtained.

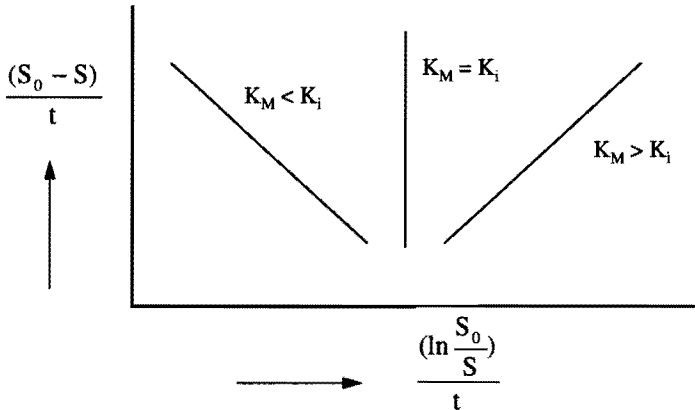


Figure 10.4 Schematic plot of equation 10.13 for a single substrate enzyme-catalyzed reaction with competitive product inhibition, for different values of K_i and K_M .

The slopes of the curves in figure 10.4 are given by equation 10.14:

$$\pm \text{slope} = K_M * \frac{(K_i + S_0)}{(K_i - K_M)} = \frac{(K_M * [S]_0)}{(K_i - K_M)} + \frac{(K_M * K_i)}{(K_i - K_M)} \tag{10.14}$$

By plotting the slopes of the graphs obtained from equation 10.13 according to equation 10.14 versus the initial substrate concentration, the inhibitor constant (K_i) can be determined. This value can be used to calculate K_M and V_{max} from the slopes and intercept of

the lines obtained from *equation 10.13*. However, an alternative and more accurate way of estimating K_M and V_{max} is by the method developed by Foster and Niemann^{21,22}. Basically it comes down to plotting lines in *figure 10.4* with a slope S_0 . These lines will intercept the lines represented by *equation 10.13*. From these intercepts a new line can be constructed which exhibits a slope equal to K_M and intercept on the vertical axis at V_{max} and on the horizontal axis at V_{max}/K_M . Concomitantly, K_i can be calculated from the values of K_M and V_{max} obtained graphically.

10.3 Experimental

Materials: All chemicals used were commercially available and of analytical grade and used without further purification. The chemicals used in the gas chromatographic analysis were of chromatographic grade. A cell suspension of poly(3-hydroxybutyrate-co-3-hydroxyvalerate) containing *Alcaligenes eutrophus* was kindly provided by Mrs. L. Naylor (ZENECA Bio Product, U.K.).

Equipment: Scanning electron microscopy (SEM) was performed on a Cambridge Stereoscan 200 microscope. For gas chromatography measurements a Hewlett-Packard 5809A gas-chromatograph was equipped with a fused silica column, a 7673A auto-sampler and a flame ionization detector. An Aminco French pressure cell was used. UV-Vis spectrophotometric measurements were performed on a Perkin-Elmer 115 spectrophotometer.

Recovery of native PHA granules from cell suspension: A cell suspension was washed twice and resuspended in 50 mM phosphate buffer pH = 7.0 (pellet diluted 10 times). The suspension was then passed through the French pressure cell at a pressure of 2000 psi. Approximately 80 % of the cells were broken and subsequently stored at - 20 °C.

Determination of the activity of granule-associated PHB synthase: The standard reaction mixture consisted of 175 μ l 0.6 M phosphate buffer (pH = 7.0), 445 μ l milli-Q water, 10 μ l granule suspension and 70 μ l substrate solution (equals 114 nmol (R,S)-3-hydroxybutyryl-CoA). The reaction progress was followed by determining the decrease in the concentration of (R,S)-3-hydroxybutyryl-CoA using a spectrophotometer operating at a wavelength of 232 nm. A cell blank was performed, in which the granule suspension was replaced by 70 μ l 50 mM phosphate buffer (pH = 7.0), to correct for the adsorption caused by cell debris. A substrate blank was performed to determine whether monomer decay processes were occurring other than the one caused by the PHB synthase enzyme. The reaction mixture and blanks were

incubated at 28 °C. At set times samples were centrifuged at 14,000 rpm for 5 minutes, after which the adsorption of the supernatant liquid was measured at 232 nm. Since the substrate used was a mixture of (R)- and (S)-3-hydroxybutyryl-CoA, experiments were conducted to determine whether one or both enantiomers were converted. It was assumed that only (R)-3-hydroxybutyryl-CoA was converted by the granule suspension used (This assumption is based *in vitro* experiments conducted by Haywood *et al.* ¹⁶). During the activity measurements no enzyme deactivation occurred (data not shown). The error in activity measurements was estimated to be $\pm 10\%$.

Protein assay: The amount of protein in the granule suspension was determined using the Pierce BCA Protein Assay ²³.

Determination of number of granules per liter of granule suspension: In order to determine the number of granules per liter of granule suspension the polymer content of the granule suspension was determined using a gas chromatographic method which has been described elsewhere ^{24,25}, while the size of the granules present was determined by SEM.

10.4 Results and Discussion

In the discussion below, instead of the steady-state solution of the Michaelis-Menten scheme, two alternative ways of analyzing the kinetic data will be used. First, a straight forward analysis of the kinetic data obtained from different experiments. Secondly, the integrated Michaelis-Menten rate equation will be used (in which competitive product inhibition is implemented).

Three experiments were conducted in which the enzyme and substrate concentrations were varied. In *figure 10.5* the progress curves for these experiments are depicted. As can be seen from *figure 10.5* the substrate concentration ([S]) decreases, to reach eventually a constant value. Since no enzyme deactivation occurred during the described experiments (see experimental section), the fact that the reaction does not go to completion may be caused either by product inhibition or by an increase in the rate of the reverse reaction.

10.4.1 Straightforward Analysis of Kinetic Data

In order to be able to compare the different experiments with each other, the conversion-time data were normalized for the enzyme concentration used. These normalized conversion-time curves are shown in *figure 10.6*. In this figure three regimes can be recognized. The first part of the conversion-time curve (from 0 - 2 hours) represent the situation in which $[S]/[E]$ is high and the rate of substrate conversion is maximum, i.e. the enzyme is saturated with substrate. The rate of substrate conversion is zero order in substrate concentration, while it is first order in enzyme concentration.

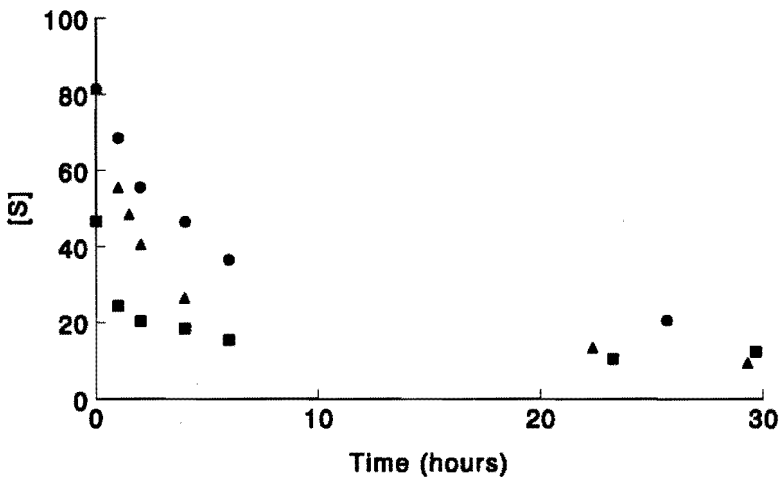


Figure 10.5 Substrate concentration ($= [S]$ in μM) as a function of time for three experiments. Experiment A: $[S] = 81.5 \mu\text{M} = [S]_{st}$, i.e. "standard" concentration of substrate, and $[E] = [E]_{st}$, i.e. "standard" concentration of enzyme (triangles), Experiment B: $[S] = [S]_{st}$ and $[E] = 0.5 * [E]_{st}$ (circles), and Experiment C: $[S] = 4/7 * [S]_{st}$ and $[E] = [E]_{st}$ (squares).

The rate of substrate conversion, V , can be represented by *equation 10.15*.

$$V = k_{ins.} * [E]_{total} \quad (10.15)$$

where $k_{ins.}$ is the rate coefficient for the insertion of a monomer unit in the enzyme-polymer complex and $[E]_{total}$ is the total enzyme concentration (= equal to the enzyme-polymer complex concentration). *Equation 10.15* assumes that all the enzyme molecules present are active and that the rate determining step in the catalytic reaction is the insertion of monomer

into the enzyme-polymer complex. If the difference between the initial substrate concentration ($[S]_0$) and the substrate concentration at time t ($[S]$) is plotted versus time the slope of this curve gives the product $k_{ins} * [E]_{total}$ (plot not shown). In *table 10.1* the values of $k_{ins} * [E]_{total}$ are shown for the different experiments.

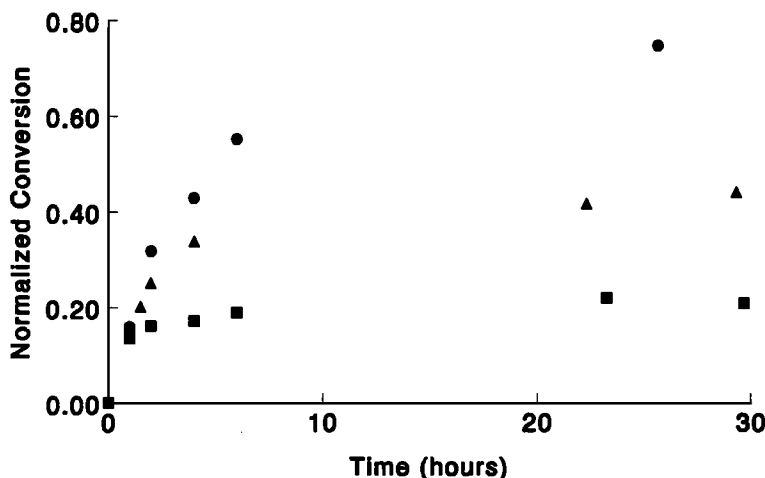


Figure 10.6 Normalized conversion as a function of time for different experiments. Experiment A (triangles), Experiment B (circles) and Experiment C (squares).

Table 10.1 $k_{ins} * [E]_{total}$ in mol/l.h for three experiments. Values were normalized for difference in substrate and enzyme concentrations.

Experiment	$k_{ins} * [E]_{total}$ (mol/l.h)
A	$1.3 * 10^{-5}$
B	$1.3 * 10^{-5}$
C	$1.1 * 10^{-5}$

As the substrate concentration in the reaction mixture decreases, $[S]/[E]$ will decrease and the enzyme will not be saturated with substrate anymore, i.e. the second part of the conversion-time curve (from 2 to 6 hours). The rate of substrate conversion becomes now dependent on the substrate concentration, as depicted in *equation 10.16*:

$$V = k * [S] * [E]_{total} \quad (10.16)$$

where k is the rate coefficient for the formation of the substrate-enzyme complex. According to *equation 10.16* the rate of substrate conversion now has become first order in substrate and enzyme concentration. Plotting $\ln([S]/[S]_0)$ versus time results in a straight line with a slope equal to $k * [E]_{total}$ (plot not shown).

Table 10.2 contains the values of $k * [E]_{total}$. From the values of $k_{ins.} * [E]_{total}$ and $k * [E]_{total}$ an estimation of K_M can be made by assuming that K_M can be approximated by the ratio of $k_{ins.}$ and k , i.e. assuming that the decomposition of the enzyme-substrate complex to enzyme and substrate can be neglected. In doing so, a value for K_M of 0.11 mM is found.

Table 10.2 $k * [E]_{total}$ in h^{-1} for three experiments. Values were normalized for difference in substrate and enzyme concentration.

Experiment	$k * [E]_{total}$ (h^{-1})
A	0.111
B	0.103
C	0.117

The third part in *figure 10.5* shows a decrease in the rate of substrate conversion and a constant substrate concentration in the reaction mixture. This can be attributed to the fact that the reverse reaction becomes increasingly important as substrate is converted. This reverse reaction will eventually cause the conversion of substrate to stop, i.e. the system reaches equilibrium. The average apparent equilibrium constant, defined as the ratio of [HS-CoA] over [S], is equal to 4.4.

10.4.2 The Use of the Integrated Rate Equation for the Analysis of Kinetic Data

In order to be able to determine characteristic kinetic parameters, such as K_M and V_{max} , for enzyme-catalyzed reaction the experimental results presented in *figure 10.5* were plotted according to *equation 10.13* (see *figure 10.7*). As can be seen from *figure 10.7*, straight lines are obtained indicating that competitive product inhibition is very likely to occur. The

inhibition constant K_i , which is equal to $17 \mu\text{M}$, is in this specific case smaller than the Michaelis-Menten constant (K_M) as can be seen from the sign of the slope in *equation 10.13*.

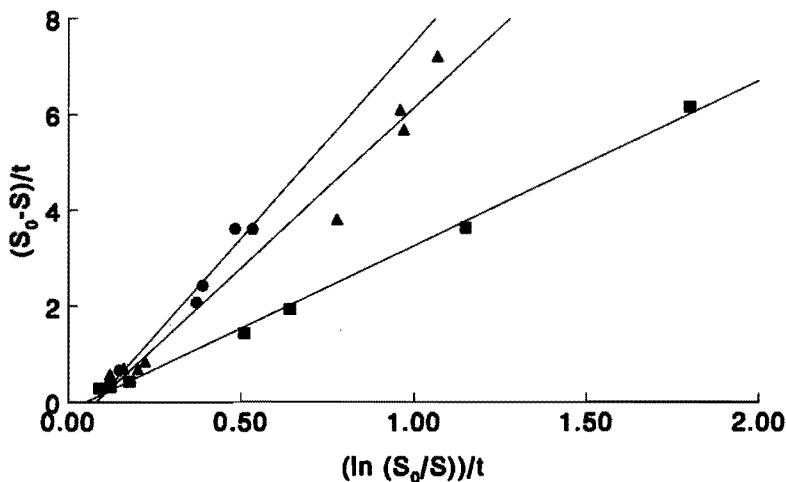


Figure 10.7 $(S_0 - S)/t$ (in 10^{-9} mol/l.s) as a function of $(\ln(S_0/S))/t$ (in 10^{-4} s^{-1}) for different experiments. Experiment A (triangles), Experiment B (circles) and Experiment C (squares).

The method of Foster and Niemann^{21,22}, described briefly in the theory section, was used for determining numerical values of K_M and V_{\max} . The values of the different kinetic parameters determined using the integrated rate equation are given in *table 10.3*.

Table 10.3 Various kinetic parameters obtained by applying *equation 10.13* to the experimental data shown in *figure 10.5*.

V_{\max} (calculated from experiment)	$1.5 * 10^{-5}$	mol/l.h
V_{\max} (experimental value)	$1.2 * 10^{-5}$	mol/l.h
K_M	$1.3 * 10^{-4}$	mol/l
K_i	$1.7 * 10^{-5}$	mol/l

The value of K_M ($= 0.13 \text{ mM}$) determined via this method is in good agreement with values reported in literature^{3,16,26}.

10.5 Concluding Remarks

In the previous section two different approaches were used for analyzing kinetic data of the conversion of (R)-3-hydroxybutyryl-CoA catalyzed by PHB synthase containing granules, which was purified from *Alcaligenes eutrophus*. Using the straightforward kinetic analysis of the progress curves and assuming that the cleavage of the enzyme-substrate complex in enzyme and substrate is negligible, a value of K_M of 0.11 mM was obtained. When the integrated rate equation which takes into account competitive product inhibition was used to describe the experimental data, a value for K_M of 0.13 mM was found. The average value for K_M (= 0.12 mM) determined here is in good agreement with values reported in literature^{3,16,26}. At the same time it was found that the inhibition constant K_i for the inhibition of PHB synthase by coenzyme-A was equal to 17 μM which is comparable to the value found in literature for the inhibition of 3-ketothiolase by coenzyme-A, i.e. 16 μM ^{16,27}. This result indicates that not only 3-ketothiolase is regulated by coenzyme-A but also PHB synthase. The major question that arises from this result is: what is the effect of the inhibition of PHB synthase by coenzyme-A during the biosynthesis of PHB?

First the situation in which no polymer is being formed will be considered. This has already been discussed earlier, but in summary the following can be said: under balanced growth conditions, coenzyme-A levels are high and the synthesis of PHB is inhibited. In this case no acetoacetyl-CoA will be formed. Concomitantly, (R)-3-hydroxybutyryl-CoA is not present in the bacterium which can be converted into PHB. Thus, PHB synthase is not operative under balanced growth conditions due to the fact that the substrate for this enzyme is not present. Therefore, it is not possible to detect an inhibition of PHB synthase by coenzyme-A under these conditions. Once the bacterium is in nutrient limitation but carbon excess, acetyl-CoA can no longer be oxidized at a high rate via the tricarboxylic acid cycle and therefore it accumulates. Under these conditions the concentration of coenzyme-A is low and acetoacetyl-CoA is being formed which is consequently converted into (R)-3-hydroxybutyryl-CoA and polymerization can occur. Again inhibition of PHB synthase by coenzyme-A is not observed during the early part of PHB accumulation since the concentration of coenzyme-A is very low. However, one has to consider the heterogeneity of the polymerization systems, i.e. the polymerization mainly takes place at the surface of the PHB granules, plus the fact that the

substrate and coenzyme-A exhibits some resemblance with biosurfactants such as rhamnolipids²⁸. Taking these two phenomena into account the following hypothesis can be made: the concentrations of substrate and coenzyme-A at the surface of the PHB granules are higher than those in the bulk of the cytoplasm. At low accumulation levels the coenzyme-A which is formed during the polymerization process can diffuse away from the surface into the cytoplasm where it is effectively recycled, thus ensuring the formation of high molar mass polymer. As the amount of polymer increases in the bacterium the volume of the surface layer of PHB granules increases compared with the volume of the cytoplasm. Hence, the concentration of coenzyme-A at the surface of the PHB granules increases, concomitantly coenzyme-A will inhibit PHB synthase. The increasing concentration of coenzyme-A at the granule surface could also account for the decreasing molar mass of the polymer formed during the accumulation process, since coenzyme-A can act as a chain transfer agent (see also *Chapters 3, 4, and 5*). This is in agreement with results recently published by Koizumi *et al.*⁶ who stated that the decrease in the molar mass of the polymer formed is probably due to an increase in chain transfer agent concentration during the polymerization process. A more detailed discussion of the above hypothesis will be given in *Chapter 5*.

A totally different approach of the conversion of (R)-3-hydroxybutyryl-CoA is by considering it as a *classical* polycondensation. In doing so, the incomplete conversion of substrate can be explained by the fact that in the closed system equilibrium is reached, since the low molar mass product of the reaction (coenzyme-A) is not removed from the system. This is also observed in a closed synthetic polycondensation system in which the low molar mass reaction product, e.g. water, is not removed, concomitantly equilibrium will set in after a certain reaction time. The apparent equilibrium constant found for the experiments described in this work, i.e. $K \sim 4.4$, is comparable to values²⁹ found for synthetic polyesterification or transesterification which are in the range of 0.1 - 10.

10.6 References

- 1 Lemoigne, M., *Bull. Soc. Chem. Biol.*, **8**, 770 (1926)
- 2 Poirier, Y., Dennis, D.E., Nawrath, C., and Somerville, C., *Adv. Mater.*, **5**, 30 (1993)
- 3 Griebel, R., and Merrick, M.J., *J. Bacteriol.*, **108**, 782 (1971)

- 4 Ballard, D.G.H., Holmes, P.A., and Senior, P.J., In *Recent Advances in Mechanistic and Synthetic Aspects of Polymerization*, Fontanille, M. and Guyot, A. (Eds.), Vol. 215, 293 (1987), Reidel (Kluwer) Publishing Co., Lancaster, U.K.
- 5 Kawaguchi, Y., and Doi, Y., *Macromolecules*, 25, 2324 (1992)
- 6 Koizumi, F., Abe, H., and Doi, Y., *J. Macromol. Sci.*, A32, 759 (1995)
- 7 De Koning, G.J.M., and Maxwell, I.A., *J. Environ. Pol. Degr.*, 3, 223 (1993)
- 8 Kurja, J., Zirkzee, H.F., De Koning, G.J.M., and Maxwell, I.A., *Macromol. Theory & Sim.*, 4, 839 (1995)
- 9 Mark, H., and Whitby, G.S., eds., "*Collected Papers of W.H. Carothers on High Polymeric Substances*", Interscience, New York (1940)
- 10 Jedlinski, Z.J., in "*Handbook of Polymer Synthesis*", Part A, Kricheldorf, H.R., Marcel Dekker, Inc., New York, p 645-683 (1992)
- 11 Sandler, S.R., and Karo, W., "*Polymer Syntheses*", Vol. 1, 2nd Edition, Chapter 2, Academic Press Inc., New York (1992)
- 12 Odian, G., "*Principles of Polymerization*", John Wiley & Sons, New York (1981)
- 13 Haywood, G.W., Anderson, A.J., Chu., L., and Dawes, E.A., *FEMS Microbiol. Lett.*, 52, 91 (1988)
- 14 Steinbüchel, A., and Schlegel, H.G., *Molecular Microbiology*, 5, 535 (1991)
- 15 Anderson, A.J., and Dawes, E.A., *Microbiol. Rev.*, 54, 450 (1990)
- 16 Haywood, G.W., Anderson, A.J., and Dawes, E.A., *FEMS Microbiol. Lett.*, 57, 1 (1989)
- 17 Fang, J-M., and Wong, C-H, *SYNLETT*, 393 (1994)
- 18 Segel, I.H., "*Enzyme Kinetics*", John Wiley & Sons, New York (1975)
- 19 Cornish-Bowden, "*Principles of Enzyme Kinetics*", Butterworth, London, p. 150 (1976)
- 20 Orsi, B.A., and Tipton, K.F., in "*Methods in Enzymology*", Volume 63, Edited by Purich, D.L., Academic Press Inc., New York, p. 159 (1979)
- 21 Foster, R.J., and Niemann, C., *Proc. Natl. Acad. Sci. U.S.A.*, 39, 999 (1953)
- 22 Foster, R.J., and Niemann, C., *J. Am. Chem. Soc.*, 77, 1886 (1955)
- 23 Smith, P.K. et al., *Anal. Biochem.*, 150, 76 (1985)
- 24 Brauneegg, G., Sonnleitner, B., and Lafferty, R.M., *Eur. J. Appl. Microbiol. Biotechnol.*, 6, 29 (1978)
- 25 Brandl, H., Gross, R.A., Lenz, R.W., and Fuller, R.C., *Appl. Environm. Microbiol*, 54, 1977 (1988)
- 26 Fukui, T., Yishimoto A., Matsumoto M., Husokawa, S., Saito T., Nishikawa H., and Tomita, K., *Arch. Microbiol.*, 110, 149 (1976)
- 27 Oeding, V., and Schlegel, H.G., *Biochem. J.*, 134, 239 (1973)
- 28 Fiechter, A., *TIBTECH*, 10, 208 (1992)
- 29 Odian, G., "*Principles of Polymerization*", John Wiley & Sons, New York (1981)

CHAPTER 11

The Accumulation of Poly-(R)-3-hydroxybutyrate in *Alcaligenes eutrophus*

2. *Granule Growth*

Synopsis: Due to the heterogeneous character of the biosynthesis of poly-(R)-3-hydroxybutyrate in *Alcaligenes eutrophus*, the accumulation has been considered in terms of a granule formation and a granule growth stage. In this chapter a quantification was made concerning the granule growth stage of the biosynthesis of poly-(R)-3-hydroxybutyrate in *Alcaligenes eutrophus*. Expressions for the rate of polymerization and the molar mass of the polymer formed were derived taking the heterogeneity of the polymerization process into account. Evidence was present for the occurrence of coagulation of granules during the granule growth stage of the accumulation process due to the fact that these granules reached a pseudo-close packing in the polymer accumulating bacteria. Further, it was shown that the molar mass of the polymer formed depended on the granule size, i.e. upon increasing granule size the molar mass of the polymer decreased.

11.1 Introduction

Since Lemoigne ¹ first isolated and characterized the poly-(R)-3-hydroxybutyrate (PHB) homopolymer in 1925, PHB has been extensively studied by biochemists to elucidate its biosynthetic pathways ^{2,3}. One year later a patent was granted to Dinsmore ⁴, working for the Goodyear Tire & Rubber Company, for a process that can be regarded as the first true synthetic emulsion polymerization. It describes the thermal polymerization over a period of six months of aqueous emulsions of various diene-monomers, with oleate salts and egg albumin as stabilizers.

In part reproduced from : (i) Kurja, J., Zirkzee, H.F., De Koning, G.J.M., and Maxwell, I.A., in : "Biodegradable Plastics and Polymers", Y. Doi and K. Fukuda (Eds.), Elsevier, Amsterdam, p. 379-386 (1994), and (ii) Kurja, J., Zirkzee, H.F., De Koning, G.J.M., and Maxwell, I.A., *Macromol. Theory and Sim.*, **4**, 839 (1995)

It was not until 1968 that Ellar *et al.*⁵, who reported on the morphology of poly-3-hydroxybutyrate granules, drew some equivalents with the emulsion polymerization process as quoted: "The model that has been developed is not too unlike the familiar emulsion polymerization equation, except that the number of chain initiation sites in this case is probably determined by a well-defined number of protein molecules which form the initial micelle".

Ballard *et al.*⁶ have drawn the conclusion that the PHB biosynthesis has some of the features of an emulsion polymerization with the individual granules corresponding to latex particles and the membrane lipid to surfactant. Though, they did not consider PHB biosynthesis as an emulsion polymerization since the PHB polymerization mechanism is not free radical but a coordination-insertion process bearing more resemblance to a Ziegler-Natta type system.

Very recently, Gerngross *et al.*⁷ proposed a model for granule formation. They assume that granule formation is caused by the formation of micelles formed from polymerase enzyme molecules which are propagating in the cytoplasm. At the same time, De Koning and Maxwell⁸ drew an analogy between the conventional emulsion polymerization process and the biosynthesis of poly-3-hydroxyalkanoates. They stated that the granule formation mechanism closely resembles a homogeneous nucleation mechanism, i.e. polymer-polymerase conjugates (a polymer-polymerase conjugate is a PHB polymer chain bound to a polymerase enzyme) which are growing in the cytoplasm form precursor granules. These precursor granules then grow until they are mature granules. In this chapter the qualitative model of De Koning and Maxwell⁸ for the granule growth stage of the PHB accumulation process is quantified. The quantification of the granule formation stage⁹ will be discussed in *Chapter 12*.

11.2 Theory

Before we discuss the analogues between the bacterial PHB accumulation and a conventional emulsion polymerization we would like to give a short overview of these processes as they are currently accepted in the open literature.

11.2.1 Emulsion Polymerization

Emulsion polymerization is often referred to as a particular case of free radical polymerization, although other types of polymerization reactions in emulsion are known¹⁰, e.g. the emulsion polymerization of siloxanes^{11,12,13} and the ring-opening metathesis polymerization of oxanorbornene derivatives¹⁴. The kinetics and mechanisms involved in an emulsion polymerization are highly complicated, since events occur in several phases, and exchange of radicals and monomer between these phases needs to be taken into account. Models and theories dealing with these aspects of emulsion polymerization are numerous and excellent reviews are available^{15,16,17}.

In contrast to bulk and solution polymerization, emulsion polymerizations are heterogeneous reaction systems¹⁸. Generally an emulsion polymerization system comprises of water, monomer, surfactant, initiator and additives such as chain transfer agents and buffers. A widely used and accepted mathematical model for the emulsion polymerization process is that of Smith and Ewart¹⁹, which is based on the descriptive model of Harkins²⁰. The Smith-Ewart model subdivides the emulsion polymerization process into three distinct intervals. A typical conversion-time curve is shown in *figure 11.1*.

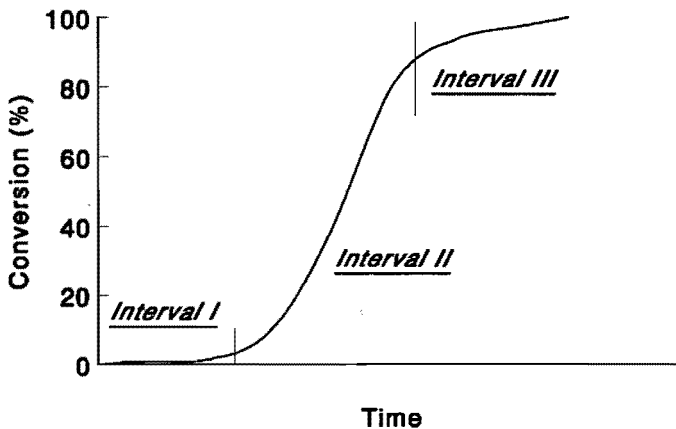


Figure 11.1 A typical conversion-time curve for an emulsion polymerization with the different intervals indicated.

For simplicity we will assume that the added surfactant is present at a concentration above the CMC (= critical micelle concentration), although this is not necessary since there are several examples of emulsifier free emulsion polymerizations described in the literature e.g. ²¹.

Interval I is the initial stage where particle formation takes place via several possible mechanisms ^{15,18,22,23,22}. The initiator (oil or water soluble) dissociates into reactive radicals. These radicals will mainly diffuse to the monomer swollen micelles, since their total surface area is much larger than that of the monomer droplets. In the monomer swollen micelles the radicals will initiate the polymerization. This process is also referred to as micellar nucleation ^{19,20}. There is also evidence that before the radical enters the micelle it has gained a certain length by addition of monomer present in the water phase ¹⁵.

Interval II is entered when no new particles are being formed (no micelles are present anymore) and is characterized by the fact that the number of polymer particles reaches a constant value. Polymerization in the particles proceeds in the presence of a separate monomer phase. The monomer droplets ensure a constant transport of monomer to the growing polymer particles (no diffusion limitation), i.e. the rate of diffusion of monomer from the monomer droplets to the water phase and subsequently to the polymer particles is equal to the rate of consumption of the monomer in the polymerization process. The monomer and radical concentration within the water phase and the polymer particles is constant during interval II, leading to a constant rate of polymerization.

Interval III begins with the disappearance of the monomer droplets, after which the monomer concentration in the polymer particles decreases continuously. Concomitantly, the rate of polymerization decreases. For clarity we would like to emphasize that the polymerization takes place **inside** the growing polymer particles, although exceptions to this are known such as the emulsion polymerization of acrylonitrile and tetrafluoroethylene ^{10,24}. In general, the rate of a free radical polymerization (R_p) is given by:

$$R_p = k_p * [M] * [R] \quad (11.1)$$

where k_p is the second order propagation rate coefficient, $[M]$ and $[R]$ the monomer and free radical concentrations, respectively. In emulsion polymerization the overall rate of polymerization can be taken as the summation of those in each individual polymer particle, leading to:

$$R_p = \frac{k_p * C_M * \bar{n} * N}{N_{Av.}} \quad (11.2)$$

where C_M is the monomer concentration within the polymer particles, \bar{n} the average number of radicals per particle, N the number of polymer particles per unit volume, and $N_{Av.}$ Avogadro's number.

11.2.2 Accumulation of Poly-(R)-3-hydroxybutyrate

Since PHB is a storage material, it is appropriate to consider its metabolism as a cycle of synthesis and breakdown^{2,3}. The enzymes of the cycle have been examined extensively in a range of organisms and found to be very similar. The carbon source supplied to the bacterium is metabolized, via several steps, into (R)-3-hydroxybutyryl-CoA. This compound is believed to be the monomer that is converted by the polymerase enzyme into PHB.

The kinetics of the synthesis of biopolymers was recently reviewed by Luong *et al.*²⁵. The models discussed^{26,27,28} involve mainly the growth kinetics of the bacteria while the polymer accumulation process was not examined in any great detail. Kawaguchi and Doi²⁹, on the other hand, proposed a reaction equation for the polymerization process of PHB; based on the usual initiation, propagation and termination concept used in polymer chemistry. However, they didn't take into account the heterogeneous character of the PHB polymerization system.

11.2.3 Physical Model for the PHB Accumulation in *Alcaligenes eutrophus*

When considering any polymerization process, the first and relatively simple approach is to consider a homogeneous system, i.e. the concentration of all reactants is equal throughout the reaction system. However, this can not be used in the present case because the PHB polymerization system is inherently heterogeneous.

11.2.3.1 Formation of Granules

Only initially the system is homogeneous. The polymerase enzyme is present in the cytoplasm^{7,30,31} and there are no granules present. Once the bacterium starts accumulating PHB, monomer will react with the polymerase enzyme in the cytoplasm, hence initiation has occurred. During chain propagation, the polymerase enzyme will stay bound to the growing polymer chain, also referred to as polymer-polymerase conjugate. These species can be regarded as a surface active species, where the polymerase enzyme is the hydrophilic headgroup while the polymer chain is the hydrophobic tail. At a certain point the growing chain will precipitate since it exceeds its water solubility, or in other words, a colloidal particle will be formed in order to minimize its hydrophobic surface area. The so-formed hydrophobic surface will attract phospholipids and other surface active cell constituents. The granule surface can also be stabilized by the endgroups of polymer chains present, i.e. the hydroxyl or carboxyl endgroups can act as cosurfactant. This stage of the PHB accumulation is similar to interval I in the conventional emulsion polymerization process. A more quantitative and extensive approach of granule formation will be discussed in detail in *Chapter 12*.

11.2.3.2 Growth of Granules

Once the granule formation process is completed the bacteria enter the stage of granule growth. This stage of PHB accumulation is characterized by two main features. First, the constant number of granules per bacterium, being typically 8-14 granules per bacterium for *Alcaligenes eutrophus*⁶. Secondly, a constant rate of polymerization. The granule growth stage can be compared to interval II of a conventional emulsion polymerization process, as the number of polymer particles, i.e. loci of polymerization, remains constant¹⁵. Monomer diffuses to the surface of the granule where it is converted into polymer by the granule-associated polymer-polymerase conjugate⁷. If a propagating polymer-polymerase conjugate has undergone chain transfer it will desorb from the granule surface due to its hydrophilic character. In the cytoplasm, a free polymerase enzyme will grow into an polymer-polymerase conjugate, which at a certain degree of polymerization of the polymer chain can precipitate onto the granule surface rather than forming a new granule as in interval I.

The propagation in the case of PHB accumulation occurs mainly *at the surface* of the granules which is somewhat different from the conventional emulsion polymerization process

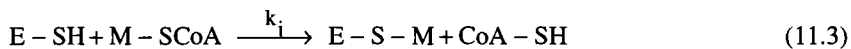
where the propagation of the polymer chain generally occurs *inside* the latex particles. Another difference lies in the monomer supply. The presence of a separate monomer phase in a conventional emulsion polymerization ensures a constant monomer concentration in the polymer particles. In the case of the PHB accumulation monomer is continuously supplied by a cascade of reactions in the cytoplasm (see also *Chapter 10*). It is known that the bacteria can continue accumulating PHB up to a weight fraction PHB of approximately 0.80, at which point PHB accumulation stops, although there is still monomer and active polymerase enzyme present ⁶.

11.2.4 Kinetic Model for the Accumulation of PHB in *Alcaligenes eutrophus*

In previous sections the different stages of PHB accumulation in terms of the emulsion polymerization process have been formulated. Here, these results are put together into a kinetic model for PHB accumulation, or more specifically the granule growth stage. At this point it is not the aim to develop a detailed kinetic model, but rather a frame-work from which further improvements can be incorporated.

11.2.4.1 Initiation

The polymerization process is initiated by the reaction of the active site of the polymerase enzyme and the monomer. The overall initiation reaction is given by *equation 11.3*.



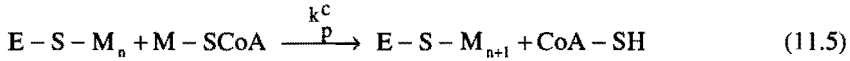
Here E-SH denotes the free polymerase enzyme, M-SCoA the monomer, CoA-SH is coenzyme-A and E-S-M is a polymerase enzyme with one monomer unit attached to it. k_i is the second order initiation rate coefficient. The rate of initiation (R_i) is given by *equation 11.4*:

$$R_i = k_i * [E - SH] * [M - SCoA] \quad (11.4)$$

here [M-SCoA] denotes the monomer concentration in the cytoplasm and [E-SH] the concentration of free polymerase enzyme in the cytoplasm.

11.2.4.2 Propagation in the Cytoplasm

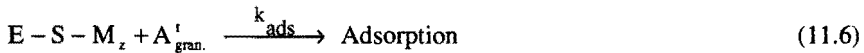
Once the active site of the polymerase enzyme has reacted with monomer, propagation in the cytoplasm, according to *equation 11.5*, can take place:



here $E-S-M_n$ represents a polymerase enzyme molecule in the cytoplasm which is attached to a polymer chain with a degree of polymerization of n or $n+1$ (also referred to as polymer-polymerase conjugate), and k_p^C is the second order propagation rate coefficient for propagation in the cytoplasm.

11.2.4.3 Adsorption of Polymer-Polymerase Conjugates onto Granules

At a degree of polymerization of z the polymer-polymerase conjugate, which is propagating in the cytoplasm, will become surface active and can adsorb onto a granule. Adsorption of these polymer-polymerase conjugates onto granules can be envisaged by:



here k_{ads} is the adsorption rate coefficient, $E-S-M_z$ the species which can adsorb, i.e. polymer-polymerase conjugate, with a degree of polymerization of z , and $A_{gran.}^t$ the total granule surface. It is not too unlikely to assume that species with a degree of polymerization of $z \pm s$ also give adsorption. Here, s is an integer which is a measure for the distribution of adsorbing polymer-polymerase conjugates. However, for simplicity we will only take the average degree of polymerization of z into account. Adsorption implied by *equation 11.6* is supposed to be irreversible. The rate of adsorption R_{ads} (in mole/liter.hour) can be easily visualized by *equation 11.7*:

$$R_{ads} = k_{ads} * [E-S-M_z] * A_{gran.}^t \quad (11.7)$$

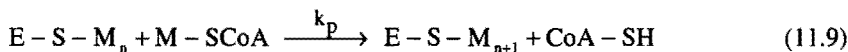
here, $A_{gran.}^t$ is the total granule surface area per liter of reaction mixture (in dm^2/l), which is equal to:

$$A'_{\text{gran.}} = \pi * d_{\text{gran.}}^2 * N_{\text{gran.}} \quad (11.8)$$

where $d_{\text{gran.}}$ denotes the average granule diameter and $N_{\text{gran.}}$ the number of granules per liter of reaction mixture.

11.2.4.4 Propagation at the Granule Surface

After adsorption has occurred the polymer-polymerase conjugate can propagate further at the granule surface. The propagation step at the granule surface can be visualized by *equation 11.9*.



It is assumed that the rate of propagation is independent of the length of the polymer chain attached to the polymerase enzyme (Flory's principle of equal reactivity)³². The rate of PHB accumulation or the rate of polymerization, R_p (in mole/liter.hour), is given by:

$$R_p = k_p * [M - SCoA]^{\text{gran.}} * [E - S - M_n] \quad (11.10)$$

where $[M - SCoA]^{\text{Gran.}}$ is the monomer concentration at the granule surface which is not necessarily equal to the monomer concentration in the cytoplasm. The monomer (see *figure 11.2*) bears some resemblance with biosurfactants such as rhamnolipids³³. Therefore, it is assumed that the monomer exhibits surface active properties. $[E - S - M_n]$ is the concentration of the propagating species at the granule surface with a degree of polymerization of n , while $n > z$, while k_p is the second order propagation rate coefficient for propagation at the granule surface. Assuming that most of the polymerization takes place *at the granule surface* the overall rate of polymerization R_p can be taken as the summation over the individual granules. This leads to *equation 11.11* which is comparable to *equation 11.2* for the emulsion polymerization process:

$$R_p = \frac{k_p * [M - SCoA]^{\text{gran.}} * n * N_{\text{gran.}}}{N_{\text{Av.}}} \quad (11.11)$$

here n^* is the average number of granule associated polymer-polymerase conjugates per granule.

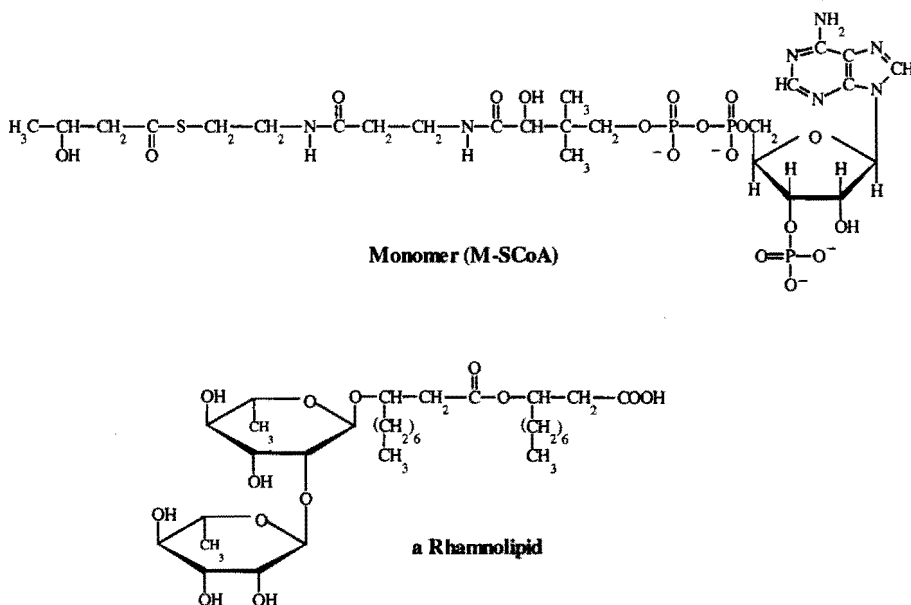
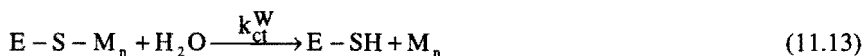
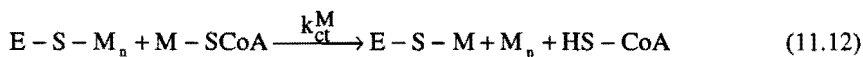


Figure 11.2 Structural formula of the monomer (M-SCoA) and a rhamnolipid.

11.2.4.5 Chain Transfer at the Granule Surface

The propagation process stops when the polymer-polymerase conjugate undergoes chain transfer. Possible chain transfer agents, amongst others, are monomer, water, acetyl-CoA, and acetoacetyl-CoA (see also *Chapter 13*). Only water and monomer will be considered here. Chain transfer to monomer and/or water can occur as depicted by *equations 11.12* and *11.13*.



here k_{ct}^M and k_{ct}^W are the rate coefficients for chain transfer to monomer and water, respectively. The total rate of chain transfer (R_{ct}) can be expressed as follows:

$$R_{ct} = (k_{ct}^M * [M - SCoA]^{gran.} + k_{ct}^W * [H_2O]) * \left(\frac{n^* * N_{gran.}}{N_{Av.}} \right) \quad (11.14)$$

Because of its hydrophilic nature, it is very likely that when a polymer-polymerase conjugate has undergone chain transfer it desorbs into the cytoplasm. In the case of chain transfer to water the resulting species is the free polymerase enzyme molecule (E-SH) which has to react with a monomer before it can participate in the polymerization process again. The product of the chain transfer to monomer reaction is already initiated (E-S-M) and can directly undergo propagation in the cytoplasm.

11.2.4.6 Molar Mass of Polymer

The molar mass of the polymer formed can be related to the number average degree of polymerization simply via the molar mass of the repeating unit. The number average degree of polymerization (\bar{x}_n) is given by *equation 11.15*:

$$\bar{x}_n = \frac{\text{rate of propagation}}{\sum \text{rates of all reactions leading to dead polymer}} = \frac{R_p}{R_{ct}^{tot}} \quad (11.15)$$

Here, the assumption is made that the system obeys steady-state conditions in the granule growth stage, i.e. the polymer-polymerase conjugate concentration at the granule surface ($\frac{n^* * N_{gran.}}{N_{Av.}}$) does not change with time (see *equation 11.16*). This is partially supported by the fact that the rate of polymerization is constant over a considerable time interval, as will be shown in *section 11.3.1*.

$$\frac{d \left(\frac{n^* * N_{gran.}}{N_{Av.}} \right)}{dt} = 0 \quad (11.16)$$

Two processes influence $\left(\frac{n^* * N_{gran.}}{N_{Av.}}\right)$: (1) the adsorption of polymer-polymerase conjugates from the cytoplasm onto the granule surface, **and** (2) chain transfer to water and/or monomer of propagating polymer-polymerase conjugates at the granule surface which, subsequently, leads to the desorption of the reaction product (free polymerase enzyme). This results in the next equation:

$$\frac{d\left(\frac{n^* * N_{gran.}}{N_{Av.}}\right)}{dt} = R_{ct}^{tot} - R_{ads}^{tot} = 0 \quad (11.17)$$

From *equations 11.16 and 11.17* it follows that the **total** rate of surface active polymer-polymerase conjugates adsorption onto granules (R_a) is equal to the **total** rate of chain transfer of propagating polymer-polymerase conjugates at the granule surface (R_{ct}), when the system obeys steady-state conditions. The number average molar mass of the polymer (\overline{M}_n) formed, which is the product of the number average degree of polymerization and the molar mass of the repeating unit, can be visualized by *equation 11.18*, using *equations 11.15 - 11.17*.

$$\overline{M}_n = \frac{M_0 * R_p}{R_{ct}^{tot}} = \frac{M_0 * R_p}{R_{ads}^{tot}} = \frac{k_p * [M - SCoA]^{gran.} * M_0 * n^*}{k_{ads} * [E - S - M_z] * N_{Av.} * \pi * d_{gran.}^2} \quad (11.18)$$

Here M_0 is the molar mass of the repeating unit. According to *equation 11.18* the number average molar mass of the polymer formed during the granule growth stage of the accumulation process scales with $\frac{1}{d_{gran.}^2}$. It should be noted that the rate of chain transfer and propagation per chain is taken constant in the derivation of *equation 11.18*.

In *Chapter 15* the time-dependent changes in the granule associated polymer-

polymerase conjugate concentration, i.e. $\frac{d\left(\frac{n^* * N_{gran.}}{N_{Av.}}\right)}{dt}$, will be discussed, when the

influence of the metabolism on monomer production and polymerization is considered. Also the effect of the periodic behavior of the metabolism on the rate of chain transfer as well as on the rate of propagation will be examined.

11.3 Granule Growth: Comparison with Experiment

11.3.1 Rate of Polymerization

It is well known that *Alcaligenes eutrophus* can accumulate PHB up to about 80 % of its cell dry weight. At this level any further accumulation proceeds at a negligible rate. It can be speculated that this is related to a diffusion limitation, caused by an increasing concentration of water soluble polymers present (e.g. DNA and RNA). At a polymer content of 80 %, the space available in the cell has been reduced to such an extent that further polymer accumulation would mean both massive polymer granule coalescence, and exclusion of other material from the bacterium, e.g. vital cell components such as DNA and proteins. This appears to limit the maximum polymer content achievable by the cell: how this limitation is achieved is as yet unknown (see also *Chapter 13* for a possible explanation for this phenomenon).

The rate of polymerization has been calculated by considering the limitation discussed above. For modeling purposes, the conversion (X) at the maximum polymer content achievable ($C_{\text{PHB}}^{\text{Max}}$) will be defined as unity. So $X(t) = (C_{\text{PHB}}^t) / (C_{\text{PHB}}^{\text{Max}})$ represents the fraction of polymer accumulated (C_{PHB}^t) compared to the ultimate level achievable ($C_{\text{PHB}}^{\text{Max}}$). Utilizing this definition of conversion the data of Ballard *et al.*⁶ and Kawaguchi and Doi²⁹ were converted into conversion-time curves (displayed in *figure 11.3*). From *figure 11.3* the rates of polymerization have been calculated and are reported in *table 11.1*. It can be seen in *figure 11.3* and *table 11.1* that there are two separate regions; in both a constant rate of polymerization is observed. The rates of polymerization in the first part for the fermentations reported by Ballard *et al.*⁶ and Kawaguchi and Doi²⁹ are almost the same. After a certain period the rate of polymerization gradually decreases to a second steady-state, which continues until the end of the accumulation process. One explanation for the two observed rates of polymerization is that at a certain volume fraction of granules in the bacterium close

packing of granules occurs (see *figure 11.4*). Therefore, only coalescence would allow the accumulation of more polymer, since for monodisperse spheres hexagonal close packing occurs at a volume fraction spheres of 0.72, whereas for polydisperse spheres fractions of dispersed phase can be above 0.9. If, indeed, coalescence would occur during polymer accumulation then, according to *equation 11.11*, the rate of polymerization would decrease because the number of granules (N_{gran}) is reduced. This is observed experimentally.

Table 11.1 Rates of polymerization (mole/l.h) for the different fermentations in *figure 11.3*.

Reference	$(R_p^{\text{region1}})^a$	$(R_p^{\text{region2}})^b$	V_{PHB}^c
Ballard <i>et al.</i> ⁶	$1.7 * 10^{-2}$	$9.2 * 10^{-3}$	0.61
Kawaguchi and Doi ²⁹	$1.8 * 10^{-2}$	$2.7 * 10^{-3}$	0.57

^a Rate of polymerization in region 1, i.e. the first part of the granule growth stage **before** coalescence.

^b Rate of polymerization in region 2, i.e. the second part of the granule growth stage **after** coalescence has occurred.

^c Volume fraction PHB in the bacterium at which the rate of polymerization declines

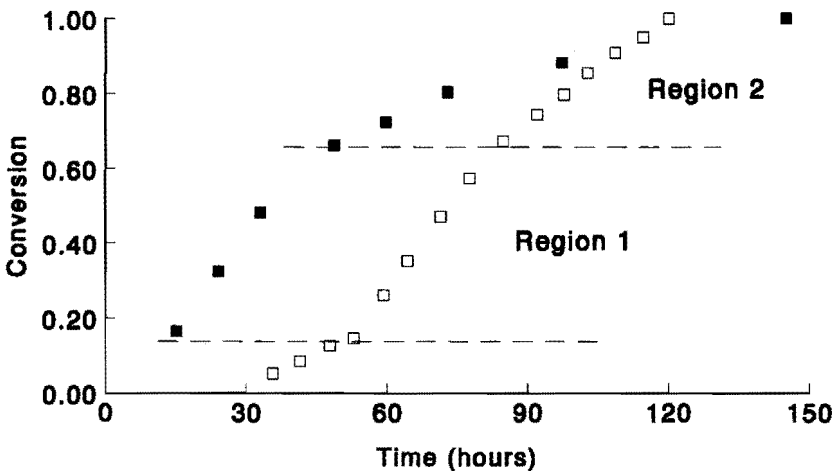


Figure 11.3 Conversion-time curves for different PHB accumulations. Open squares represent data taken from Ballard *et al.* ⁶ and closed squares represent data taken from Kawaguchi & Doi ²⁹.

The volume fraction of polymer in the bacterium equals 0.59 (average value, see *table 11.1*) at the point where the rate of polymerization slows down. This is in good agreement with Ballard *et al.* ⁶ who reported a value of 0.58 at which the bacteria's shape became more

spherical, suggesting the onset of coalescence. This latter supposition, that the change in shape of the bacterium is related to coalescence, rests on the assumption that a bacterium changes shape because it is 'full' of granules. Further, the fact that the polymer is in an amorphous state³⁴ in the granules allows them to coagulate much easier than when the polymer would have been in the crystalline state.

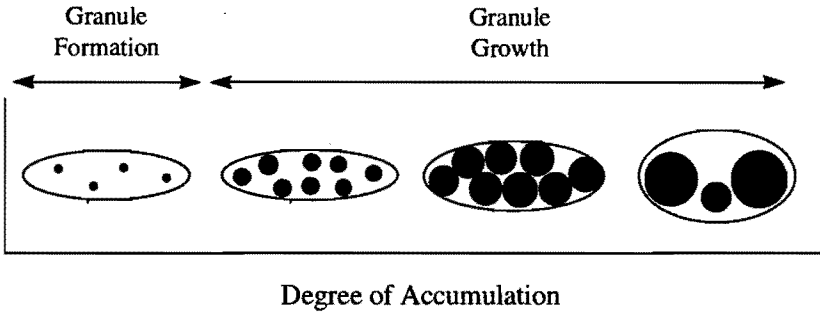


Figure 11.4 The degree of accumulation of PHB accumulating bacteria.

Ideally the concept of 'incipient coagulation' could be tested with a knowledge of the granule diameter as a function of conversion. Unfortunately, these data do not exist, therefore, experimental rate of polymerization (= rate of polymer accumulation) and molar mass data must be used to calculate the granule diameter ($d_{\text{gran.}}$) as a function of conversion. These model based '*experimental*' data can be compared with simulated curves where no coagulation and controlled coagulation occur, respectively. This is done below.

a. *Experimental: Granule diameter according to the volume growth rate.* In the next approach mechanistic effects will be introduced by using the volume growth rate coefficient³⁵. This coefficient (K) may be evaluated from the knowledge of the propagation reaction and the conversion-time curve of the polymerization system. The mass of polymer added per unit of time to a single growing chain is given by:

$$K = \frac{k_p * [M - SCoA]^{\text{gran.}} * M_0}{N_{\text{Av.}} * \rho_p} \quad (11.19)$$

where ρ_p is the density of the polymer. The volume growth rate coefficient will change during the polymerization, as can be seen in the extended form in *equation 11.20* where the change in volume growth per unit of time is calculated once the molar conversion is known.

$$\Delta K = K \cdot (X_2 - X_1) \cdot (t_2 - t_1) \quad (11.20)$$

With *equation 11.20* the increase in granule diameter per unit of time and conversion can be calculated according to

$$\Delta d_{\text{gran.}} = \left(\frac{6 \cdot \Delta K}{\pi} \right)^{1/3} \quad (11.21)$$

Once the granule size $d_{\text{gran.,1}}$ at time t_1 is known then the theoretical granule size ($d_{\text{gran.,2}}$) at time t_2 and X_2 can be calculated

$$d_{\text{gran.,2}} = d_{\text{gran.,1}} + \Delta d_{\text{gran.}} \quad (11.22)$$

This value can subsequently be compared with the experimental value. *Equations 11.19-11.22* are applied to the conversion-time curve reported by Ballard *et al.*⁶ which is displayed in *figure 11.3*. In *figure 11.5* the granule diameter as a function of conversion is depicted as calculated from *equations 11.19-11.22* using the conversion-time data before coagulation is supposed to occur. In the same picture the theoretical diameter of a granule is plotted for a granule which grows solely via the formation of monomer into polymer (no coagulation takes place). As can be seen from *figure 11.5* the diameter of the granules increase with increasing conversion, i.e. during this part of the accumulation process the growth of the granules occurs via the formation of monomer to polymer.

In *figures 11.6* and *11.7* the data of the entire conversion-time curves represented in *figure 11.3* are used to calculate the granule diameter utilizing *equations 11.19-11.22*. Curve **a** in *figures 11.6* and *11.7* shows a constant increase with conversion until a conversion of approximately 0.70 is reached after which the diameter increases more steeply.

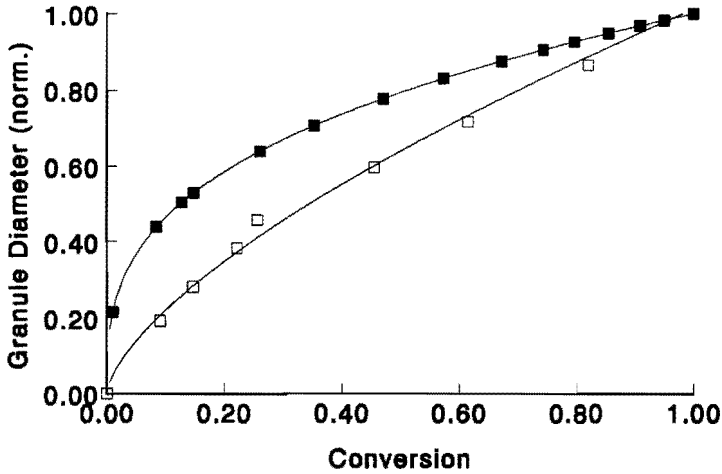


Figure 11.5 The normalized granule diameter as a function of conversion. Open squares represent the granule diameter according to equations 11.19-11.22, closed squares calculated granule diameter according to equation 11.24.

b. Experimental: Granule diameter calculated from the molar mass. The last method by which the diameter of the granules can be determined is by using the experimental molar mass data. According to equation 11.18 the granule diameter is a function of the number average molar mass (M_n) of the polymer formed, rewriting equation 11.18 gives equation 11.23:

$$d_{\text{gran.}} = \sqrt{\left(\frac{B}{M_n}\right)} \quad (11.23)$$

here B is comprised of different parameters that are assumed to be constant during the granule growth stage of the accumulation process, such as M_0 , $[M\text{-SCoA}]^{\text{Gran.}}$, n^* , k_p , k_{ads} , and $[E\text{-S-M}_2]$. Equation 11.23 is applied to the instantaneous number average molar mass given in figures 11.8 and 11.9 and are represented in figures 11.6 and 11.7 by curve **b**, respectively. The data in figures 11.6 and 11.7 are normalized to the last data point, concomitantly it is possible to plot the data without detailed knowledge of the value of the constant B. Curve **b** in figure 11.6 shows a constant increase with conversion until a conversion of approximately 0.70 is reached after which the diameter increases more steeply. In the case of curve **b** in

figure 11.7 this behavior, i.e. an increase in diameter up to a conversion of approximately 0.70 and then a more steeper increase, is less pronounced. This is probably due to the fact that less experimental data were available in the first part of the accumulation process, i.e. the part before coagulation occurs.

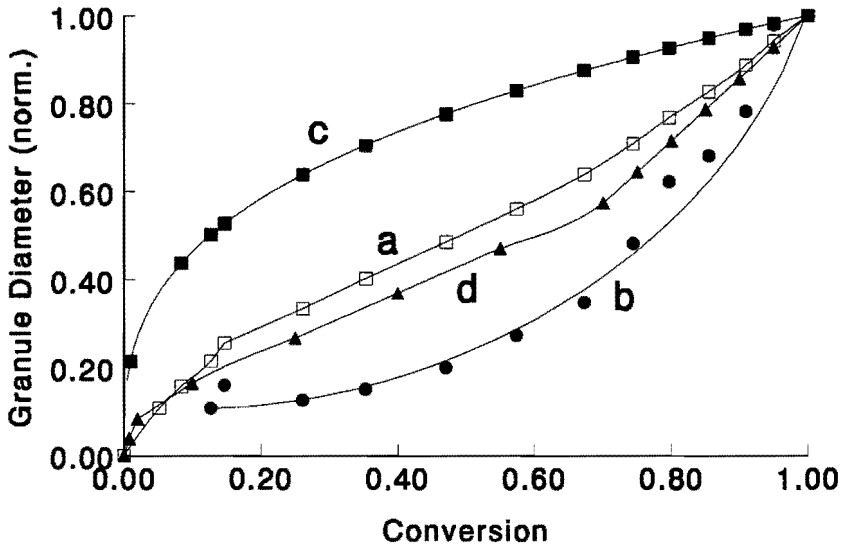


Figure 11.6 The normalized granule diameter as a function of conversion. Open squares represent the granule diameter according to equations 11.19-11.22 (curve a), closed circles the granule diameter from the instantaneous number average molar mass data according to equation 11.23 (curve b), closed squares calculated granule diameter according to equation 11.24 (curve c), and the closed triangles theoretical latex particle diameter if coagulation is simulated for a conventional emulsion polymerization, the number of latex particles decreased with a factor of 5 after a conversion of 0.70 (curve d).

c. Simulation: Course of granule diameter as a function of conversion. It can be shown that if monomer is converted into polymer and this polymer is then put into a sphere, i.e. a granule, the resulting granule diameter is given by equation 11.24:

$$d_{\text{gran.}} = \left(\frac{6 * M_0 * n_m^{X-1} * X}{\pi * \rho_p} \right)^{1/3} \quad (11.24)$$

$n_m^{X=1}$ is the total number of moles of monomer converted into polymer at a conversion equal to unity. Equation 11.24 is represented by curve **c** in figures 11.6 and 11.7. The diameter of the growing granule increases rapidly in the beginning and gradually reaches its maximum value at the end of the polymerization.

d. Simulation: Latex particle diameter during an emulsion polymerization with coagulation. Curve **d** in figures 11.6 and 11.7 represents the latex particle diameter of a simulated emulsion polymerization where after a conversion of 0.70, coagulation is simulated. This coagulation decreased the number of latex particles per liter by a factor of 5.

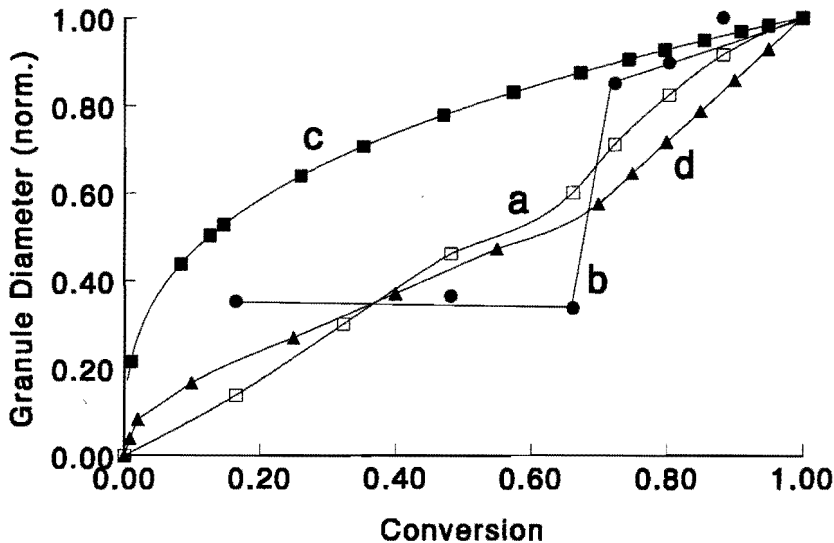


Figure 11.7 The normalized granule diameter as a function of conversion. Open squares represent the granule diameter according to equations 11.19-11.22 (curve a), closed circles the granule diameter from the instantaneous number average molar mass data according to equation 11.23 (curve b), closed squares the calculated granule diameter according to equation 11.24 (curve c), and closed triangles theoretical latex particle diameter if coagulation is simulated for a conventional emulsion polymerization, the number of latex particles decreased with a factor of 5 after a conversion of 0.70 (curve d).

From the above it can be seen that both 'experimental' curves follow more closely the simulation where coagulation occurred. It is believed that this is evidence for both the

assumption that coagulation occurs during polymer accumulation, and also for the kinetic model derived in this chapter. Further testing of these ideas will necessarily involve the measurement of granule size as a function of conversion.

11.3.2 Molar Mass

According to *equation 11.18* the molar mass of the PHB formed, during the granule growth stage, will decrease as the granules grow, i.e. with increasing granule diameter. In *figures 11.8 and 11.9* the cumulative and instantaneous number average molar mass of PHB formed during two different fermentations as a function of conversion are plotted ^{6,29}.

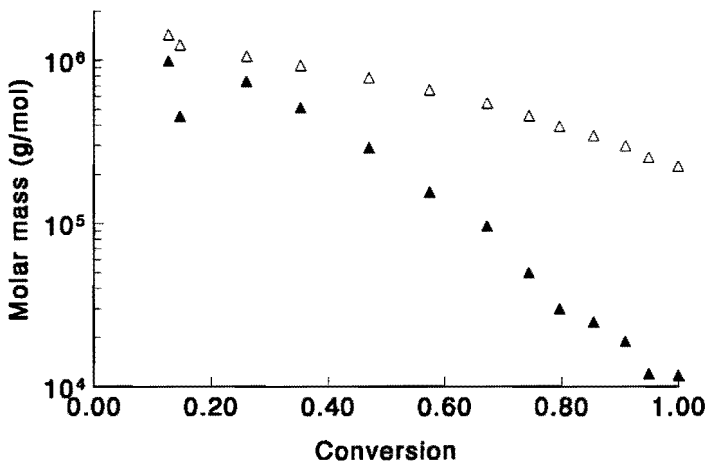


Figure 11.8 Instantaneous and cumulative number average molar mass of PHB formed as a function of conversion. Cumulative number average molar mass (open triangles), and instantaneous number average molar mass (closed triangles). Data taken from Ballard et al. ⁶.

Figures 11.8 and 11.9 show that the molar mass of the PHB formed decreases with conversion, as predicted by the model. The fact that the molar mass shows a stronger decrease after approximately 70 % conversion can be explained by the fact that coagulation occurs, as already pointed out in the previous section. When this coagulation occurs the number of granules decreases while the diameter of the remaining granules increases. This results initially in a sudden decrease of the molar mass which will decrease constantly as the rate of polymerization becomes constant again, i.e. N_{gran} is constant again. After the coagulation the

decrease in molar mass is solely determined by the increase in granule diameter due to the formation of new polymer.

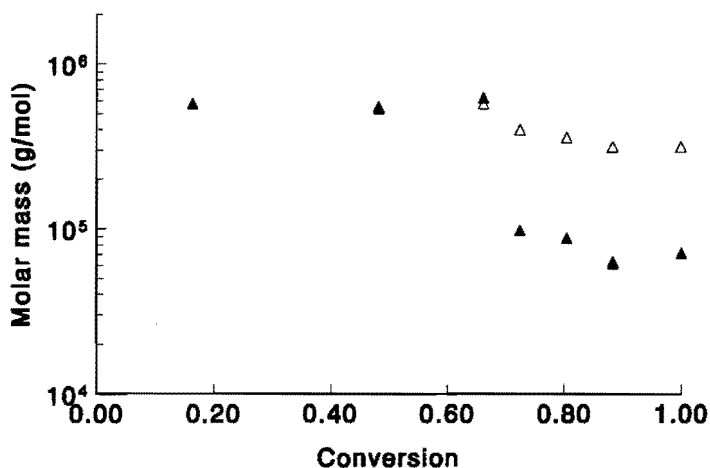


Figure 11.9 Instantaneous and cumulative number average molar mass of PHB formed as a function of conversion. Cumulative number average molar mass (open triangles), and instantaneous number average molar mass (closed triangles). Data taken from Kawaguchi and Doi²⁹.

11.4 Conclusions

In the foregoing sections a kinetic model has been developed which is able to describe the experimental data on PHB accumulation, during the granule growth stage, in *Alcaligenes eutrophus* reported in open literature. In contrast to previous models, the heterogeneous nature of the PHB accumulation is taken into account. The accumulation of PHB is projected on different aspects known to be important in the conventional emulsion polymerization process, such like particle formation and interval II kinetics. Further, adsorption and desorption of propagating and terminated polymer-polymerase conjugates are believed to play an important role in the PHB accumulation process. The experimentally observed decrease in the rate of polymerization can be explained by coalescence of the granules present due to the fact that these granules reach a pseudo-close packing in the accumulating bacterium. Evidence is given for the occurrence of coalescence of these granules during the accumulation process

by two independent approaches, i.e. via the volume growth factor K and via the relation between the molar mass of the polymer formed and the granule diameter.

The decrease in the molar mass of the polymer formed during the PHB accumulation process can be explained in terms of the kinetics of the polymerization process and the effect of the granule size thereon. This is in contrast with the explanation^{36,37} that the decrease in molar mass is due to the simultaneous operation of the polymerase enzyme and the depolymerase enzyme (see also *Chapters 10* and *13*). The developed model focuses on the PHB accumulating bacterium *Alcaligenes eutrophus*, but it is believed that this model might also be applicable to other PHB accumulating species (see also *Chapter 15*).

11.5 References

- 1 Lemoigne, M., *Ann. Inst. Pasteur Paris*, **39**, 144 (1925)
- 2 Dawes, E.A. and Senior, P.J., *Adv. Microbiol. Physiol.*, **10**, 135 (1973)
- 3 Anderson, A.J. and Dawes, E.A., *Microbiol. Rev.*, **54**, 450 (1990)
- 4 US 1,732,795 (1927), Goodyear Tire and Rubber Co., Dinsmore, R.P., *Chem Abstr.* **24**, 266
- 5 Ellar, D., Lundgren, D.G., Okamura, K., and Marchessault, R.H., *J. Mol. Biol.*, **35**, 489 (1968)
- 6 Ballard, D.G.H., Holmes, P.A., and Senior, P.J., *Recent Adv. Mech. Synth. Aspects Pol.*, **215** 293 (1987)
- 7 Gerngross, T.U., Reilly, P., Stubbe, J., Sinskey, A.J., and Peoples, O.P., *J. Bacteriol.*, **175**, 5289 (1993)
- 8 De Koning, G.J.M., and Maxwell, I.A., *J. Environ. Pol. Degr.*, **3**, 223 (1993)
- 9 *Chapters 12, 13, and 14.*
- 10 Kurja, J., Zirkzee, H.F., and Maxwell, I.A., "Unconventional Emulsion Polymerizations", in "Emulsion Polymers and Emulsion Polymerization", M.S. El-Aasser and P. Lovell (Eds.), Wiley, Chapter 23, 763 (1997)
- 11 Weyenberg, D.R., Findlay, D.E., Cekada, J., and Bey, A.E., *J. Pol. Sci., Part C*, **27**, 27 (1969)
- 12 US 4,273,634 (1981), Dow Corning Corp., invs.: Saam, J.C., Wegener, R.L., *Chem Abstr.* **95**, 82044r
- 13 Saam, J.C., and Huebner, D.J., *J. Pol. Sci., Polym Chem. Ed.*, **20**(12), 3351 (1982)
- 14 Lu, S-Y, Quayle, P., Booth, C., Yeates, S.G., and Padget, J.C., *Polymer Int.*, **32**, 1 (1993)
- 15 Maxwell, I.A., Morrison, B.R., Gilbert, R.G., and Napper, D.H., *Macromolecules*, **24**, 1629 (1991)
- 16 Hansen, F.K., and Ugelstad, J., 'Particle Formation Mechanisms', in 'Emulsion Polymerization', Ed. I. Piirma, Academic Press, New York, (1982)
- 17 Gilbert, R.G., and Napper, D.H., *J. Macromol. Sci. - Rev. Macromol. Chem. Phys.*, **C23**, 127 (1983)
- 18 Blackley, D.C., 'Emulsion Polymerization', Applied Science Publishers LTD, London, (1975)
- 19 Smith, W.V., and Ewart, R.H., *J. Chem. Phys.*, **16**, 592 (1948)
- 20 Harkins, W.D., *J. Am. Chem. Soc.*, **69**, 1428 (1947)
- 21 Goodwin, J.W., Hearn, J., Ho, C.C., and Ottewill, R.M., *Col. Polym. Sci.*, **252**, 464 (1974)

- 22 Fitch, R.M., and Tsai, C.H., in '*Polymer Colloids*', Ed. R.M. Fitch, Plenum, New York, (1971)
- 23 Ugelstad, J., and Hansen, F.K., *Rubber Chem. Technol.*, 49, 536 (1976)
- 24 McCarthy, S.J., Elbing, E.E., Wilson, I.R., Gilbert, R.G., Napper, D.H., and Sanger, D.F., *Macromolecules*, 19, 2440 (1986)
- 25 Luong, J.H.T., Mulchandani, A., and Leduy, A., *Enzyme Microb. Technol.*, 10, 326 (1988)
- 26 Mulchandani, A., Luong, J.H.T., and Groom, C., *Appl. Microbiol. Biotechnol.*, 30, 11 (1989)
- 27 Quinlan, A.V., *Ann. N.Y. Acad. Sci.*, 469, 259 (1986)
- 28 Ollis, D.F., *Ann. N.Y. Acad. Sci.*, 413, 144 (1983)
- 29 Kawaguchi, Y., and Doi, Y., *Macromolecules*, 25, 2324 (1992)
- 30 Griebel, R., Smith, Z., and Merrick, J.M., *Biochemistry*, 7(10), 3676 (1968)
- 31 Haywood, G.W., Anderson, A.J., and Dawes, E.A., *FEMS Microbiol. Lett.*, 57, 1 (1989)
- 32 Flory, P.J., "*Principles of Polymer Chemistry*", New York, (1953)
- 33 Fiechter, A., *TIBTECH*, 10, 208 (1992)
- 34 De Koning, G.J.M., and Lemstra, P.J., *Polymer*, 33, 3292 (1992)
- 35 Lichti, G., Hawkett, B.S., Gilbert, R.G., and Napper, D.H., *J. Pol. Sci., Pol. Chem. Ed.*, 19, 925 (1981)
- 36 Doi, Y., Kawaguchi, Y., and Kunioka, M., *FEMS Microbiol. Lett.*, 67, 165 (1990)
- 37 Doi, Y., "*Microbial Polyesters*", New York, VCH Publishers, Inc., (1990)

CHAPTER 12

The Accumulation of Poly-(R)-3-hydroxybutyrate in *Alcaligenes eutrophus* 3. Granule Formation

Synopsis: Due to the heterogeneous character of the biosynthesis of poly-(R)-3-hydroxybutyrate in *Alcaligenes eutrophus*, the accumulation has been considered in terms of a granule formation and a granule growth stage. Several nucleation mechanism reported in literature for various, synthetic and biological, emulsion polymerizations were reviewed. After this a quantification was made concerning the granule formation stage of the biosynthesis of poly-(R)-3-hydroxybutyrate in *Alcaligenes eutrophus*, based on a homogeneous nucleation model followed by growth. Further, an expression was derived describing the molar mass of the polymer formed during the granule formation stage. Good agreement was obtained by comparing model calculations based on the homogeneous nucleation model and experimental result on the accumulation of poly-(R)-3-hydroxybutyrate in *Alcaligenes eutrophus*. Finally, it has been shown that the molar mass of the polymer formed during the whole course of the accumulation process is related to the amount of polymer in the bacterium.

12.1 Introduction

Numerous genera of micro-organisms and fungi are capable of accumulating poly-3-hydroxyalkanoates (PHAs) as intracellular granules. Due to the intrinsic heterogeneity of this biological polymerization process a subdivision has to be made. On the bases of its colloidal appearance this polymerization system can be divided into a so-called granule formation and granule growth stage. In the previous chapter, the granule growth stage of the accumulation of

In part reproduced from : (i) Kurja, J., Zirkzee, H.F., De Koning, G.J.M., and Maxwell, I.A., in : "Biodegradable Plastics and Polymers", Y. Doi and K. Fukuda (Eds.), Elsevier, Amsterdam, p. 379-386 (1994), and (ii) Kurja, J., Zirkzee, H.F., and Maxwell, I.A., "Unconventional Emulsion Polymerizations", in : "Emulsion Polymers and Emulsion Polymerization", M.S. El-Aasser and P. Lovell (Eds.), Wiley, Chapter 23, 763 (1997)

poly-(R)-3-hydroxybutyrate in *Alcaligenes eutrophus* has been discussed and quantified. The major conclusion that could be drawn from *Chapter 11* is that the heterogeneity of the polymerization system has a profound effect on the polymerization process and thus on the polymer formed. In this chapter, the granule formation stage of the accumulation of PHB in *Alcaligenes eutrophus* will be discussed and equations will be derived describing this process. Before doing so, a literature overview will be given which summarizes the mechanisms and models proposed for the formation of latex particles in **synthetic** as well as in **natural** (biological) emulsion polymerizations.

12.2 Latex Particle Formation in Emulsion Polymerization Processes

12.2.1 Synthetic Emulsion Polymerizations

If the formation of latex particles in an emulsion polymerization is considered, one of the key factors is the amount of surfactant added. Two cases can be distinguished: (1) the surfactant concentration is below its critical micelle concentration (CMC), or (2) above its CMC under the polymerization conditions. If the nucleation mechanisms proposed for emulsion polymerizations are summarized according to the added surfactant concentration, one can distinguish among several mechanisms, as will be summarized below.

a. Nucleation models for systems above the CMC: Oligomeric radicals formed in the aqueous phase during the initial phase of an emulsion polymerization can either enter existing micelles when these radicals reach a critical degree of polymerization of z at which they become surface active and can enter the monomer swollen micelles (*Micellar Nucleation*¹). However, these z -mers can also propagate further in the aqueous phase until they reach a critical degree of polymerization of j at which they become insoluble. Concomitantly, these j -mers want to minimize their surface area and will collapse forming a precursor particle. This latter case is also known as the *Homogeneous Nucleation* mechanism, and first quantified by Fitch and Tsai² (also known as the 'HUFT' (Hansen-Ugelstad-Fitch-Tsai) theory³). The micelles initiated via the micellar nucleation mechanism as well as the precursor particles formed via the homogeneous nucleation mechanism are colloiddally unstable and can coagulate until colloidal

stability is attained. This nucleation mechanism is also known as the coagulative nucleation theory ⁴.

b. Nucleation models for emulsifier free systems : For emulsifier free emulsion polymerization systems precursor particle formation takes place via the homogeneous nucleation process, because no micelles exist. This implies that aqueous phase kinetics play a very important role in the formation of latex particles. After the precursor particles have been formed a number of mechanisms for latex particle formation can occur :

1. *Homogeneous-coagulative nucleation mechanism*: here the growth of precursor particles is dominated by coagulation events which will lead to a continuously decreasing number of particles (*figure 12.1*, curve *A*).

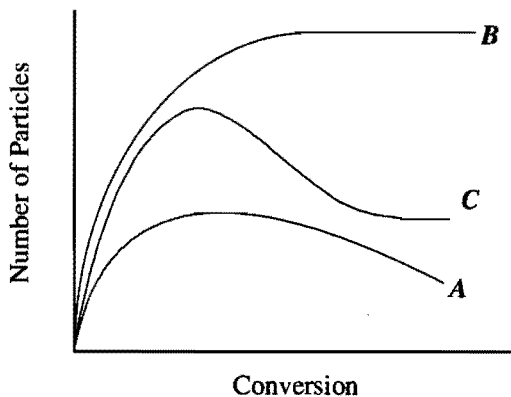


Figure 12.1 Schematic representation of the number of particles formed as a function of conversion for the different nucleation mechanisms. Curve *A*: Homogeneous-coagulative nucleation mechanism, Curve *B*: Homogeneous nucleation followed by growth, and Curve *C*: Homogeneous nucleation followed by limited coagulation

2. *Homogeneous nucleation followed by growth*: in this theory it is assumed that after the formation of the precursor particles no coagulation occurs and the particles will only grow by the entry of oligomeric radicals formed in the aqueous phase (*figure 12.1*, curve *B*). Concomitantly, the number of latex particles will become constant in time and conversion.

3. *Homogeneous nucleation followed by limited coagulation*: this model is an extension of the HUFT theory which claims that nucleation of precursor particles occurs by homogeneous nucleation followed by limited coagulation until the particles attain colloidal stability. This mechanism will cause the number of particles to increase rapidly after which it will decrease again (figure 12.1, curve C).

4. *In situ micellization*: takes account for the formation of *in situ* formed surfactant which is derived from utilizing a water soluble initiator. These *in situ* formed surfactant species are products of the termination of oligomeric radicals propagating in the aqueous phase. It should be stressed here that only unanchored species can participate in *in situ* micellization. This form of nucleation is expected to be rare since the total amount of unanchored species formed during an emulsion polymerization is rather low and probably will not exceed its CMC on the time scale of the nucleation period usually observed in an emulsion polymerization. However, if this would be the case the polymerization system can be modeled as a system in which surfactant is present in amount which exceeds the CMC, i.e. as a micellar nucleating system.

Out of the above discussed mechanisms none can exclusively deal with experimental observations concerning the nucleation stage during an emulsion polymerization. Often a combination of mechanisms is operative.

12.2.2 Latex Particle Formation in Biological Emulsion Polymerizations ⁵

12.2.2.1 The Biosynthesis of Poly-*cis*-isoprene (Natural Rubber)

Natural rubber is synthesized by a wide variety of plants. The botanic rationale for this synthesis is still a mystery. The biosynthesis of natural rubber has been studied extensively in the past ^{6,7,8,9}, and the basic polymerization reactions have been defined. However, the full mechanism of the formation of rubber particles has still not been elucidated, although some suggestions have been made ^{7, 9, 10}. The formation of poly-*cis*-1,4-isoprene is a heterogeneous polymerization where the polymerization mainly occurs at the surface of the rubber particles. The propagating rubber transferase molecule is mainly situated at the surface of a rubber latex particle ^{11,12}. The sizes of

rubber latex particles can vary from 10 nm to several microns⁹. The outer layer of these latex particles mainly consists of phospholipids and proteins.

Archer and Audley⁷ suggested that the rubber particles are formed via a micellar nucleation mechanism, where the micelles consist of geranylgeranyl diphosphate (GGDP), rubber transferase and, possibly, other molecules. These micelles are either dispersed in the cytoplasm or attached to some surface. Paterson-Jones *et al.*⁹ assumed that, initially, rubber transferase acts on a molecule of farnesyl diphosphate (FDP) or GGDP at some site in a suitable cell membrane. Via a complicated mechanism it is assumed that at a critical chain length the polymer chain, together with both a portion of the membrane and the rubber transferase, detaches to form a separate entity. This is a latex particle composed of a rubber coil, stabilized by phospholipid chains containing the rubber transferase, through which protrude the active growing ends of the rubber molecules. These authors⁹ also stated that the existence of rubber latex particles in the cell is a simple reflection of their chemical incompatibility with either the cytoplasm or the cell membranes.

Hager *et al.*¹⁰ proposed another mechanism for rubber particle formation that suggests that the low molar mass rubber formed during the biosynthesis represents the first stable rubber particles that can exist as stable latex particles (*figure 12.2*).

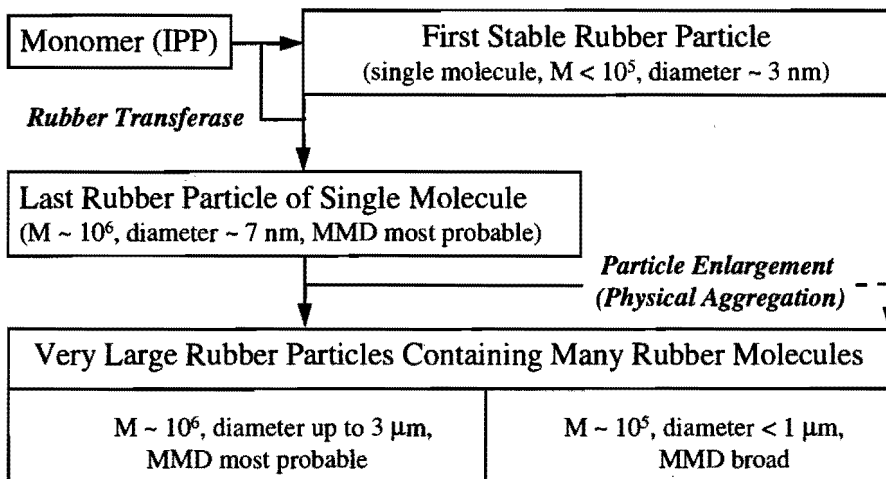


Figure 12.2 Schematic representation of the biosynthesis of natural rubber as proposed by Hager *et al.*¹⁰ (MMD: Molar Mass Distribution, M: Molar mass in g/mole)

These precursor particles can further polymerize until their large size hinders the geometrical positioning required for further polymerization. The precursor particles can also coagulate to form larger particles (see *figure 12.2*). A similarity of this process to the synthetic emulsion polymerization process of particle growth is the repeated initiation, propagation and termination of rubber transferase at the particle surfaces. The nucleation mechanism proposed by Hager *et al.*¹⁰ for the formation of rubber latex particles is closely related to the homogeneous nucleation model known from the conventional emulsion polymerization process. For this reason it is likely that useful comparisons can be made between the mechanisms of conventional emulsion polymerization and the emulsion polymerization of rubber, particularly in a fashion already applied to PHB¹⁸.

12.2.2.2 The Biosynthesis of Cellulose

Cellulose is the most abundant biopolymer and is produced by nearly all green plants and some fungi and bacteria in order to strengthen cell walls. The enzyme responsible for the formation of cellulose is cellulase, and it is active on the monomer, uridine diphosphoglucose¹³. Under normal circumstances the cellulose is formed as microfibrils on the exterior of the cell walls. Initially the cellulase enzyme molecule is active within the cell, but the oligomeric cellulase chains are adsorbed onto the cell wall, and further polymerization occurs through and beyond the cell walls, forming microfibrils. In a sense the polymer is 'extruded' through the cell walls by the cellulase, and the polymer chains external to the cell walls crystallize, thus giving their strengthening properties. If the cellulose biosynthesis outside the cell walls is delayed or repressed, the polymer can accumulate as latex particles within the cells. This supports the association-crystallization hypothesis¹⁴ for cellulose biosynthesis. According to this model the cellulose is synthesized as individual chains within the cytoplasm, which then adsorb onto the cell walls. This in contrast to other models where it is presumed that the enzyme is only active at the microfibril ends embedded in cell walls. If the former model is correct, and it is supported by experimental evidence, then the biosynthesis of cellulose can be considered, in part, as an emulsion polymerization.

12.2.2.3 The Biosynthesis of Poly-3-hydroxyalkanoates

Already 25 years ago Ellar *et al.*¹⁵ and Griebel *et al.*¹⁶ compared the formation of PHB granules with the formation of latex particles in the conventional emulsion polymerization process. In doing so, they stated that: "The model that has been developed is not too unlike

the familiar emulsion polymerization equation, except that the number of chain initiation sites in this case is probably determined by a well-defined number of protein molecules which form the initial micelle".

Recently, Gerngross *et al.*¹⁷ developed a model for PHB granule assembly based on the finding from a study on the localization of the PHB synthase enzyme at the surface of the PHB granules (*figure 12.3*).

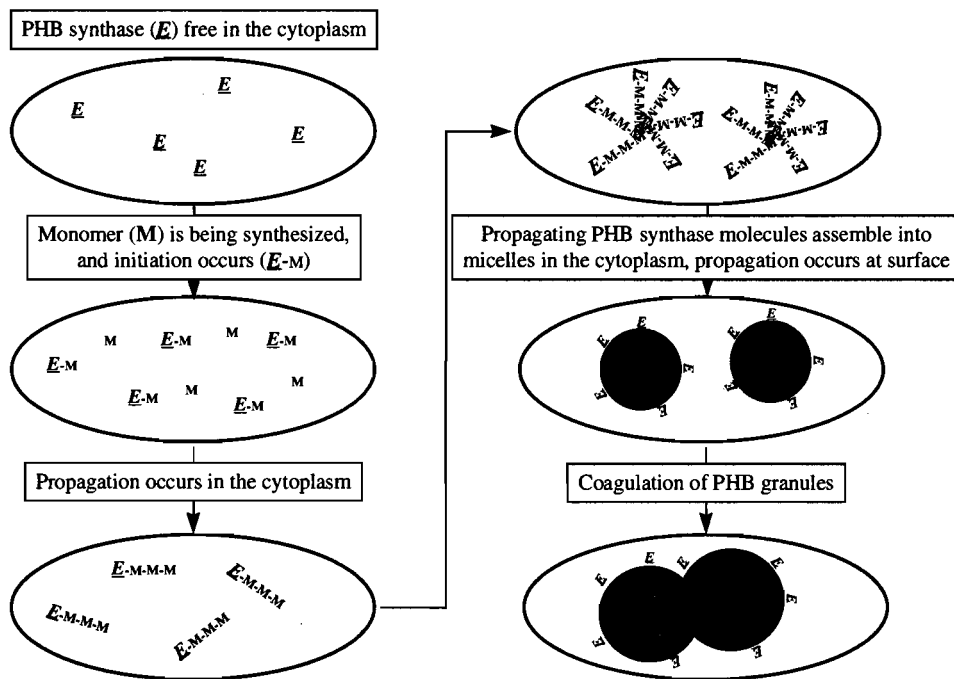


Figure 12.3 Nucleation mechanism for Granule Formation in *Alcaligenes eutrophus* according to Gerngross *et al.*¹⁷.

Assuming that the polymerization starts in the total absence of PHB and the growing polymer chain remains bound to the PHB synthase enzyme, PHB granule assembly would proceed in the following five steps: First, the metabolism of the bacterium will reach a situation at which coenzyme-A is depleted, acetyl-CoA and (R)-3-hydroxybutyryl-CoA, i.e. the monomer in the polymerization process, are produced. Then, the PHB synthase will be initiated and polymerization can occur. After which, the length of the polymer chain which is

attached to the PHB synthase increases. This will generate a number of propagating polymer chains, which are hydrophobic and attached to hydrophilic PHB synthase enzyme molecules. These propagating polymer chains can assemble in the aqueous cytoplasm into micelle-like structures, where the polymer chains form the hydrophobic core while the PHB synthase molecules reside at the surface. Here, the PHB synthase will continue polymerizing monomer into polymer. Finally, inside the bacterium several granules can be formed initially, but as conversion of monomer into polymer continues, the space available for the granules present can become confined. As a consequence of this phenomenon granules can coagulate as monomer is still converted into polymer.

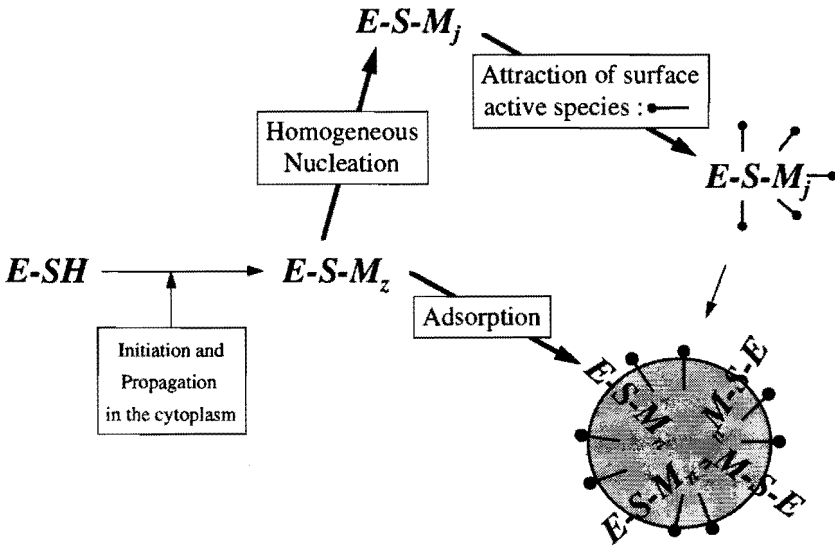


Figure 12.4 Homogeneous nucleation of PHB granules according to De Koning and Maxwell¹⁸, with $z < j$, and $n > z$.

At the same time as Gerngross *et al.*¹⁷ postulated a modified version of the model of Ellar *et al.*¹⁵ and Griebel *et al.*¹⁶, De Koning and Maxwell¹⁸ drew a clear analogy between the emulsion polymerization process and the biosynthesis of PHB. They proposed a homogeneous nucleation mechanism for granule formation similar to the homogeneous nucleation model of Fitch and Tsai²⁶, which is widely accepted in conventional emulsion polymerization (see figure 12.4). According to this model, the polymerase molecules react with monomer in the cytoplasm (initiation) followed by propagation, resulting in the formation

of a so-called polymer-polymerase conjugate. The polymer-polymerase conjugate can act as a surfactant since the polymerase enzyme "head" is hydrophilic and the PHB tail is hydrophobic. As the chain grows, it becomes increasingly hydrophobic and at a certain degree of polymerization (j) it collapses in order to minimize its surface area. A precursor granule (nucleus) is formed now. Growing chains in the cell water can either form a nucleus or adsorb onto existing, precursor, granules if the tail length is sufficient for adsorption (length z) and enough granule surface is present. This model is schematically presented in *figure 12.4*.

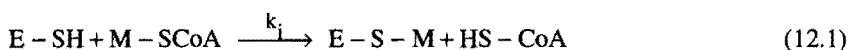
In conclusion it can be said that the models proposed by Ellar *et al.*¹⁵, Griebel *et al.*¹⁶ and Gerngross *et al.*¹⁷ are similar to the *in situ* micellization model proposed for synthetic emulsion polymerizations with zero or low amounts of added surfactant. The model proposed by De Koning and Maxwell¹⁸ is derived, as they stated in the original paper, from the homogeneous nucleation mechanism known from the conventional emulsion polymerization process. This last model will be quantified in the next section.

12.3 Granule Formation during the Biosynthesis of PHB in *Alcaligenes eutrophus*

In this section the kinetic processes which are involved in the formation of granules during the accumulation of PHB in *Alcaligenes eutrophus* will be evaluated. At the same time rate equations will be derived which will be used to establish expressions for the number of granules formed during this stage of the accumulation process and the molar mass of the polymer formed.

12.3.1 Initiation

Only initially the system is homogeneous. The polymerase enzyme is present in the cytoplasm^{16,17,19} and there are no granules present. Once the bacterium starts accumulating PHB, monomer will react with the polymerase enzyme in the cytoplasm, hence initiation has occurred. This can be envisaged by *equation 12.1*:



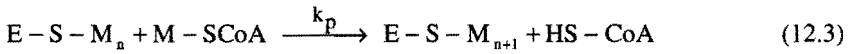
here, E-SH denotes the free polymerase enzyme, M-SCoA the monomer, HS-CoA is coenzyme-A and E-S-M is a polymerase enzyme with one monomer unit attached to it. k_i is the second order initiation rate coefficient. The rate of initiation (R_i) is given by *equation 12.2*:

$$R_i = k_i * [E - SH] * [M - SCoA] \quad (12.2)$$

here [M-SCoA] denotes the monomer concentration in the cytoplasm and [E-SH] the concentration of free polymerase enzyme in the cytoplasm.

12.3.2 Propagation in the Cytoplasm

Once initiation of the polymerization has occurred, propagation in the cytoplasm can take place according to *equation 12.3*:



here E-S- M_i represents the polymerase enzymes in the cytoplasm which is attached to a polymer chain with a degree of polymerization of n or $n+1$ (also referred to polymer-polymerase conjugate), and k_p is the second order propagation rate coefficient for propagation in the cytoplasm (it is assumed that the propagation rate coefficient in the cytoplasm is equal to that at the granule surface). The rate of propagation (R_p) in the cytoplasm is equal to:

$$R_p = k_p * [M - SCoA] * [E - S - M_n] \quad (12.4)$$

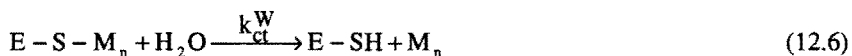
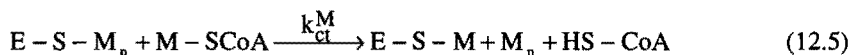
During propagation, the polymerase enzyme will stay bound to the growing polymer chain. The polymerization leads to the formation of polymer-polymerase conjugates. At a certain degree of polymerization z the polymer-polymerase conjugate can be regarded as a surface active species, where the polymerase enzyme is the hydrophilic head group while the polymer chain is the hydrophobic tail. This surface active polymer-polymerase conjugate can undergo either: 1. *Adsorption of a polymer-polymerase conjugate, with a degree of polymerization of z , onto existing granules* (This process has been discussed and quantified in *Chapter 3*) or 2. *A polymer-polymerase conjugate propagates further in the cytoplasm until it*

reaches a degree of polymerization of j at which it becomes insoluble and will collapse in order to minimize its surface area, resulting in the formation of a new granule.

In other words, a colloidal particle will be formed from the polymer-polymerase conjugate with a degree of polymerization of the polymer of j in order to minimize its hydrophobic surface area. The so-formed hydrophobic surface will attract phospholipids and other surface active cell constituents. The granule surface can also be stabilized by the end groups of polymer chains present, i.e. the hydroxyl or carboxyl end groups can act as co-surfactant.

12.3.3 Chain Transfer in the Cytoplasm

Polymer-polymerase conjugates can undergo in the cytoplasm chain transfer to water and/or monomer, although other chain transfer agents can be operative such as acetyl-CoA or acetoacetyl-CoA. In *Chapter 13* a new chain transfer agent will be discussed, not reported in literature yet, i.e. coenzyme-A. This chain transfer agent can have, according to the hypothesis postulated in the following chapter, a profound influence on the accumulation process. However, in the present case only water and monomer will be considered as chain transfer agents (see also *Chapter 11*). For these reactions the following equations can be postulated.



here k_{ct}^M and k_{ct}^W are the rate coefficients for chain transfer to monomer and water, respectively, and are assumed to be the same as for chain transfer at the granule surface (see *Chapter 11*). The rate of chain transfer (R_{ct}) in the cytoplasm can be expressed as follows:

$$R_{ct} = (k_{ct}^M * [M-SCoA] + k_{ct}^W * [H_2O]) * [E-S-M_n] \quad (12.7)$$

12.3.4 Quantitative Description of Granule Formation during PHB Accumulation

It is assumed that the process of granule formation can be described, in a first approximation, with the model developed by De Koning and Maxwell¹⁸. This model is in principle equivalent to the model proposed by Hager *et al.*¹⁰ for the formation of latex particles during the biosynthesis of natural rubber. According to the homogeneous nucleation mechanism followed by growth² the number of granules ($N_{\text{gran.}}$) formed can be calculated by integrating the rate equation for the formation of polymer-polymerase conjugates with a degree of polymerization of j , which is simply the rate equation for the propagation of a polymer-polymerase conjugate with a degree of polymerization of $j-1$ (E-S- M_{j-1}):

$$\frac{dN_{\text{gran.}}}{dt} = k_p * [M - \text{SCoA}] * [E - S - M_{j-1}] * N_{\text{Av.}} \quad (12.8)$$

In order to be able to calculate the number of granules, the concentration of the polymer-polymerase conjugates with a degree of polymerization of $j-1$ has to be known. This concentration can be evaluated from the concentrations of all the intermediate polymer-polymerase conjugates with degrees of polymerization between 1 and $j-2$. The necessary differential equations are listed below:

$$\frac{d[E - \text{SH}]}{dt} = -k_i * [M - \text{SCoA}] * [E - \text{SH}] + k_{\text{ct}}^w * [\text{H}_2\text{O}] * [E - S - M_n] \quad (12.9)$$

with $1 < n < x$

$$\begin{aligned} \frac{d[E - S - M]}{dt} = & k_i * [M - \text{SCoA}] * [E - \text{SH}] - k_{\text{ct}}^w * [\text{H}_2\text{O}] * [E - S - M] \\ & + k_{\text{ct}}^M * [M - \text{SCoA}] * [E - S - M_n] - k_p * [M - \text{SCoA}] * [E - S - M] \end{aligned} \quad (12.10)$$

$$\begin{aligned} \frac{d[E - S - M_n]}{dt} = & k_p * [M - \text{SCoA}] * [E - S - M_{n-1}] - k_{\text{ct}}^w * [\text{H}_2\text{O}] * [E - S - M_n] \\ & - k_{\text{ct}}^M * [M - \text{SCoA}] * [E - S - M_n] - k_p * [M - \text{SCoA}] * [E - S - M_n] \end{aligned} \quad (12.11)$$

with $2 < n < z-1$

$$\begin{aligned} \frac{d[E-S-M_n]}{dt} = & k_p * [M-SCoA] * [E-S-M_{n-1}] - k_{ct}^W * [H_2O] * [E-S-M_n] \\ & - k_{ct}^M * [M-SCoA] * [E-S-M_n] \\ & - k_p * [M-SCoA] * [E-S-M_n] - k_{ads} * [E-S-M_n] * A_{gran}^t \end{aligned} \quad (12.12)$$

with $z < n < j-1$

Although, in *Chapter 14*, equations 12.8 - 12.12 are solved simultaneously, concomitantly, amongst other things, the number of granules formed during the accumulation process can be calculated, some word will be addressed at this point with respect to the granule formation process. From the above rate equations it can be seen that during a certain period of time in the beginning of the accumulation process no granules will be present. Fitch and Tsai² proposed that the nucleation of precursor particles (granules) starts after a certain time (t_{begin}) according to *equation 12.13*.

$$t_{begin} = \frac{j}{k_p * [M-SCoA]} \quad (12.13)$$

It is not too unlikely that the degree of polymerization at which granules are being formed (j) is relatively high compared with values found for conventional emulsion polymerizations of sparsely water soluble vinyl monomers. This is probably due to the fact that the molar mass of the hydrophilic polymerase enzyme molecule is extremely high¹⁹ compared with that of water soluble free radical initiators normally used in emulsion polymerization. Therefore, t_{begin} can be rather long compared with the conventional emulsion polymerization process. The value of t_{begin} will be evaluated in *Chapter 14*.

12.3.5 Influence of Granule Formation on the Molar Mass of the Polymer

During a chain-growth polymerization, the kinetic chain length of the polymer formed is the ratio of the rate of propagation over the total rate of active site formation (see *equation 12.14*).

$$v_{cyto} = \frac{k_p * [E-S-M_n]}{k_i * [E-SH] + k_{ct}^M * [E-S-M_n]} \approx \frac{k_p * [E-S-M_n]}{k_i * [E-SH]} \quad (12.14)$$

Here v_{Cyto} is the kinetic chain length of the polymer formed in the cytoplasm. *Equation 12.14* only holds in the very early part of the accumulation process where polymerization only occurs in the cytoplasm and no granules are present, while at the same time the rate of chain transfer is low compared with the rate of initiation since the active specie concentration is very low during the initial part of the accumulation process. Once granules are being formed the expression for the kinetic chain length changes, i.e. propagation and chain transfer at the granule surface start to affect the molar mass of the polymer formed. During the granule growth stage of the accumulation process, the kinetic chain length (v_{Gran}) of the polymer formed is related to the rate of propagation of the polymer-polymerase conjugate at the granule surface and the rate of adsorption (R_{ads}) of polymer-polymerase conjugates from the cytoplasm onto the PHB granules. As discussed in *Chapter 11* this can be visualized by the following equation (see also *section 11.2.4.6*) :

$$v_{\text{Gran.}} = \frac{R_p}{R_{\text{ads}}} \approx \frac{1}{d_{\text{gran.}}^2} \quad (12.15)$$

During the granule formation stage the polymerization process slowly shifts from the cytoplasm to the granule surface. Eventually, the polymerization is completely determined by the granule surface and the granule growth stage is entered. The kinetic chain length of the polymer formed during the granule formation (v_{GF}) stage can be expressed as a linear combination of *equations 12.14* and *12.15*. The coefficients in the linear expression are a measure for the extent at which the kinetic processes occurring at the granule surface are contributing to the total polymerization process.

$$v_{\text{GF}} = \left(\frac{N_{\text{gran.}}^t}{N_{\text{gran.}}^{\text{max}}} \right) * v_{\text{Gran.}} + \left(1 - \frac{N_{\text{gran.}}^t}{N_{\text{gran.}}^{\text{max}}} \right) * v_{\text{Cyto}} \quad (12.16)$$

In *equation 12.16*, $N_{\text{gran.}}^t$ and $N_{\text{gran.}}^{\text{max}}$ represent the number of granules at time t during the granule formation stage and the maximum number of granules, respectively. Once all granules have been formed, the instantaneous molar mass of the polymer will mainly be determined by the kinetic processes occurring at the granule surface.

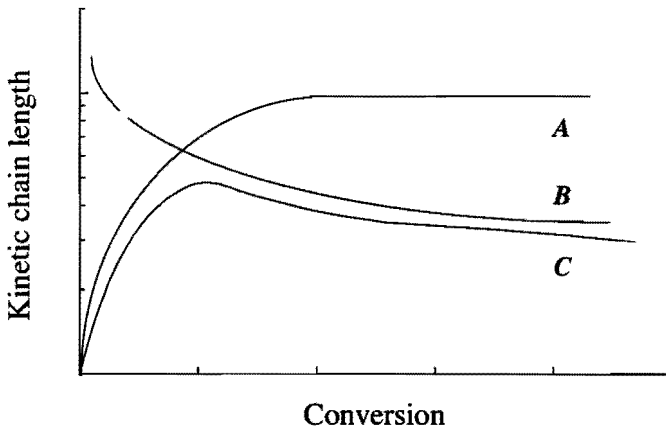


Figure 12.5 Schematic representation of the kinetic chain length of the polymer formed versus conversion according to equation 12.16 assuming a homogeneous nucleation mechanism followed by growth. Curve A: represents the v_{Cyto} -term in equation 12.16, curve B: represents the v_{Gran} -term in equation 12.16, and curve C: represents the resulting kinetic chain length, i.e. v_{GF} .

Figure 12.5 gives a schematic representation of equation 12.16. Initially, the kinetic chain length of the polymer formed will be determined by the kinetic processes in the cytoplasm. Gradually, the surface of the newly formed granules becomes involved in the polymerization process. In the limit where no new granules will be formed the kinetic chain length of the polymer formed will exclusively be determined by the granule growth process, i.e. v_{GF} is equal to v_{Gran} .

12.4 Experimental Molar Mass versus Accumulation Time and Conversion

12.4.1 Molar Mass of PHB formed during a Two-step Batch Fermentation

During a two-step batch fermentation bacteria are grown in a nutrient rich medium, and do not contain any detectable amount of PHB at the end of the bacterial growth process. After this the bacteria are transferred into a nitrogen-free medium, and incubated with a carbon source leading to the accumulation of polymer. Kawaguchi and Doi²⁰ measured the molar mass of PHB formed during such a two-step batch fermentation (see figure 12.6). Figure 12.6 represents a set of fermentations of different carbon source concentrations (5, 10, and 20 g/l fructose). The reason why these different fermentations are plotted in one figure is

the fact that the fructose concentration only has an influence on the amount of PHB accumulated in the bacteria, and not on the rate of polymerization (accumulation) and the relationship between molar mass and conversion/time.

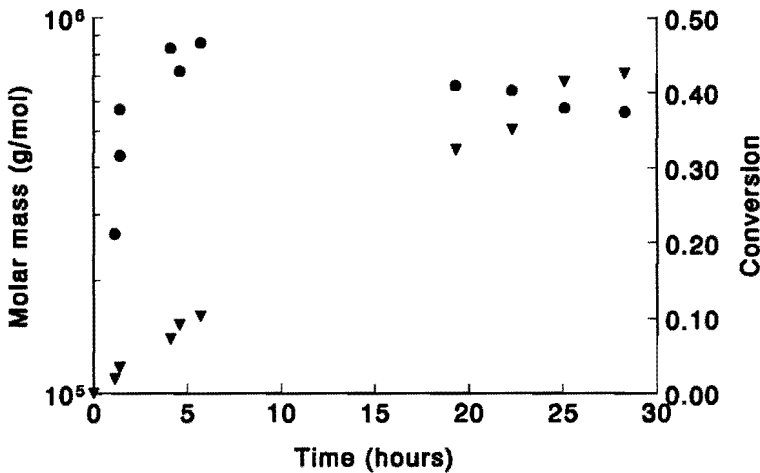


Figure 12.6 Cumulative number average molar mass and conversion of PHB formed as a function of time. Circles: experimental cumulative number average molar mass, and triangles: conversion of PHB. Experimental data obtained from Kawaguchi & Doi²⁰.

From figure 12.6 it can be clearly seen that the molar mass of the polymer formed during the accumulation process first increases, but after a certain period time starts to decrease. This increase during the initial stage of the accumulation process is a reproducible phenomenon²⁰. The course of the experimental molar mass as a function of conversion is comparable with the course predicted by equation 12.16 (see figure 12.5, curve C). Since the rate of polymerization is constant during the initial stage of the accumulation process and declines at higher accumulation levels (typically at conversions higher than approximately 0.70) (Please note that conversion is defined as the fraction of polymer accumulated compared to the ultimate level achievable). Initially the molar mass of the polymer formed is low since the polymerization process is mainly located in the cytoplasm. However, granules are being formed so the cumulative molar mass of the polymer present becomes more and more determined by the kinetic processes at the granule surface. The polymer produced at the granule surface can be of relatively high molar mass for small granules (Note that the number

average degree of polymerization is inversely proportional to the square of the granule diameter; see also *figure 12.5*, curves *A* and *B*).

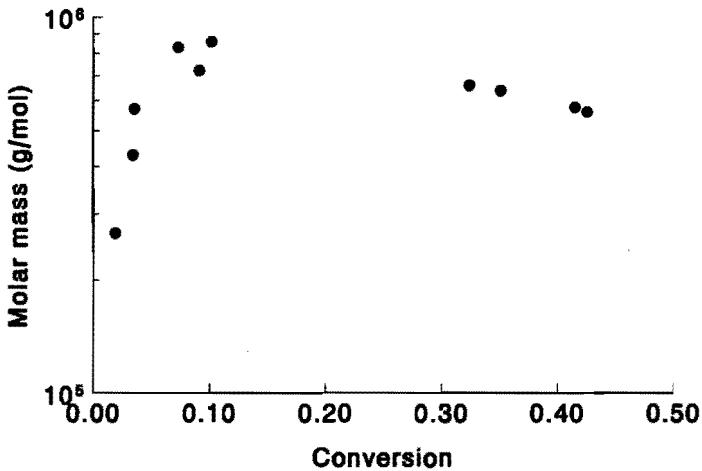


Figure 12.7 Molar mass of PHB as a function of conversion for a two-step batch fermentation. Data obtained from Kawaguchi and Doi²⁰.

Once, no new granules are being formed the molar mass of the polymer will be mainly determined by the granule surface available for the polymerization process (see *Chapter 11*). *Figure 12.7* clearly demonstrates that the molar mass of PHB depends on conversion, i.e. on the amount of polymer present in the bacterium or in other words on the size of the granules present.

12.4.2 Influence of Multiple Carbon Source Addition on Accumulation Process

In the previous section it was clearly shown that the molar mass of PHB accumulated by *Alcaligenes eutrophus* during a two-step fermentation is related to conversion. A supportive evidence of the above phenomenon is given by the experiment described in *figure 12.8*. In this experiment, reported by Kawaguchi and Doi²⁰, fructose was added to the fermenter which contained a certain number of bacteria. After the addition of fructose the bacteria started to accumulate PHB. After $t = 24$ hours a new charge of fructose was added upon which the bacteria started to accumulate polymer again.

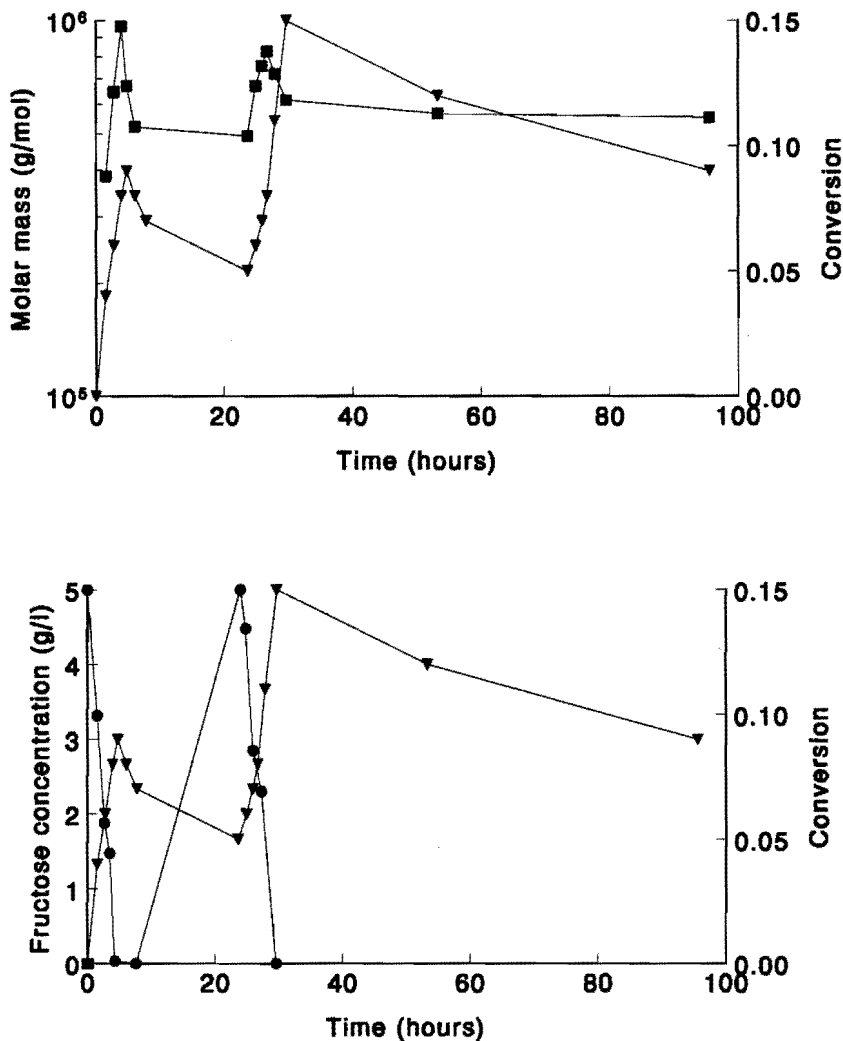


Figure 12.8 Top figure: Fructose concentration and conversion as a function of time. Closed circles: fructose concentration, and closed triangles: conversion. Bottom figure: Cumulative number average molar mass of PHB formed as a function of time. Squares: molar mass, and triangles: conversion. Experimental data obtained from Kawaguchi & Doi²⁰.

First, a qualitative discussion of figure 12.8 will be given after which a semi-quantitative explanation of the observed phenomena will be discussed. In doing so, figure 12.8 has been plotted in such a way that the different stages, i.e. accumulation and degradation, are represented in separate plots (see figure 12.9.a - 12.9.b).

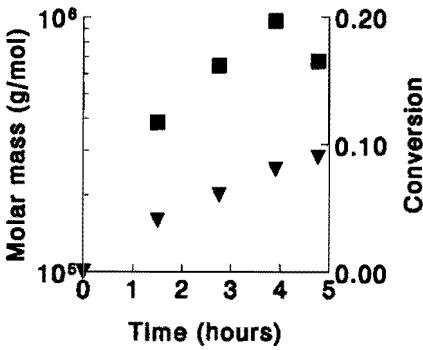


Figure 12.9a: PHB Accumulation

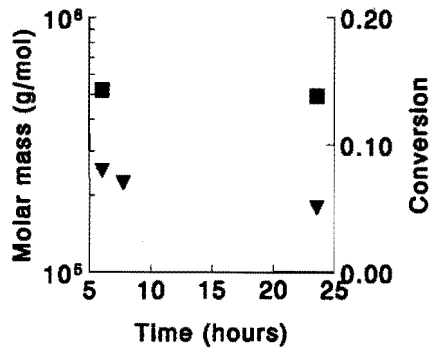


Figure 12.9b: PHB Degradation

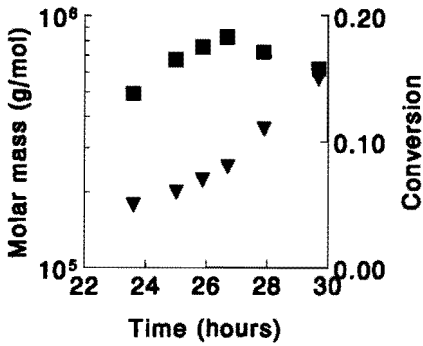


Figure 12.9c: PHB Accumulation

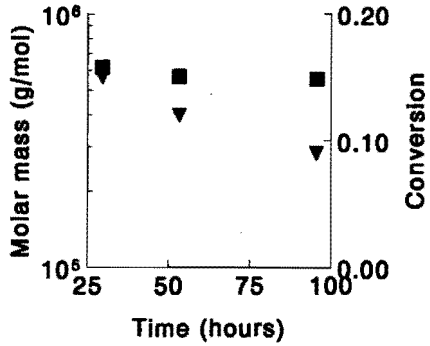


Figure 12.9d: PHB Degradation

Figure 12.9 Figure 12.8 plotted with respect to the stage of the accumulation process, i.e. accumulation or degradation of polymer which is indicated in the different figures. Squares: molar mass data, and triangles: conversion data.

Figure 12.9.a represents the initial stage of the accumulation process, fructose is being metabolized, thus conversion increases, i.e. the polymer content in the bacteria increases. As can be seen from this plot the molar mass of the polymer formed reaches a maximum value at a conversion of approximately 0.08, after which it decrease as conversion increases to the final value of 0.09. After approximately 5 hours polymer degradation sets in since no carbon source is present anymore (see figure 12.9.b). The molar mass of the polymer decreases slightly, while conversion decreases during this degradation period from 0.09 to 0.05. After 24 hours a second amount of fructose is added to the medium, concomitantly the bacteria starts to accumulate polymer again (second accumulation stage, figure 12.9.c). Conversion increases

from 0.05 to 0.15, while the molar mass of the polymer first increase and then decreases. Again the maximum in molar mass is reached when the conversion is approximately 0.09 (see *figure 12.9.c*). The bacteria start to degrade the polymer once all the fructose has been metabolized (*figure 12.9.d*).

Before discussing *figures 12.8* and *12.9* in a semi-quantitative way it should be stressed that the molar mass of the polymer formed is related to conversion as discussed in the previous section and shown by *figures 12.5* (schematically) and *12.7* (experimentally). In *figure 12.10* the dependency of molar mass on conversion for the first accumulation stage is plotted. First, the molar mass increases as expected since in the initial stage of the accumulation process the molar mass is determined by the kinetic processes in the cytoplasm (see *equation 12.16*). Since granules are being formed the polymerization becomes gradually more located at the granule surface, concomitantly the molar mass decreases due to an increase in granule surface (closed circles in *figure 12.10*).

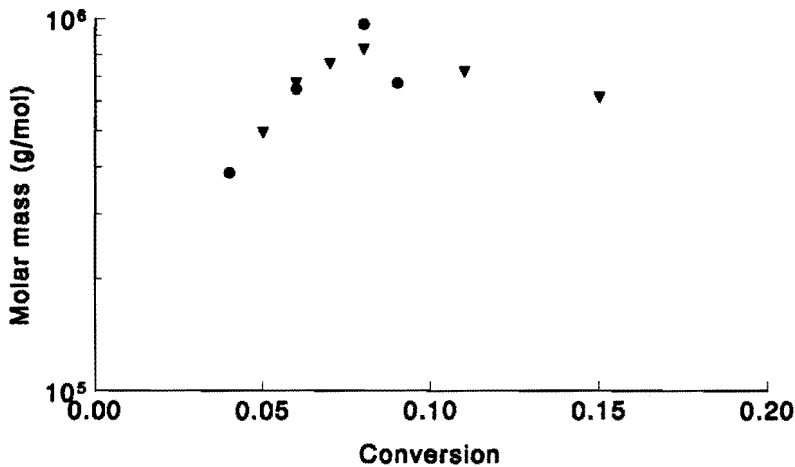


Figure 12.10 Cumulative molar mass of PHB versus conversion for the polymer accumulation stages of the experiment described in *figure 12.8* and *figures 12.9.a* and *c*. Circles: first accumulation stage, and triangles: second accumulation stage.

After this initial accumulation stage the bacteria start to degrade the polymer (first degradation stage), since the carbon source is depleted. The molar mass of the polymer during

the first degradation stage decrease only slightly (see *figure 12.11*, closed circles), due to the fact that the depolymerase enzyme is an *exo*-type hydrolase²⁰, which implies that the degradation of the polymer molecules takes place at the end of the chain. Conversion decreases in the degradation stage from 0.09 to 0.05, concomitantly the granules present decrease in size.

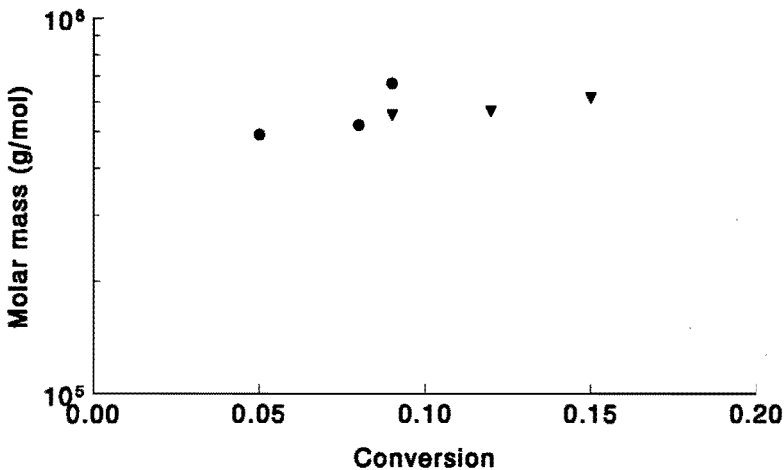


Figure 12.11 Cumulative molar mass of PHB versus conversion for the polymer degradation stages of the experiment described in *figure 12.8* and *figures 12.9.b* and *d*. Circles: first degradation stage, and triangles: second degradation stage.

The second accumulation stage is entered as soon as a fresh amount of fructose is added to the medium. During this second accumulation the conversion increases from 0.05 to 0.15, while the molar mass first increases and then decreases. This is due to the fact that at a conversion of 0.05 the molar mass of the polymer formed is mainly determined by the kinetic processes in the cytoplasm. As conversion increases the kinetic processes at the granule surface become more important (see *figure 12.7*). Again the maximum molar mass is synthesized at a conversion of 0.09 comparable with the first accumulation stage and the two-step batch fermentation discussed in the previous section (*figure 12.7*). Summarizing, during the experiment described above the molar mass of the polymer formed during the accumulation of PHB in *Alcaligenes eutrophus* is directly related to conversion, i.e. to the amount of polymer present in the bacterium, and thus to the granule surface available for the polymerization process.

12.5 Concluding Remarks

In the present chapter a clear relation between the kinetic processes in the cytoplasm, the influence of newly formed granules and the molar mass of the polymer formed during the *granule formation stage* has been established. This is also schematically indicated in *figure 12.12*.

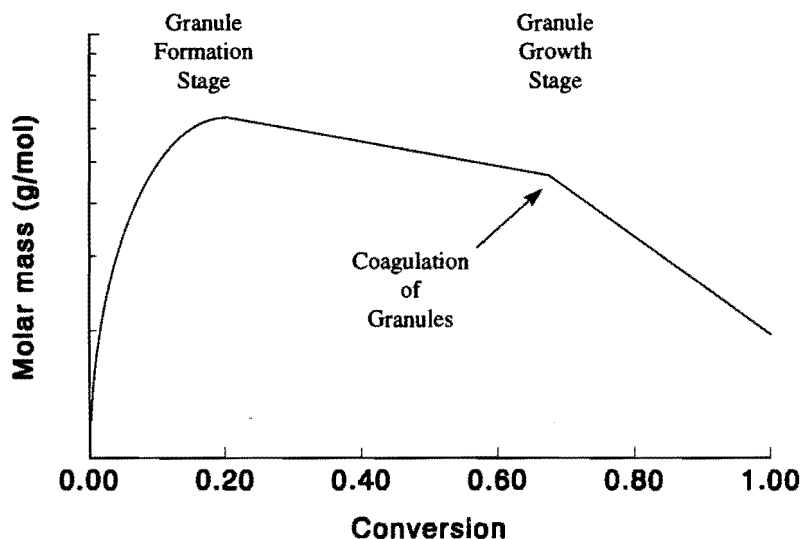


Figure 12.12 Schematic representation of the course of the molar mass as a function of conversion during the accumulation of PHB in *Alcaligenes eutrophus*. The different stages during the accumulation process are indicated.

The course of the molar mass of the polymer formed during the *granule growth stage* of the accumulation process can be explained in terms of the kinetic mechanisms of propagation and chain transfer, and the affect of granule size on these. The molar mass of the polymer is related to the granule surface (see also *Chapter 11*). During the granule growth process the surface of the granules will increase due to the formation of polymer. At a certain volume fraction of PHB granules in the bacteria, typically in the order of 0.6, coagulation can occur since a pseudo-close packing of granules in the bacterium is reached. This effect causes an additional decrease in the molar mass of the polymer after a conversion of approximately 0.72. This is schematically represented in *figure 12.12* by the latter part of the curve as

indicated. In figure 12.13 the experimental molar mass of PHB is plotted as a function of conversion for different fermentations.

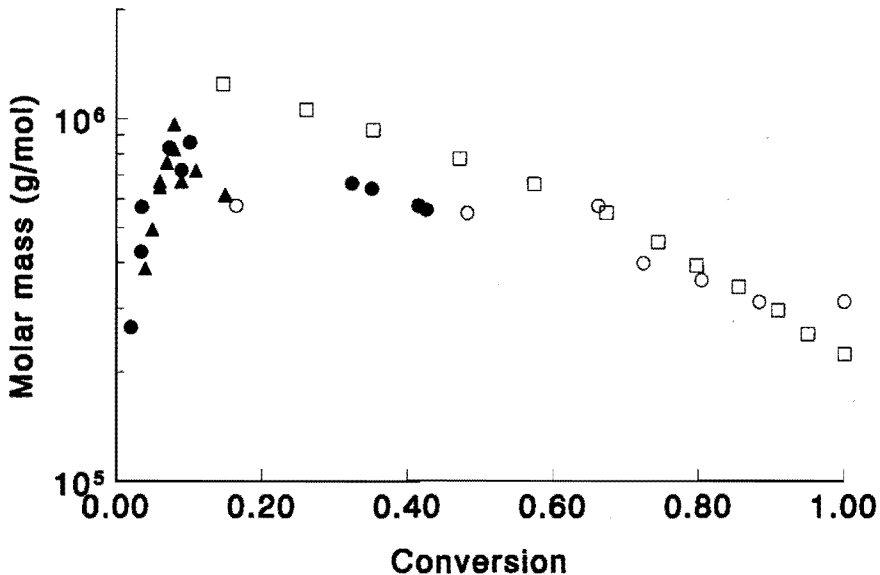


Figure 12.13 Molar mass versus conversion for different experiments. Closed triangles: data from figure 12.10, closed circles: data from figure 12.7, open circles: data from Kawaguchi and Doi²⁰, and open squares: data from Ballard et al.²¹.

The major conclusion that can be drawn from this plot is that the molar mass of the polymer formed during the accumulation process is indeed directly related to conversion, i.e. the amount of polymer present in the bacterium. Concomitantly, the accumulation of PHB in *Alcaligenes eutrophus* has to be regarded as a heterogeneous polymerization in order to model the polymerization process successfully.

12.6 References

- 1 Harkins, W.D., *J. Pol. Sci.*, **5**, 217 (1947)
- 2 Fitch, R.M., and Tsai, C.H., in "Polymer Colloids", Fitch, R.M. (Ed.), Plenum, New York (1971)
- 3 Ugelstad, J., and Hansen, F.K., *Rubber Chem. Techn.*, **49**, 536 (1976)
- 4 Napper, D.H., and Gilbert, R.G., *Makromol. Chem., Macromol. Symp.*, **10/11**, 503 (1987)

- 5 Kurja, J., Zirkzee, H.F., and Maxwell, I.A., "Unconventional Emulsion Polymerizations", in : "Emulsion Polymers and Emulsion Polymerization", M.S. El-Aasser and P. Lovell (Eds.), Wiley, Chapter 23, 763 (1997)
- 6 Backhaus, R.A., *Isr. J. Bot.*, 34, 283 (1985)
- 7 Archer, B.L. and Audley, B.G., *Bot. J. Lin. Soc.*, 94, 181 (1987)
- 8 Tanaka, Y., *Prog. Polym. Sci.*, 14, 339 (1989)
- 9 Paterson-Jones, J.C., Gilliland, M.G., and van Staden, J., *J. Plant Physiol.*, 136, 257 (1990)
- 10 Hager, T., MacArthur, A., McIntyre, D., and Seeger, R., *Rubber Chem. Techn.*, 52, 693 (1979)
- 11 Cornish, K., *Eur. J. Biochem.*, 218, 267 (1993)
- 12 Lynen, F., *J. Rubb. Res. Inst. Malaya*, 21, 389 (1969)
- 13 Colvin, J.R., in "Encyclopedia of Polymer Science and Engineering", Krischwitz, J.L. (Ed.), Vol. 3, pp 60-68, John Wiley & Sons, New York (1985)
- 14 B.W.W. Grout, *Planta*, 123, 275 (1975)
- 15 Ellar, D., Lundgren, D.G., Okamura, K., and Marchessault, R.H., *J. Mol. Biol.*, 35, 489 (1968)
- 16 Griebel, R., Smith, Z., and Merrick, J.M., *Biochemistry*, 7(10), 3676 (1968)
- 17 Gerngross, T.U., Reilly, P., Subbe, J., Sinsky, A.J., and Peoples, O.P., *J. Bacteriol.*, 175, 5289 (1993)
- 18 De Koning, G.J.M., and Maxwell, I.A., *J. Environmental Degrad.*, 1, 223 (1993)
- 19 Haywood, G.W., Anderson, A.J., and Dawes, E.A., *FEMS Microbiol. Lett.*, 57, 1 (1989)
- 20 Kawaguchi, Y., and Doi, Y., *Macromolecules*, 25, 2324 (1995)
- 21 Ballard, D.G.H., Holmes, P.A., and Senior, P.J., *Recent Adv. Mech. Synth. Aspects Pol.*, 215, 293 (1987)

CHAPTER 13

The Accumulation of Poly-(R)-3-hydroxybutyrate in *Alcaligenes eutrophus*

4. Influence of the Granule Surface

Synopsis: In this chapter it has been shown, via the introduction of the concept of boundary layers, that kinetic processes at or near the granule surface play an important role during the accumulation of poly-(R)-3-hydroxybutyrate in *Alcaligenes eutrophus*. The role of coenzyme-A in the polymerization process has been investigated, i.e. coenzyme-A has been considered as the only chain transfer agent present. A possible explanation has been given for the experimental observation that at high accumulation levels the rate of polymerization declines and eventually becomes zero, via the concept of boundary layers together with the fact that coenzyme-A can act as an inhibitor for the polymerase enzyme.

13.1 Introduction

Early research on the biosynthesis of bacterial polyhydroxyalkanoates (PHAs) mainly concentrated on the biological pathway of the PHA biosynthesis. Lately, due to an increasing interest for the application of these polymers, investigations are also concerned with the polymerization process, i.e. kinetics as well as physico-chemical aspects. Ballard *et al.*¹ where the first who considered the biosynthesis of polyhydroxybutyrate (PHB) in *Alcaligenes eutrophus* as a polymerization process. They suggested that the enzymatic polymerization had several features which resembled an emulsion polymerization, but it could not be one since the propagation reaction was a thiolcondensation where the polymerase enzyme acts like a catalyst, just like transition metals do in Ziegler-Natta catalysis. Some years later, Kawaguchi and Doi² developed a kinetic scheme for the polymerization process, and stated that the biopolymerization consisted of an initiation, propagation and chain transfer reaction as is observed in conventional chain type of polymerizations. Further, they posed that chain transfer with water was the only chain stopping event. Although, this model stated the individual steps

of the polymerization process, it did not take into account the heterogeneity of the polymerization system. Recently, De Koning and Maxwell³ drew a clear analogy between the biosynthesis of PHB and the conventional emulsion polymerization process. They proposed that the granule formation stage of the biosynthesis of PHB is very similar to the process of homogeneous nucleation during interval I of an emulsion polymerization⁴. This model was later quantified by Kurja *et al.*⁵, showing that the heterogeneity of the process needs to be taken into account when the kinetics of the polymerization process are considered/described. They divided the polymerization process into two stages, i.e. in a granule formation and growth stage. Since granule formation and granule growth are processes which occur simultaneously, one must be able to describe the granule growth process before the granule formation stage can be considered. As was demonstrated by Kurja *et al.*⁵, kinetic processes at or near the granule surface play an important role during the biosynthesis of PHB in *Alcaligenes eutrophus*. As a first approximation, the concentrations of monomer and coenzyme-A (HS-CoA) were considered constant throughout the polymerization system, although they recognized that this might not be the case. Coenzyme-A plays a important role in the regulation and kinetics of the biopolymerization^{6,7}. Here, the difference in the concentration of coenzyme-A in the cytoplasm and at the granule surface is investigated. In doing so, the concept of boundary layers is introduced, which is also used in the description of heterogeneous catalysis or mass transport processes near interfaces⁸. The molar mass of the polymer formed during the polymerization process will be calculated using the boundary layer concept. Among the most major results of the introduction of boundary layers is the fact that a plausible explanation can be given for the experimental observation that at high accumulation levels the rate of polymerization decreases and eventually goes to zero. This shows again that the heterogeneity of the polymerization system has to be taken into account in describing the biosynthesis of PHB.

13.2 Theory

13.2.1 Introduction

The work presented in this chapter is an extension of the model developed by Kurja *et al.*⁵. This model regards the biosynthesis of PHB by *Alcaligenes eutrophus* as a heterogeneous polymerization system. Concomitantly, processes occurring at or near the

granule surface, like for instance the adsorption of surface active polymer-polymerase conjugates and desorption of polymerase enzyme molecules, determine the characteristics of the polymer formed, i.e. molar mass. According to this model, initially all polymerase enzyme is present in the cytoplasm, due to its hydrophilic nature. Once the bacterium starts accumulating PHB, monomer will react with the polymerase enzyme in the cytoplasm, hence initiation of the polymerization has occurred. During the propagation, the polymerase enzyme will stay associated to the growing polymer chain. The polymerization leads to the formation of polymer-polymerase conjugates. With increasing tail length, the polymer-polymerase conjugate becomes more hydrophobic, and at a critical degree of polymerization, j , the PHB tail will collapse in order to minimize its surface area, and thus a precursor granule is formed. Once granules are formed, surface active polymer-polymerase conjugates in the cytoplasm can undergo either further propagation in the cytoplasm to form a new granule or adsorb onto an already existing granule. Adsorption will only take place if the polymer-polymerase conjugate has a degree of polymerization of at least z , while $z < j$. Once the polymer-polymerase conjugate is adsorbed onto an existing granule, it will propagate further at the granule surface. As chain transfer occurs, the polymerase enzyme molecule can desorb from the granule surface due to its hydrophilic nature. This chain transfer reaction can be with water² and/or monomer⁵, however, coenzyme-A can also act as a chain transfer agent, as will be discussed later (section 13.2.2). Instead of coenzyme-A, other coenzyme-A linked molecules, like acetyl and acetoacetyl-CoA, can act as chain transfer agents. In the cytoplasm, the polymerase enzyme molecule can react with monomer and join the polymerization process again. In quantifying the model of De Koning and Maxwell³, Kurja *et al.*⁵ assumed that the polymerization mainly takes place at the granule surface and that the average number of granule associated polymer-polymerase conjugates is constant:

$$\frac{d\left(\frac{n^* \cdot N_{\text{gran.}}}{N_{\text{Av.}}}\right)}{dt} = 0 \quad (13.1)$$

here n^* represents the average number of granule associated polymer-polymerase conjugates per granule and N_{gran} the number of granules. A consequence of equation 13.1 is

that in steady state the total rate of adsorption (R_{ads}^{tot}) equals the total rate of chain transfer (R_{ct}^{tot})⁵.

$$R_{ct}^{tot} = R_{ads}^{tot} \quad (13.2)$$

Further, it was shown that the kinetic chain length of the polymer formed at the granule surface (\bar{M}_n^S) could be described by the following equation⁵:

$$v_{Gran.} = \frac{R_p}{R_{ads}^{tot}} \approx \frac{1}{d_{gran.}^2} \quad (13.3)$$

where $d_{gran.}^2$ is the diameter of the granule. The kinetic chain length of the polymer formed in the cytoplasm (v_{cyto}), i.e. the aqueous phase, is expressed by the following equation (see also *Chapter 12, equation 12.14*):

$$v_{cyto} = \frac{k_p * [E-S-M_n]}{k_i * [E-SH]} \quad (13.4)$$

here, k_p and k_i represent the propagation and initiation rate coefficients, respectively. $[E-S-M_n]$ and $[E-SH]$ denote the propagating polymer-polymerase conjugate and free polymerase enzyme concentration, respectively. During the initial stage of the polymerization process the kinetic chain length of the polymer formed is not only determined by processes occurring at the granule surface but also by processes occurring in the cytoplasm⁹. This can be envisaged by the following equation:

$$v_{GF} = \xi_{ss} * v_{Gran.} + (1 - \xi_{ss}) * v_{Cyto} \quad (13.5)$$

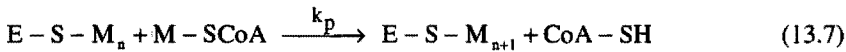
where ξ_{ss} represents a kind of “*degree of steady state*”, expressing the fact that once all granules have been formed the molar mass of the polymer will be determined by processes occurring at the granule surface. ξ_{ss} is defined as:

$$\xi_{ss} = \frac{N_{gran.}}{N_{gran.}^{ss}} \quad (13.6)$$

here $N_{gran.}$ is the number of granules and $N_{gran.}^{ss}$ the number of granules in the "steady state" situation, i.e. the maximum number of granules (see also *Chapter 12*).

13.2.2 Introduction of Boundary Layers

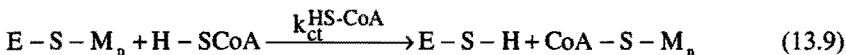
Before introducing the concept of boundary layers, a short overview will be given of the propagation and chain transfer processes which are involved in the biosynthesis of PHB in *Alcaligenes eutrophus*. The propagation reaction for the biosynthesis of PHB can be envisaged in the following way^{1,2,5}:



while rate of polymerization (R_p) of this reaction is:

$$R_p = k_p * [M-SCoA] * [E-S-M_n] \quad (13.8)$$

where k_p is the propagation rate coefficient, $E-S-M_n$ a polymer-polymerase conjugate with degree of polymerization n , $HS-CoA$ is free coenzyme-A and $M-SCoA$ is the monomer, i.e. (R)-3-hydroxybutyryl-CoA. The reaction represented in *equation 13.7* is an equilibrium reaction. However, coenzyme-A is rapidly converted in the cytoplasm into for instance acetyl-CoA. Concomitantly, the concentration of coenzyme-A will be relatively low shifting the equilibrium to the right-hand side favoring polymerization. It should be noted that enzymes do not alter the equilibrium of a chemical reaction. This means that an enzyme accelerates the forward and reverse reaction by precisely the same factor¹⁰. Coenzyme-A can also act as a chain transfer agent as depicted in *figure 13.1* and *equation 13.9*.



Since coenzyme-A is the only chain transfer agent which is considered, low concentrations of coenzyme-A can not be neglected. The rate of chain transfer (R_{ct}) to coenzyme-A can be expressed now by:

$$R_{ct} = k_{ct}^{HS-CoA} * [HS - CoA] * [E - S - M_n] \quad (13.10)$$

where k_{ct}^{HS-CoA} is the rate coefficient for chain transfer to coenzyme-A. As mentioned before, the concentration of coenzyme-A is relatively low during the polymerization process.

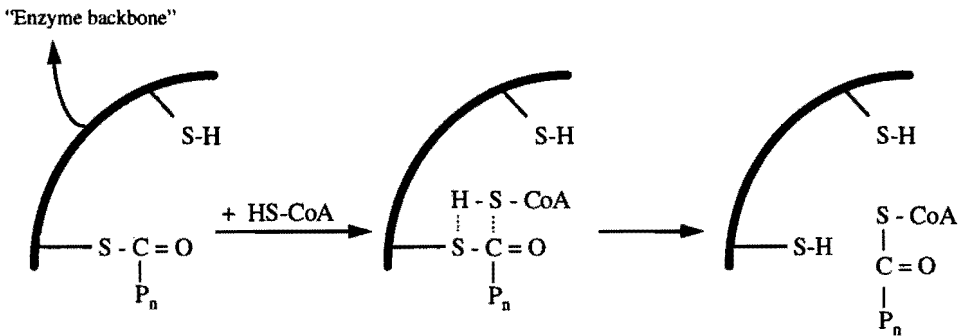


Figure 13.1 Mechanism for chain transfer to coenzyme-A.

However, near the granule surface higher coenzyme-A concentrations can be expected for the following reasons. Firstly, coenzyme-A exhibits a hydrophilic-hydrophobic character⁵. Secondly, coenzyme-A is generated at the granule surface due to the conversion of (R)-3-hydroxybutyryl-CoA into PHB. Thirdly, coenzyme-A concentration is lower in the cytoplasm due to the conversion into for instance acetyl-CoA, a precursor for the monomer. As a consequence of this, a concentration profile near the granule surface is created (see figure 13.2). When two polymer-polymerase conjugates are located at the granule surface, a coenzyme-A molecule, released after a propagation step from one polymer-polymerase conjugate, can easily flip over to a nearby located polymer-polymerase conjugate and cause chain transfer (see figure 13.3). As a result of this, the rate of chain transfer to coenzyme-A will be higher at or near the granule surface than in the cytoplasm, since local concentrations of both coenzyme-A and polymerase enzyme are higher at the granule surface. It can be expected that in the boundary layer the concentration of coenzyme-A does not change if the

surface concentration of the polymer-polymerase conjugate is constant. This can be seen in the following way: if the surface concentration of polymer-polymerase conjugates is at the optimum surface concentration, additional adsorption will increase the local polymer-polymerase conjugate and HS-CoA concentrations.

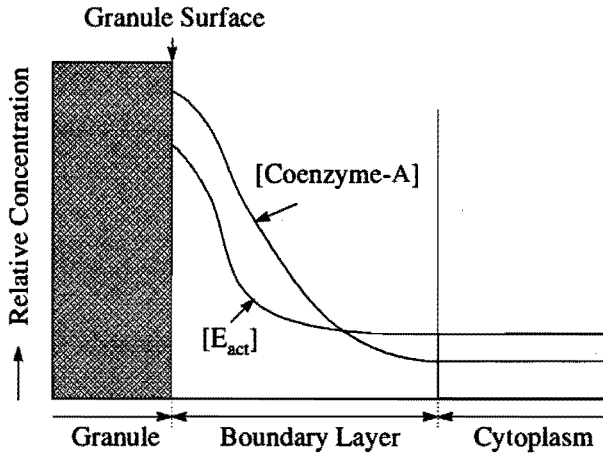


Figure 13.2 Concentration profiles of coenzyme-A ($[Coenzyme-A]$) and polymerase enzyme ($[E_{act}]$) near the granule surface.

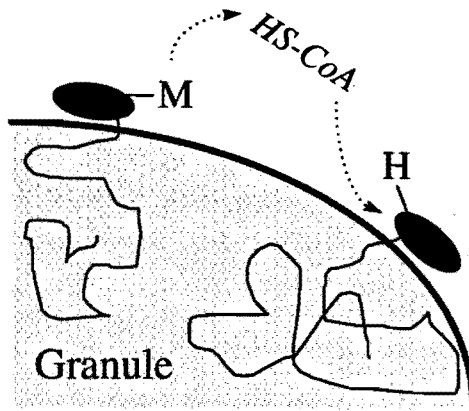


Figure 13.3 Chain transfer at the granule surface.

As a result of this the rate of chain transfer to coenzyme-A will increase. This means that the concentration of polymer-polymerase conjugates at the granule surface decreases,

since chain transfer leads to desorption of the hydrophilic polymerase enzyme molecule⁵. On the other hand, if the surface concentration of polymer-polymerase conjugates is **below** the average concentration, the rate of chain transfer will be lower and less chain transfer will occur. Consequently, the surface concentration of polymer-polymerase conjugates will increase. In other words, deviations from the steady state surface concentration of polymer-polymerase conjugates will therefore be suppressed. This leads to a time-average constant polymer-polymerase conjugate concentration at the granule surface (see also *Chapter 11* (section 11.2.4.6) and *Chapter 15* (section 15.2.2)).

13.2.3 Influence of the Boundary Layer on Polymerization Kinetics

During the polymerization process, the granule surface will grow. This means that the total number of polymer-polymerase conjugates at the granule surface also grow. Granule growth will cause an increasing volume of the boundary layer. This results in a higher surface related rate of chain transfer (R_{ct}^S) to coenzyme-A, which is proportional to the total granule surface (A_{gran}^t):

$$R_{ct}^S = \frac{k_{ct}^{HS-CoA} * [HS - CoA]^s * [E - S - M_n]^s * A_{gran}^t * L}{V_{Cyto}} = k_{ct}^S * A_{gran}^t \quad (13.11)$$

here $[E-S-M_n]^s$ is the polymer-polymerase conjugate concentration in the boundary layer, k_{ct}^{HS-CoA} the rate coefficient for chain transfer to coenzyme-A, $[HS-CoA]^s$ the concentration of coenzyme-A in the boundary layer, L the width of the boundary layer, and V_{Cyto} the volume of cytoplasm, while k_{ct}^S is equal to $\frac{k_{ct}^{HS-CoA} * [HS - CoA]^s * [E - S - M_n]^s * L}{V_{Cyto}}$. The rate of chain transfer to coenzyme-A in the aqueous phase, i.e. cytoplasm, (R_{ct}^A), can be described by the following equation:

$$R_{ct}^A = k_{ct}^{HS-CoA} * [HS - CoA]^{cyto} * [E - S - M_n]^{cyto} \quad (13.12)$$

where $[E-S-M_n]^{cyto}$ and $[HS-CoA]^{cyto}$ represent the concentration of the propagating polymer-polymerase conjugates and coenzyme-A in the cytoplasm, respectively. Chain growth in the cytoplasm can be stopped by two processes. i.e. by chain transfer in the cytoplasm or adsorption of the surface active polymer-polymerase conjugates onto a granule. In the latter case, chain growth will continue at the granule surface until it is stopped by a chain transfer reaction at the granule surface. Whether adsorption or chain transfer occurs, depends on the amount of granule surface available. If adsorption occurs the molar mass of the polymer formed will be controlled by chain transfer at the granule surface. If little or no surface is present, chain transfer will be mainly determined by the kinetic processes in the cytoplasm. If all the polymerase enzyme is bound to polymer and present in the cytoplasm, the molar mass of the polymer formed will be determined by the rate of polymerization in the cytoplasm (R_p^A) and the rate of chain transfer to coenzyme-A in the cytoplasm (R_{ct}^A):

$$\bar{M}_n^A = \frac{M_0 * R_p^A}{R_{ct}^A} \quad (13.13)$$

where \bar{M}_n^A is the molar mass of polymer formed in the cytoplasm. In the case that all the polymerase enzyme is bound to polymer and located at the granule surface, the molar mass of the polymer formed at the granule surface (\bar{M}_n^S) is the sum of the degree of polymerization of the adsorbed polymer-polymerase conjugate (z) and the number of propagation steps of same polymer-polymerase conjugate at the granule surface times the molar mass of the monomer unit (M_0). This is shown in the following equation:

$$\bar{M}_n^S = M_0 * \left(z + \frac{R_p^S}{R_{ct}^S} \right) \quad (13.14)$$

where R_p^S represents the rate of polymerization at the granule surface. The molar mass of the polymer formed during the polymerization process is determined by a combination of process occurring in the cytoplasm and at the granule surface for which can be accounted for by equations 13.13 and 13.14. In the following section an expression will be derived representing the molar mass of the polymer formed.

13.2.4 Chain Transfer in the Cytoplasm vs. Chain Transfer in the Boundary Layer

Chain transfer in the cytoplasm will occur if the average time needed for chain transfer is smaller than the time needed for adsorption ($\Delta t_{aw} \ll \Delta t_{ads}$), i.e. the rate of chain transfer (R_{ct}^A) exceeds the rate of adsorption (R_{ads}). On the other hand, if the rate of chain transfer in the cytoplasm is lower than the rate of adsorption, chain transfer will occur at the granule surface. Therefore, the “*degree of surface controlled chain transfer*” is defined as:

$$\xi = \frac{R_{ads}}{R_{ads} + R_{ct}^A} \quad (13.15)$$

One difficulty in using *equation 13.15* is to describe the rate of adsorption, since values for the (total) concentration of active polymerase enzyme, i.e. bound to polymer, and the critical degree of polymerization for adsorption z can only be estimated. However, when the rate of adsorption approaches the rate of chain transfer at the granule surface (R_{ct}^S) *equation 13.15* can be written as:

$$\xi = \frac{R_{ct}^S}{R_{ct}^S + R_{ct}^A} \quad (13.16)$$

This equation is valid when the *increase in the number* of granule associated polymer-polymerase conjugates is relatively small compared to the *total number* of granule associated polymer-polymerase conjugates, i.e. the number of adsorption events due to the growing granule surface is negligible to the total number of adsorption events.

The growth time of a propagating polymer-polymerase conjugate, typically in the order of 15 minutes, is small compared with the total polymerization time, which can be in the order of 6,000 minutes. Values for R_{ct}^A and R_{ct}^S can be estimated from the molar mass of the polymer formed, assuming that in early stages of the polymerization $\xi = 0$ and the molar mass is determined by chain transfer in the cytoplasm, while at higher conversions $\xi = 1$ and the molar mass is determined by chain transfer at the granule surface. The instantaneous molar

mass of the polymer formed is expressed as a linear combination of \overline{M}_n^S and \overline{M}_n^A as shown in equation 13.17:

$$\overline{M}_n = (1-\xi) * \overline{M}_n^A + \xi * \overline{M}_n^S \quad (13.17)$$

This equation for the molar mass is very similar to the expression for the kinetic chain length derived in Chapter 12 (see equation 12.16)⁹. From the previous, it is obvious that according to the boundary layer concept, a higher chain transfer agent concentration is present at or near the granule surface than in the cytoplasm. It should be noted that besides coenzyme-A, water, and monomer also amphoteric molecules, like phospholipids, might act as a chain transfer agent, although they are not taken into account in the current treatment.

13.3 Theory, Model and Experiment

In this section, model calculations (see also Chapter 14), based on the equations derived in the previous section, will be compared with experimental data. First, the assumption that the number of granule associated polymer-polymerase conjugates is proportional to the amount of granule surface will be tested. Secondly, a typical one step batch fermentation of PHB in *Alcaligenes eutrophus* will be discussed in light of the boundary layer concept. Finally, a possible mechanism for the end of the polymerization is discussed, using the concept described above.

13.3.1 Constant Surface Concentration of Polymer-Polymerase Conjugates

The assumption that a constant polymer-polymerase conjugate surface concentration can be expected, will be validated using data from Haywood *et al*¹¹. They measured the granule associated and soluble polymer-polymerase conjugate activity during the accumulation of PHB in *Alcaligenes eutrophus* (see figure 13.4). If it is assumed that the specific activity of a single granule associated polymer-polymerase conjugate is equal to that of a single soluble polymer-polymerase conjugate, then the activity of the polymer-polymerase conjugate at the granule surface or in the cytoplasm is proportional to the amount of polymer-polymerase conjugate at the granule surface or in cytoplasm.

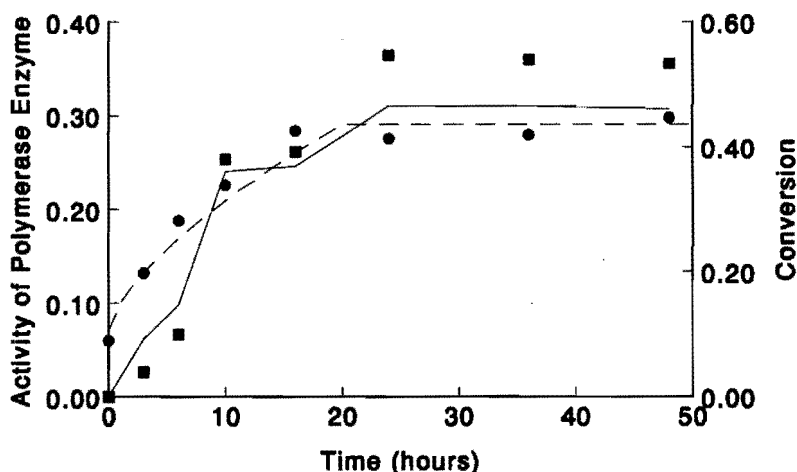


Figure 13.4 Activity of granule associated polymer-polymerase conjugate and conversion as a function of accumulation time. Circles: activity of granule associated polymerase enzyme measured by Haywood *et al.*¹¹, squares: conversion data, solid line: calculated activity related to the mass of polymer formed, and dashed line: calculated activity related to accumulation time.

Further, Haywood *et al.*¹¹ also measured the mass of polymer produced during polymerization. If it is also assumed that the PHB granules are formed in the earliest stages of the polymerization process and the number of granules remains constant up to high accumulation levels, typically in the order of 60 vol-% (see *Chapter 11*), the total granule surface ($A_{\text{gran.}}^t$) is equal to the mass of polymer produced (m_{PHB}) to the power 2/3 ($A_{\text{gran.}}^t \sim m_{\text{PHB}}^{2/3}$, solid line in *figure 13.4*). Assuming that the total rate of polymerization is constant throughout the accumulation process, the granule surface is proportional to the accumulation time (t_{acc}) to the power 2/3 ($A_{\text{gran.}}^t \sim t_{\text{acc}}^{2/3}$, dashed line in *figure 13.4*) (Bear in mind that the total rate of polymerization is equal to the sum of the rate of polymerization in the cytoplasm and at the granule surface). The calculated lines in *figure 13.4* are in good agreement with the measured values of the activity of the granule associated polymer-polymerase conjugate. Therefore, the assumption that the increase in the number of granule associated polymer-polymerase conjugates is proportional to the increase of granule surface, seems to be valid. It should be noted, however, that the calculated lines only represent the course of the activity of the granule associated polymer-polymerase conjugate as a function of accumulation time rather than the absolute values.

13.3.2 An Example: One step Batch Fermentation of PHB in *Alcaligenes eutrophus*

Ballard *et al.*¹ performed an experiment in which PHB was produced by *Alcaligenes eutrophus* from glucose as the carbon source under phosphorus limitation in a one step batch fermentation. Figure 13.5 represent the conversion time behavior of this reaction, while figure 13.6 shows the change of the molar mass of the polymer formed as a function of time. For modeling purposes the time scale has been shifted in such a way that start of the accumulation process coincides with time t equals zero.

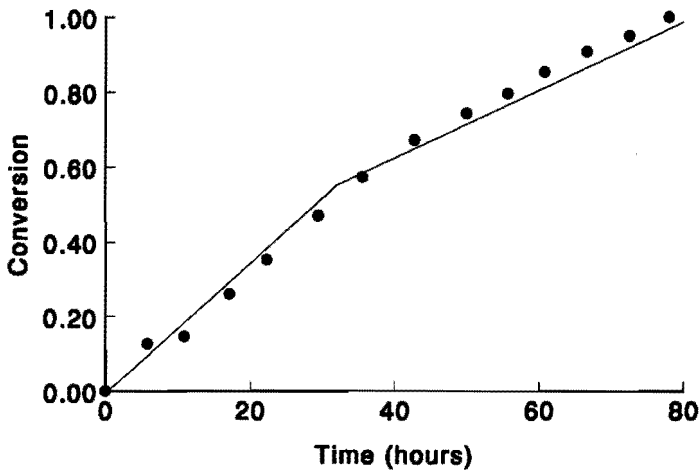


Figure 13.5 Conversion versus time plot. Experimental data according to Ballard *et al.*¹, and solid line: simulated conversion-time plot with coagulation.

The constant slope of the conversion time plot in figure 13.5 indicates that the rate of polymerization is constant, at least up to a conversion of approximately 60 %, after which the rate of polymerization declines to a somewhat lower value. This decrease in the rate of polymerization is accounted for by an increasing coenzyme-A concentration at or near the granule surface (see also section 13.3.3) which results in a lower propagation rate, due to the inhibition of the polymerase enzyme by coenzyme-A. The solid line in figure 13.5 represents a model calculation implementing the above. The fact that the rate of polymerization is constant during the first part of the accumulation process indicates that during the polymerization process the monomer concentration is virtually constant, since the decrease in the rate of polymerization can be accounted for by a decreasing in the polymer-polymerase conjugate concentration at the granule surface after coagulation. Figure 13.6 clearly shows that the

molar mass of the polymer formed increases very rapidly during the initial stage of the accumulation process, after which it gradually decreases.

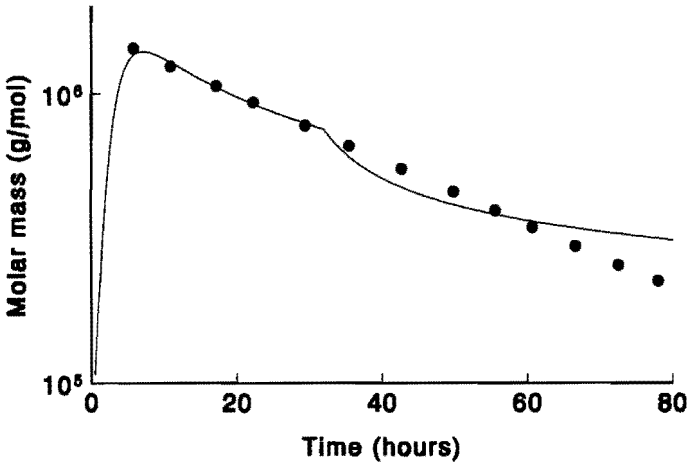


Figure 13.6 Cumulative molar mass versus time plot. Experimental molar mass-time plot according to Ballard *et al.*¹, and solid line: simulated molar mass-time plot.

The initially observed increasing molar mass can be accounted for in different ways. (i) *The kinetic processes in the cytoplasm strongly influence the molar mass of the polymer formed during the initial stage, i.e. the granule formation stage, of the accumulation process (see Chapter 11 and 12).* (ii) *Variation of the chain transfer agent concentration during polymerization:* This would mean that initially the overall chain transfer agent concentration is high in the cytoplasm, and decreases in time. Coenzyme-A exhibits a time-concentration dependency which resembles this behavior¹². This can be envisaged in the following way: Coenzyme-A is released in relatively large amounts in the TCA-cycle¹³. Once the concentration is under a certain value, 3-ketothiolase⁶ and the polymerase enzyme⁷ are no longer inhibited by coenzyme-A, and the accumulation of PHB starts. The concentration of coenzyme-A is still relatively high during the initial stage of the accumulation process, causing a high rate of chain transfer resulting in relatively low molar mass polymer. Once the concentration of coenzyme-A decreases further the molar mass of the polymer will be higher. Later in the accumulation process the molar mass of the polymer formed is determined mainly by the kinetic processes occurring at the granule surface resulting in a decreasing molar mass as a function of accumulation time^{5,9} (see also *section 13.2.4*). Koizumi *et al.*¹⁴ also related

the change in molar mass of the polymer formed to changes in the chain transfer agent concentration, however, these authors did not mention what this chain transfer agent would be. (iii) *Low molar mass polymer is present in the cytoplasm at $t = 0$* : It is possible that during the initial stage of the accumulation process the instantaneous molar mass of the polymer formed is high but the measured, cumulative, molar mass is lower due to the presence of low molar mass polymer in the bacterium. This would mean, however, that polymer was already present before the actual accumulation process started. This is probably the case in one step fermentation processes. The solid lines in figures 13.5 and 13.6 are model calculations utilizing values for the different input parameters as shown in table 13.1.

Table 13.1 Numerical values for different input parameters used in model calculations

k_p^I	=	$5.8 \cdot 10^5$	l/mole.s ^a
k_p^{II}	=	$3.0 \cdot 10^5$	l/mole.s ^b
k_{ct}^A	=	$5 \cdot 10^{-2}$ to $4.2 \cdot 10^{-4}$	s ⁻¹
k_{ct}^S	=	$3 \cdot 10^{-14}$	mole/l.dm ² .s
[M-SCoA]	=	$2 \cdot 10^{-5}$	mole/l
[E-SH] ₀ ^c	=	$2 \cdot 10^{-5}$	mole/l
N_{gran}	=	$3 \cdot 10^{16}$	l ⁻¹
z	=	580	units

^a represent the propagation rate coefficient in the first part of the accumulation process

^b represent the propagation rate coefficient in the second part of the accumulation process

^c initial free polymerase enzyme concentration, which is equal to the total active polymerase enzyme concentration (fast initiation)

In these calculations it is assumed that the granule formation period is short compared with the total accumulation time. Therefore, the number of granules is taken constant from the beginning of the accumulation process (*Chapter 14* will be mainly concerned with the estimation of input parameters, and their influence on the number of granules calculated as a function of time).

13.3.3 Influence of the Boundary Layer on the End of Polymerization

In *in vitro* experiments it is observed that high levels of coenzyme-A inhibit the polymerase enzyme⁷. Since the propagation reaction is an equilibrium reaction (see *section 13.2.2*), it can easily be seen that high levels of coenzyme-A enhance the depolymerization reaction. Further, at high accumulation levels the rate of polymerization decreases and

eventually goes to zero while active polymerase enzyme and monomer are still present¹. With the introduction of the boundary layer concept, it is possible to explain the above mentioned phenomena. First, the assumption will be made that the total amount of coenzyme-A in the bacterium stays constant throughout the accumulation process. At low conversions, the boundary layers of the granules will not overlap due to the relatively large distance between the separate granules (stage I in *figure 13.7*), coenzyme-A concentrations will be relatively low due to the large volume of the cytoplasm compared with the volume of the polymer phase.

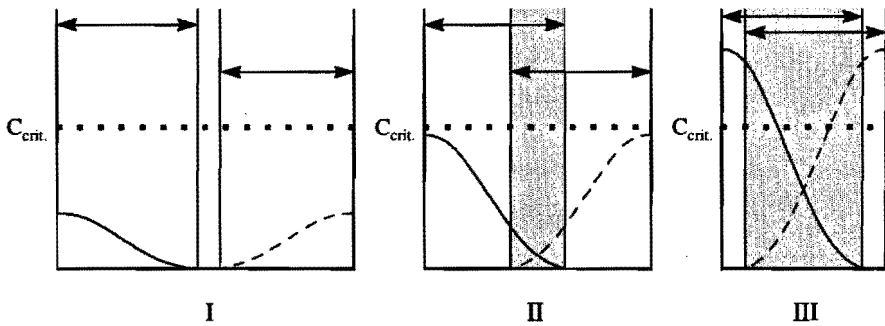


Figure 13.7 Different phases of the approach of granules: overlap of boundary layers

As the polymerization proceeds, the granules grow, and will approach each other causing a little overlap of the boundary layers of the separate granules at this point higher coenzyme-A concentrations in the boundary layer can be expected due to a decrease of the volume of the cytoplasm. In this situation, however, the coenzyme-A concentration is still below the critical value above which inhibition starts to play a significant role in the overall polymerization process (stage II in *figure 13.7*). At very high volume fractions, however, the boundary layers give an overlap and most of the water is located in a water-film between the granules. As a result of this, the concentration of coenzyme-A exceeds its critical concentration and polymerization will cease due to inhibition of the polymerase enzyme (stage III in *figure 13.7*) (see also *Chapter 10*)

13.4 Concluding Remarks

In this chapter, it is shown that the kinetic processes which occur at or near the granule surface play an important role during the accumulation of PHB in *Alcaligenes eutrophus*. With the introduction of a boundary layer near the granule surface, it is possible to describe and predict the molar mass of the polymer formed during the accumulation process. Coenzyme-A is put forward as a possible chain transfer agent and its effect on the polymerization processes has been discussed (Coenzyme-A can inhibit the polymerase enzyme (see also *Chapter 10*)). As a result of this, high coenzyme-A concentrations at the end of the polymerization process can shift the equilibrium of the polymerization reaction in such a way that polymerization will stop. Even depolymerization can occur if the coenzyme-A concentration is high enough. In this case the *polymerase enzyme* can act as the *depolymerase enzyme*, which is also suggested by Fukui *et al.*¹⁵ in the case of the PHB accumulation in *Zoogloea ramigera*.

The polymerization of (R)-3-hydroxybutyryl-CoA into PHB catalyzed by the polymerase enzyme can be regarded as a simple chemical reaction in which the relative concentrations of monomer, polymer and coenzyme-A determine the direction of the reaction, i.e. polymerization or depolymerization. The polymerase enzyme only lowers the activation energy of the transition state in the polymerization/depolymerization step¹⁰.

13.5 References

- 1 Ballard, D.H.G., Holmes, P.A., and Senior, P.J., *Recent Adv. Mech. Synth. Aspects. Pol.*, 215, 293 (1987)
- 2 Kawaguchi, Y., and Doi, Y., *Macromolecules*, 25, 2324 (1992)
- 3 De Koning, G.J.M., and Maxwell, I.A., *J. Environm. Pol. Degr.*, 1, 223 (1993)
- 4 Fitch, R.M., and Tsai, C.H., in "*Polymer Colloids*", ed. by R.M. Fitch, Plenum Press, 91 (1971)
- 5 *Chapter 11* of this thesis
- 6 Anderson, A.J., and Dawes, E.A., *Microbiol. Rev.*, 54, 450 (1990)
- 7 *Chapter 10* of this thesis
- 8 Froment, G.F., and Bischoff, K.B., "*Chemical Reactor Analysis and Design*", 2nd. edition, Wiley, (1990)
- 9 *Chapter 12* of this thesis
- 10 Stryer, L., "*Biochemistry*", W.H. Freeman and Co., New York, (1981)
- 11 Haywood, G.W., Anderson, A.J., and Dawes, E.A., *FEMS Microbiol. Lett.*, 57, 1 (1989)

- 12 Mansfield, D.A., Anderson, A.J., and Naylor, L.A., *Can. J. Microbiol.*, 41, 44 (1995)
- 13 Doi, Y., "Microbial Polyesters", New York, VCH Publishers, (1990)
- 14 Koizumi, K., Abe, H., and Doi, Y., *J. Macromol. Sci., Pure Appl. Chem.*, 32, 759 (1995)
- 15 Fukui, T., Yishimoto A., Matsumoto M., Husokawa, S., Saito T., Nishikawa H., and Tomita, K., *Arch. Microbiol.*, 110, 149 (1976)

CHAPTER 14

The Accumulation of Poly-(R)-3-hydroxybutyrate in *Alcaligenes eutrophus*

5. Model Calculations versus Experiments

Synopsis: Values for the different kinetic parameters and the monomer and polymerase enzyme concentrations were estimated from experimental data. These values were used to perform some model calculations which were compared with experimental data. Good agreement between model calculations and experimental data was obtained.

14.1 Introduction

In order to get more insight in the validity of the kinetic model developed in *Chapters 11, 12, and 13*, model calculation have to be performed which subsequently must be compared with experimental results. Therefore, values for the different kinetic parameters and concentrations of monomer and polymerase enzyme during the polymerization process have to be known. Therefore, estimates of different kinetic parameters, monomer, and enzyme concentrations have to be made, most conveniently these estimates are based on experimental data. First, the monomer and enzyme concentration during the accumulation process will be considered. Secondly, values for the different kinetic parameters such as the propagation and initiation rate coefficient will be evaluated. After this, the influence of the variation in numerical value, within physical limits, of the different input parameters on the number of granules formed during the accumulation process will be discussed. Finally, the molar mass of PHB formed during different accumulations in *Alcaligenes eutrophus* will be discussed. During these accumulations several process parameters such as pH, temperature, and carbon source concentration are varied.

14.2 Monomer and Polymerase Enzyme Concentration

The rate of polymerization depends directly, among other things, on the monomer and polymerase enzyme concentration. Therefore, in this section a rationalization will be given for the values of the separate concentrations used in the model calculations which are discussed in the latter part of this chapter.

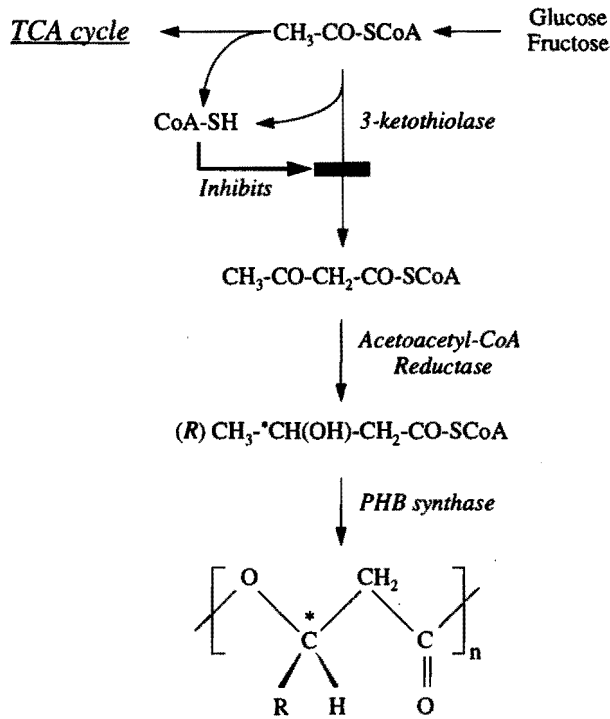


Figure 14.1 Schematic representation of the metabolic pathway of the biosynthesis of PHB in *Alcaligenes eutrophus*¹.

14.2.1 Monomer Concentration during the Accumulation Process

In conventional polymerizations, the monomer is added to the polymerization system where it is polymerized into polymer. In biological polymerization systems, however, the monomer is often synthesized from other components present. In the case of the biosynthesis of PHB, a carbon source is fed to the bacteria which is metabolized via several steps into the monomer which is subsequently polymerized into polymer catalyzed by the polymerase

enzyme, also referred to as PHB-synthase. In *figure 14.1* the metabolic pathway of fructose is given. Fructose is metabolized, under balanced growth conditions, into acetyl-CoA which subsequently is oxidized by the tricarboxylic acid cycle (TCA cycle). Concomitantly, no acetoacetyl-CoA and (R)-3-hydroxybutyryl-CoA (which is the monomer in the polymerization process) are formed. In this case the monomer concentration is zero. Once the bacteria are in nutrient limitations, but carbon excess, acetyl-CoA accumulates and acetoacetyl-CoA is formed which is converted into (R)-3-hydroxybutyryl-CoA. Consequently, the monomer concentration starts to increase and eventually will reach its maximum value, thus enabling polymerization.

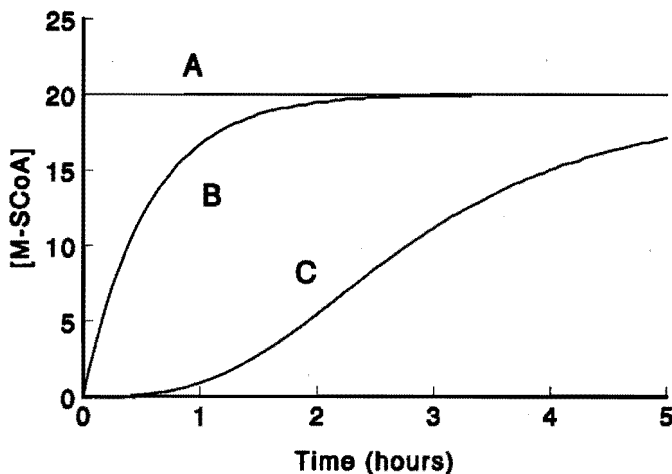


Figure 14.2 Schematic representation of the monomer concentration (μM) versus accumulation time (hours), for the initial stage of the accumulation process.

In *figure 14.2* three courses of the monomer concentration versus accumulation time are shown. Curve *A* represents the case where the monomer reaches its maximum concentration immediately after the start of the accumulation process after which it stays constant throughout the polymerization process. Curve *B*, on the other hand, shows a course of the monomer concentration $[\text{M-SCoA}]$ in which it gradually increases to its maximum value (see *figure 14.2*). This can be represented by the following equation:

$$[\text{M-SCoA}] = [\text{M-SCoA}]_{ss} * (1 - e^{-k^*t}) \quad (14.1)$$

here $[M-SCoA]_{ss}$ is the steady-state monomer concentration, t is time and k is a constant. Curve *C* in *figure 14.2* represents the case where the monomer concentration only slowly reaches its maximum value, which can be visualized by the following equation:

$$[M-SCoA] = \frac{[M-SCoA]_{ss} * k * t^3}{1 + k * t^3} \quad (14.2)$$

Estimates for the maximum monomer concentration have been given by several authors. Mansfield *et al.*² for instance have measured the amount of monomer per gram of residual biomass during the accumulation of, PHB in *Alcaligenes eutrophus*, and found a value of 0.03 μ mole monomer per gram of residual biomass, which corresponds with a concentration of 21 μ M (assuming 1.4 μ l cell water per mg bacterial dry weight). Bradel and Reichert³, on the other hand, stated that the monomer concentration corresponds with 0.53 mg/l acetyl-CoA, leading to a value of 7 μ M.

14.2.2 Polymerase Enzyme Concentration

The polymerization of (R)-3-hydroxybutyryl-CoA is catalyzed by a polymerase enzyme. Just like the monomer concentration, the concentration of the polymerase enzyme is a crucial parameter in the kinetics of the polymerization process. Unfortunately, measured values for the polymerase enzyme concentration ($[E-SH]$) have not been found in literature. However, estimations of the polymerase enzyme concentration have been made by several investigators. Bowien *et al.*⁴ estimated the active polymerase enzyme concentration in *Alcaligenes eutrophus* at 46 μ M. They based their estimate on the specific activities of the polymerase enzyme in the bacteria and the purified specific activity, being 0.24 and 22.4 units, respectively), the molar mass of the enzyme (105,000 g/mole) and 2.2 μ l cell water per mg protein. Kawaguchi and Doi¹ estimated the active polymerase enzyme concentration from the increasing number of dead polymer chains formed during the polymerization. Extrapolation to time zero gives an amount of 18,000 polymerase enzyme molecules per cell. From this the polymerase enzyme concentration can be calculated which gave a value of 25 μ M. Bradel and Reichert³ estimated a polymerase enzyme concentration of 0.025 μ M. In *table 14.1* different values of the monomer and polymerase enzyme concentration are summarized.

Table 14.1 Estimates for the monomer ([M-S-CoA]) and polymerase enzyme ([E-SH]) concentration.

[M-S-CoA]	[E-SH]	Reference
21 μM	-	Mansfield <i>et al.</i> ²
7 μM	0.025 μM	Bradel and Reichert ³
-	46 μM	Bowien <i>et al.</i> ⁴
-	25 μM	Kawaguchi and Doi ¹

14.3 Estimation of Rate Coefficients

In this section estimates will be made for different kinetic parameters utilizing kinetic expressions derived in the previous chapters.

Values for the *propagation rate coefficient* (k_p) can be obtained using conversion time data. From the slope of the conversion-time plot the rate of polymerization can be estimated, which is in a first approximation equal to the rate of propagation. Assuming that all the polymerase enzyme present is active (i.e. present in polymer-polymerase conjugates), an estimate can be made of k_p . Using a monomer and active polymerase enzyme concentration of each 20 μM , a value for k_p in the order of $10^5 - 10^6$ l/mole.s is found. This would mean that one polymerase enzyme molecule catalyses about 10 propagation steps per second. This is in the same order of magnitude as the value of 2 for the number of propagation steps per second per polymerase enzyme molecule reported by Doi *et al.* ⁵.

A value for k_i , the *initiation rate coefficient*, can be estimated using data from the earliest stages of the polymerization process. According to definition, the number average molar mass of a polymer (\overline{M}_n) is determined by the ratio of the propagation rate (R_p) and the initiation rate (R_i). After some rearrangements the following expression for k_i can be found:

$$k_i = \frac{M_0 * k_p * [E - S - M_n]}{\overline{M}_n * [E - SH]} \quad (14.3)$$

where $[E-S-M_n]$ represents the concentration of propagating polymer-polymerase conjugates, M_0 the molar mass of the monomer unit, k_p the propagation rate coefficient, and $[E-SH]$ the free soluble polymerase enzyme concentration. Using experimental molar mass data from the earliest stage of the accumulation process and the partitioning of the polymer-polymerase conjugates over the cytoplasm and the granule phase ⁶, a value for k_i can be estimated. This leads to an estimation of k_i , which is in the order of 10^{-2} l/mole.s.

Since several chain transfer agents can operative during the accumulation process, an overall pseudo-first order chain transfer coefficient for the aqueous phase and the granule surface is used for the model calculations. In the evaluation of the chain transfer coefficient an estimate for the *overall chain transfer rate coefficient in the aqueous phase* (k_{ct}^A) and *at the granule surface* (k_{ct}^S) will be given separately. Values for k_{ct}^A are estimated in a similar way as k_i , with the difference that in this case the molar mass is determined by the rate of chain transfer in the water phase (i.e. steady state is reached), which is expressed by *equation 14.4*:

$$k_{ct}^A = \frac{M_0 * k_p * [M - SCoA]}{M_n} \quad (14.4)$$

where $[M-SCoA]$ represents the monomer concentration. It has to be stressed that k_{ct}^A is an overall chain transfer coefficient and combines the separate chain transfer coefficients and chain transfer agent concentrations that contribute to all the chain transfer processes in the water phase, i.e. k_{ct}^A is a pseudo first order rate coefficient. Substituting values for the different variables in *equation 14.4* results in a value for k_{ct}^A in the order of $10^{-3} - 10^{-4} s^{-1}$. A value for the surface related overall chain transfer coefficient (k_{ct}^S) can be obtained by using the same method as used above, i.e. a value for k_{ct}^S can be estimated if values for the molar mass (M_n), rate of propagation (R_p) and the total granule surface (A_{gran}^l) are known. If this is the case k_{ct}^S can be calculated according to the following equation:

$$k_{ct}^S = \frac{M_0 * R_p}{M_n * A_{gran}^l} \quad (14.5)$$

which results in a value for k_{ct}^S in the order of 10^{-13} - 10^{-14} mole/l.dm².s.

The *adsorption rate coefficient* (k_{ads}) can be calculated in two different ways. The first one is equivalent to the previously used approach, i.e. using the general expression for the molar mass. In doing so, the following expression is found for k_{ads} :

$$k_{ads} = \frac{M_0 * R_p}{M_n * [E - S - M_z] * A'_{gran.}} \quad (14.6)$$

From *equation 14.6* a value in the order of 10^{-3} - 10^{-5} dm/s, using the steady-state concentration for [E-S-M_z] which is in the order of 10^{-12} mole/l.

An alternative way of calculating the adsorption rate coefficient (k_{ads}) is via a chemical engineering approach of the adsorption of the surface active polymer-polymerase conjugate onto a PHB granule. If a PHB granule is considered in an isotropic turbulence, the following equation holds ⁷:

$$Sh = 2 = \frac{k_{ads} * d_p}{D_z} \quad (14.7)$$

where Sh is the Sherwood number, D_z the diffusion coefficient of the surface active species which can adsorb with a degree of polymerization of z , d_p is the diameter of the PHB granule, and N_{av} is Avogadro's number. The diffusion coefficient can be calculated using the Einstein-Stokes relation:

$$D_z = \frac{k_b * T}{6 * \pi * r_z * \eta} \quad (14.8)$$

here k_b is Boltzmann's constant, T is temperature, r_z the radius of the surface active species which can adsorb, while η represents the viscosity of the cytoplasm (which is set equal to that of pure water being 0.01 Poise). The radius of the adsorbing species can be easily calculated by assuming that this species is spherical, this leads to the following equation:

$$r_z = \left(\frac{3 * (z * V_{mu} + V_{enz})}{4 * \pi} \right)^{1/3} \quad (14.9)$$

In *equation 14.9*, V_{mu} represents the volume of one monomer unit and V_{enz} the volume of the polymerase enzyme molecule. The volume of the monomer unit can be calculated using the volume contribution of structural groups⁸ leading to a value for V_{mu} of $8 * 10^{-29} \text{ m}^3$. The volume of the polymerase enzyme can be evaluated from the molar mass of the enzyme (approximately 110,000 g/mole) and the assumption that the density of the polymerase enzyme is equal to unity, this leads to a value of V_{enz} of $2 * 10^{-25} \text{ m}^3$. In the next section an estimate for z will be made, which is in the order of 500. This results in a radius for the adsorbing species of approximately 4 nm. Leading to a diffusion coefficient of $5 * 10^{-12} \text{ m}^2/\text{s}$. Finally, an adsorption rate coefficient of approximately $4 * 10^{-5} \text{ dm/s}$ is obtained, assuming an average diameter of the PHB granules of 250 nm. This value for the adsorption rate coefficient is in good agreement with the value found from *equation 14.6*.

14.4 Estimation of Granule Formation Parameters

14.4.1 Estimation of z from *in vivo* Polymerizations

It is difficult to estimate a value for z , i.e. the degree of polymerization of the surface active species which can adsorb, therefore only a rough estimate can be made utilizing the following assumptions: First, 5 - 10 % of the total polymerase enzyme is present in the cytoplasm⁶. Secondly, initiation is fast, and finally k_p and $[\text{M-S-CoA}]$ are equal at the granule surface and in the cytoplasm. If initiation is fast, it can be assumed that almost all the polymerase enzyme in the cytoplasm is present as active polymerase enzyme, i.e. in the form of polymer-polymerase conjugate. This means that the ratio of the polymerase enzyme concentration at the granule surface, in the form of polymer-polymerase conjugates, and in the cytoplasm is equal to the ratio of the growth-time of one polymer-polymerase conjugate at the granule surface and in the cytoplasm. Since the rate of polymerization for a single chain is constant (assumption 3), the ratio between the degree of polymerization at the granule surface and the cytoplasm (z) is equal to ratio of the number polymer-polymerase conjugates at the granule surface and in the cytoplasm. Assuming an average degree of polymerization of approximately 10,000 a value for z is obtained which is in the order of 500 - 1000.

14.4.2 Estimation of j

The homogeneous nucleation model for the formation of latex particles in an emulsion polymerization states that nucleation of newly formed latex particles is a homogeneous process, while early growth of polymer chains occurs in the continuous aqueous phase⁹. As the growing polymer chain reaches a critical degree of polymerization of j , at which it exceeds its water solubility, the polymer chain will collapse in order to minimize its surface area. One of the factors which controls the value of j is the difference in water solubility between the monomer, or monomer unit, and the radical. In the process of granule formation of PHB, the polymer-polymerase conjugate can be regarded as a surfactant in which the polymerase enzyme is the hydrophilic headgroup, and the growing polymer chain the hydrophobic tail. The value of j in the biosynthesis of PHB depends on the hydrophilicity of the polymerase enzyme and the hydrophobicity of the PHB tail (which is related to the water solubility of the monomer or better the monomer unit in the case of the biosynthesis of PHB).

For the conventional emulsion polymerization of methyl methacrylate (MMA, saturation concentration in water = 0.15 M) a value for j of 65 has been reported¹⁰, in this case the hydrophilic part was a sulfate radical. Whereas for styrene (S, saturation concentration in water = 0.003 mM) with the same sulfate radical, a value of only 5 has been found¹¹.

Studies on the stabilizing effect of polystyrene-polyethylene oxide block copolymers on emulsions revealed that the optimum ratio (mass ratio) of the polystyrene and the polyethylene oxide block turned out to be 0.4. Comparison of the polyethylene oxide part with the polymerase enzyme and the polystyrene part with the hydrophobic PHB tail, an estimate of j can be made. The molar mass of the polymerase enzyme has been reported to be between 63,900 and 160,000 g/mole^{6,12,13}, if at the same time the mass ratio of 0.4 is taken into account j can be estimated to be in the order of 520.

From studies on the formation of latex particles during the biosynthesis of natural rubber, the molar mass of the adsorbing surface active poly-*cis*-isoprene-polymerase conjugates was determined to be approximately 10^5 g/mole¹⁴. For the biosynthesis of natural rubber, j would be in the order of 600, assuming that the molar mass of the poly-*cis*-isoprene

polymerase enzyme is approximately 50,000 g/mole. Which is comparable with the value for j estimated from the flocculation experiments for the biosynthesis of PHB.

From the previous, it is obvious that only rough estimates of the values for z and j can be made. However, a value for both z and j in the order of 500 will be used, with the restriction that z has to be smaller than j .

14.5 Model Calculations

In this section the differential equations which were derived in *Chapter 12 (section 12.3.4)* for the granule formation stage during the accumulation of PHB in *Alcaligenes eutrophus* will be solved simultaneously. In doing so, results of the calculations will be mainly concerned with the change in the number of granules formed upon changing the value of the input parameters. At the same time, the sensitivity of the model with respect to the variation in input parameters will be investigated. *Table 14.2* gives the default values of the different input parameters as derived in the previous section.

Table 14.2 Numerical value of input parameters

Input parameter	Minimum	Default	Maximum	
k_p	$5 \cdot 10^4$	10^5	$5 \cdot 10^6$	l/mole.s
k_i	10^{-1}	10^2	10^4	l/mole.s
k_{ct}^A	10^{-6}	10^{-4}	10^{-2}	s^{-1}
k_{ct}^S		$5 \cdot 10^{-13}$		mole/l.dm ² .s
k_{ads}	10^{-8}	$5 \cdot 10^{-5}$	$5 \cdot 10^{-2}$	dm/s
z/j	0.5	0.98	0.992	
j	250	500	750	
$[M-SCoA]^a$	10^{-7}	10^{-6}	10^{-4}	mole/l
$[E-SH]_0^b$	10^{-7}	$2 \cdot 10^{-5}$	10^{-3}	mole/l

^a steady-state value for the monomer concentration

^b initial free polymerase enzyme concentration

Figure 14.3 represents the normalized concentrations of different intermediate species formed during the polymerization process as a function of time. This figure shows that once an

intermediate has been formed it will rapidly increase to its maximum concentration after which it decreases again to its steady-state value.

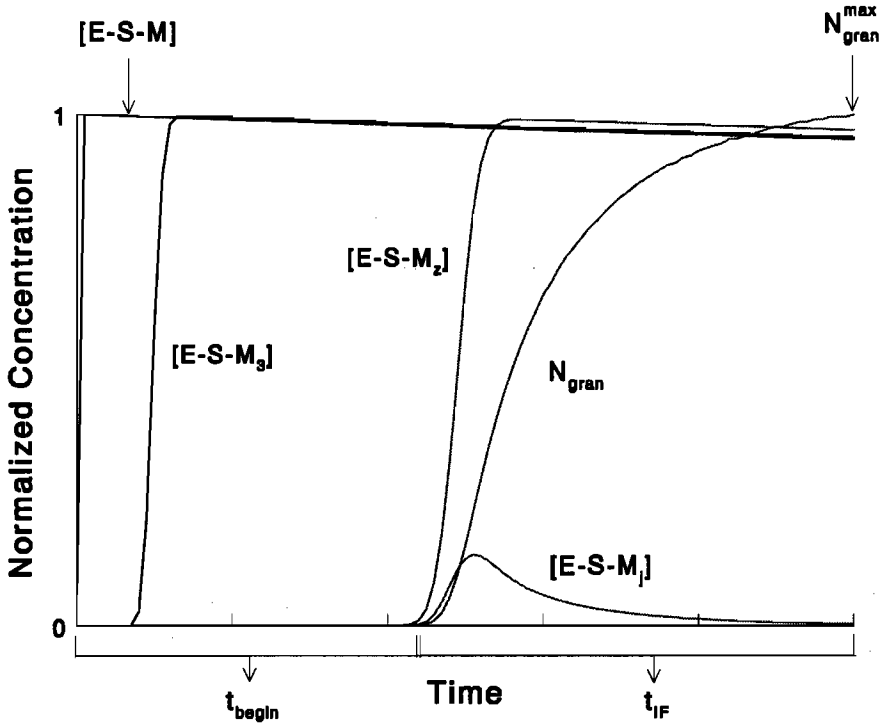


Figure 14.3 Normalized concentration of different intermediates formed during the polymerization as a function time. All input parameters were set at their default value as shown in table 14.3. $[E-S-M_x]$ represents the relative concentration of a propagating polymer-polymerase conjugate with a degree of polymerization of x , N_{gran} the number of granules, and N_{gran}^{max} the total number of granules. While t_{begin} and t_{IF} represent the time before the first granule is formed and the interval of granule formation, respectively.

If the number of granules is considered, i.e. the integrated curve of $[E-SM_1]$ versus time, the following is observed: it takes considerable time before the first granules are formed, after this the concentration of $[E-SM_1]$ increases relatively fast to reach its maximum values. Once $[E-SM_1]$ reaches its maximum value it decreases again to zero. These observations can be explained in the following way: According to the homogeneous nucleation model¹⁰, the time needed before a degree of polymerization of j is obtained ($= t_{begin}$, see also figure 14.3) is represented by the next equation:

$$t_{\text{begin}} = \frac{j}{k_p * [M - SCoA]} \quad (14.10)$$

In this equation the denominator represents the growth rate of one single polymer chain. In the case of *figure 14.3*, t_{begin} is equal to 16 minutes. *Figure 14.3* also shows that after the first granules have been formed, the concentration of the species with a degree of polymerization smaller than z , which is the critical degree of polymerization for adsorption, decreases very rapidly, due to adsorption of these species onto the newly formed granules. The total granule surface ($A_{\text{gran.}}^t$) increases rather fast during the early stage of the polymerization process due to the following two reasons. First, the surface of the granules will grow due to the presence of propagating polymer-polymerase conjugates at the granule surface which causes granule growth. Secondly, new granule surface is also formed due to the nucleation process which is still operative in the earliest stage of the polymerization process. Due to this increase in surface more and more polymer-polymerase conjugates from the cytoplasm can adsorb onto already existing granules rather than propagating further in the cytoplasm to form new granules. Once no new granules are being formed all the surface active polymer-polymerase conjugates grown in the cytoplasm will adsorb onto existing granules. The time during which granules are formed is referred to as the interval of granule formation (t_{IF}).

14.5.1 Influence of Variations in Input Parameters on the Number of Granules

In all the calculations discussed in this section the input parameters were kept at their default value and only the parameters under discussion were varied over at least two orders of magnitude. The deviation from the default value of the parameter under discussion will always be expressed on a logarithmic scale. Three features of the outcome of the model calculations will be discussed below, i.e. the time needed for the formation of the first granule (t_{begin}), the interval of granule formation (t_{IF}), and the total number of granules formed ($N_{\text{gran.}}^{\text{max}}$).

In *section 14.2.1* an estimation has been made of the *steady-state concentration of the monomer ([M-SCoA])* during the accumulation process. At the same time three arbitrarily chosen courses of the monomer concentration as a function of time, i.e. monomer profiles, have been suggested according to which the steady-state concentration of the monomer could

be reached. *Figure 14.4* represent model calculations in which the monomer concentration and all the other input parameters were kept at their default value (see *table 14.2*), however, the course of the monomer concentration as a function of time was changed as discussed in *section 14.2.1*. From *figure 14.4* it is obvious that the number of granules formed as a function of time depends on the monomer profile. The time it takes to form all granules (interval of formation) is for both the constant and the exponential monomer profiles small, as could be expected if *equation 14.10* is considered. For the sigmoidal profile, however, a longer interval of formation is calculated. This is caused by the lower concentration of the monomer in the cytoplasm, which results in a slower initiation process. As a result of this the granule formation process will be slower, which can be explained by *equation 14.10*.

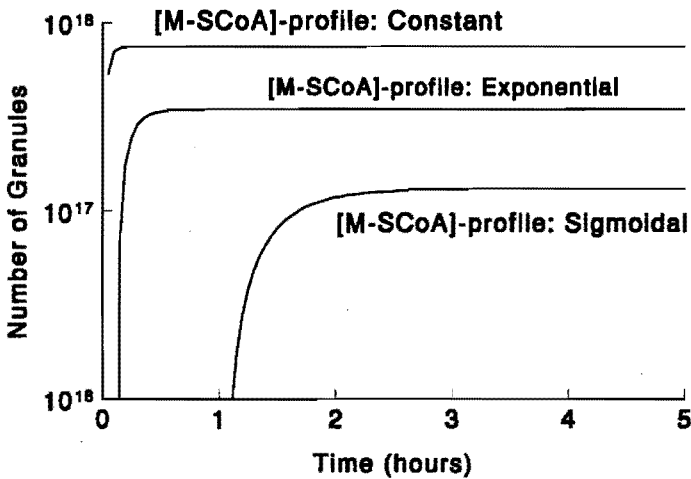


Figure 14.4 Number of granules per liter of cytoplasm as a function of time for different monomer concentration profiles as indicated in plot (see also *section 14.2.1*).

In order to see to what extent the **monomer concentration** ($[M-SCoA]$) influences the process of granule formation, the monomer concentration was varied. The monomer concentration was kept constant during polymerization. The results of these calculations are shown in *figure 14.5* (open circles). The time needed before the first granule is formed increases with decreasing monomer concentration as is predicted by *equation 14.10*. Also the interval of granule formation increases with decreasing monomer concentration. On the other hand, the total number of granules increases with higher monomer concentrations, this can be

attributed to the increasing rate of propagation over the rate of adsorption, i.e. more E-S-M_j species, which precipitate from the cytoplasm to form precursor granules, will be formed.

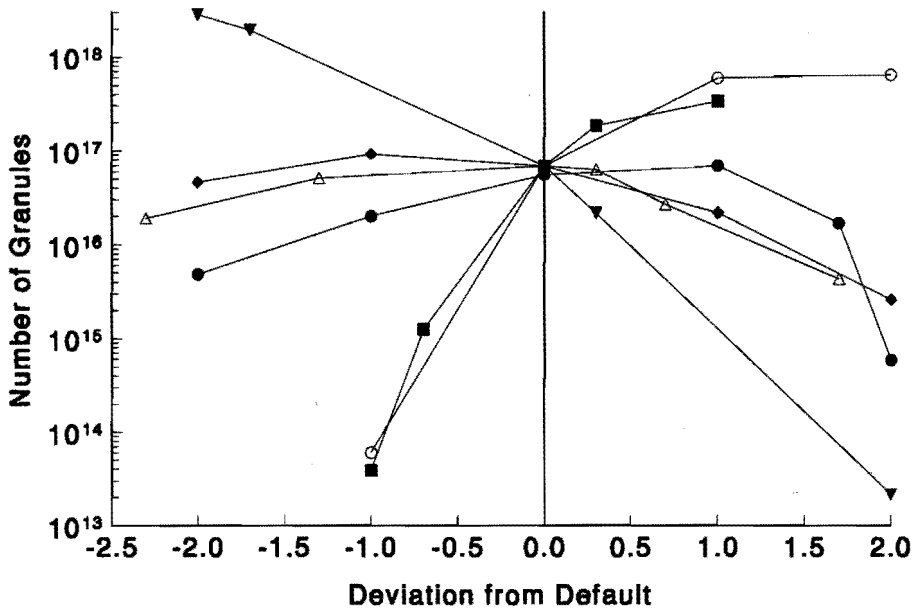


Figure 14.5 Number of granules per liter of cytoplasm as a function of the deviation from the default value of different input parameters. Please note that the deviations are taken relative with respect to the default value of the input parameter on a **logarithmic** scale. The different input parameters are denoted as follows: Monomer concentration by open circles, Initial free polymerase enzyme concentration ($[E-SH]_0$) by open triangles, k_p by closed squares, k_i by closed chevrons, k_w by closed circles, and k_{ads} by closed triangles. Lines are to guide the eye.

The influence of varying the **initial free polymerase enzyme concentration ($[E-SH]_0$)** on the number of granules formed during the granule formation stage is also shown in **figure 14.5** (open triangles). A rather striking result of these calculations is that the number of granules formed as a function of the polymerase enzyme concentration goes through an optimum. This can be envisaged in the following way: When the initial free polymerase enzyme concentration increases the number of granules increases due to a low rate of adsorption. This low rate of adsorption is caused by two effects: First, less active enzyme will be present in the cytoplasm since the absolute polymerase enzyme concentration will be low. Secondly, the increase in granule surface will be smaller at low active enzyme concentrations.

As a result, the number of granules formed at low polymerase enzyme concentrations will increase as this concentration increases. However, at higher initial polymerase enzyme concentrations, the rate of adsorption will become higher due to the higher concentration of "adsorbable" species and larger total granule surface. In summary, it can be said that at very low polymerase enzyme concentrations, initiation, propagation and granule formation and thus formation of granule surface are slow, which causes a slower adsorption process resulting in more granules. While at higher polymerase enzyme concentration these processes are faster, especially the rate of adsorption. This results in a decreasing number of granules with an increasing polymerase enzyme concentration.

The influence of the *propagation rate coefficient* (k_p) on the number of granules is represented in *figure 14.5* by the closed squares. It is clearly demonstrated by this figure that k_p has a rather strong influence on the number of granules formed. It also shows that the time needed to form the first granules (t_{begin}) increases with decreasing k_p , as would be expected. The interval of formation, on the other hand, is affected less by a change in the propagation rate coefficient. The increase in the number of granules with increasing k_p can be explained by the fact that if the rate of propagation increases, more propagating polymer-polymerase conjugates in the cytoplasm will grow until they become insoluble, i.e. they reach their critical degree of polymerization j for precipitation, rather than adsorbing onto already existing granules. Here again it is the competition between the propagation versus the adsorption process.

Figure 14.5 also shows the influence of the *initiation rate coefficient* (k_i) on the granule formation stage, i.e. on the number of granules formed. The number of granules decreases with increasing k_i due to the increasing concentration of surface active polymer-polymerase conjugates in the cytoplasm. Thus, not only the concentration of these surface active species increases but also the total granule surface, whereas the rate of polymerization for a single species remains constant. The result is that the rate of adsorption increases in relation to the rate of polymerization, leading to a lower number of granules. The time interval of formation (t_{IF}) is strongly influenced by k_i , while t_{begin} is virtually unaffected by the change in initiation rate coefficient. This can be attributed to the fact that t_{begin} depends on k_p and the monomer concentration.

The influence of *chain transfer coefficient in the water phase* (k_{ct}^A) on the formation of granules is represented by the closed circles in *figure 14.5*. k_{ct}^A also has a strong influence on the number of particles formed during the accumulation process. At relatively high values for k_{ct}^A ($> \frac{k_p * [M - SCoA]}{j}$), however, the number of granules decreases sharply. This is due to the fact that at high values of k_{ct}^A the polymer chain will not reach the length of j at which granules are formed. When this is the case, granule formation will also be the result of coagulation of low(er) molar mass polymer chains present in the cytoplasm. This is not accounted for in the model since only homogeneous nucleation with growth is considered and not homogeneous nucleation with limited coagulation (see also *Chapter 12*). Therefore, the number of granules decreases when the rate of chain transfer increases. The interval of granule formation is not affected by changes in the value for k_{ct}^A . The time needed for the formation of the first granule is independent of the chain transfer rate coefficient just like in the case of the initiation rate coefficient. Again t_{begin} only depends on the propagation rate coefficient (k_p) and the monomer concentration ($[M - SCoA]$) according to *equation 14.10*.

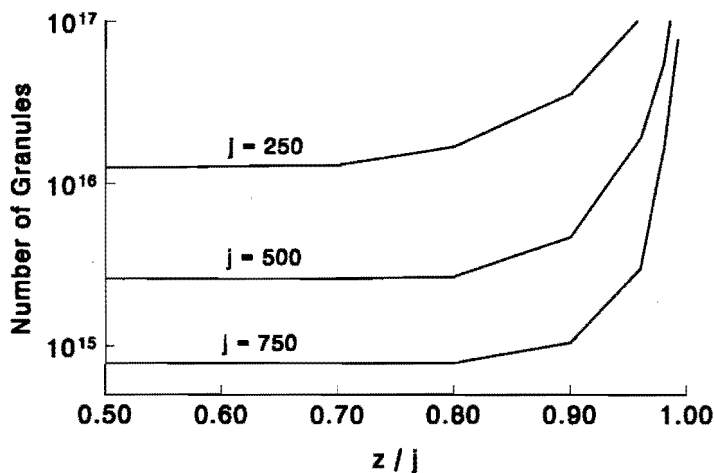


Figure 14.6 Number of granules per liter of cytoplasm as a function of the ratio of z/j at different values for j

Calculations with increasing *adsorption rate coefficient* (k_{ads}) show that the number of granules formed decreases with increasing k_{ads} (figure 14.5, closed triangles). If the rate of adsorption is high, less granules will be formed. The interval of granule formation (t_{IF}) increases with a decreasing value of the adsorption rate coefficient.

The influence of z and j , i.e. the *degree of polymerization at which the oligomeric polymerase enzyme molecule becomes surface active and precipitates, respectively*, on the number of granules formed is shown in figures 14.6 and 14.7. Figure 14.6 shows that the number of granules increases with a decreasing value for j at the same z/j -ratio. This can be attributed to the fact that as j increases the probability that adsorption occurs becomes more likely since the number of different species which can adsorb increases.

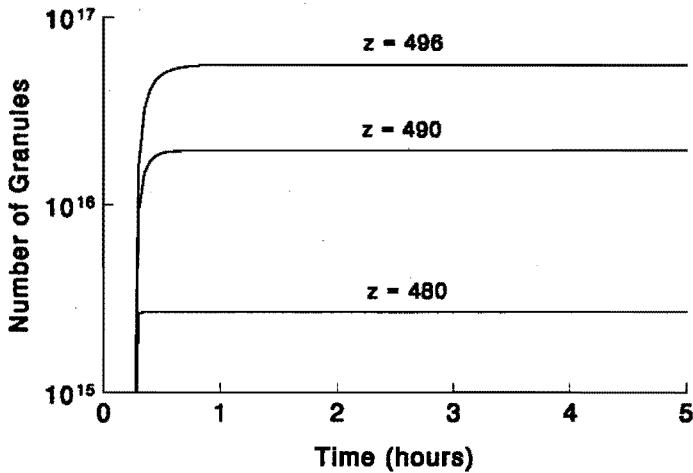


Figure 14.7 Number of granules as a function time for different values of z , j is kept at a value of 500.

As the ratio of z and j approaches unity, i.e. z approaches j (see also figure 14.7), the number of granules formed increases sharply since the probability that adsorption occurs decreases as z approaches j . The time needed for the formation of the first granule (t_{begin}) strongly depends on j as is shown by equation 14.10. Figures 14.6 and 14.7 show that the number of granules is very sensitive for the values of z and j .

14.6 Experimental Results and Model Calculations

In the previous section the influence of different input parameters on the number of granules formed has been evaluated. A logical approach would now be to compare the number of granules formed during the accumulation of PHB in *Alcaligenes eutrophus*, using experimental data, with the calculated value. In literature, however, only little experimental data are available on the formation of granules.

Ballard *et al.*¹⁵ stated that the number of granules is constant, typically being in the order of 8-12 granules per bacterium, already during the earliest stage of the accumulation process. This would mean that the time interval of granule formation (t_{IF}) and the time the first granule is formed (t_{begin}) are rather short. Although they did not mention an explicit time or time interval. In most of the model calculation present in the previous section t_{begin} and t_{IF} are also rather short indicating some coherence between the model calculation and the experimental observations concerning the granule formation stage.

Hustede *et al.*¹⁶ cloned the poly-(R)-3-hydroxybutyric acid synthase (in this thesis referred to as polymerase enzyme) genes of *Rhodobacter sphaeroides* and *Rhodospirillum rubrum* and heterologous expression in *Alcaligenes eutrophus*. In doing so, they determined the PHB synthase activity in different strains of *Alcaligenes eutrophus* and *Escherichia coli*. In the case of the latter bacterium almost no PHB synthase activity was measured, while for *Alcaligenes eutrophus* the measured activity varied from almost zero up to the value determined for the wild type from which the cloned genes originated. The number of granules per bacterium varied from 2-3 up to over 30, depending on the origin of the genes. A quantitative measure of the number of granules per bacterium can not be made since only thin sections of the polymer containing bacteria were investigated. The above results indicated that the total activity of the polymerase enzyme (PHB synthase), which can be expressed in terms of the propagation rate coefficient or as the product of the propagation rate coefficient and the polymerase enzyme concentration, clearly has an influence on the number of granules per bacterium. At this moment, however, it is not possible to make any quantitative statements about the above experimental results.

It is clear from the above that the amount of experimental data on the number of granules formed during the accumulation process is insufficient. On the other hand, a vast amount of experimental data exists on the molar mass of PHB formed during its accumulation in *Alcaligenes eutrophus*. As has been clearly demonstrated in *Chapters 11, 12 and 13* the number of granules present strongly influences the molar mass of the polymer formed. Therefore, in the following sections the molar mass of PHB accumulated under different accumulation conditions, such as different carbon source concentrations, temperature and pH will be discussed. In doing so, experimental results on the molar mass of PHB formed during these accumulation processes will be compared with model calculations utilizing values of the input parameters which are within reasonable physical limits.

14.6.1 Influence of Carbon Source Concentration

Kawaguchi and Doi ¹, have conducted two-step batch experiments varying the initial fructose (carbon source) concentration using *Alcaligenes eutrophus*. *Figures 14.8 and 14.9* show the conversion versus time and molar mass versus time graphs, respectively, of accumulations utilizing different fructose concentrations. The solid lines in *figures 14.8 and 14.9* represent model calculations using values for the different input parameters as shown in *table 14.3*.

Table 14.3 Numerical value of input parameters used for different model calculations.

Input Parameter	[Fructose]	pH	Temperature		units
			16 °C	35 °C	
k_p	$4.5 * 10^5$	$4.7 * 10^5$	$2.8 * 10^5$	$6 * 10^5$	l/mole.s
k_i	----- 10^3 -----				l/mole.s
k_{ct}^A ⁱ	----- from $5 * 10^{-2}$ to $3 * 10^{-4}$ -----				s ⁻¹
k_{ct}^S ⁱⁱ	----- $5 * 10^{-14}$ -----				mole/l.dm ² .s
[M-SCoA] ⁱⁱⁱ	----- $2 * 10^{-5}$ -----				mole/l
[E-SH] ^{iv}	----- $2 * 10^{-5}$ -----				mole/l

ⁱ k_{ct}^A changes to account for the change in the chain transfer concentration during the initial stage of the accumulation process

ⁱⁱ k_{ct}^S is related with k_{ads} via: $k_{ads} = k_{ct}^S / [E-S-M_2]$, [E-S-M₂] is the concentration of "adsorbable" species

ⁱⁱⁱ steady-state concentration of the monomer

^{iv} initial free polymerase enzyme concentration

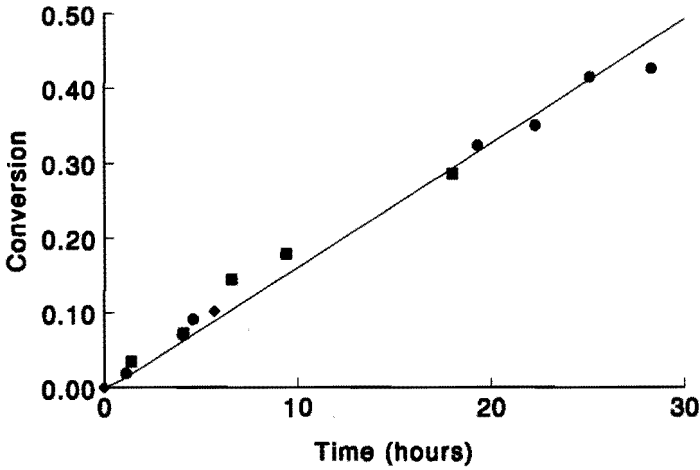


Figure 14.8 Conversion versus time measured for different fructose concentrations. Circles: [Fructose] = 20 g/l, squares: [Fructose] = 10 g/l, and triangles: [Fructose] = 5 g/l. Solid line: model calculation. Data taken from Kawaguchi and Doi¹.

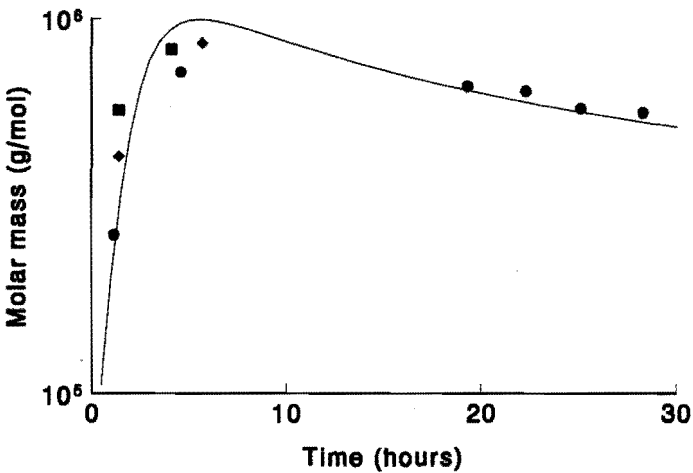


Figure 14.9 Molar mass versus time measured for different fructose concentrations. Circles: [Fructose] = 20 g/l, squares: [Fructose] = 10 g/l, and triangles: [Fructose] = 5 g/l. Solid line: model calculation. Data taken from Kawaguchi and Doi¹.

It can be clearly seen from figure 14.8 that the initial fructose concentration does not influence the rate of polymerization, i.e. the slope of the conversion versus time graph, or the molar mass of the polymer formed versus the accumulation time. This could be due to the fact

that not the polymerization is the rate determining step but for instance the conversion of acetyl-CoA in acetoacetyl-CoA. This step is known to be a key reaction in the metabolic regulation of the biosynthesis of PHB¹⁷.

14.6.2 Influence of pH

Changes in the pH of an enzyme containing solution can cause a number of effects on the activity of the enzyme. The enzyme may be even irreversibly denatured by acid or base. The most important effects of pH are on the rate of the reaction. The effect of pH on the activity of the enzyme in question can be tested by incubation of the particular enzyme at the pH in question, followed by assaying of the sample at the pH optimum. Figure 14.10 shows the dependency of the relative activity of two PHB synthase enzymes from different microorganisms. Both PHB synthase enzymes showed a pH optimum at 7.

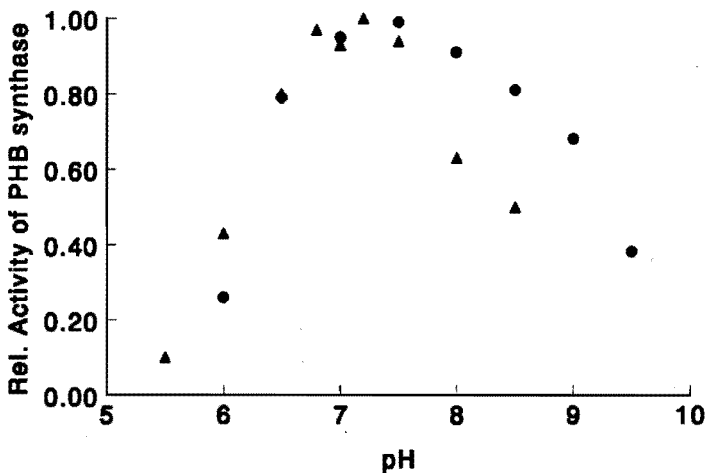


Figure 14.10 Relative activity of granule associated polymer-polymerase conjugates versus pH. Triangles: PHB synthase from *Zoogloea ramigera*, according to Fukui et al.¹⁸, and circles: PHB synthase from *Bacillus megaterium*, according to Griebel et al.¹⁹

Another enzyme which plays an important role in the biosynthesis of PHB is 3-ketothiolase. Nishimura et al.²⁰ reported that 3-ketothiolase from *Zoogloea ramigera* showed a pH optimum of 7.5 in the condensation reaction, and 8.5 in the thiolysis reaction. Although the origin of the enzymes mentioned above is different from the bacterium under discussion here, i.e. *Alcaligenes eutrophus*, it is assumed that the pH optima of the enzymes is virtually

the same in different bacteria. During the biosynthesis of PHB several enzymes are active which all have their own pH optimum. By performing fermentations at different pH the net result of the pH can be rather large, i.e. all enzyme show a pH optimum at approximately the same value, or relatively small due to compensation of extremes. Koizumi *et al.*²¹ conducted two step batch experiments varying the pH of the fermentation medium. The results of these experiments are shown in *figures 14.11* and *14.12*. From the experimental data, it can be seen that pH, ranging from 5.8 to 8, does not have a large influence on the conversion or molar mass of the polymer formed versus time. The solid line in *figures 14.11* and *14.12* represents model calculations using the input parameters given in *table 14.3*.

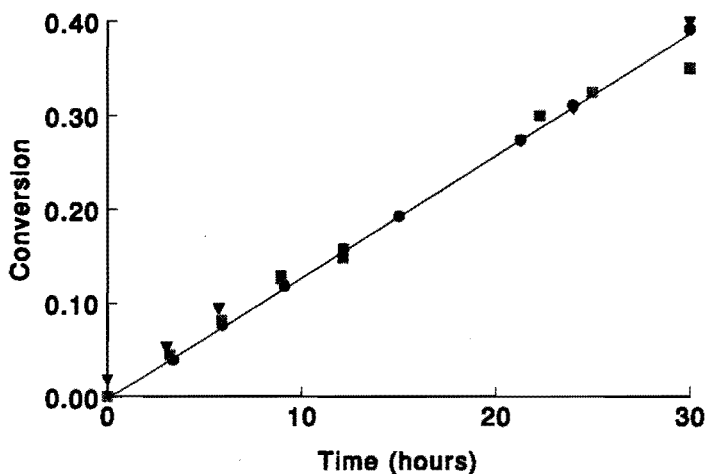


Figure 14.11 Conversion time plot measured at different pH values. Squares: pH = 5.8, circles: pH = 7, and triangles: pH = 8. Data taken from Koizumi *et al.*²¹.

14.6.3 Influence of Temperature

An increase in temperature can have several effects on an enzyme catalyzed reaction. The two major effects are an increase in the rate of the catalyzed reaction and an increase in the rate of enzyme denaturation. Since these processes are competing reactions that both increase with increasing temperature, no temperature optimum can be defined for an enzyme. Therefore, it is very difficult to predict whether the rate of an enzymatic reaction increases or decreases with increasing temperature. The effect of temperature on the reaction rate can be interpreted for simple enzymatic reactions from measurements made over a wide temperature range in which the enzyme is stable. Koizumi *et al.*²¹ investigated the influence of temperature

on the production of PHB by *Alcaligenes eutrophus* (see figures 14.13 and 14.14). The results indicated that with an increasing temperature, the rate of accumulation increased.

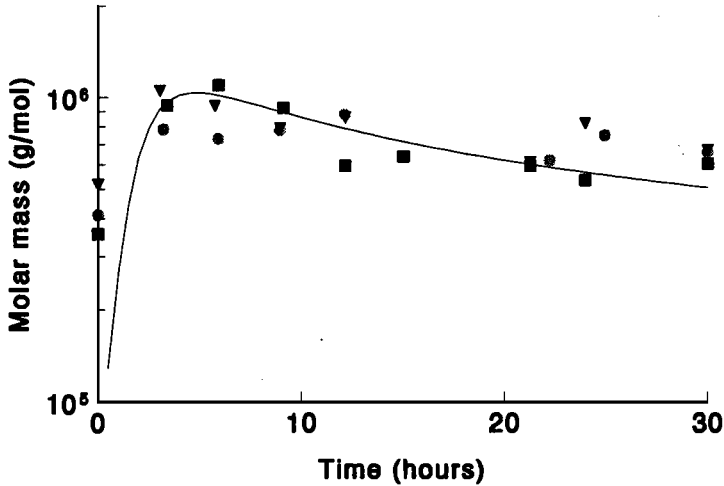


Figure 14.12 Molar mass of PHB versus time, for fermentations conducted at different pHs. Squares: pH = 5.8, circles: pH = 7, and triangles: pH = 8. Data taken from Koizumi et al. ²¹.

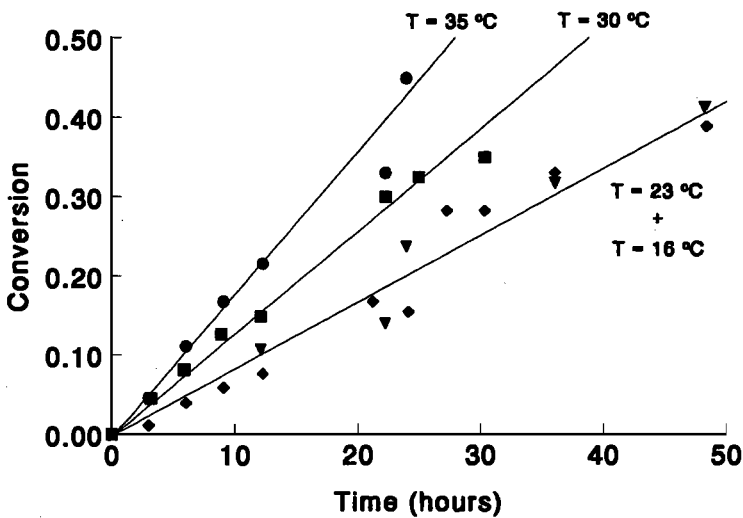


Figure 14.13 Conversion time plot measured at different temperatures. Circles: $T = 35\text{ }^{\circ}\text{C}$, squares: $T = 30\text{ }^{\circ}\text{C}$, triangles: $T = 23\text{ }^{\circ}\text{C}$, and chevrons: $T = 16\text{ }^{\circ}\text{C}$. The solid lines represent model calculations as indicated. Data taken from Koizumi et al. ²¹.

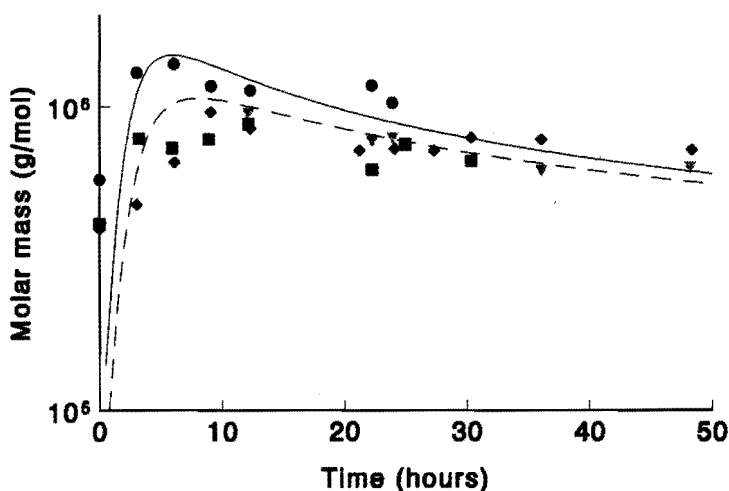


Figure 14.14 Molar mass as a function of accumulation time at different temperatures. Circles: $T = 35\text{ }^{\circ}\text{C}$, squares: $T = 30\text{ }^{\circ}\text{C}$, triangles: $T = 23\text{ }^{\circ}\text{C}$, and chevrons: $T = 16\text{ }^{\circ}\text{C}$. Solid line and dashed line are model calculations for $T = 35\text{ }^{\circ}\text{C}$ and $16\text{ }^{\circ}\text{C}$, respectively. Experimental data taken from Koizumi et al.²¹.

14.7 Concluding Remarks

In the foregoing sections estimates have been made for the different kinetic parameters and concentrations of monomer and polymerase enzyme from experimental data. With these estimates, model calculations have been performed to investigate the influence of the different input parameters on the predicted number of granules during the accumulation of PHB in *Alcaligenes eutrophus*. Model calculations clearly showed that the adsorption rate coefficient, propagation rate coefficient, and monomer concentration have the most profound effect on the predicted number of granules. The modeling of the biosynthesis of PHB exhibits some intrinsic difficulties compared with the modeling of conventional polymerization processes. In conventional polymerizations only reactions which are directly related to the polymerization processes such as propagation and termination are considered. When biological polymerizations are modeled, however, many reactions occur which are not necessarily directly related to the polymerization process. One of these reactions is for instance the production of monomer which has been synthesized *in vivo* before it can be polymerized into

polymer. Further, in the case of the biosynthesis of PHB many bacteria are present in the reaction mixture. These bacteria are considered as single batch reactors and the whole reaction mixture is considered as a summation of all the individual batch reactors. The residence time distribution of the reaction mixture is considered to be very narrow. In practice, however, this is not necessarily the case since during the accumulation process some new biomass will be formed, which means that new bacteria are formed, resulting in a broadening of the residence time distribution. The developed kinetic model does not account for this broadening and assumes that all the bacteria start to accumulate PHB at the same moment and all have the same overall rate of polymerization. Another problem of modeling the biosynthesis of PHB is the fact that the start of the polymerization is often not exactly defined with respect to time. Further, the reproducibility and the accuracy of the experimental data can be questioned. For instance, the way the polymer is extracted from the biomass might influence the molar mass of the polymer. For this reason, the actual intracellular molar mass might be higher than the reported molar mass.

In spite of the above comments, it seems that the molar mass of PHB in *Alcaligenes eutrophus* is related to the granule surface as is predicted by the model. The model developed can describe the experimental results relative well, especially if it is considered the model contains only one adjustable parameter, i.e. the propagation rate coefficient, which is fitted to the conversion versus time curve. Furthermore, the model is applicable to *in vitro* polymerizations utilizing purified polymerase enzyme and monomer. In *in vitro* experiments the influence of the initial coenzyme-A, monomer and polymerase enzyme concentration on the accumulation processes can be investigated more easily. While at the same time, the course of the molar mass of the polymer formed as a function of time/conversion and the rate of polymerization can be monitored.

14.8 References

- 1 Kawaguchi, Y., and Doi, Y., *Macromolecules*, **25**, 2324 (1992)
- 2 Mansfield, D.A., Anderson, A.J., and Naylor, L.A., *Can. J. Microbiol.*, **41**, 44 (1995)
- 3 Bradel, R., and Reichert, K.H., *Makromol. Chem.*, **194**, 1983 (1993)
- 4 Bowien, B., Cook, A.M., and Schlegel, H.G., *Arch. Microbiol.*, **97**, 273 (1974)
- 5 Doi, Y., Kawaguchi, Y., Koyama, N., Nakamura, S., Hiramitsu, Y., Yoshida, and Kimura, H., *FEMS Microbiology Rev.*, **103**, 103 (1992)

- 6 Haywood, G.W., Anderson, A.J., and Dawes, E.A., *FEMS Microbiol. Lett.*, 57, 1 (1989)
- 7 Froment, G.F., and Bischoff, K.B., "Chemical Reactor Analysis and Design", 2nd. edition, Wiley (1990)
- 8 Krevelen, van, D.W., "Properties of Polymers", Elsevier, Amsterdam (1990)
- 9 Chapter 12 of this thesis
- 10 Fitch, R.M. and Tsai, C.H., in "Polymer Colloids", Fitch, R.M. (Ed.), Plenum, New York (1971)
- 11 Maxwell, I.A., Morrison, B.R., Napper, D.H., and Gilbert, R.G., *Macromolecules*, 24, 1629 (1991)
- 12 Steinbüchel, A., Hustede, E., Liebergesell, M., Pieper, U., Timm, A., and Valentin, H., *FEMS Microbiol. Rev.*, 103, 217 (1992)
- 13 Peoples, O.P., and Sinskey, A.J., *J. Biol. Chem.*, 264, 15298 (1989)
- 14 Hager, T., MacArthur, A., McIntyre, D., and Seeger, R., *Rubber Chem. Techn.*, 52, 693 (1979)
- 15 Ballard, D.G.H., Holmes, P.A., and Senior, P.J., *Recent Adv. Mech. Synth. Aspects Pol.*, 215, 293 (1987)
- 16 Hustede, E. Steinbüchel, A., and Schlegel, H.G., *FEMS Microbiol. Lett.*, 93, 285 (1992)
- 17 Anderson, A.J. and Dawes, E.A., *Microbiol. Rev.*, 54, 450 (1990)
- 18 Fukui, T., Yishimoto A., Matsumoto M., Husokawa, S., Saito T., Nishikawa H., and Tomita, K., *Arch. Microbiol.*, 110, 149, (1976)
- 19 Griebel, R., Smith, Z., and Merrick, J.M., *Biochemistry*, 7(10), 3676, (1968)
- 20 Nishimura T., Saito, T., and Tomita, K., *Arch. Microbiol.*, 116, 21 (1978)
- 21 Koizumi, K., Abe, H., and Doi, Y., *J. Macromol. Sci., Pure Appl. Chem.*, 32, 759 (1995)

CHAPTER 15

The Accumulation of Poly-(R)-3-hydroxybutyrate in *Alcaligenes eutrophus*

6. On the Applicability of the Developed Model

Synopsis: The model developed and tested in the previous chapters has been applied to other polyhydroxyalkanoates accumulating bacteria and transgenic plants. Most of the observed polymer chemical features of the investigated polyhydroxyalkanoates accumulating systems could be explained qualitatively by the previously developed model.

15.1 Introduction

A large diversity of bacterial polyhydroxyalkanoates (PHAs) have been found to accumulate in over 80 species ¹. Research on PHA production has mainly been concentrated on two micro-organisms, i.e. *Alcaligenes eutrophus*, which produces short-chain PHAs, and *Pseudomonas putida/oleovorans*, which produces medium-chain PHAs (see figure 15.1) ².

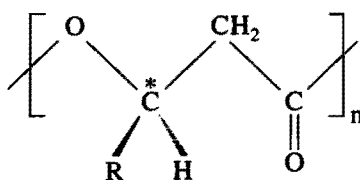


Figure 15.1 Polyhydroxyalkanoates. In short-chain PHAs R represents a hydrogen atom, methyl group, or an ethyl group, while in medium-chain PHAs R ranges from a hexyl up to a cetyl group.

The most versatile PHA, i.e. poly-(R)-3-hydroxybutyrate (PHB), is synthesized by *Alcaligenes eutrophus*. In the previous chapters a kinetic model has been developed and tested for the accumulation of PHB in *Alcaligenes eutrophus*. However, in addition to PHB homopolymer, *Alcaligenes eutrophus* is capable of producing other polyhydroxyalkanoates (PHAs) containing a number of different monomer units, which nature and proportion depends

on the carbon source used. These PHAs have a melting point of approximately 175 °C depending on the composition. In addition to PHB and copolymers containing hydroxybutyrate, there is another general class of PHAs containing monomer units ranging from hexyl to cetyl pendant groups. *Pseudomonas oleovorans* is the prototypical bacterium synthesizing these PHAs from *n*-alkanes or *n*-alkanoic acids. In contrast to PHB, medium-chain PHAs (mcl-PHA) are elastomers with a melting point ranging from 40 to 60 °C.

In this chapter an attempt will be made to extend the model developed in the previous chapters for other PHAs accumulated by different species. In doing so, first the accumulation of different copolymers by *Alcaligenes eutrophus* will be discussed. Secondly, the accumulation of mcl-PHA by *Pseudomonas putida* and/or *oleovorans* will be considered. After this the use of genetic engineering with respect to the biosynthesis PHAs will be thought over, from the point of view of the developed model. However, before the above mentioned subjects are discussed a critical evaluation of the developed model will be given.

15.2 Some Critical Comments on the Developed Model

The development of a model would not be complete without a critical evaluation of the model, especially in this chapter where the applicability of the developed model is tested with respect to other PHAs and PHA accumulating species. Therefore, in the underlying section some critical remarks will be addressed with respect to different aspects of the developed model. First, the possible implementations of enzyme kinetics on the accumulation process will be considered. Secondly, the physical chemistry of the accumulation process is thought over from a somewhat different point of view as has been done in the previous chapters. In *section 15.2.3* different topics will be discussed in a somewhat random way.

15.2.1 Enzyme Kinetics and the Biosynthesis of PHB

In *Chapter 10* the kinetics and mechanisms of the biosynthesis of PHB were discussed using the simple Michaelis-Menten model to account for the action of the polymerase enzyme on the substrate, i.e. (R)-3-hydroxybutyryl-CoA. However, in this case the polymerization process was not taken into account as such. In *Chapters 11, 12, and 13*, a kinetic scheme was presented which assumed that all the reactions involved in the polymerization process were

going to completion without considering the fact that in principle these reactions tend to reach an equilibrium. *Figure 15.2* shows a simple Michaelis-Menten scheme in which the different steps occurring during the polymerization process are accounted for. In principle, this scheme should have been used to describe the experiments discussed in *Chapter 10, 11, 12, and 13*.

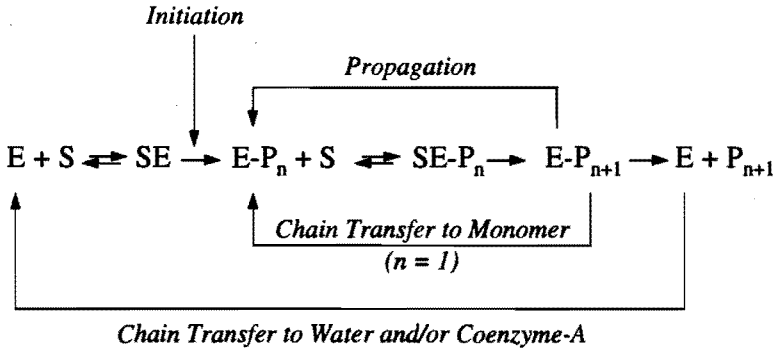


Figure 15.2 A simple Michaelis-Menten scheme for the biosynthesis of PHB. *E* represents the polymerase enzyme, *SE* the substrate-polymerase enzyme complex, *E-P_n* the polymer-polymerase conjugate, *SE-P_n* the substrate-polymer-polymerase conjugate, and *S* the substrate.

The scheme depicted in *figure 15.2* does not consider the release of coenzyme-A during the polymerization process and its influence on the metabolism. Coenzyme-A inhibits 3-ketothiolase and the polymerase enzyme^{3,4,5}. It is not the objective of this thesis to consider the influence of the metabolism, i.e. monomer production, of the PHB accumulating species on the production of PHB in detail. However, some comments will be made in the following section how this problem could be dealt with. In doing so, the possible influence of coenzyme-A on the production of the substrate, i.e. (R)-3-hydroxybutyryl-CoA, and the polymerization process will be discussed.

15.2.2 Does the Biosynthesis of PHB exhibit Oscillatory Behavior ?

Until recently it was common knowledge that biochemical reactions inevitably converged rapidly to their thermodynamic steady-state and this steady-state was unique. Similarly, a restrictive view of the concept of homeostasis dominated physiological thinking. It was supposed that physiological control functioned solely to restore transiently disturbed systems to a steady-state. It is now recognized that this is not the case and complex dynamical

behavior is an aspect of biological regulation, of which sustained oscillations is a typical example. At the macroscopic level, oscillatory processes seem relatively common in biological systems, e.g. rhythmic heartbeat. It was not until 1964 that Ghosh and Chance⁶ observed, as first, oscillations in a biochemical system, i.e. the glycolytic pathway, on a microscopic level. Nowadays, oscillatory behavior is commonly recognized in biological systems. Periods range from fractions of seconds to the annual rhythms of plants⁷. The glycolytic oscillator is probably the most widely studied biochemical oscillator. For instance, Goldbeter and Lefever⁸ proposed a model for the glycolytic oscillator where feedback activation is essential to the destabilization of the thermodynamic steady state and the resulting oscillations. However, it can be shown that positive feedback was not sufficient to produce sustained oscillations. On the other hand, negative feedback systems can exhibit periodic behavior. An example of a negative feedback system is the intracellular calcium-cyclic AMP system⁹. Below the following hypothesis is postulated: The biosynthesis of poly-(R)-3hydroxybutyrate in *Alcaligenes eutrophus* exhibits oscillatory behavior.

If the production of monomer during the biosynthesis of PHB and its subsequent polymerization is considered, a combination of positive feedback, auto-acceleration, and negative feedback, inhibition of 3-ketothiolase and PHB synthase, by coenzyme-A can be recognized. In *figure 15.3* a carbon source, typically fructose or glucose, is converted to pyruvate. From pyruvate, the monomer, i.e. (R)-3-hydroxybutyryl-CoA, is formed in several steps catalyzed by different enzymes (see *figure 15.3*). When the bacterium is triggered to accumulate polymer, two acetyl-CoA molecules are converted into acetoacetyl-CoA and coenzyme-A. This reaction is catalyzed by 3-ketothiolase. As more acetyl-CoA is converted, concentrations of acetoacetyl-CoA and coenzyme-A increase. Acetoacetyl-CoA is converted by the enzyme acetoacetyl-CoA reductase into (R)-3-hydroxybutyryl-CoA, which is subsequently polymerized into PHB, catalyzed by the polymerase enzyme. During this polymerization reaction, coenzyme-A is formed again. The concentration of coenzyme-A in the system increases via reactions **2** and **4**, while reaction 1, i.e. the formation of acetyl-CoA, causes a decrease. As the concentration of coenzyme-A increases the rate of acetyl-CoA formation will increase, leading ultimately to a higher rate of polymerization (reaction **4**). Thus, higher acetyl-CoA concentrations will cause a higher rate of coenzyme-A release via

reactions 2 and 4, which again can increase the rate of acetyl-CoA formation and so on. This indicates a positive feedback, i.e. coenzyme-A catalyzes its own production.

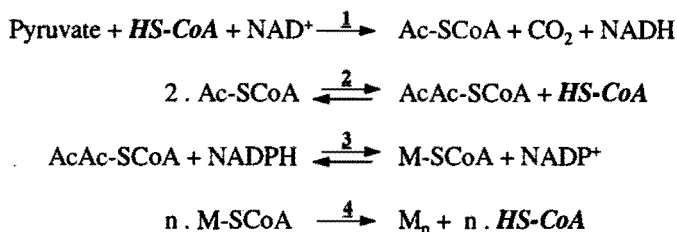


Figure 15.3 The metabolism of monomer production from pyruvate and its subsequent polymerization. HS-CoA represents coenzyme-A, Ac-SCoA acetyl-CoA, AcAc-SCoA acetoacetyl-CoA, M-SCoA the monomer, i.e. (R)-3-hydroxybutyryl-CoA. NAD⁺, NADH, NADPH, and NADP⁺ have their usual meaning. 1 represents the pyruvate dehydrogenase complex, 2 the 3-ketothiolase enzyme, 3 the NADPH-linked acetoacetyl-CoA reductase, while 4 is the polymerase enzyme (PHB synthase).

However, when coenzyme-A concentrations are too high, 3-ketothiolase and PHB synthase will be inhibited^{3,4,5} leading to a lower rate of acetoacetyl-CoA and polymer formation and thus lowering the rate at which coenzyme-A is released from reactions 2 and 4, indicating a negative feedback. This results in a lower rate of release of coenzyme-A, decreasing the coenzyme-A concentration. As a result of the lowering of the coenzyme-A concentration the inhibition of reactions 2 and 4 can cease, thus increasing the rate of acetoacetyl-CoA and polymer formation again. Eventually, the oscillations may lead to steady-state. The alternation of positive and negative feedback causes the concentration of different intermediates to oscillate. As a result of this, the rate of propagation, initiation, and chain transfer will also oscillate with a certain frequency. In the following section the concept of oscillations in biochemical reaction and its potential influence on the biosynthesis of PHB will be discussed in somewhat more detail for the model developed in this thesis.

15.2.3 The Granule Formation and Granule Growth Stage

The granule formation stage of the biosynthesis of PHB in *Alcaligenes eutrophus* is considered in this thesis as a homogeneous nucleation process followed by growth of the granules formed. However, polymer-polymerase conjugates which are terminated in the cytoplasm result in the formation of hydrophobic polymer in the cytoplasm. This hydrophobic

polymer can form precursor granules but can also coagulate with existing granules. In the case of coagulation the growth of granules is not only caused by the adsorption of oligomeric polymerase enzyme or propagation of granule associated polymer-polymerase conjugates. Also the possibility of coagulation of small precursor granules should be taken into account. Concomitantly, a better model for the formation of granules would be a homogeneous nucleation model with limited coagulation of polymer present in the cytoplasm, resulting from the chain transfer of polymer-polymerase conjugates present in the cytoplasm, and small precursor granules which have not yet attained colloidal stability (see also *Chapter 12*). Further, the adsorption of surface active polymer-polymerase conjugates onto the granule surface should be considered as a coagulation event rather than an adsorption event, although, the equations describing this adsorption/coagulation process are basically the same. After considering the granule formation stage some words will be addressed now to the granule growth process.

In the description of the granule growth process it is assumed that polymer-polymerase conjugates which are propagating at the granule surface desorb from the granule surface once they are terminated. After this desorption, the polymerase enzyme molecules can react with monomer again (initiation) in the cytoplasm and propagate until they reach a critical degree of polymerization, z , at which coagulation/adsorption of these polymer-polymerase conjugates can occur onto already existing granules. In this process, the exchange of polymerase enzyme between the cytoplasm and the granule surface plays a crucial role in the determination of the molecular mass of the polymer formed, i.e. as the granule surface increases the molar mass of the polymer is lowered as depicted by *equation 11.18* in *Chapter 11*. This equation is deduced by assuming steady-state for the concentration of granule associated polymer-polymerase conjugates, i.e. the concentration of granule associated and cytoplasmatic polymer-polymerase conjugates does not change with time. This has also been observed experimentally by Haywood *et al.*¹⁰ Fukui *et al.*¹¹ showed that after PHB accumulation ceased in *Zoogloea ramigera*, polymerase enzyme which was present at the granule surface during polymer accumulation was released from the granule surface and mainly present in the cytoplasm. Nonetheless, the steady-state assumption that was used in the deduction of *equation 11.18* in *Chapter 11* also led to the conclusion that during the granule growth stage the rate of adsorption of surface active polymer-polymerase conjugates from the cytoplasm onto the PHB granules has to be equal to the rate of chain transfer of polymer-polymerase conjugates. At

first sight this seems strange since the rate of adsorption is proportional with the granule surface while the rate of chain transfer should be constant since all parameters determining the rate of chain transfer are constant, viz. the polymer-polymerase conjugate concentration, chain transfer constant, and chain transfer agent concentration. In *Chapter 13* this has been solved by changing the chain transfer agent concentration as a function of granule surface. As has been pointed out in the previous section the concentration of different intermediate species in a metabolic pathway may oscillate. In fact, this is the case if the polymer-polymerase conjugate concentration is considered. The adsorption of oligomeric polymerase enzyme caused the polymer-polymerase conjugate concentration to increase, while the chain transfer of polymer-polymerase conjugate and subsequent desorption of the polymerase enzyme decreases this concentration. In terms of *section 15.2.2*, the process of adsorption causes a positive feedback on the rate of propagation and chain transfer since these rates are proportional with the polymer-polymerase conjugate concentration. The chain transfer process on itself gives a strong negative feedback with respect to the rate of propagation and chain transfer, since it decreases the polymer-polymerase conjugate concentration. The rate of adsorption increases when the granules grow in size thus resulting in more polymer-polymerase conjugates at the granule surface, which leads to a higher rate of chain transfer. In summary, the average granule associated polymer-polymerase conjugate concentration remains constant, while the period of the oscillation of this concentration can change with time. Concomitantly, the rate of chain transfer, which is proportional with the average polymerase enzyme concentration at the granule surface, is expected to remain constant. However, the instantaneous rate of chain transfer oscillates with the same frequency as the polymer-polymerase conjugate concentration does.

In the deduction of an expression for the molar mass of the polymer formed during the biosynthesis of PHB in *Alcaligenes eutrophus* a steady-state approximation was made. The major reason for this was the fact that in this way the influence of the heterogeneity of the polymerization system on the molar mass of the polymer formed could be pointed out, i.e. the molar mass of the polymer formed is inversely proportional with the diameter of the granules present^{12,13}. Further, the assumption was made that after a polymer-polymerase conjugate molecule was terminated, the polymerase enzyme would desorb from the granule surface due to its hydrophilic character. Here, a different approach will be discussed which does not involve a steady-state approximation and the "desorption-assumption", but only the fact that

the polymerization system becomes heterogeneous during the accumulation process, i.e. granules are being formed. According to definition, the kinetic chain length of a polymer is the number of propagation steps per initiated chain. *Equation 15.1* represents the kinetic chain length of the polymer formed in the cytoplasm (v^{cyto}).

$$v^{\text{cyto}} = \frac{R_p^{\text{cyto}}}{R_i^{\text{cyto}} + R_{\text{ct},M}^{\text{cyto}}} = \frac{k_p * [E - S - M_n]^{\text{cyto}}}{k_i * [E - SH]^{\text{cyto}} + k_{\text{ct}}^M * [E - S - M_n]^{\text{cyto}}} \quad (15.1)$$

here R_p^{cyto} and R_i^{cyto} are the rate of propagation and initiation in the cytoplasm, respectively, and $R_{\text{ct},M}^{\text{cyto}}$ the rate of chain transfer to monomer in the cytoplasm. $[E-SH]^{\text{cyto}}$ represents the free polymerase enzyme concentration in the cytoplasm, $[E-S-M_n]^{\text{cyto}}$ the propagating polymer-polymerase conjugate concentration in the cytoplasm, while k_p , k_i , and k_{ct}^M are the propagation, initiation, and chain transfer to monomer rate coefficient, respectively. When polymerization starts the initiation rate will be high since $[E-SH]$ is high, and the rate of propagation and rate of chain transfer to monomer low, due to the low concentration of propagating polymer-polymerase conjugates. As the polymerization proceeds, the concentration of free polymerase enzyme decreases, while that of the propagating conjugates increases. This results in an increase of the molar mass of the polymer formed as a function of conversion. During the polymerization process granules will be formed and the propagating polymer-polymerase conjugates will become associated with these granules¹⁴. When propagating polymer-polymerase conjugates in the cytoplasm are terminated the resulting free polymerase enzyme molecules remain in the cytoplasm. For that part of the polymerization process which occurs at the granule surface an identical expression for the molar mass of the polymer formed can be given (see *equation 15.2*). *Equation 15.2* represent the kinetic chain length of the polymer formed at the granule surface (v^{gran}).

$$v^{\text{gran}} = \frac{R_p^{\text{gran}}}{R_i^{\text{gran}} + R_{\text{ct},M}^{\text{gran}}} = \frac{k_p * [E - S - M_n]^{\text{gran}}}{k_i * [E - SH]^{\text{gran}} + k_{\text{ct}}^M * [E - S - M_n]^{\text{gran}}} \quad (15.2)$$

here the different parameters have the same meaning as in *equation 15.1*, the superscript *gran.* refers to the granule surface. As the granules are just formed only

propagating polymer-polymerase conjugates are present at the granule surface. Once these propagating molecules are terminated free polymerase enzyme molecules are formed which could reside at the granule surface. The termination process increases the concentration of the free polymerase enzyme molecules at the granule surface ($[E-SH]^{gran}$) and thus enhances the rate of initiation at the granule surface. Initially the molar mass of the polymer formed at the granule surface is high due to the low free polymerase enzyme concentration at the granule surface. However, as the polymerization process proceeds the concentration of granule associated propagating polymer-polymerase conjugates ($[E-S-M_n]^{gran}$) decreases, while the concentration of free polymerase enzyme molecules increases. Concomitantly, the molar mass of the polymer formed at the granule surface decreases as a function of time/conversion. The overall molar mass of the polymer formed is determined by both the processes occurring in the cytoplasm and at the granule surface.

In conclusion it can be said that the molar mass of the polymer formed during the biosynthesis of PHB in *Alcaligenes eutrophus*, initially increases due to the kinetic processes in the cytoplasm. Then a transient period follows in which both the processes in the cytoplasm and at the granule surface determine the overall molar mass of the polymer formed, i.e. the molar mass of the polymer as a function of time/conversion goes through a maximum. After this transient period only the kinetic processes occurring at the granule surface determine the molar mass of the polymer, i.e. the molar mass decreases as a function of time/conversion due to an increasing granule surface. The above discussed approach gives the same (qualitative) result as the approach discussed in *Chapters 11, 12, and 13* (see *figures 12.12 and 12.13*). This is not so surprising since in both approaches the heterogeneity of the polymerization process is taken into account. However, the approach discussed in *Chapters 11, 12, and 13*, is preferred, since an expression for the molar mass of the polymer formed is found which contains experimentally accessible parameters. After these critical comments the developed model will be applied to several cases in which PHAs are formed by different bacteria, plants, and even during an *in vitro* polymerization.

15.3 Copolymers from Different Bacteria

Most of the polyhydroxyalkanoates synthesized by micro-organisms are copolymers, consisting of two or more hydroxyalkanoate repeating units. The composition of the copolymer formed depends on the micro-organism and the carbon substrate used (for more details on different bacterial polyhydroxyalkanoates see Steinbüchel and Valentin ²).

15.3.1 Copolymers from *Alcaligenes eutrophus*

When conventional copolymerizations are considered, the composition of the copolymer formed depends on the ratio of monomers and the reactivity ratios of the different comonomers present. The reactivity ratios can differ in such a way that the chemical composition of the copolymer formed changes with conversion or reaction time. This is typically the case when the reactivity ratios strongly deviate from unity, i.e. one of the comonomers is consumed at a faster rate than the other. In the case of the emulsion polymerization process where the continuous aqueous phase acts as a reservoir of monomer, differences in water solubility of the comonomers can magnify this effect. The phenomenon that the chemical composition of the copolymer formed changes as function of time/conversion is also referred to as composition drift ¹⁵. *Figure 15.4* gives a typical molar mass chemical composition distribution (MMCCD) of a styrene-methyl acrylate (S-MA) copolymer prepared via an emulsion polymerization. Methyl acrylate is the more water soluble monomer, while styrene is built in the copolymer at a higher relative rate. As can be clearly seen from this figure, the chemical composition distribution of the copolymer formed is extremely broad. In this particular case, the chemical composition of the polymer formed changes in such a way that at the end of polymerization even homopolymer, i.e. poly(methyl acrylate), is formed.

One of the most abundant copolymers synthesized by *Alcaligenes eutrophus* is poly-3-hydroxybutyrate-*co*-3-valerate (PHB-*co*-HV), which is currently produced industrially by Monsanto (formally ZENECA Bioproducts) and marketed under the trade name Biopol[®]. During the commercial process glucose and propionate are used as carbon sources. The HV content of PHB-*co*-HV is controlled by variation of the glucose to propionate ratio in the feed.

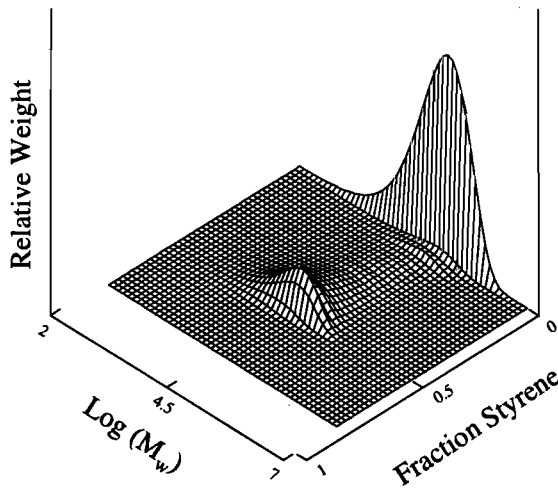


Figure 15.4 Model MMCCD of a high conversion S-MA emulsion copolymer. $(S/MA)_0 = 0.33$ (mole/mole), monomer over water ratio of 0.5 (g/g), 1 wt-% chain transfer agent, and $M_w = 110,000$ g/mole. Data taken from Van Doremaele¹⁵.

Recently, Yoshie *et al.*¹⁶ investigated the chemical composition distribution of commercially available PHB-*co*-HV. By subjecting the, as received, PHB-*co*-HV samples to a fractionation method utilizing a solvent/non-solvent combination (chloroform acted as a solvent and n-heptane as a non-solvent). The major conclusion which can be drawn from this investigation is the fact that during the bacterial production of PHB-*co*-HV the chemical composition of the polymer changed as a function of accumulation time. This resulted in a broad chemical composition distribution of the polymer produced. In some cases the difference in chemical composition was large enough to cause phase separation. During the biosynthesis of PHB-*co*-HV composition drift occurs as is also observed in the case of the conventional emulsion polymerization process.

Nakamura *et al.*¹⁷ reported on the influence of the ratio of 4-hydroxybutyrate and butyric acid in the carbon feed on the chemical composition of the poly-3-hydroxybutyrate-*co*-4-hydroxybutyrate copolymer formed. Figure 15.5 represents the fraction of 4-hydroxybutyrate units in the copolymer as a function of accumulation time at different ratios of 4-hydroxybutyrate and butyric acid in the carbon feed. This figure clearly shows that the

composition of the copolymer formed changes with accumulation time. It is clear from the above that the concentrations of the different monomers during the biosynthesis of copolymers in *Alcaligenes eutrophus* change with time, which is directly reflected in the changing chemical composition of the copolymer with time. This is caused by two effects.

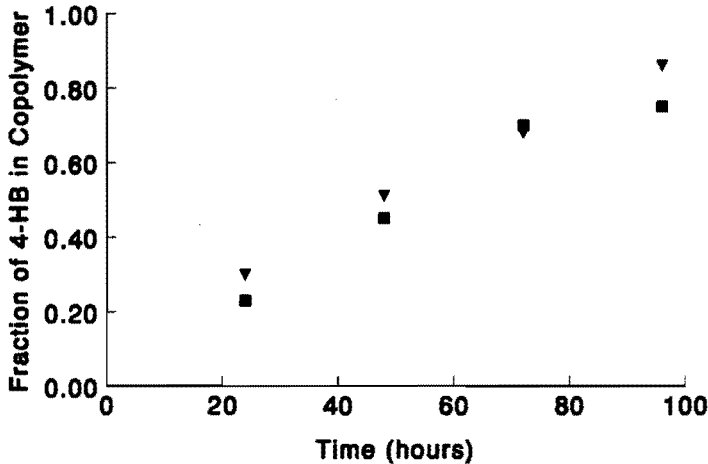


Figure 15.5 Fraction of 4-hydroxybutyrate in copolymer as function of accumulation time at different ratios of 4-hydroxybutyrate (4-HB) and butyric acid (BA) in the carbon feed. Closed triangles represent a ratio of 4-HB/BA of 10, while in the case of the closed squares this ratio is 3. Data taken from Nakamura et al.¹⁷.

First, the rate at which the different carbon sources are metabolized determines the actual monomer concentrations. While on the other hand, the relative rates at which the comonomers are consumed also influences the monomer concentration in the polymerization system. Another difficulty in the biosynthesis of copolymers is the fact that a certain carbon source does not necessarily result in the formation of one typical monomer, but often a mixture of monomers is obtained. For instance, if 4-hydroxybutyrate is used as a single carbon source, the fractions of 3-hydroxybutyrate and 4-hydroxybutyrate in the copolymer are approximately 0.75 and 0.25, respectively¹⁷.

The developed model for the accumulation of PHB homopolymer in *Alcaligenes eutrophus*^{12,13} can serve as a basis for a model which can describe the accumulation of copolymers. In doing so, the polymer chemical part of the model for homopolymer

accumulation has to be extended to account for the use of different carbon sources which results in the synthesis of different monomers and monomer concentrations. Also the difference in reactivity of the monomers present has to be accounted for. The model has to be adjusted for the difference in hydrophobicity of the different monomer units which influence the granule formation parameters such as the critical degree of polymerization for surface activity of the polymer-polymerase conjugate, z , and precipitation, j .

15.3.2 Copolymers from *Pseudomonas putida/oleovorans*

In addition to PHB and copolymers containing 3-hydroxybutyrate, there is another general class of PHAs where the pendant R group (see *figure 15.1*) ranges from hexyl to cetyl, depending on the carbon source fed, typically being n-alkanes, n-alcohols, or n-alkanoates. *Pseudomonas putida* and *oleovorans* are typical examples of bacteria which are capable of accumulating these so-called medium-chain PHAs (mcl-PHA) ^{18,19}. Furthermore, unique polymers containing unsaturations or branches in the pendant R group (see *figure 15.1*), as well as chloride or fluoride in the side groups, can be obtained by changing the fermentation feedstock ^{20,21,22}. Recently, Hori *et al.* ²³ investigated the time-dependent changes in the molar mass of mcl-PHA accumulated by *Pseudomonas putida*, by varying pH, carbon source concentration, and temperature during the accumulation process. The chemical composition of the mcl-PHA formed did not change with accumulation time, and remained constant at a mol fraction of 0.94 and 0.06 for 3-hydroxyoctanoate and 3-hydroxyhexanoate, respectively. *Figure 15.6* represents the conversion-time plot of several fermentations conducted at different accumulation temperatures. As temperature increases from 15 °C to 30 °C, the rate of initiation increases. While the rate of initiation for the fermentation conducted at 35 °C was considerably lower. The rate of polymer formation, however, is basically the same for the fermentations conducted at 20, 25 and 30 °C, i.e. the slope of the different curves is virtually the same. The rate of polymer formation in the case of the fermentations performed at 15 and 35 °C are lower than those performed at 20, 25 and 30 °C. In *figure 15.7* the molar mass of the polymer formed at different fermentation temperatures as a function of conversion are shown. For the fermentations performed at 15 up to 30 °C the molar mass reached a high value already after a very short period of time, i.e. at conversions below 0.01. However, for the fermentation conducted at 35 °C, the molar mass of the polymer formed first increases to reach a maximum value at a conversion of approximately 0.02, after which it decreases it again.

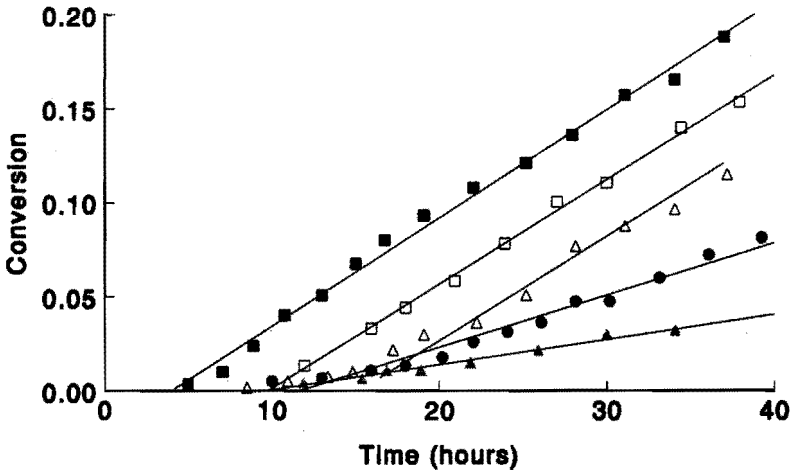


Figure 15.6 Conversion as a function of accumulation time at different accumulation temperatures. Closed circles represent an accumulation temperature of 15 °C, the open triangles of 20 °C, the open squares of 25 °C, the closed squares of 30 °C, and the closed triangles of 35 °C. Data taken from Hori et al.²³ Lines are to guide the eye.

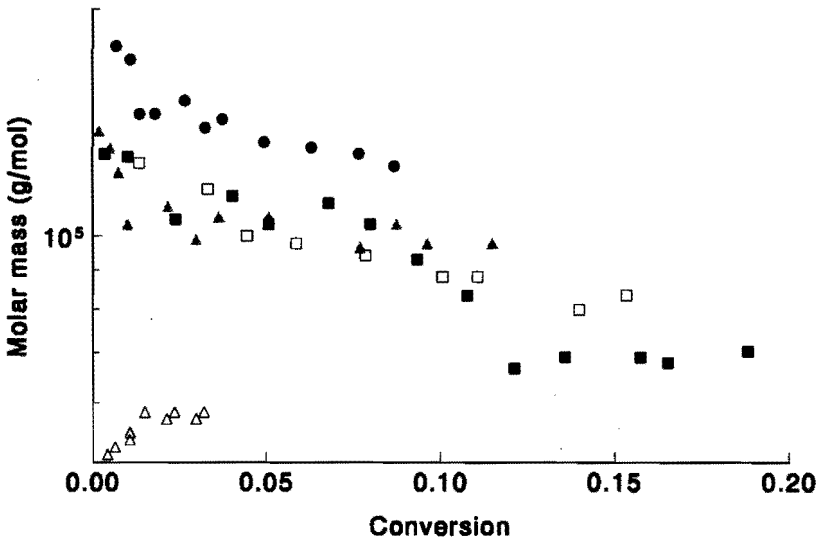


Figure 15.7 Molar mass as a function of conversion at different accumulation temperatures. Closed circles represent an accumulation temperature of 15 °C, the closed triangles of 20 °C, the open squares of 25 °C, the closed squares of 30 °C, and the open triangles of 35 °C. Data taken from Hori et al.²³

These results can be explained qualitatively, in terms of the model developed for the accumulation of PHB in *Alcaligenes eutrophus* in the following way: As has been discussed in *Chapter 11* the molar mass of PHB formed in *Alcaligenes eutrophus* first increases to reach its maximum value after a conversion of approximately 0.10 after which the molar mass decreases continuously until the granules in the bacteria coagulate. This coagulation results in a steeper decrease of the molar mass as a function of conversion or time. The transition from an increasing to a decreasing molar mass is attributed to the fact that as soon as all granules have been formed the kinetic processes occurring at the granule surface mainly determine the molar mass of the polymer formed, i.e. a decreasing molar mass as function of conversion which is due to the inversely proportional relationship between granule surface and molar mass (see also *Chapter 12*). In the case of the biosynthesis of mcl-PHA by *Pseudomonas putida* the maximum in the course of the molar mass as a function of conversion is observed at conversions below 0.01. The shift in the maximum to a lower conversion can be explained by the fact that probably the period of granule formation during the accumulation of mcl-PHA by *Pseudomonas putida* is shorter than in the case of the accumulation of PHB by *Alcaligenes eutrophus*. This can be attributed to the fact that the value for the granule formation parameters, i.e. the degree of polymerization at which the polymer-polymerase conjugate becomes surface active, z , and precipitates, j , are somewhat lower in the case of the biosynthesis of mcl-PHA. In other words, the mcl-hydroxyalkanoate monomer unit is more hydrophobic than the hydroxybutyrate unit. The time needed for the formation of the first granule (t_{begin} , see *Chapter 14*) in the case of the formation of mcl-PHA is shorter, compared with the biosynthesis of PHB, if only the value for j is considered. Also the time needed for a surface active polymer-polymerase conjugate to form is shorter, since z will be lower in this case. The effects of pH and carbon source concentration on the conversion-time and molar mass-conversion behavior reported by Hori *et al.*²³ can be explained in a similar manner as the effect of temperature on the fermentation process.

In summary, it can be said that the maximum in the course of the molar mass of the polymer formed as function of conversion are mainly caused by lower values of z and j . Just like in the case of the accumulation of PHB by *Alcaligenes eutrophus*, the molar mass of the polymer formed during the biosynthesis of mcl-PHA by *Pseudomonas putida* seems to be related to conversion, i.e. to the amount of polymer present in the bacterium. For the accumulation of mcl-PHA by *Pseudomonas oleovorans*, Preusting *et al.*²⁴ mentioned a

potential relation between the degree of polymerization of the polymer and the intracellular amount of PHA. The absolute value found for the molar mass of mcl-PHA is approximately a factor 6 lower than that found generally for PHB, this can be accounted for in terms of differences in the values for the separate kinetic parameters, monomer and/or polymerase enzyme concentrations.

15.4 Genetic Engineering and the Biosynthesis of Polyhydroxyalkanoates

Although PHAs exhibit interesting features, such as biodegradability and thermoplastic processability, relatively high production costs limited the number of applications in the past. Two major contributors to the cost of production are the carbon source added to the feedstock and the purification of the polymer at the end of the fermentation process. Reduction in cost can be achieved in several ways of which alternative carbon sources and genetic engineering of the genes of PHA synthesis are probably the most important ones. Here, the genetic engineering of the genes of PHA synthesis will be considered in some what more detail with respect to the model developed in the previous chapters. In doing so, only qualitative explanations will be given for the observed phenomena.

15.4.1 Cloning of Genes Responsible for the Biosynthesis of PHB

Genes encoding the ketothiolase, acetoacetyl-reductase and PHB synthase enzyme of *Alcaligenes eutrophus* have been expressed in species such as *Escherichia coli*²⁵ and *Pseudomonas oleovorans*²⁶, but also in transgenic plants such as *Arabidopsis thaliana*²⁷. By transferring the genes responsible for PHB biosynthesis by *Alcaligenes eutrophus* to an appropriate strain of *Escherichia coli* which was altered in fatty-acid uptake and utilization, this bacterium accumulated PHB-co-HV from glucose and propionate as carbon sources²⁸. This indicates that the three enzymes responsible for the production of the monomer and the subsequent polymerization of this monomer are perhaps the only requirements for the biosynthesis of PHB. There exist unique strains of PHA accumulating *Escherichia coli* have been developed which lyse when exposed to a temperature of 42 °C, making downstream processing of the polymer easier²⁹. The biosynthesis of PHB by recombinant *Escherichia coli* yields larger PHB granules than typically obtained by wild type micro-organisms. This can also be preferable from a downstream processing point of view³⁰. The fact that larger, and

probably less, PHB granules are formed by the recombinant bacterium than in the wild type micro-organisms can be attributed to differences in e.g. monomer and/or polymerase enzyme concentration between in the different bacteria. However, the granule formation parameters, i.e. z and j , will be the same in both systems.

In addition, *Pseudomonas oleovorans*, which is capable of accumulating mcl-PHA, has also been "equipped" with the genes responsible for PHB biosynthesis by *Alcaligenes eutrophus*²⁶. The recombinant bacterium synthesizes different monomers, i.e. 3-hydroxybutyryl-CoA (HB), 3-hydroxyoctanoate (HO), and 3-hydroxyhexanoate (HH), which can be polymerized by the polymerase enzymes present. A remarkable result of the accumulation process is the fact that the recombinant bacterium did not accumulate a copolymer consisting of mcl-HA and 3-hydroxybutyrate units, but a blend of PHB and mcl-PHA. This is in accordance with the fact that PHB producing bacteria have never been reported to incorporate significant amounts of mcl-HA (medium chain length-hydroxyalkanoates) into the accumulated polymer. Antithetically, mcl-PHA accumulating bacteria only incorporate trace amounts of short chain HA (hydroxyalkanoates) in their mcl-PHA. These results indicate that the PHB and mcl-PHA polymerase enzymes are specific for the HB-unit and HO-unit or HH-unit, respectively. Preusting *et al.*³¹ showed that these polymers were stored in separate granules. Initially, it was believed that the storage of PHB and mcl-PHA in separate granules was caused by the isolation procedure. Horowitz and Sanders³², on the other hand, concluded from a study on the formation of artificial granules from PHB and mcl-PHA that in the *in vitro* case the different polymers are found in the same granule which is in contrast with the *in vivo* observations. The following explanation was given by Horowitz and Sanders for the observed phenomena: In the *in vitro* experiments both polymers are initially present in a chloroform solution. Upon removal of the chloroform from the artificial emulsion, the composition of the resulting submicron polymeric granules was the same, i.e. all the granules contained equal ratios of PHB and mcl-PHA. Furthermore, they stated that the observation that in the *in vivo* situation separate populations of pure PHB and mcl-PHA granules existed, must be caused by a biological property of granule formation, rather than a physical property of the two polyesters.

In terms of the model developed in this thesis, especially the part which is concerned with the granule formation stage of the biosynthesis of PHB, a relatively simple explanation

can be given for the formation of two generations of PHA granules during the accumulation of PHA by the recombinant strain of *Pseudomonas oleovorans*. For simplicity, it is assumed that the recombinant *Pseudomonas oleovorans* contains two different polymerase enzyme molecules, i.e. one PHB synthase and one mcl-PHA synthase enzyme, although it is known that *Pseudomonas oleovorans* contains two very similar PHA synthases^{33,34}. Basically what may happen is the following: PHB and mcl-PHA polymerase enzymes synthesize PHB and mcl-PHA, respectively. As these polymer-polymerase conjugates exceed their water solubility, they want to minimize their surface area, and granules are formed. However, in the model developed in *Chapter 12* for the granule formation coagulation events which can occur after this homogeneous nucleation are not included which is also put forward as a shortcoming of the developed model (see *section 15.2*). Concomitantly, according to the homogeneous coagulation model with limited coagulation precursor granules will coagulate until they reach colloidal stability. These precursor granules differ in chemical composition, i.e. either being PHB or mcl-PHA. As a rule of thumb in polymer science the following holds: *Two (different) polymers do not mix*. DSC thermal analysis of a PHB/mcl-PHA mixture exhibited two independent glass transition temperatures at 5 °C and - 36 °C, respectively^{31,32}, belonging to the separate polymers. This indicates that PHB and mcl-PHA do not mix. Therefore, it can be concluded that during the coagulation step in the nucleation stage surface active polymer-polymerase conjugates will only coagulate with granules which exhibit the same chemical composition. But also during the granule growth process surface active polymer-polymerase conjugates will only adsorb onto granules exhibiting the same polymer composition. This results in the formation of two generations of granules which contain different PHAs.

Genes that encoded acetoacetyl-CoA reductase and PHB synthase have been introduced into *Arabidopsis thaliana*^{27, 35, 36}. Transgenic plants which contained both genes accumulated PHB in the form of granules in the cytoplasm, nucleus, and vacuole. The size of the PHB granules found in the transgenic plant has been shown to be heterogeneous, with the granules present in the nucleus being typically in the order of 0.2 μm , smaller than those found in the cytoplasm and vacuole, which were in the order of 0.5 μm ^{35,36}. Analysis of the molar mass distribution of the plant PHB revealed the presence of three different fractions which resulted in a rather broad multi-modal molar mass distribution (see *figure 15.8*).

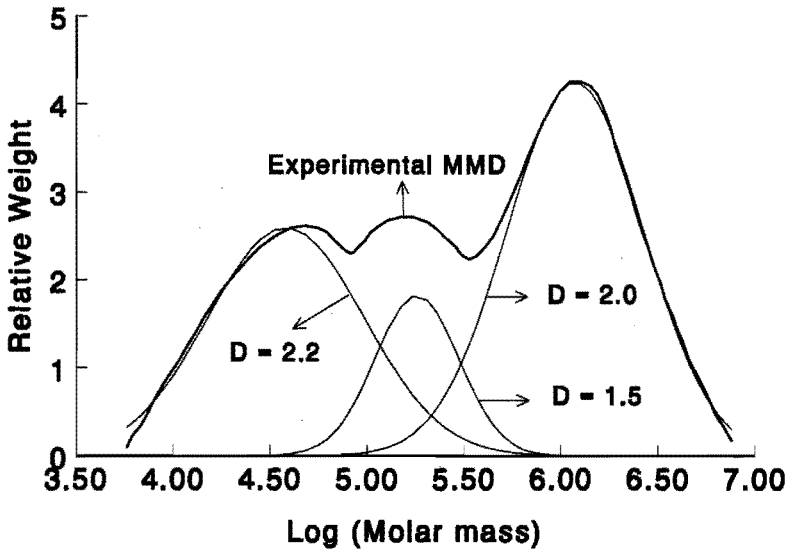


Figure 15.8 Molar mass distribution (MMD) expressed as a relative weight factor of the amount of polymer present in the sample as function of the logarithm of the molar mass of the polymer. The separate MMDs are a result of a Gaussian deconvolution of the experimental molar mass distribution. Experimental data taken from Poirier et al. ³⁶.

When this distribution is subjected to a Gaussian deconvolution, three peaks are obtained. The polydispersity (D), i.e. the ratio of the weight and number average molar mass, of the separate peaks is shown in *figure 15.8*. On average the polydispersity is approximately 2, which is the same value found for bacterial PHB ³⁷. Since PHB is accumulated at three different places in the plant it is not too unlikely that the three different peaks in *figure 15.6* correspond with these three different places, i.e. in every part of the plant, polymer is formed with different molar mass and different granule sizes. A rationalization for this is given by the fact that the activity and concentration of the polymerase enzyme and other metabolites do not have to be necessarily the same in different parts of the plant. In conclusion, it can be said that the biosynthesis of PHB seems not to be restricted to very specific systems, i.e. a minimum of requirements have to be met for the successful accumulation of this polymer in different micro-organisms and even in plants.

15.4.2 Towards the *in vitro* Synthesis of Polyhydroxalkanoates

In the previous section it was postulated that for the formation of PHB the substrate and polymerase enzyme are probably the only requirements. In fact, Gerngross *et al.*^{38,39} showed very recently, that if the polymerase enzyme from *Alcaligenes eutrophus* was incubated with substrate, i.e. (R)-3-hydroxybutyryl-CoA, PHB was formed. The polymer formed was present in granules which were significantly larger, approximately 3 μm , than those formed *in vivo*, in the order of 0.2 - 0.5 μm . This can be attributed to the fact that during the granule formation stage, coagulation occurs, since no surfactants (e.g. lipids and protein) are present to stabilize the granule surface. In order to attain colloidal stability the granules will coagulate, which results in larger granules (see also *Chapter 12*). Further, the molar mass of the *in vitro* polymer was considerably higher, i.e. $\sim 10^7$ g/mol³⁹, than for the polymer formed in the *in vivo* polymerization process, i.e. $\sim 10^6$ g/mol⁴⁰. The molar mass of the polymer formed remained constant during the *in vitro* polymerization process. The higher molar mass polymer formed in the *in vitro* case can be attributed to the fact that in the *in vivo* system more substances are present which can cause chain transfer, e.g. acetyl-CoA, acetoacetyl-CoA, lipids etc., which are not present in the *in vitro* system. As a general rule it was stated that upon lowering the polymerase enzyme concentration, the molar mass of the polymer increased while the granules formed became larger. Both these phenomena can be explained very easily. The higher molar mass at lower polymerase enzyme concentration is due to less initiation events at a constant number of propagation steps. The larger granules at lower polymerase enzyme concentration can be explained by the fact that less nucleation events occur during the granule formation stage which leads to larger granules. Attempts to promote chain transfer by overburdening the polymerase enzyme with excessive amounts of monomer (1,200,000 monomer equivalents) led to incomplete monomer conversion ($\sim 60\%$), whereas low monomer amounts (48,000 monomer equivalents) were completely converted by the same amount of polymerase enzyme. For both the polymerizations the molar mass of the polymer formed was in the order of 10^7 g/mol. The incomplete monomer conversion in the case of the high amount of monomer is probably due to the fact that the polymerase enzyme is inhibited by the large amount of coenzyme-A released during the polymerization process.

15.5 Concluding Remarks

In this chapter the applicability of the model developed in this thesis has been considered. It was stated that the chemical kinetics of the accumulation process should be considered in terms of enzyme kinetics. After this a link has to be established between conventional enzyme and polymerization kinetics. Further, the possible occurrence of oscillations during the accumulation process has been discussed by considering a model which describes the metabolism of the biosynthesis of PHB in a very simple way. It has been shown that these oscillations can occur and what their potential influence is on the accumulation process. However, direct exclusive experimental evidence is not available.

The homogeneous nucleation model with growth, used to describe the granule formation stage, has to be extended to account for coagulation events which occur during the earliest stage of the accumulation process. *In vitro* polymerizations forming PHB already have shown that the granule size increases dramatically when no, or very low amounts of surface active species are present, i.e. approximately 3 μm , compared with the *in vivo* polymerization process where the granules are in the range of 0.2 - 0.5 μm . The granule growth process can be considered as a dynamic process where the exchange of polymerase enzyme between the granule surface and the cytoplasm mainly determines the accumulation process. On the other hand, it has been shown that an alternative approach based on the basic definition of molar mass is also able to explain the course of the molar mass of the polymer formed during the accumulation process.

The developed model has to be extended at several points before it can be quantitatively applied to the accumulation of copolymers. Nonetheless, the model can be used to deal with some features in a qualitative way. In doing so, the phenomenon known as composition drift can occur during the accumulation of copolymers in *Alcaligenes eutrophus* and can be explained using the developed model.

The use of genetic engineering in the biosynthesis of PHAs can be of great help, not only with respect to the more efficient production of PHAs, but also in the elucidation of the kinetics and mechanisms governing the accumulation process. The observation that a mutant

of *Pseudomonas oleovorans* containing both the PHB and mcl-PHA synthase enzyme, is capable of accumulating PHB and mcl-PHA in separate granules can be explained using the developed model. Further, the trimodality of the molar mass distribution observed when PHB is accumulated by a transgenic plant can be explained by the fact that polymer is accumulated at three different places in the plant, each place with its own specific accumulation conditions. The *in vitro* polymerization of PHB clearly showed that this polymerization process can be considered as a conventional polymerization process, exhibiting the normal processes of initiation, propagation and termination. While at the same time the polymerization process is also affected by the heterogeneity of the polymerization system.

In conclusion, it can be stated that the developed model is applicable not only to the biosynthesis of PHB by *Alcaligenes eutrophus*, where it originally was developed for, but also to other PHAs and PHA accumulating species.

15.6 References

- 1 Doi, Y., "Microbial Polyesters", New York, VCH Publishers, Inc., (1990)
- 2 Steinbüchel, A., and Valentin, H.E., *FEMS Microbiol. Lett.*, 128, 219 (1995)
- 3 Oeding, V., and Schlegel, H.G., *Biochem. J.*, 134, 239 (1973)
- 4 Haywood, G.W., Anderson, A.J., Chu, L., and Dawes, E.A., *FEMS Microbiol. Lett.*, 52, 91 (1988)
- 5 Chapter 10 of this thesis
- 6 Ghosh, A., and Chance, B., *Biochem. Biophys. Res. Commun.*, 16, 174 (1964)
- 7 Winfree, A.T., "The Geometry of Biological Time", Springer, New York, (1980)
- 8 Goldbeter, A., and Lefever, R., *Biophys. J.*, 12, 1302 (1972)
- 9 Rapp, P.E., and Berridge, M.J., *J. Theor. Biol.*, 66, 497 (1977)
- 10 Haywood, G.W., Anderson, A.J., and Dawes, E.A., *FEMS Microbiol. Lett.*, 57, 1 (1989)
- 11 Fukui, T., Yishimoto A., Matsumoto M., Husokawa, S., Saito T., Nishikawa H., and Tomita, K., *Arch. Microbiol.*, 110, 149 (1976)
- 12 Kurja, J., Zirkzee, H.F., De Koning, G.J.M., and Maxwell, I.A., *Macromol. Theory and Sim.*, 4, 839 (1995)
- 13 Chapter 11 of this thesis
- 14 Gerngross, T.U., Reilly, P., Stubbe, J., Sinskey, A.J., and Peoples, O.P., *J. Bacteriol.*, 175, 5289 (1993)
- 15 Van Doremaele, G.H.J., "Model Prediction, Experimental Determination, and Control of Emulsion Copolymer Microstructure", PhD. Thesis, Eindhoven University of Technology, The Netherlands (1990)
- 16 Yoshie, N., Menju, H., Sato, H., and Inoue, Y., *Macromolecules*, 28, 6516 (1995)
- 17 Nakamura, S., Doi, Y., and Scandola, M., *Macromolecules*, 17, 4237 (1992)
- 18 De Smet, M.J., Eggink, G., Witholt, B., Kingma, J., and Wynberg, H., *J. Bacteriol.*, 154, 870 (1983)
- 19 Huisman, G.W., de Leeuw, O., Eggink, G., and Witholt, B., *Appl. Environ. Microbiol.*, 55, 1949 (1989)

- 20 Lageveen, R.G., Huisman, G.W., Preusting, H., Ketelaar, P., Eggink, G., and Witholt, B., *Appl. Environ. Microbiol.*, 54, 2924 (1988)
- 21 Fritzsche, K., Lenz, R.W., and Fuller, R.C., *Int. J. Biol. Macromol.*, 12, 85 (1990)
- 22 Fritzsche, K., Lenz, R.W., and Fuller, R.C., *Int. J. Biol. Macromol.*, 12, 92 (1990)
- 23 Hori, K., Soga, K., and Doi, Y., *Biotechnology Lett.*, 16, 709 (1994)
- 24 Preusting, H., Nijenhuis, A., and Witholt, B., *Macromolecules*, 23, 4220 (1990)
- 25 Slater, S.C., Voige, W.H., and Dennis, D.E., *J. Bacteriol.*, 170, 4431 (1988)
- 26 Timm, A., Byrom, D., and Steinbüchel, A., *Appl. Microbiol. Biotechnol.*, 33, 296 (1990)
- 27 Poirier, Y., Dennis, D.E., Klomparens, K., and Somerville, C., *Science*, 256, 520 (1992)
- 28 Slater, S., Gallaher, T., and Dennis, D., *Appl. Environ. Microbiol.*, 58, 1089 (1992)
- 29 Fidler, S., and Dennis, D., *FEMS Microbiol. Rev.*, 103, 231 (1992)
- 30 Middelberg, A.P.J., Lee, S.Y., Martin, J., Williams, D.R.G., and Chang, H.N., *Biotechnol. Lett.*, 17, 205 (1995)
- 31 Preusting, H., Kingma, J., Huisman, G., Steinbüchel, A., and Witholt, B., *J. Envir. Pol. Deg.*, 1, 11 (1993)
- 32 Horowitz, D. M., and Sanders, J.K.M., *Polymer*, 35, 5079 (1994)
- 33 Huisman, G.W., Wonink, E., Meima, R., Kazemier, B., Terpstra, P., and Witholt, B., *J. Biol. Chem.*, 266, 2191 (1991)
- 34 Huisman, G.W., Wonink, E., de Koning, G.J.M., Preusting, H., and Witholt, B., *Appl. Microbiol. Biotechnol.*, 38, 1 (1992)
- 35 Poirier, Y., Dennis, D., Klomparens, K., Nawrath, C., and Somerville, C., *FEMS Microbiol. Rev.*, 103, 237 (1992)
- 36 Poirier, Y., Sommerville, C., Schechtman, L.A., Satkowski, M.M., and Noda, I., *Int. J. Biol. Macromol.*, 17, 7 (1995)
- 37 Doi, Y., "Microbial Polyesters", New York, VCH Publishers, Inc., (1990)
- 38 Gerngross, T.U., Snell, K.D., Peoples, O.P., and Sinskey, A.J., *Biochemistry*, 33, 9311 (1994)
- 39 Gerngross, T.U., and Martin, D.P., *Proc. Natl. Acad. Sci. USA*, 92, 6279 (1995)
- 40 Anderson, A.J., and Dawes, E.A., *Microbiol. Rev.*, 54, 450 (1990)

Epilogue

In this thesis some outstanding problems concerning heterogeneous polymerization in aqueous media have been studied. Three areas were identified that embody problems, thermodynamic and/or kinetic in nature, of which solutions are of key importance for further development in emulsion polymerization or emulsion polymerization-like processes. These three areas were: (1) monomer partitioning during emulsion polymerization, (2) the control of latex particle morphology during emulsion polymerization (via the use of specific surfactant structures like vesicles), and (3) the kinetics of unconventional emulsion polymerizations. These areas were embedded in the following two objectives. The *first* objective of this thesis was to describe, explain and predict the partitioning of monomer(s) between the separate phases (such as water, latex particles, monomer droplets, and vesicle bilayers) present during the course of an emulsion polymerization. The *second* objective of this thesis was directed towards the applicability of the concepts known from conventional free-radical emulsion polymerizations, such as particle nucleation and growth, to polymerizations processes that, until recently, were not recognized as emulsion polymerization due to the fact that the propagating species involved in the polymerization reaction had a non-free-radical character. The biosynthesis of poly-(R)-3-hydroxybutyrate (PHB) in *Alcaligenes eutrophus* has served as a model system.

The results obtained during the investigation described in this thesis concerning the above objectives can be epitomized as follows:

With respect to the *first* objective the insight obtained can be summarized as follows: The monomer concentration in the latex particles directly determines the rate of polymerization and thus the molar mass, while the ratio of monomers in the latex particles dictates the chemical composition of the copolymer formed. Therefore, a detailed knowledge of the partitioning of monomer(s) is of utmost importance with respect to the modeling and control of emulsion polymerization processes and the characteristics of the formed product. To achieve this goal a new experimental method was developed to determine the monomer concentration in the different phases present during an emulsion polymerization, i.e. the

aqueous phase, the monomer droplets and the latex particles. Concomitantly, it was possible to test a thermodynamic model based on the Flory-Huggins theory and to evaluate its use in predicting experimental partitioning data. In doing so, a simple relationship has been derived for predicting the monomer concentrations in the latex particles during an emulsion copolymerization based on the saturation concentration of the monomer in the latex particles and the composition of the monomer droplets. The developed theoretical model has been extended successfully to polymer-monomer mixtures which exhibit only limited miscibility, e.g. the emulsion copolymerization of styrene and acrylonitrile, and to vesicles (surfactant bilayers which were swollen with different organic solvents). In order to visualize the partitioning of monomer(s) during an emulsion polymerization, phase diagrams have been constructed which can be of great practical relevance. These phase diagrams provide insight in the phase behavior and can be helpful in the study of the morphology of composite latex particles. Detailed knowledge of this phase behavior opens the possibility of controlling the final morphology of composite latex particles and ultimately the properties of the formed product. Although a start has been made with the construction of phase diagrams of emulsion polymerization processes, there is still a large amount of research to be done. Special attention has to be paid not only to the kinetic processes occurring during an emulsion polymerization and their effect on the phase behavior of the polymerizing system, but also to the interesting morphology and phase behavior of polymers formed during so-called unconventional emulsion polymerizations, which can yield, for instance, semi-crystalline polymers like in the biosynthesis of polyhydroxyalkanoates (PHAs).

By applying the concepts known from conventional emulsion polymerization to the biosynthesis of PHB by *Alcaligenes eutrophus*, i.e. the *second* objective of this thesis, some plausible explanations have been found for experimentally observed phenomena which were until recently only poorly understood. The biosynthesis of PHB has been considered as an emulsion polymerization, and the polymerization process has been divided into a granule ("latex particle") formation and growth stage. The principal reactions occurring during the enzyme catalyzed chain-growth polymerization, viz. initiation, propagation and chain termination, were defined. Further, by taking into account the exchange of reactive species between the cytoplasm (continuous aqueous phase) and the granule surface (polymer phase), a kinetic model has been developed. This model is capable of predicting/describing not only the experimentally observed relation between conversion and the molar mass of the polymer

formed, but also a rationalization is given for the fact that polymerization ceases at high polymer accumulation levels in the bacterium. The developed model has been shown to be able to explain the accumulation of PHB by *Alcaligenes eutrophus*, as well as by plants, and the accumulation of other PHAs by *Pseudomonas putidaloleovorans*. Since the *in vivo* synthesis of PHAs is difficult to manipulate in such a way that the exclusive effect of the separate parameters on the polymerization process can be investigated, the recently reported *in vitro* synthesis of PHAs offers enormous opportunities of testing kinetic models such as described in this thesis. Kinetic experiments, *in vivo* as well as *in vitro*, have to be designed that can contribute to a better understanding of the biosynthesis of PHAs, in particular, and enzyme catalyzed polymerizations, in general.

It can be concluded, exemplified by the systems investigated in this thesis, that due to the complexity of heterogeneous polymerization reactions and processes, it is of utmost importance that a unified experimental and theoretical approach is developed leading to a better understanding of these systems. Therefore, scientists from different disciplines should collaborate, thus establishing a *Chain-of-Knowledge* linking chemistry with physics, mathematics, and life sciences.

Summary

This thesis describes an investigation of two relevant aspects of heterogeneous polymerizations in aqueous media, viz. (1) the partitioning of one or two monomers between the different phases present during emulsion polymerization, and (2) the kinetics of the biosynthesis of poly-(R)-3-hydroxybutyrate (PHB) by *Alcaligenes eutrophus* which results in the formation of a latex very similar to the product of a conventional emulsion polymerization.

The partial and saturation swelling of latex particles by one or two monomers has been studied. Experimental partitioning results have been described, modeled, and predicted utilizing a model based on the Flory-Huggins lattice theory. It has been shown that during partial swelling the combinatorial entropy of mixing polymer and monomer is the significant term determining the degree of partial swelling. The degree of saturation swelling is mainly determined by the residual energy term consisting of the enthalpy of mixing and the interfacial free energy. It is experimentally observed that in an ideal latex system, i.e. the monomer(s) present is a good solvent for the polymer in the latex particles, the fraction of any monomer is the same in the latex particles and in the monomer droplets. This can be explained and predicted by a model based on a simplified Flory-Huggins lattice theory. In the case of the non-ideal system, i.e. the monomer(s) are a poor(er) solvent for the polymer in the latex particles, the same model can be used, without the simplifications made in the case of the ideal latex systems, to describe the experimental partitioning results. For the ideal, as well as the non-ideal latex systems, a simple empirical relationship has been developed whereby the concentration of the monomers in the latex particles at any composition of the monomer droplet phase can be calculated from the individual saturation concentrations of the monomers in the latex particles of interest. Further, phase diagrams have been constructed which visualize the partial and saturation swelling of latex particles by one or two monomers. The Gibbs phase rule has been applied to heterogeneous polymerization systems with curved surfaces, such as latices, and to the constructed phase diagrams.

A brief survey is given of those heterogeneous polymerization processes in aqueous media that can be considered as emulsion polymerizations due to the fact that the product of

the polymerization process can be designated as a latex; because of the resemblance to natural rubber latex particles. The polymerization of an unsaturated monomer in the hydrophobic bilayer of a vesicle can be considered as an unconventional emulsion polymerization from a kinetic as well as from a thermodynamic point of view. Guidelines have been presented for the successful polymerization of an unsaturated monomer in vesicle bilayers. The equilibrium partitioning of solvent between water and vesicle bilayers above their phase transition temperature has been discussed in terms of the classical Flory-Huggins lattice theory. The vesicle surface free energy has been described by the Gibbs-Thomson equation and was justified via the modified Gibbs phase rule.

Unconventional emulsion polymerizations hardly have been the subject of in-depth kinetic studies. Therefore, a highly relevant example, i.e. the biosynthesis of bacterial polyhydroxyalkanoates (PHAs), more specifically the biosynthesis of PHB by *Alcaligenes eutrophus* has been investigated. In doing so, the concepts known from the conventional emulsion polymerization process have been used, such as the division of the polymerization process in a granule formation and a granule growth stage. First, the kinetics and metabolic regulation of the accumulation of PHB in *Alcaligenes eutrophus* have been studied. It has been shown that the bacterial polycondensation can be understood in terms of classical polymerization reactions. The polymerization process is controlled via competitive product inhibition, i.e. the low molar mass product of the polycondensation reaction, coenzyme-A, can inhibit the polymerization reaction if its concentration exceeds a certain critical value. By dividing the accumulation process in a granule formation and a granule growth stage, the effect of both processes on the polymerization and the polymer characteristics, most notably the molar mass of the polymer formed, has been studied. The molar mass of the polymer formed during the polymerization process is strongly related to the accumulation stage of the polymer in the bacterium, i.e. during the granule formation stage the molar mass of the polymer increases while during the granule growth stage the molar mass of the polymer formed decreases. As in conventional free-radical emulsion polymerizations the exchange of reactive species between the different phases has a profound effect on the characteristics of the polymerization process. This has been shown by the concept of boundary layers and their role at the end of the polymerization process, i.e. although monomer and active polymerase enzyme are present, the polymerization ceases due to the overlap of the boundary layers resulting in a high coenzyme-A concentration which inhibits the polymerase enzyme. Values

for the different kinetic parameters and the concentrations of monomer and polymerase enzyme have been estimated from experimental data. These values have been used to perform model calculations which were compared with experimental results. Good agreement was obtained between the model calculations and the experimental data. Finally, the model developed for the accumulation of PHB in *Alcaligenes eutrophus* has been applied to other PHAs accumulating bacteria, transgenic plants, and the *in vitro* synthesis of PHB. Most of the observed phenomena could be explained qualitatively by the developed model. The occurrences of oscillations during the biosynthesis of PHB in *Alcaligenes eutrophus* has been postulated. Very recently, model calculations have been performed, indicating that this could indeed be the case (result not included in this thesis).

The major conclusion that can be drawn from this thesis is that the large surface to volume ratio of heterogeneous polymerizations, most notably emulsion polymerization and emulsion polymerization-like processes, has a profound effect, not only on the polymerization kinetics, due to the fact that the reaction system is compartmentalized, but also on the thermodynamics, i.e. on the partitioning of for instance monomer between the separate phases present. It is of utmost importance to understand the interrelation between kinetics and thermodynamics and the effect of these two phenomena on the polymerization process since they directly determine the properties and characteristics of the end product.

Samenvatting

Dit proefschrift beschrijft een onderzoek naar een aantal relevante aspecten van heterogeen polymerisaties in waterig milieu. Bestudeerd werden: (1) de verdeling van één of twee monomeren over de verschillende fasen die aanwezig zijn tijdens een emulsie(co)polymerisatie en (2) de biosynthese van poly-(R)-3-hydroxybutyraat (PHB) in *Alcaligenes eutrophus*.

De partiële en verzadigingszwellbaarheden van latex deeltjes door één of twee monomeren werd onderzocht. Experimentele verdelingsgegevens werden beschreven, gemodelleerd en voorspeld met behulp van een thermodynamisch model gebaseerd op de Flory-Huggins roostertheorie. Hierbij werd aangetoond dat gedurende de partiële zwelling van latex deeltjes de combinatoriële mengentropie van het polymeer en het monomeer de belangrijkste bijdrage is aan de partiële molaire vrije energie die de mate van de partiële zwelbaarheid bepaalt. De mate van verzadigingszwelling wordt hoofdzakelijk bepaald door de residuele vrije energie term, die bestaat uit de mengenthalpie en de grensvlak vrije energie. Het is een experimenteel gegeven dat in het geval van ideale latex systemen (d.w.z. het monomeer is een goed oplosmiddel voor het polymeer) de fractie van elk monomeer in de latex deeltjes gelijk is aan dat in de monomeer fase. Dit kan verklaard worden met een model gebaseerd op een vereenvoudigde Flory-Huggins roostertheorie. Ook in het geval van niet-ideale latex systemen (d.w.z. het monomeer is een slecht(er) oplosmiddel voor het polymeer) kan de Flory-Huggins roostertheorie gebruikt worden om de experimentele verdelingsgegevens te beschrijven. Voor zowel de ideale als de niet-ideale latex systemen, werd een eenvoudige empirische vergelijking afgeleid waarmee de concentratie van de verschillende monomeren in de latex deeltjes als functie van de samenstelling van de monomeer fase, kan worden berekend op basis van de verzadigingsconcentraties van de monomeren in de latex deeltjes. Verder zijn fasendiagrammen opgesteld die de partiële en de verzadigingszwellbaarheden van latex deeltjes door één of twee monomeren visualiseren. Tegelijkertijd is de fasenregel van Gibbs toegepast op multi-component systemen die fasen bezitten met gekromde oppervlakken, zoals latices.

Een beknopt overzicht werd gegeven van niet-conventionele heterogene polymerisatieprocessen in waterig milieu die desalniettemin opgevat kunnen worden als emulsiopolymerisaties omdat het product van het polymerisatieproces een latex is. De polymerisatie van een onverzadigd monomeer in de hydrofobe bilaag van vesicles werd bestudeerd, zowel vanuit een kinetisch als thermodynamisch oogpunt. Richtlijnen zijn opgesteld voor een succesvolle polymerisatie van een onverzadigd monomeer in de vesicle bilaag. De evenwichtsverdeling van het monomeer/oplosmiddel tussen de waterfase en de hydrofobe bilaag werd beschreven met behulp van de klassieke Flory-Huggins roostertheorie. De grensvlakspanning van de vesicle bilaag is beschreven met behulp van de Gibbs-Thomson vergelijking op basis van de gemodificeerde fasenregel van Gibbs.

De kinetische en mechanistische processen die een rol spelen tijdens de biosynthese van PHB in *Alcaligenes eutrophus* (een niet-conventionele emulsiopolymerisatie) werden onderzocht. Hierbij werd gebruik gemaakt van concepten en principes die bekend zijn in conventionele emulsiopolymerisaties, zoals de onderverdeling van het polymerisatieproces in een deeltjesvormings- en een deeltjesgroei-stadium. Allereerst werden de kinetiek en de metabolische regulatie van de biosynthese van PHB in *Alcaligenes eutrophus* bestudeerd. Het belangrijkste resultaat is dat de bacteriële polycondensatie opgevat kan worden als een klassiek polymerisatiereactie. De biopolymerisatie wordt gereguleerd via competitieve produktinhibitie, d.w.z. het laag moleculaire produkt van de polycondensatie, co-enzyme-A, kan de polymerisatiereactie inhibiteren wanneer het een bepaalde kritische concentratie overschrijdt. Door de biopolymerisatie onder te verdelen in een granule vormingsproces en een granule groeiproces kon de invloed van de afzonderlijke processen op bijvoorbeeld het molecuulgewicht van het gevormde polymeer onderzocht worden. Het molecuulgewicht van het gevormde polymeer hangt sterk af van de hoeveelheid polymeer dat reeds door de bacterie is opgeslagen. Gedurende het granule vormingsproces neemt het molecuulgewicht toe terwijl tijdens het granule groeiproces het molecuulgewicht afneemt. Zoals in conventionele emulsiopolymerisatieprocessen speelt ook bij de biosynthese van PHB in *Alcaligenes eutrophus* de uitwisseling van monomeer en polymerase enzyme een belangrijke, en mogelijk cruciale rol. Dit is ondermeer aangetoond met behulp van de invloed van grenslagen op het stoppen van de polymerisatie bij een grote hoeveelheid opgeslagen polymeer. De grenslagen overlappen elkaar dan waardoor de lokale co-enzyme-A concentratie zo hoog wordt dat deze het polymerase enzym inhibiteert. De concentraties van de verschillende metabolieten en de

waarden van de verschillende kinetische parameters zijn geschat aan de hand van experimentele gegevens. Deze zijn vervolgens gebruikt in modelberekeningen die werden vergeleken met experimentele gegevens. Een goede overeenkomst is gevonden tussen modelberekeningen en experimentele data. Uiteindelijk werd het model dat ontwikkeld was voor de biosynthese van PHB in *Alcaligenes eutrophus* ook toegepast op andere polyhydroxyalkanoaten accumulerende bacteriën, transgene planten en de *in vitro* synthese van PHB. Een groot gedeelte van de experimentele gegevens konden kwalitatief verklaard worden met behulp van het ontwikkelde model. Verder werd een hypothese geponeerd die het optreden van oscillaties gedurende de biosynthese van PHB in *Alcaligenes eutrophus* kan verklaren.

De belangrijkste conclusie uit beide fenomenen die werden bestudeerd in dit proefschrift is dat de grote oppervlak-volume verhouding in heterogene polymerisaties, met name in emulsiepolymerisaties en "emulsiepolymerisatie-achtige" processen, een cruciale rol speelt. Niet alleen de kinetische processen maar ook de thermodynamische evenwichten worden door deze compartimentalisatie sterk beïnvloed. Het is van vitaal belang de correlatie tussen kinetiek en thermodynamica en hun effect op het polymerisatieproces te begrijpen, daar de kinetiek en de thermodynamica direct de eigenschappen en karakteristieken van het gevormde eindproduct bepalen.

Curriculum Vitae

Jenci Kurja werd geboren op 4 april 1966 te Maastricht. Hij behaalde het diploma MAVO in 1982 en het diploma MLO in 1986. Vier jaar later, in 1990, behaalde hij het diploma HLO, met lof. In september van datzelfde jaar begon hij aan de verkorte opleiding Scheikunde aan de Katholieke Universiteit Nijmegen. Het doctoraal examen werd, met lof, afgelegd op 30 maart 1992. Vanaf 1 november 1992 is hij werkzaam in de vakgroep voor Polymeerchemie en Kunststoftechnologie (TPK) deeltmakende van het Centrum voor Polymeren en Composieten (CPC) van Eindhoven Polymer Laboratories (EPL) aan de Technische Universiteit Eindhoven (TUE) onder leiding van prof. dr. P.J. Lemstra.

Langs deze weg wil ik iedereen bedanken die heeft bijgedragen tot het totstandkomen van dit proeschrift. In het bijzonder alle afstudeer(d)(st)ers, t.w. Eelco, Willianne, Mariëlle, Nanette, Maarten, Mark, Eric, Angela, Erwin en Jacques.

“Woran arbeiten Sie?” wurde Herr K. gefragt.

Herr K. antwortete: “Ich habe viel Mühe, ich bereite meinen nächsten Irrtum vor.”

Bertolt Brecht: *Geschichten*,

Bibliothek Suhrkamp, Frankfurt am Main 1962, S. 167,

Herr K. war sicher Wissenschaftler! Oder?

Stellingen

behorende bij het proefschrift

Some Outstanding Problems concerning Heterogeneous Polymerizations in Aqueous Media: *Thermodynamics, Kinetics and Modeling*

van

Jenci Kurja

1. Het kinetisch model van Kawaguchi en Doi voor de biosynthese van PHB in *Alcaligenes eutrophus*, waarbij het polymerisatieproces als een homogeen systeem wordt beschouwd, gaat voorbij aan de invloed van de ratio van het grote oppervlak-volume op het polymerisatieproces.

- Kawaguchi, Y., and Doi, Y., *Macromolecules*, 25, 2324 (1992)

2. Bij een emulsiepolymerisatie, waarbij een watermengbaar monomeer wordt gebruikt, gaat men voorbij aan het feit dat dit monomeer vaak een slecht oplosmiddel is voor het polymeer in de latexdeeltjes.

- Hoofdstuk 3 van dit proefschrift

3. Door tijdens de biosynthese van polyhydroxyalkanoaten conversie te definiëren als de hoeveelheid polymeer in de bacterie ten opzichte van de maximale hoeveelheid polymeer in dezelfde bacterie, kunnen experimentele gegevens uit verschillende experimenten en van verschillende systemen met elkaar vergeleken worden.

- Hoofdstuk 11 van dit proefschrift

4. Enzymen zijn meer dan polymerisatiekatalysatoren.

- Hoofdstukken 10 en 13 van dit proefschrift

5. Het feit dat Ellar *et al.* de biosynthese van PHB niet als een emulsiepolymerisatie wilde opvatten op basis van het polymerisatiemechanisme is onjuist.

- Ellar, D., Lundgren, D.G., Okamura, K., and Marchessault, R.H., *J. Mol. Biol.*, 35, 489 (1968)
- Hoofdstuk 9 van dit proefschrift

6. Om binnen drie jaar twee verschillende en tegenstrijdige verklaringen te geven voor het verloop van het molecuulgewicht van het gevormde polymeer als functie van de accumulatie tijd, tijdens de biosynthese van PHB in *Alcaligenes eutrophus*, is op zijn minst vreemd te noemen, zeker indien in de laatste publicatie de eerste verklaring niet wordt besproken of niet naar wordt verwezen.

- Koizumi, F., Abe, H., and Doi, Y., *J. Macromol. Sci., Pure Appl. Chem.*, **A32(4)**, 759 (1995)
- Kawaguchi, Y., and Doi, Y., *Macromolecules*, **25**, 2324 (1992)

7. Voor slecht te verwerken polymeren is er vaak een oplossing.

- Lemstra, P.J., Kurja, J., Meijer, H.E.H., "Processing of Polymers using Reactive Solvents" in: *Materials Science and Technology: A Comprehensive Treatment*, R.W. Cahn and E.J. Kramer (Eds.), VCH Verlagsgesellschaft, Chapter 10, in press (1997)

8. Oude maten meten vaak met oude maten.

9. Het probleem van Dhr. Boonstra (president Philips) dat Philips qua organisatie vergelijkbaar is met een bord spaghetti, waarbij het moeilijk is één sliert te verwijderen is minder groot dan het lijkt. Polymeerkundigen hebben reeds grote ervaring met het ontwarren van met elkaar verstrengelde spaghetti-achtige moleculen.

- Interview met Cor Boonstra in *De Telegraaf*, Zaterdag 11 januari 1997
- DeGennes, P.G., *Scaling Concepts in Polymer Physics*, Cornell Univ. Press, Ithaca, New York (1978)
- Smith, P., and Lemstra, P.J., UK patent 2.040.414 (1979)

10. "There is nothing more difficult to carry out, nor more doubtful of success, nor more dangerous to handle, than to initiate a new order of things".

- Niccolò Machiavelli (1469 - 1527)
- Hoofstukken 10 tot en met 15 van dit proefschrift

11. Om fraude met Euro-cheques tegen te gaan, zouden deze, net zoals in België, door de eigenaar gebarreerd moeten kunnen worden.

12. Een biodegradeerbaar polymeer hoeft niet altijd milieuvriendelijker te zijn dan een polymeer dat niet biodegradeerbaar is.

- "Environmental economic assessment of biotechnological processes and products", by B. Kothuis and F. Schelleman, TME report, The Hague, May 1996

13. Kurja betekent ellende, ofschoon dit proefschrift nu gereed is.

- Fins-Nederlands woordenboek